Characterization of the Immunoproteasome Subunits LMP2 and LMP7 in the Mouse Brain

Dissertation

zur Erlangung des akademischen Grades

doctor rerum naturalium

(Dr. rer. nat.)

Genehmigt Fakultät für Naturwissenschaften

der Otto-von-Guericke-Universität Magdeburg

von   M.Sc. Paula Säring

geb. am 14.08.1987 in Finsterwalde

Gutachter: Prof. Dr. Daniela C. Dieterich

Prof. Dr. Frank Kirchhoff

Eingereicht am: 22. Mai 2018

Verteidigt am: 16. November 2018

Table of content

List of abbreviations

Abbreviation	Meaning
AB	antibody
ABC	avidin biotin complex
AD	Alzheimer´s disease
ALS	amyotrophic lateral sclerosis
AMP	adenosine monophosphate
AMPA	α-amino-3-hydroxy-5-methyl-4-isoxazolepropionic acid
APS	ammonium peroxide sulfate
ATP	adenosine triphosphate
BSA	bovine serum albumin
BT	biotin tyramin
°C	degree Celsius
cAMP	cyclic adenosine monophosphate
CANDLE	chronic atypical neutrophil dermatosis with lipodystrophy
CDK	cyclin-dependent kinase
chk	chicken
CNS	central nervous system
CREB	cAMP response element-binding protein
d	day
DAPI	4`,6-diamidino-2-phenylindole
DAMP	damage-associated molecular pattern
DC	dendritic cell
ddH$_2$O	double distilled water
DNA	deoxyribonucleic acid
DRiP	defective ribosomal products
DUB	deubiquitinating enzyme
E1	ubiquitin-activating enzyme
E2	ubiquitin-conjugating enzyme
E3	ubiquitin-protein ligase
ECL	enhanced chemical luminescence
EDTA	ethylenediaminetetraacetic acid
ER	endoplasmic reticulum
FACS	flow cytometric analysis
Fig.	figure
g	gram
GFAP	glial fibrillary acidic protein
GluR1	AMPA-selective glutamate receptor 1
GluR2	AMPA-selective glutamate receptor 2
gp	guinea pig
gt	goat
h	hour
HBSS	Hank´s balanced salt solution
HD	Huntington´s disease
HEPES	2-(4-(2-hydroxyethyl)-1-piperanzinyl)-ethansulfonic acid
Hom	homogenate
HRP	horseradish peroxidase
Iba-1	ionized calcium-binding adapter molecule 1
IF	immunofluorescence
IFN-γ	interferon γ
IL1a	interleukin 1 alpha
IL1b	interleukin 1 beta
IL10	interleukin 10
IP	immunoproteasome
IPTG	isopropyl-β-D-thiogalactopyranoside
JMP	joint contracture, muscle atrophy, microcytic anemia and panniculitis-induced lipodystrophy
kDa	kilo Dalton

6

kg	kilo gram
KO	knockout
KPSI	kilo-pound per square inch
l	liter
LMP2	low molecular mass protein 2
LMP7	low molecular mass protein 7
M	molar
mA	milli Ampere
Map2	microtubule-associated protein 2
MBP	maltose binding protein
MCA	middle cerebral artery
MCAO	middle cerebral artery occlusion
MECL-1	multicatalytic endopeptidase complex subunit-1
MFG-E8	mild-fat globule epidermal growth factor-like factor 8
µg	micro gram
mg	milli gram
MHCI	major histocompatibility complex class I
MHCII	major histocompatibility complex class II
min	minute
µl	micro liter
ml	milli liter
mM	milli molar
mRNA	messenger RNA
ms	mouse
NB	neurobasal medium
NEDD8	neural precursor cell expressed developmentally down-regulated protein 8
NeuN	neuronal nuclei protein
NF-κB	nuclear factor kappa-light-chain-enhancer of activated B cells
ng	nano gram
nm	nano meter
NR1	N-methyl-D-aspartate receptor subunit 1
NR2A	N-methyl-D-aspartate receptor subunit 2A
NR2B	N-methyl-D-aspartate receptor subunit 2B
P1	pellet 1 (after 1st centrifugation at 100 x g)
P2	pellet 2 (after 2nd centrifugation at 12 000 x g)
P3	pellet 3 (after hypo-osmotically lysis and centrifugation at 100 000 x g)
PAC	proteasome assembly chaperone
PBS	phosphate buffered saline
pCREB	phosphorylated CREB
PD	Parkinson´s disease
PFA	paraformaldehyde
PGPH	peptidylglutamyl-peptide hydrolysing
pH	potentia hydrogenii
PI	protease inhibitor
PLP	periodate-lysine-paraformaldehyde
POMP	proteasome maturation protein
PRR	pattern recognition receptor
PSD95	postsynaptic density protein 95
rb	rabbit
RNA	ribonucleic acid
RNS	reactive nitrogen species
ROS	reactive oxygen species
rpm	rounds per minute
RT	room temperature
S	Svedberg
S1	supernatant 1 (after 1st centrifugation at 100 x g)
S2	supernatant 2 (after 2nd centrifugation at 12 000 x g)
SDS	sodium dodecyl sulfate
SDS-PAGE	sodium dodecyl sulfate polyacrylamide gel
SEM	standard error of the mean

SJ	synaptic junction
SUMO	small ubiquitin-like modifier
Syphy	synaptophysin 1
TAP	transporter associated with antigen processing
TBS	tris buffered saline
TBS-T	tris buffered saline, 0.1% Tween20
TEMED	tetramethylethylendiamine
TGF-β	transforming growth factor
TMT	trimethylthiazoline
TNF-α	tumor necrosis factor
TPBS	tris phosphate buffered saline
TPBS-T	tris phosphate buffered saline, 0.1% Tween20
tRNA	transfer RNA
Ub	Ubiquitin
UBL	ubiquitin-like protein
UPS	ubiquitin-proteasome system
URM1	ubiquitin-related modifier 1
WB	western blot
WT	wild type
x g	gravity

List of figures

List of tables

Zusammenfassung

Die hier verfasste Dissertation beinhaltet eine Lokalisationsstudie sowie eine funktionelle Charakterisierung der katalytischen Untereinheiten LMP2 und LMP7 des Immunoproteasomes (IPs) im Gehirn der Maus. Das IP ist eine spezifische Form des Proteasoms, welches konstitutiv in Zellen des Immunsystems exprimiert wird und auf Grund seiner speziellen proteolytischen Eigenschaften eine wichtige Rolle für die Prozessierung der MHCI Antigene spielt. Interessanterweise können entzündungsfördernde Zytokine auch zu einer Induktion von IPs im Gehirn führen. Dabei wurde die Existenz des IP vor allem mit neurodegenerativen Erkrankungen in Verbindung gebracht. Die genaue zelluläre Expression sowie mögliche Funktionen sind in diesem Zusammenhang jedoch noch weitestgehend unerforscht.

Anhand von immunohistologischen Verfahren und konfokaler Mikroskopie konnte die Expression der IP Untereinheiten LMP2 und LMP7 hauptsächlich in Iba1-positiven Mikroglia nach zerebraler Ischämie gezeigt werden. Des Weiteren konnte mit biochemischen Methoden ein anhaltender, massiver Anstieg LMP2- und LMP7-Proteingehalts in einer Zeitspanne von bis zu 4 Tagen nach Ischämie detektiert werden. Die Expression konstitutiver Proteasomuntereinheiten als auch ubiquitinierter Proteine scheinen dabei unverändert und implizieren eine spezialisierte Funktion des IPs neben dem physiologischen Proteinabbau in diesem Zusammenhang. Außerdem konnte mit Hilfe eines LMP7-defizienten Mausmodells im Vergleich zu Wildtyp-Kontrollen gezeigt werden, dass die Expression von LMP7 anscheinend neuroprotektive Eigenschaften besitzt und das Ausmaß der neuralen Gewebeschäden sowie der sensomotorischen Störungen nach zerebraler Ischämie limitiert. Darüber hinaus scheint LMP7 eine wichtige Rolle für die Aktivierung und morphologische Ausprägung der Mikroglia Zellen zu besitzen. Ein Mangel an LMP7 führt zwar zu einem Anstieg an Mikroglia innerhalb der Infarktregion, aber auch zu einer signifikanten Reduktion an peripheren infiltrierenden Immunzellen einschließlich Monozyten, Dendritische Zellen und Makrophagen. Auf Grund dessen und der vermehrten Detektion von Aktivitätsmarkern in LMP7-defizienten Mikroglia können ein vermindertes phagozytisches Leistungsvermögen sowie veränderte inflammatorische Prozesse nach Ischämie angenommen werden. Diese Hypothese spiegelt sich zudem in einer tendenziell veränderten Zytokininduktion in LMP7-defizienten Mikroglia wieder. Zusammenfassend zeigen diese Ergebnisse eine relevante Bedeutung des IPs für die zelluläre Funktionalität von Mikroglia Zellen im Allgemeinen und unter ischämischen Bedingungen im Besonderen sowie möglicherweise anderer neuraler Pathologien. Neben einem grundlegenden wissenschaftliches Ergenntnisgewinn hinsichtlich der Präsenz, Induktion und funktionellen Rolle von IPs im Säugetiergehirn, deuten diese Daten auch auf eine potentielle klinische Relevanz hin. Die gezielte

therapeutische Aktivierung und/oder Inhibition des IP in bestimmten Bereichen des geschädigten und/oder bedrohten Hirngewebes nach zerebraler Ischämie könnte zu einer vorteilhaften Modulation der Mikrogliaaktivität genutzt werden und den Verlauf von zerebralen Pathophysiologien im Zusammenhang mit neuroinflammatorischen und neurodegenerativen Prozessen positiv beeinflussen.

Abstract

This dissertation comprises a localization analysis as well as a functional characterization of the hitherto barely assessed, specific immunoproteasome (IP) subunits LMP2 and LMP7 in the mouse brain.

The IP is a specialized proteasome subtype, which is constitutively expressed in immune cells and plays an important role for the MHCI antigen processing due to its proteolytic activities. Interestingly, IP formation can be induced by pro-inflammatory cytokines also in non-immune tissue including the brain. Notably, the presence of IPs is mainly associated with neurodegenerative diseases or pathologies, even though the functional repertoire of IP subunits in this context remains largely unidentified.

Using immunohistological methods and confocal microscopy, Iba1-positive microglia cells were determined as the predominant cell type expressing the IP subunits LMP2 and LMP7 under normal and ischemic conditions in the mouse brain. Further, a massive increase in gene expression of LMP2 and LMP7 over a period of 4 days after ischemia was confirmed by biochemical approaches. Interestingly, protein levels of the constitutive standard proteasome subunits and levels of ubiquitinated proteins were not altered and imply a specialized function of the IP beside the physiological proteolysis within this context. Moreover, LMP7 seems to exert a neuroprotective effect during cerebral ischemia. Notably, in an LMP7-deficient mouse model, the extent of neural damage and sensorimotor deficits was increased compared to wild type littermates after cerebral ischemia. In addition, LMP7 seems to play an important role for the activation and morphological phenotype of microglia cells. Moreover, LMP7 deficiency leads to an increased numerical density of microglia within the infarct area, but more importantly to a significant reduction of infiltrating peripheral immune cells including monocytes, dendritic cells and macrophages. Furthermore, expression of microglial activation markers were enhanced, and cytokine induction seemed altered in LMP7-deficient mice. These results indicate a potentially reduced phagocytic capability as well as altered inflammatory processes after ischemia in these mice. In conclusion, these data point towards a functional relevance of microglial IP expression under ischemic conditions and potentially also under other neuropathological cicumstances. This work does not only contribute to a deeper understanding of the presence, induction and functional repertoire of IPs in the mammalian brain, but also provides evidence for a possible clinical and translational value of the obtained data in the context of neuroprotection. The specific clinical targeting of the IP activity and the subsequent modulation of microglia activity within certain vulnerable brain regions could introduce beneficial therapeutic strategies after cerebral ischemia and other brain injuries accompanied by neuroinflammatory and neurodegenerative processes.

1 Introduction

Current definitions of life itself contain as criteria the processes of metabolism and homeostasis, growth and reproduction as well as the ability to react and adapt to environmental stimuli [1], [2]. The smallest units of living organisms are cells, which exist in two types: eukaryotic and prokaryotic cells. Eukaryotes feature different cellular compartments, including the nucleus, which are absent in prokaryotes [3]. For cellular vitality, proteins are essential biochemical components to enable the afore mentioned capabilities. Their functions range from structural support and movement possibilities to signaling functions, catalysis of chemical reactions, transport and storage capacities as well as key roles for the immune system [4]–[6]. The maintenance and regulation of the cellular protein homeostasis generally depends on three principles: firstly, the continuous synthesis of proteins, secondly, protein modifications, which are able to control and regulate many cellular processes [7], [8], and thirdly, the degradation of proteins.

The major interest for this work concerns mainly the latter aspect of proteome homeostasis, i.e. the process of protein degradation. This primarily comprises the removal and clearance of damaged and non-functional proteins as well as proteins no longer needed within the cell. The coordinated balance of protein synthesis and degradation plays an important role in remodeling the cellular protein composition and, thereby, determines the cell's ability to adapt and react to its environment. Inhibition and suppression of each or both processes are extremely harmful and lead to massive cellular stress and consequently cell death. As for instance, proteasome inhibitors interfere and block the process of protein degradation and lead to cytotoxic consequences that are exploited in cancer therapy [9], [10]. Two intracellular ways exist for protein degradation. On the one hand, phagocytized protein aggregates and complete organelles can be cleaved by several proteases in lysosomes and on the other hand, the ubiquitin-proteasome system enables selective degradation of targeted cellular proteins [11], [12].

1.1 Proteasomal degradation

The majority of intracellular proteins is degraded by the ubiquitin-proteasome system (UPS) that enables a selective and highly efficient proteolysis of client proteins [13]. For this work, I will focus on the eukaryotic structures and processes only. Eukaryotic proteasomal degradation of regulatory and short-lived proteins occurs mainly in conjugation with the process of ubiquitination. However, proteasomal clearance of damaged or misfolded proteins by oxidation can be also achieved in an ubiquitin-independent way to prevent the formation of protein aggregates under cellular stress [14].

1.1.1 Molecular components

The proteolysis of proteins destined for degradation is performed by the proteasome, a multi-catalytic protein complex. Different proteasome subtypes and associations of the core complex exist with several regulatory particles (Fig. 1).
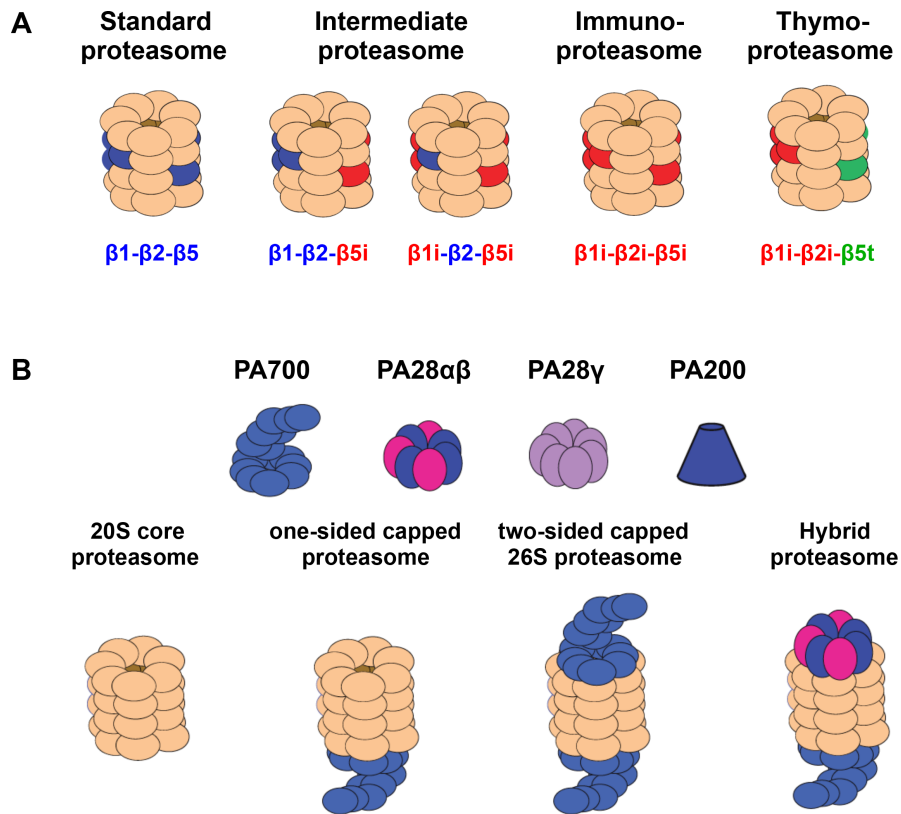
Figure 1: Proteasome subtypes and regulatory particles

The core complex of proteasomes is built by four stacked rings harboring the catalytically active β-subunits (A). The constitutive subunits β1, β2, and β5 are incorporated into standard proteasomes and can be replaced by the inducible subunits β1i, β2i and β5i to form IPs or intermediate proteasomes. An additional form of proteasomes exists in the thymus and is characterized by the subunit β5t instead of β5. The 20S core can be associated to one or two regulatory particles that can influence the proteolytic activity of the whole complex (B). Modified from Vigneron & Van den Eynde, 2014 [15]

Most abundant is the ubiquitous standard proteasome [15], [16]. Additional subtypes that can be found in vertebrates are the IP, the thymoproteasome and the testis-specific proteasome, whose subunit compositions slightly differ compared to the standard proteasome and will be mentioned below.

In general, the 20S core complex that is part of every proteasome subtype harbors four homologous and axial stacked rings consisting of two inner rings of seven alpha subunits α1-α7 and two outer rings of seven beta subunits β1-β7. The term 20S refers to its

sedimentation coefficient. The whole complex features an overall mass of ca. 700 kDa [17]–[19].

Within the core complex, only three subunits of each β-ring contain the catalytically active sites of the proteasome formation, responsible for the proteolysis. The standard 20S core harbors the β1, β2 and β5 subunit, which expose N-terminal threonine residues serving as nucleophiles for the peptide bond hydrolysis and have a caspase-like/peptidylglutamyl-peptide hydrolyzing- (PGPH), trypsin-like and chymotrypsin-like activity, respectively. In the so-called IP, which plays a major role in immune relevant tissues, these subunits are replaced by the β1i (LMP2), β2i (MECL1) and β5i (LMP7) subunits. The IP features an increased chymotrypsin-like activity due to the altered activity of LMP2, which results in reduced cleavage after acidic residues. The other two subunits, MECL-1 and LMP7, exhibit similar proteolytic activities like their standard counterparts [20]–[22].

The subunit β5t is part of a subtype referred to as the thymoproteasome. Likewise to the IP it contains the β1i and β2i subunits and substitutes β5 by β5t. This subtype is exclusively expressed in cortical thymic epithelial cells and is of major importance for the positive selection of CD8^{+} cells [23]–[25]. Tanaka proposed another putative proteasome subtype as the "mammalian testis-specific proteasome", which differs in the composition of the proteasomal α subunits and harbors the α8 subunit instead of the constitutive α4 and was first discovered in *Drosophila* flies and seems to be crucial for spermatogenesis [26]–[30].

The assembly of proteasomes is a very intricate and strictly controlled process in order to guarantee a proper formation and maturation of the whole complex [27]. Initially, the α-ring formation takes place and is coordinated by four proteasome assembling chaperones (PACs), which form the heterodimers PAC1-PAC2 and PAC3-PAC4. In the next step, the β-ring formation is promoted by attachment of the β subunits to the α-ring. After incorporation of all β subunits, the β5 pro-peptide as well as interactions among the N-terminal extensions of β6 and the C-terminals of β7 facilitate the dimerization of two half-proteasomes. For these steps in proteasome assembly, the molecular chaperone POMP (proteasome maturation protein) is essential [31]. After formation of the 20S core, successive cleavage of the N-terminal pro-peptides of the β-subunits is initiated and the PACs and POMP are degraded as a signal for successful proteasome maturation [13], [26], [31]–[33]. Notably, the incorporation of LMP2 is preferred over the β1 subunit in newly synthesized proteasome complexes. This in turn favors the incorporation of the MECL-1 subunit and subsequently the assembly with LMP7 compared to the constitutive β5 subunit [34]–[38]. Interestingly, the maturation rate of IPs is estimated to be four times faster than that of the standard proteasome [26].

Depending on the rate and specificity of proteolysis, the 20S core proteasome is present in cells without any associations or attached to either one or two regulatory particles forming a one- or two-sided capped proteasome. These regulators enable a specific recognition of ubiquitin-tagged client proteins and can modulate the proteolytic activity [13], [39]. Most thoroughly investigated is the 19S regulatory particle, also referred to as PA700, serving as an ATP-dependent proteasome activator (Fig. 1B). In complex with the 20S core proteasome, PA700 forms the standard 26S proteasome, whereas in literature often no differences are made between the final complex of one (26S) or two (30S) PA700 regulators in association with the 20S core [26], [40]. PA700 consists of at least ten different subunits that form a base sub complex (regulatory particle triple-ATPase subunits Rpt1-6 and non-ATPase subunits Rpn1, Rpn2, Rpn10, and Rpn13) and additional nine subunits that are components of the lid sub complex (Rpn3, Rpn5-9, Rpn11, Rpn12, Rpn15). In association with the 20S core, PA700 facilitates under ATP hydrolysis the recognition and binding of polyubiquitin-tagged proteins as well as the protein deubiquitination and unfolding, controlled opening of the α-ring structure, and translocation of the substrate to the β-ring compartment [12], [26], [41].

Other regulatory proteasome activators are the complexes of the PA28 family. From this family, the PA28α/β complex is probably the most interesting for this work as the expression of PA28α/β is associated with the expression and formation of IPs. Levels of PA28α/β are increased in the presence of interferon-γ (IFN-γ). Its structure is a hetero-heptameric ring, formed by either α4β3 or α3β4 subunits [42], [43]. PA28α/β in association with the 20S core of primarily the IP but also the standard proteasome subtype accelerates the proteolysis of polypeptides without an effect on large polyubiquitinated proteins and promotes an efficient generation of small peptides, which could function as antigens [44]. The function of the PA28γ complex is still under investigation, but there is evidence about a function in nuclear proteolysis [45], [46] and cell cycle control [47], [48]. In addition, Ustrell and colleagues discovered a further regulatory particle, called PA200 [49]. It is suggested to play a unique role during the maturation process of the proteasome and also in genomic stability due to its main cellular localization within the nucleus. Additional, PI31 was described as a inhibitory regulator of the proteasome, although the precise functional repertoire needs further characterization [50].

The assembly of the regulatory caps is very complex, too, and has not yet been fully elucidated [39]. For the formation process of the base exist two assumptions, a 20S core-independent and a 20S core-dependent assembly. However, both models and also the hypothetical formation of the lid sub complex are mediated in analogy to the core assembly by several chaperones that coordinate the pairing of the different subunits [51]–[53].

The expression pattern and tissue distribution vary among the different proteasome subtypes. As already mentioned, the thymoproteasome and the testis-specific proteasome are exclusively found in specific cells of the concerned organs. In contrast, the standard proteasome and also the IP can be found in all tissues [13]. Consequently, a constitutive expression of the standard proteasomal subunits is characteristic in nearly all cell types. In contrast, the basal expression of IP is limited to the spleen, hematopoietic cells and immune relevant tissue Upon stress situations with concomitant pro-inflammatory cytokine release such as IFN-γ or tumor necrosis factor (TNF-α), the expression of immunoproteasomal subunits is also induced in other cell types [26], [54]. Interestingly, the presence of IPs was detected also in immune-suppressed tissue like the eye and the brain, mainly in the context of viral infections or neurodegenerative disease [55]–[60].

In addition, the several proteasome subtypes can be distributed in different proportions within cells. Especially under pathological circumstances or after oxidative stress, the ratio of the expressed β subunits is shifted towards the inducible subunits of the IP accompanied by an increase in specific regulatory particles [61]–[63].

1.1.2 Ubiquitination

The targeting of the majority of proteins for degradation is realized by ubiquitination, a process that links ubiquitin molecules to a protein and thereby functions as a signal for proteasome-mediated degradation [11], [41].

Three types of enzymes mainly perform the process of ubiquitination (Fig. 2). First, ubiquitin is activated under ATP consumption by an ubiquitin-activating enzyme E1. Thereby, a thioester intermediate is formed between the cysteine residue of E1 and the C-terminal of the ubiquitin molecule. This enables the association with an ubiquitin-conjugating enzyme E2 once again by the formation of a thiol-intermediate of ubiquitin and E2. Finally, a substrate-specific ubiquitin ligase E3 promotes the formation of an isopeptide bond between the C-terminal carboxyl group of the ubiquitin molecule and the ε-amino group of a lysine on the client protein [13].
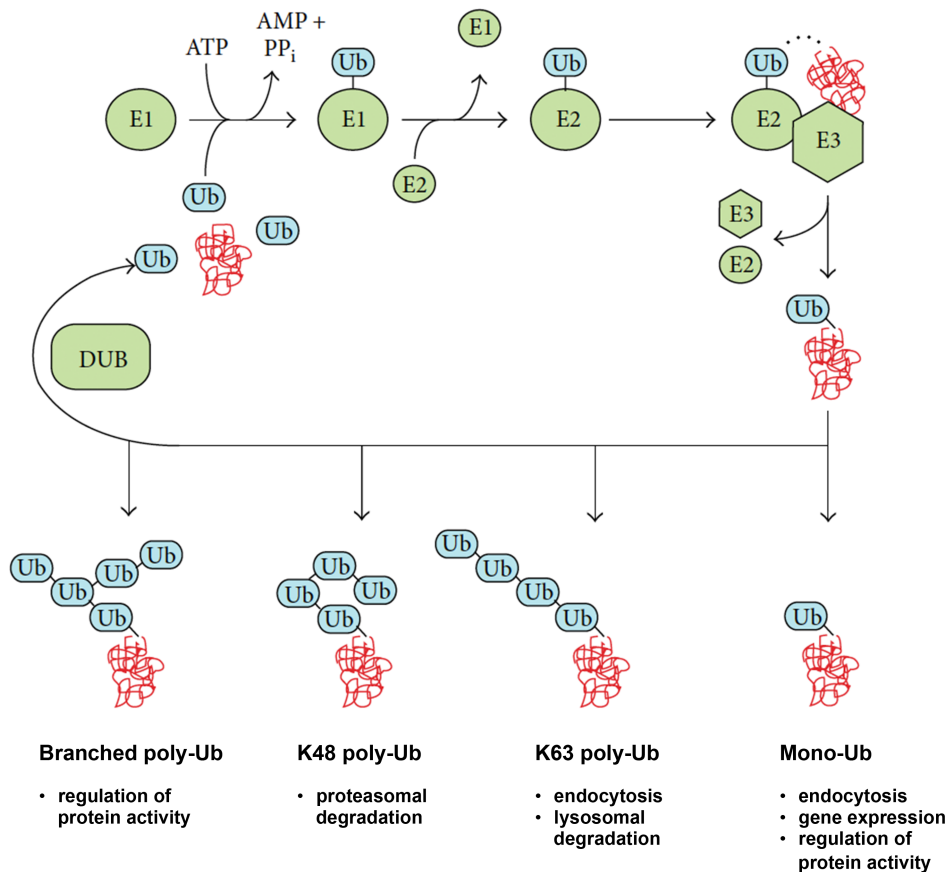
Figure 2: Process and consequences of ubiquitination

The attachment of ubiquitin to a client protein is achieved by three enzymes: ubiquitin-activating enzyme E1, ubiquitin-conjugating enzyme E2 and an ubiquitin ligase E3 under ATP hydrolysis. The pattern of ubiquitination determines the following cellular implications of the tagged protein.
Ub: Ubiquitin, DUB: deubiquitinating enzyme
Modified from Hamilton & Zito, 2013 [64]

The ubiquitin molecule itself features seven lysine residues that can be used for further ubiquitination. By this, different patterns of ubiquitination can be generated, including mono- and polyubiquitin chains, which in turn can be rearranged by deubiquitinating enzymes (DUB). Depending on the length and degree of branching of the ubiquitin chain as well as the site of the lysine linkage, this process can lead to different consequences including DNA repair, protein trafficking and signal transduction. For example, mono-ubiquitination serves among other function as a signal for endocytosis if attached to plasma membrane proteins or is an important regulator of gene expression if linked to the histones H2A, H2B or H1 [65]. Interestingly, poly-ubiquitin chains linked to lysine 63 (K63) of the initial ubiquitin can also serve as a signal for internalization of plasma membranes [66]. Furthermore, this ubiquitination pattern plays an important role within DNA repair pathways [67], [68]. The covalent attachment of multiple ubiquitin moieties building polyubiquitin chains that are linked to the lysine 48 (K48) of the initial ubiquitin target a protein for proteasomal degradation (Fig. 2). The result of the proteolysis are oligo-

peptides with a length of 2 to 35 amino acids and an average length about 8 to 12 amino acids [69], [70].

In addition, several ubiquitin-like modifications exist that diversely entail additional functions in protein stability by reinforcement, cross-regulation or counteraction to the ubiquitin pathway [71]. To name a few: SUMOylation plays a role during transcription, cell cycle progression, stress responses as well as apoptosis by attachment of SUMO (small ubiquitin-like modifier) proteins to the client proteins [72], [73]. NEDDylation attaches the ubiquitin-like protein NEDD8 (neural precursor cell expressed developmentally down-regulated protein 8) to substrates and is involved in cell cycle progression, DNA repair and critical for certain ubiquitin conjugations as it facilitates activation of specific E3 ubiquitin ligases [74], [75]. Another ubiquitin-like protein (UBL) called URM1 (ubiquitin-related modifier 1) is part of the URMylation process and has been implicated in tRNA processing and oxidative stress responses [76], [77]. UBLs and ubiquitin may be very different in their primary amino acid sequence, but possess a similar tertiary protein structure, which is referred to as the β-grasp fold [78]. The enzymatic pathways of UBL-conjugation and -deconjugation of client proteins are very similar to the corresponding process for ubiquitin as described above [79].

1.1.3 Functional repertoire of proteasomes

The variety of different proteasome subtypes and their possible associations with the diverse regulators implies a broad functional repertoire of these complexes besides the removal of damaged proteins. Indeed, the UPS plays an important role in many cellular processes and mechanisms including cell cycle control, regulation of gene expression and control of protein folding as well as during stress and immune responses [26]. This will be discussed in the following sections.

1.1.3.1 Degradation of damaged proteins

One major function of the proteasome is the intracellular clearance of damaged proteins that are constantly produced. This prevents an accumulation of these proteins and the formation of protein aggregates, which is essential in maintaining the protein homeostasis and in order to keep cellular viability [62]. Protein damage is a natural process due to aging or environmental circumstances and can be caused by several intrinsic and extrinsic aspects. Protein oxidation and shifts in the cellular redox state under both normal, but especially inflammatory or stress conditions, are suspected to be one of the most frequent modifications leading to a constant formation of damaged proteins [14]. As a factor of aerobic metabolism, free radicals are constantly produced and can be classified into reactive oxygen species (ROS) and reactive nitrogen species (RNS) [69]. For instance, remarkable amounts of the superoxide anion $O_2^{-\bullet}$ are released by

mitochondria. Other highly reactive oxidants are the hydroxyl radical ˙OH or the nitrogen oxide ˙NO and dioxide ˙NO$_2$, which can generate other reactive radicals in several chemical reactions [69]. However, they are also able to react and oxidize proteins, which can lead to changes in protein function and ultimately malfunction, a process that can be summarized as oxidative stress. Normally, this is compensated by the reaction with various anti-oxidant components and enzymes, but can cause especially under even short periods of elevated oxidative stress an accumulation of oxidatively modified proteins. Depending on the degree of oxidation, proteins transform from an only slightly reduced functional state with minimally exposed hydrophobic structures to fully exposed hydrophobic structures accompanied with a total loss of functionality [13], [80]. These hydrophobic structures tend to form aggregates with each other that can be further oxidized and subsequently reach a completely unfolded state with insoluble structures due to cross-linking. At this state, these super aggregates cannot be degraded by cellular proteases anymore and lead to massive cellular stress. Due to this an efficient clearance of this pool of oxidized proteins is of pivotal importance to efficiently avoid the formation of super aggregates to preserve a functional cellular protein pool [13], [69], [81], [82].

Interestingly, numerous studies could show different abilities of the various proteasome subtypes to regulate and compensate disturbances in the proteome by oxidation [14], [62], [63]. The 20S core proteasome is not able to degrade native, folded proteins, but was shown to exhibit a high degree of selectivity in an ATP-independent manner for oxidatively damaged proteins that lost their tertiary structure. The precise mechanism of recognition by the 20S core proteasome is not yet fully understood, but it has been suggested, that the α-ring structure is able to recognize and bind the exposed hydrophobic structures of unfolded and oxidized proteins [83]–[85]. Oxidized proteins that underwent solely moderate structural changes and are additionally ubiquitinated, can be also degraded by the standard 26S proteasome [14]. In addition, the IP, especially in complex with the PA28 regulator, exhibits a higher proteolytic susceptibility of oxidatively modified proteins. Thereby it can compensate an enhanced demand for proteasomal degradation after transient oxidative stress with subsequent protein aggregation more efficient than the standard proteasome [63], [86], [87].

Oxidative stress can be also caused by extrinsic factors including exposure to oxidants in the environment such as ozone and other toxic chemicals or UV radiation as well as by tissue damage and injuries. One of the most severe cases of oxidative stress is induced by an ischemic event such as stroke [88]. Due to the disturbances in oxygen supply during ischemia, the mitochondrial respiratory chain is impaired and large amounts of superoxide are released. In addition, the influence of NF-κB signaling on iNOS induction leads to the massive production of nitrogen oxide ˙NO. Superoxide O$_2$˙$^-$ and ˙NO radicals react to the

highly oxidative peroxynitrite ONOO$^-$ that is capable to significantly damaged surrounding cells and tissue [13], [89].

In this context, proteasome activity is tremendously necessary to efficiently remove protein debris in order to prevent cell death by apoptosis, which is even more important in post-mitotic cells such as neurons. At the same time, proteasomes play a damage-promoting role after ischemia due to the UPS-mediated degradation of signaling molecules, which initiates inflammatory responses [90], [91].

Next to stress-induced protein oxidation, additional protein modifications including glycation and methylation as well as deamidation severely affect cellular function; notably these also often occur during aging [92].

1.1.3.2 Clearance of short-lived and regulatory proteins

In addition, there are several other crucial functions of the proteasome, which have a strong influence on various metabolic processes like the participation in controlled protein folding as well as the clearance of short-lived regulatory proteins that are no longer needed in the cell.

The UPS is involved in the "quality control" of newly synthesized proteins and is responsible for the degradation of misfolded translational products. During the generation of newly synthesized proteins, a considerable fraction of defective ribosomal products (DRiPs) is produced due to missense or nonsense mutations or translational errors. For instance, about 30-80 % of the newly synthesized protein pool meant to enter the ER lumen undergoes incorrect folding [13]. As this concerns in large parts a variety of transmembrane proteins, a rapid degradation of these DRiPs is required in order to preserve functional integrity of cells and additionally to recycle the amino acids used [93]–[96]. The importance of this UPS-mediated quality control of protein folding could be emphasized by studies demonstrating a link of exceeding proteolytic susceptibility and the induction of apoptosis, also known as the "unfolded protein response" [97]–[99]. Especially after short periods of cellular stress, the specific 26S proteasome-mediated degradation prevents an increase in DRiP and abnormal protein levels [100]. These transient accumulations of protein debris can also induce the expression of IPs, which have a supportive function in restoration of the cellular protein homeostasis [63].

The UPS has also a major role in cell cycle control and development. The temporally coordinated cleavage and, therefore, inactivation of proteins that regulate the cell cycle such as cyclins, cyclin-dependent kinases (CDKs), and also CDK inhibitors allows tight control of a correct and successful cell cycle progression. Moreover, the precise elimination of transcription factors that operate as cue stimuli in particular stages during development depends on 26S proteasome-mediated degradation [101], [102].

Furthermore, the proteasomal degradation plays an important role for the regulation of gene expression. Proteolysis of inhibitory regulator proteins, signaling molecules, and transcription factors can either promote or terminate signal transduction and directly influence transcription [103], [104]. This task is mainly accomplished by the standard proteasome in complex with the PA700 regulator in an ATP-dependent manner, which enables a rapid adaption to environmental changes due to the highly specific degradation of natively folded and completely functional proteins that are tagged with polyubiquitin chains [69].

1.1.3.3 MHCI-associated antigen processing

Another important function of proteasomes is their participation in antigen processing. Some peptides, which are generated by proteasomal degradation will be not further degraded by other proteases into single amino acids, but indeed function as antigens and, thus, are presented on the cell surface together with molecules of the major histocompatibility complex class I (MHCI) [13]. As mentioned above, a considerable pool of proteins (30-80 %) emerge as DRiPs. Benefiting, the UPS-mediated proteolysis of DRiPs enables a constant delivery of cellular antigenic peptides to the cell surface. During this process, the antigens are first transported into the ER lumen via the TAP (transporter associated with antigen processing) transporter and are then attached to MHCI molecules by the action of several different chaperones [105]. After passing the Golgi apparatus, these antigenic oligo-peptides are presented on the cell surface and enable surveillance by T lymphocytes [106]. This becomes in particular important during infections as the presentation of antigens from originated viral proteins induces proliferation of cytotoxic CD8^{+} T-cells and apoptosis initiation of the infected cells [107]. IPs have been shown to play an outstanding and important role for the adaptive immune system [108]–[111].

The genes for LMP2 and LMP7 are placed in the MHC II region and located very close to the antigen peptide transporters genes TAP-1 and TAP-2. This and the observation that the expression of the immunoproteasomal subunits is upregulated by IFN-γ together with other genes associated with antigenic peptide generation as well as MHCI and MHCII molecules implies a specialized role of this proteasome subtype in MHCI antigen processing and presentation during infections [112].

Due to the chymotryptic activity of LMP2 IP-mediated proteolysis results in the generation of an increased amount of peptides with a hydrophobic C-terminus compared to the standard proteasome. These hydrophobic peptides are optimal to function as MHCI ligands and exhibit a high affinity to the groove of MHCI complexes [21], [113]. In consequence, this extends the repertoire of intracellular MHCI-associated antigenic peptides presented on the cell surface and allows an improved verification by the immune system. In case of viral or microbial (mutant, infectious or tumoral) epitopes are

presented, the altered set of antigens produced by the IP has been demonstrated to lead to a more efficient recruitment and activation of specific CD8^{+} T cells [54], [114]–[117].

The importance of IP-generated peptide sets for an optimized MHCI antigen presentation is supported by several studies using knockout animals. In 1994, Fehling et al. and Van Kaer and colleagues could demonstrate an inefficient presentation of the endogenous HY antigen and of an epitope of an influenza nucleoprotein in LMP7- and LMP2-deficient mouse models, respectively [111], [118]. *In vitro* and *in vivo* experiments to measure antigen presentation of dendritic cells of a knockout mouse model for all three inducible β subunits revealed an impaired antigen presentation for several antigens including epitopes for the male antigens HY and $Uty_{246-254}$, an influenza peptide, the ovalbumin peptide SIINFEKL and epitopes of the lymphocytic choriomeningitis virus [110].

However, current investigations rather would suggest a generation of different peptide quantities, which will lead to different probabilities of the single peptides to become presented on the cell surface [119], [120].

In addition, it could be shown that several knockout mouse models exhibit reduced expression of MHCI molecules and have deficits in T cell recruitment and activation [108], [117], [121]–[124].

1.1.3.4 The Proteasome and its Influence on Synaptic plasticity

Interestingly, several studies could demonstrate an important contribution of the UPS in the brain for the process of learning and memory formation [125]–[127]. After synaptic stimulation, the cellular localization of proteasomes is shifted from dendritic shafts towards synaptic spines, suggesting an involvement of the UPS in the modulation of synaptic strength [128]. Thereby, proteasome-mediated degradation might be involved in several aspects of synaptic plasticity. In combination with a temporary and spatially regulated protein synthesis, proteasomes reshape the protein composition at the pre- and postsynapse and thereby regulate synaptic vesicle homeostasis [129], the amount of neurotransmission receptors [130]–[134], and the quantity of structural components of the postsynaptic density [135], [136]. Furthermore, the UPS-mediated degradation of transcription inhibitors like CREB repressors [137], [138] as well as the transient modulation of histone modifications [139]–[141] has been suggested to facilitate the expression of essential genes for efficient memory formation.

Participation of the UPS was additionally shown for the regulation of synaptogenesis and synapse elimination during synapse formation in development [142].

Within these cellular mechanisms underlying synaptic plasticity, the 26S standard proteasome seems to have the strongest impact due to the highly selective proteolysis of client proteins and its prominent presence in the CNS. Even though, low levels of basal IP expression could be detected in the brain [143], [144] a potential involvement of IPs in

processes like synaptic plasticity, learning and memory have been not yet under investigation.

1.2 Proteasomes in aging and disease

Proteasomal degradation contributes to the constant turnover and reconstruction of the cellular protein pool and thereby maintains protein homeostasis and cell viability. The process of aging is accompanied by substantial changes of cell functionality and a decline in any quick adaption to environmental stimuli [145]. Even though the underlying mechanism of aging is yet to be fully elucidated, a decrease in proteasomal activity has been implicated in this process [146]–[148]. Additionally, it has been suggested that mitochondria functionality diminishes during aging. This and the decrease in anti-oxidative capabilities lead to a chronic shift in the intracellular redox state and to an accumulation of free radicals and oxidants [13]. Consequently, amounts of oxidized proteins are increased and facilitate the formation and accumulation of protein aggregates. If the amount of damaged proteins due to oxidative modifications exceeds proteasomal susceptibility, very large protein aggregates are formed due to cross-linking between the hydrophobic structures. Moreover, these highly cross-linked structures have been shown to be able to inhibit proteasomal degradation beyond the baseline level of proteolysis [69], [149]. In addition, the functional decline in mitochondria could limit the availability of ATP for UPS activity [13], [150]. All these aspects point towards a correlation between efficient and functional proteasomal degradation, maintenance of protein homeostasis and cellular longevity.

In general, an impairment of the UPS and disturbances in protein degradation are assumed to have an extensive influence on pathogenesis. An involvement of the UPS has been suggested for numerous diseases including amyotrophic lateral sclerosis (ALS) [151]–[153], autoimmune disorders like cystic fibrosis [154]–[156], atherosclerosis [157], [158], rheumatism [159], [160], and viral infections [161], [162]. Further, an inappropriate proteolysis of insulin signaling components in combination with a chronic decline of the cellular anti-oxidative capacity promotes diabetes [163], [164]. Especially in post-mitotic cells like neurons, a compromised proteolytic susceptibility is detrimental for cell viability. A series of neurodegenerative diseases, including Alzheimer´s disease (AD), Huntington´s disease (HD) and Parkinson´s disease (PD), exhibit elevated levels of aggregated proteins [57].

A typical marker of AD is the formation of extracellular plaques by β-amyloid fragments of the amyloid precursor protein and an abnormal presence of hyperphosphorylated tau-filaments. Although, these proteins are polyubiquitinated, they are not degraded by proteasomes indicating a dysfunction of the UPS [13]. In the past it has been suggested that the β-amyloid protein acts like a proteasome inhibitor by occupying the proteolytic

chamber of the 20S core and that aggregates of β-amyloid are resistant to proteolysis because of their cross-linked peptides [165]. This theory was recently questioned by Orre and colleagues, who could demonstrate via a subunit-specific ELISA assay a rather increased proteasome activity in cell cultures of astrocytes, neurons and microglia after stimulation with oligomeric and fibrilliar amyloid-β_{1-42} [166]. Similarly in HD, the formation of polyubiquitinated protein aggregates, so-called inclusion bodies, is a characteristic observation. These accumulations are predominantly formed by the mutant huntingtin protein and are not degradable by proteasomes [167], [168]. It has been suggested that the interaction of the polyubiquitinated huntingtin with the PA700 regulator contributes to the decreased proteolytic activity in this disease [167]. Alike, PD is characterized by the formation of cellular Lewy bodies which are protein aggregates containing mainly polyubiquitinated α-synuclein and parkin [169], [170]. In addition, for all of these neurodegenerative diseases oxidative stress seems to be one of the main reasons for the development of the pathology. Whether these observations are caused by an impaired activity of the UPS or the proteasome-mediated degradation process is inhibited by the overproduction of abnormal proteins due to oxidation, needs further investigation [13], [171]. Interestingly, the presence of IPs in the brain was mainly associated to the mentioned neurodegenerative diseases. Based on this observation and the constitutive expression of IPs in immune-specific tissue as well as the upregulation under inflammatory conditions, a central role of this subtype in the development and progression of immune responses under pathological conditions can be hypthesized [112], [123]. On the one hand studies could demonstrate a regulatory function of IPs in proinflammatory cytokine production [172]. On the other hand, IPs could efficiently remove increased amounts of DRiPs and aggregates of damaged proteins produced by induction of the mTOR-signaling pathway in inflammation and viral infections [63].

Furthermore, mutations in the gene encoding the LMP7 subunit are linked to some rare disease like JMP (joint contracture, muscle atrophy, microcytic anemia and panniculitis-induced lipodystrophy), the Nakajo-Nishimura syndrome, the Japanese autoinflammatory syndrome lipodystrophy as well as CANDLE (chronic atypical neutrophil dermatosis with lipodystrophy) [61], [173]–[175].

Another case in which the UPS in general and the IP in particular seem to be a key player is the progression of cancer [176], [177]. Normally, a controlled proteasome-mediated degradation of oncogene products and tumor suppressors as well as distinct transcription factors supports the regulation of cell cycle progression, cell growth, and anti-apoptosis. However, an increased abundance and proteolytic activity of the UPS including the standard and IP subtype have been discovered in cancer cells leading to uncontrolled cell division and the promotion of cancer [178]. Tumorgenesis is directly promoted by UPS-

mediated degradation of the CDK inhibitor p21, p27 and the tumor suppressor p53. In addition, a prolonged activation of NF-κB signaling, mediated by increased degradation of NF-κB inhibitors, is found in cancer cells and sustains the expression of growth factors and apoptosis inhibitors [179]–[181]. Due to the accelerated metabolism and the higher demand of protein degradation in cancer cells, proteasome inhibition in these malignant cells is indeed a promising clinical target for therapeutic strategies. Inhibition of the UPS results in the rapid accumulation of damaged proteins and the upregulation of pro-apoptotic factors, which induces apoptosis [182]. An example for an inhibitor of the standard proteasome is Bortezomib, which is approved for multiple myeloma therapy. Excitingly, several studies suggest the IP as a promising clinical target for cancer therapy, in particular for hematopoietic malignancies [183]–[185]. Selective inhibition of the IP promises lower side effects and neurotoxicity in cancer therapy because of the cell type-specific upregulation of the IP in cancer cells and, thus, only low effects on healthy tissue with minimal IP expression [186].

1.3 Presence of IPs in the brain

As mentioned above, the induction and presence of IPs in the brain has been mainly associated to neurodegenerative disease such as AD, HD and PD or ALS, but also viral infections [58] and brain injury [187], [188] so far. Furthermore, it has been suggested that the IP plays a role in immunosenescence and accumulates also in the brain during aging due to increasing levels of chronic inflammation [61], [189]. In healthy brain tissue, IPs seem to be almost absent pointing towards a major role in neuropathology, even though their precise functional repertoire remains largely unknown in the CNS. Besides a neuroinflammatory milieu, which would explain the induction of IPs, these pathologies are characterized by elevated oxidative stress and consequently a proceeded formation and accumulation of toxic protein aggregates. It has been suggested that the proteolytic capacity of the standard proteasome is reduced in the mentioned disease, although recent findings of Orre et al. (2013) could demonstrate rather an increased activity of the standard proteasome in cell culture after β-amyloid stimulations. However, the increased induction of IPs in neurodegenerative diseases could most likely be a compensatory mechanism as consequence of the increased demand for a highly efficient removal of accumulating pathology-associated proteins [63], [190]–[192]. Thereby, the IP could possess an important participation in the brain immune response to stress or injury and in the brains reaction to a disturbed cellular protein homeostasis.

Apart from the research regarding IP function in the brain, the distinct cellular localization of the immunoproteasomal subunits as well as the observed tissue distribution varies between the studies in part considerably. For instance, increased levels of LMP2 and LMP7 on transcript level could be detected by Gavilán et al. in aged rat hippocampus

[189]. Mishto et al. observed an expression of LMP2 and LMP7 in neurons and astrocytes in samples of hippocampus and cerebellum from AD patients using immunohistochemical stainings [59]. More recently, immunohistochemical stainings of Orre et al. in an AD mouse model revealed on the contrary a separate expression of LMP2 in astrocytes and LMP7 in microglia indicated by the overlap of fluorescent signals for LMP2 together with GFAP as well as signal co-localization of LMP7 and Iba1 [166]. Studies of Díaz-Hernández et al. proposed an increased expression of LMP2 and to a similar extent of LMP7 in neurons in a mouse model for HD [55], [56]. An induction of all three inducible subunits (LMP2, MECL-1, LMP7) was further detected in astrocytes and microglia of the spinal cord of an ALS mouse model [193]. In 2015, Chen et al. analyzed the induction and cellular localization of LMP2 and LMP7 in rats after transient cerebral ischemia. Both subunits were upregulated after the ischemic event. Whereas LMP2 was mainly detected in GFAP-positive astrocytes, the authors observed an expression for LMP7 mainly in OX42-positive microglia/macrophages, which would confirm the studies of Orre et al. [166], [187]. In contrast, a previous study analyzing induction and localization of LMP2 and LMP7 after transient ischemia in C57BL/6 mice has seen the two immunoproteasomal subunits only in NeuN-positive neurons [194]. Moreover, an expression of LMP2 and MECL-1 in Iba1-positve cells was observed in lymphocytic choriomeningitis virus-infected mice. Additional, an accumulation of these subunits was also suggested in nuclei of astrocytes but could be not observed in neurons or oligodendrocytes [58].

In summary, the listed studies provide inconsistent results regarding the expression of immunoproteasomal subunits in the brain, which presumably depends on the selected experimental design and pathological conditions. The cellular expression of IPs seems to be most likely in microglia concerning these cells as the resident immune cells of the brain and the constitutive expression of IPs in peripheral immune-relevant tissue. This theory is supported by recent *in vitro* experiments demonstrating an increased formation of IPs in rat primary microglia cultures after IFN-γ stimulation [195]. Under pathological conditions, microglia cells become rapidly activated due to the release of pro-inflammatory cytokines and differentiate into certain phenotypes with specialized functional properties [196]. In addition, microglia are concerned as the main antigen-presenting cells within the brain and mediate important processes including cytokine production and recruitment of peripheral myeloid cells. Neurons express, however, if at all, only minimal levels of MHCI molecules [197]. With regard to the function of IPs in antigen presentation, an expression of this proteasome subtype in neurons would be actually more unexpected, but needs further investigation.

Apart from the potential function of IPs in the context of neuropathology, the question arises, whether the higher proteolytic capacity of the IP could be also required for normal brain function in addition to the constitutive standard proteasome under non-pathological conditions. So far, the functional relevance of low levels of IP expression in the healthy brain and in this context whether, and especially how the IP might be involved for normal brain function, including synaptic plasticity and processes of learning and memory formation, has not been under investigation.

1.4 Objectives

Several studies could show the presence of IPs in the brain, but the results concerning the precise cellular localization as well as the functional repertoire of immunoproteasomal subunits remain contradictory and incomplete. Therefore, this work aims to (i) analyze the expression of the immunoproteasomal subunits LMP2 and LMP7 in neural cell types under physiological and pathological conditions, (ii) to investigate the regulation of LMP2 and LMP7 during neuroinflammation as well as (iii) the influence of an impaired IP formation on the neural damage caused by an ischemic event and (iv) to examine the effect of LMP7 expression on microglia morphology and function.

In order to perform reliable experiments, it was essential to ensure the successful establishment of certain tools and methods. This concerned mainly the evaluation of the selected LMP7 knockout (LMP7$^{-/-}$) mouse strain in comparison to control mice of the C57BL/6 strain and the characterization of generated antibodies raised against LMP2 and LMP7. Furthermore, existing protocols for the preparation of primary neuronal cell cultures of WT and LMP7$^{-/-}$ and a FISH assay were optimized. In addition, the fractionation protocol for the preparation of synaptic junctions was modified for optimization. A model of focal cerebral ischemia was chosen as a stress model to induce IP expression in the mouse brain. This enables a reliable and controllable analysis under oxidative stress and inflammatory conditions including a locally restricted release of cytokines.

Moreover, a characterization and analysis of the induction and regulation of IPs in cerebral ischemia as performed in this thesis, is essential in order to evaluate the immunoproteasomal subunits as potential clinical targets for therapies directly linked to stroke, but potentially also for other neurodegenerative disease.

2 Material and Methods

Sections 2.3.1, 2.4.9 and 2.5.4 have been modified from my master thesis "Functional Characterization of the IP Subunit LMP7 in the Mammalian Brain" (Säring, 2013).

2.1 Chemicals

All used chemicals were molecular-biology grade and purchased from Biorad laboratories, Invitrogen, Merck, Roth, and Sigma Aldrich. For buffers double distilled water (ddH$_2$O) of a Milli-Q System (Millipore) and for protein biochemical experiments molecular biology-grade water from Roth was used. Specialized chemicals and solutions are mentioned before each corresponding method section.

2.1.1 Primary Antibodies (AB)

Antibody	Species, Clonality	Application	Supplier
anti- α6	rb, polyclonal	WB, diluted 1:750	Thermo Scientific (PA5-22288)
anti-actin	ms, monoclonal	WB, diluted 1:2500	Cell Signaling (#3700)
anti-actin	rb, monoclonal	WB, diluted 1:2500	Cell Signaling (#8457)
anti-β1	rb, monoclonal	WB, diluted 1:500	Cell Signaling (#13267)
Anti-β5	rb, monoclonal	WB, diluted 1:750	Cell Signaling (#12919)
anti-CREB	rb, monoclonal	WB, diluted 1:1500	Cell Signaling (#9197)
anti-FK2	ms, monoclonal	WB, diluted 1:1000	Enzo lifescience (PW8810)
anti-GFAP	chk, polyclonal	IF, diluted 1:1000	abcam (ab4674)
anti-GluR1	rb, polyclonal	WB, diluted 1:1000	Cell Signaling (#13185)
anti-GluR2	ms, monoclonal	WB, diluted 1:250	Neuromab (75-002)
anti-Iba1	gt, polyclonal	IF, diluted 1:1000 WB, diluted 1:500	abcam (5076)
anti-LMP2 #1*	rb, polyclonal	not further used after AB characterization	Pineda Antikörper Service
anti-LMP2 #1*	gp, polyclonal	not further used after AB characterization	Pineda Antikörper Service
anti-LMP2 #2*	rb, polyclonal	not further used after AB characterization	Pineda Antikörper Service
anti-LMP2 #2*	gp, polyclonal	IF, diluted 1:10 000	Pineda Antikörper Service
anti-LMP2 #3*	gp, polyclonal	WB, diluted 1:2500	Pineda Antikörper Service
anti-LMP2 #4*	rb, polyclonal	WB, diluted 1:2500 IF, diluted 1:10 000	Pineda Antikörper Service
anti-LMP7 #1*	rb, polyclonal	not further used after AB characterization	Pineda Antikörper Service
anti-LMP7 #1*	gp, polyclonal	not further used after AB characterization	Pineda Antikörper Service
anti-LMP7 #2*	rb, polyclonal	IF, diluted 1:10 000	Pineda Antikörper Service

anti-LMP7 #2*	gp, polyclonal	WB, diluted 1:2500 IF, diluted 1:10 000	Pineda Antikörper Service
anti-LMP7 #3*	rb, polyclonal	WB, diluted 1:2500	Pineda Antikörper Service
anti-LMP7 #3*	gp, polyclonal	not further used after AB characterization	Pineda Antikörper Service
anti-Map2	ms, monoclonal	ICC, diluted 1:1000	Sigma-Aldrich (M4403)
anti-Map2 (2a+2b)	ms, monoclonal	IHC, diluted 1:500	Sigma-Aldrich (M1406)
anti-NeuN	ms, monoclonal	IF, diluted 1:1000 WB, diluted 1:500	Millipore (MAB377)
anti-NR1	rb, monoclonal	WB, diluted 1:500	Cell Signaling (#5704)
anti-NR2A	rb, polyclonal	WB, diluted 1:500	Alomone Labs (AGC-002)
anti-NR2B	ms, monoclonal	WB, diluted 1:500	Neuromab (75-101)
anti-pCREB	rb, monoclonal	WB, diluted 1:1500	Cell Signaling (#9198)
anti-PSD95	ms, monoclonal	WB, diluted 1:1000	Neuromab (75-028)
anti-Shank2	gp, polyclonal	WB, diluted 1:1000	SySy (162204)
anti-Synaptophysin	gp, polyclonal	WB, diluted 1:1000	SySy (101004)

Table 1 Primary antibodies (* indicates antibodies kindly provided by Prof. Dr. Ulrike Seifert).

2.1.2 Secondary Antibodies

Antibody	Application	Company
anti-mouse IgG, HRP-conjugated	WB, diluted 1:7500	Dianova (115-035-146)
anti-rabbit IgG, HRP-conjugated	WB, diluted 1:7500	Dianova (711-035-152)
anti-chicken IgG, HRP-conjugated	WB, diluted 1:7500	Dianova (103-035-155)
anti-guinea pig IgG, HRP-conjugated	WB, diluted 1:7500	Dianova (706-035-148)
anti-goat IgG, HRP-conjugated	WB, diluted 1:7500	Dianova (705-035-147)
anti-rabbit IgG, biotin-conjugated	IF, diluted 1:500	Dianova (711-065-152)
Streptavidin, Alexa^{TM}Fluor488-conjugated	IF, diluted 1:2000	Invitrogen (S11223)
Streptavidin, Alexa^{TM}Fluor555-conjugated	IF, diluted 1:2000	Invitrogen (S21381)
anti-mouse F(ab`)$_2$ fragment, Alexa^{TM}Fluor546-conjugated	IF, diluted 1:1000	Invitrogen (A-11018)
anti-mouse IgG, Cy^{TM}3-conjugated	IF, diluted 1:2000	Dianova (715-165-150)
anti-mouse IgG, Alexa^{TM}Fluor488-conjugated	IF, diluted 1:2000	Invitrogen (A21202)
anti-goat IgG, Cy^{TM}3-conjugated	IF, diluted 1:1000	Dianova (705-165-003)
anti-goat IgG, Cy^{TM}5-conjugated	IF, diluted 1:1000	Dianova (705-175-147)
anti-chicken IgG, Alexa^{TM}Fluor647-conjugated	IF, diluted 1:1000	Dianova (703-606-155)
anti-rabbit, Alexa^{TM}Fluor488-conjugated	IF, diluted 1:2000	Invitrogen (A21206)

anti-rabbit IgG, Cy™3-conjugated	IF, diluted 1:2000	Dianova (711-165-152)

Table 2 Secondary antibodies.

2.2 Animals

In this work C57BL/6J wild type (WT) and C57BL/6J LMP7 knockout (LMP7$^{-/-}$) mice, originally generated and described by Fehling et al. (1994) [109], were used. For homozygote breeding WT and LMP7$^{-/-}$ mice were obtained from Charles River (Sulzfeld, Germany). In addition, a heterozygote breeding-scheme was applied using LMP7$^{+/-}$ mice in order to produce littermates of both genotypes.

Mice were kept under controlled conditions concerning temperature and humidity (18-23° C, 40-60% humidity) at the animal facilities of the Otto-von-Guericke-University in Magdeburg. They were housed on a 12-h day/night cycle with food and water *ad libitum*.

All animal experiments were performed in compliance with international guidelines regarding the care and use of animals for experimental procedures (2010/63/EU) and with confirmed ethical approval (Landesverwaltungsamt Sachsen-Anhalt, IPT/G/04-1227/13, University Magdeburg).

2.3 Animal experiments

The following experiments were partially conducted and performed in collaboration with the research groups of Prof. Dr. Markus Fendt, Prof. Dr. Frank Angenstein, and Prof. Dr. Ildiko Dunay. Within these collaborations, I was able to compare general behavior in WT and LMP7$^{-/-}$ mice, the temporal development of the infarction using MRI scans, and the cell composition and activation using flow cytometric analysis (FACS), respectively.

2.3.1 Mouse model of focal cerebral ischemia

Permanent middle cerebral artery occlusion (MCAO) was performed as described previously [198], [199]. For these experiments, we used gender-matched 11 to 14-weeks old C57BL/6J WT and LMP7$^{-/-}$ mice, which were littermates. Mice were anesthetized by intraperitoneal injection of 2,2,2-tribromethanol (supplier, 343 mg/kg in 0.9 % NaCl). During the surgical procedure the body temperature was controlled rectally and maintained at 37 °C with a heating pad. After removing skin and muscles, a hole was drilled into the skull between orbit and ear on the fronto-temporal region to expose the middle cerebral artery (MCA). Subsequently, the MCA stem was permanently closed by electrocoagulation using bipolar forceps. After occlusion, the lesion was cleaned with 0.9 % NaCl, disinfected with 70 % ethanol, and closed with fibrin glue (supplier). After MCAO, mice were kept in individual cages at an ambient temperature of 30 °C for 2h. Body temperature and physical status were constantly checked. Sham operation was performed as described above omitting the occlusion step of the MCA.

2.3.2 Adhesive tape removal test

Adhesive tape, (ALBUPLAST, obtained from pharmacy), trimmed to 1x2 mm pieces

To assess potential long-term sensorimotor deficits after MCAO, WT and LMP7$^{-/-}$ mice were subjected to an adhesive tape removal test after Bouet et al. [200].

Briefly, mice were trained for 3 days before MCAO and then tested 1 d after MCAO as follows: First, mice were raised and fixed by holding the neck. Small adhesive tapes of 1 x 2 mm were rapidly stuck to both fore paws with alternating placement order. Following this, the mouse was placed in a transparent testing box and time was measured until the mouse recognized and removed the tape on each side. Recognition behavior was defined by the following reactions: shaking taped paw or directly bring the paw to the mouth. Removal time was taken when the tape was completely removed from the paw. Only mice that performed the task within 2 min were taken into account.

2.3.3 Behavioral tests

In collaboration with the research group of Prof. Dr. Markus Fendt, basic assessment of mouse behavior including locomotor activity and anxiety were performed with WT, LMP7$^{+/-}$ and LMP7$^{-/-}$ littermates.

In the open field paradigm [201], mice were placed in boxes of 45 cm x 45 cm x 30 cm and their movements were recorded over 10 min by a frame with infrared light sensors (14 mm distance between two sensors, sample rate 100 Hz; TSE Systems). Data were analyzed with the tracking software (EthoVision XT 11, Noldus) in order to obtain the parameter "distance travelled" and "time spent in the center" of the open field. The light-dark boxes (49.5 cm x 49.5 cm x 41.5 cm) feature a bright (135-310 lux) and a dark (0.2-1.5 lux) area of the same size, which are separated by a divider with a 6 x 8 cm opening. Mice were placed into the center of the dark area and movements were measured for 5 min using infrared sensors (TSE Systems). In addition, the carnivore odor-induced fear behavior [202] was analyzed in a Makrolon type 3 cage (37.5 cm x 21.5 cm x 15.0 cm, self construction) equipped with a fixed glass vial in one corner. Mice were expose to either Trimethylthiazoline (TMT), a component of fox urine or water as a control. The locomotor activity was recorded with a camera (TVCC50011, Abus) and analysis of behavioral data was performed with EthoVision XL software.

2.3.4 MRI measurements

For comparison of the temporal progression of the infarction, two couples of WT and LMP7$^{-/-}$ littermates were subjected to MCAO as described above. After 1, 6 and 14 days of MCAO, MRI measurements were performed in collaboration with Prof. Dr. Frank Angenstein and Karla Krautwald at the Leibniz Institute for Neurobiology Magdeburg (LIN). For this, mice were anesthetized with 1.5% isoflurane (in 50:50 N2:O2, v/v) and

fixed using a head holder with a bite bar to reduce movement artifacts. MRI was performed on a Bruker Biospec 47/20 scanner (Bruker Biospin GmbH, Ettlingen, Germany) at 4.7 T equipped with a BGA 12 (200 mT/m) gradient system as previously described in Angenstein et al. [203]. A 25-mm Litzcage small animal imaging system (DotyScientific Inc., Colombus, SC) was used for radiofrequency excitation and signal reception. Twenty one coronal T_2-weighted spin echo images were obtained using a rapid acquisition relaxation enhanced (RARE) sequence [204] with the following parameters: repetition time (TR) = 4000ms, echo time (TE) = 15ms, slice thickness = 800 µm, field of view (FOV) = 25.6x25.6 mm, matrix = 256 x 256 (i.e., in plane resolution: 100x100µm), RARE factor 8, number of averages = 6. The total scanning time was 12 min 48 s. Paravision4.0 (Bruker Biospin MRI GmbH) was used to convert the obtained raw data to images that were then further processed using the public domain Java-based image processing and analysis program ImageJ software (https://imagej.nih.gov/ij/).

2.3.5 FACS
10x PBS: 1.37 M NaCl, 27 mM KCl, 43 mM Na_2HPO_4, 14 mM KH_2PO_4, pH 7.4

In collaboration with Prof. Dr. Ildiko Dunay, Dr. Luisa Möhle, and Henning Düsedau a series of FACS experiments with samples from WT and LMP7$^{-/-}$ mice after 1 day of MCAO was performed according to established methods with minor modifications [205], [206]. Briefly, animals were subjected to MCAO as described above and intracardially perfused with 1x PBS 1 day post MCAO. Brains were collected and separated into infarct region, remaining damaged hemisphere, and intact hemisphere. The samples were homogenized in a buffer containing 1M HEPES (pH 7.3, Thermo Fisher) and 45 % glucose before sieving through a 70 µm cell strainer (Fisher Scientific). The resulting cell mixture was fractioned on a 30-70 % Percoll gradient (GE Healthcare), and obtained cells were washed in PBS and incubated with ZOMBIE NIR™ fixable dye (Biolegend) for live/dead discrimination. To prevent unspecific binding of antibodies, anti-Fc γ III/II receptor antibody (clone 93) was applied to the cells before staining with fluochrome-conjugated antibodies. The following antibodies against cell surface markers were applied in FACS buffer: CD45 (30-F11), CD11b (M1/70), Ly6C (HK1.4), MHCII I-A/I-E (M5/114.15.2), CD11c (N418), F4/80 (BM8) (all from eBioscience), and Ly6G (1A8) (Biolegend). Fluorescence Minus One (FMO) controls were used to determine the level of auto fluorescence.

2.4 Molecular and biochemical approaches

2.4.1 Genotyping
2.4.1.1 DNA extraction from mouse tail cuts and polymerase chain reaction (PCR)
TC buffer: 100 mM NaCl, 10 mM Tris-HCl, pH=8.0

Protein kinase K solution: 10mg/ml in 40 % glycerol, 1 mM Calciumacetate,10 mM Tris-HCl, pH=7.5

DreamTaq Green PCR Master Mix (2x) (Thermo Scientific)

For mouse genotyping, tail biopsies (2-3 mm length) of the pups were lysed overnight at 55 °C under constant shaking with 900 rpm (Thermomixer *comfort*, Eppendorf) in 500 µl TC buffer containing 20 µl protein kinase K solution. The next day, protein kinase K was inactivated by a heating step of 95 °C for 10 min and shaking at 300 rpm. Afterwards, samples were centrifuged for 6 min at 4 °C with 21 000 x g and either stored temporarily at -20 °C or directly subjected to the PCR assay.

The PCR reaction mix contained 10 µl of the DreamTaq Green master mix, 0.5 µl of each primer (0.25 µM), 7 µl nuclease free water and 2 µl template. Primers for detection of the WT gene were *LMP7wt-fw* (5' GGA CCA GGA CTT TAC TAC GTA GAT G 3') and *LMP7wt-rev* (5' CTT GTA CAG CAG GTC ACT GAC ATC G 3'). Primer *LMP7wt-rev* and *Neo-fw_LMP7-KO* (5' CCG ACG GCG AGG ATC TCG TCG TGA 3') were used for amplification of the LMP7$^{-/-}$ gene.

The PCR reaction started with a single denaturation step (2 min, 94 °C), followed by 35 cycles of denaturation (30 s, 94 °C), annealing (45 s, 58 °C), and elongation (50 s, 72 °C), and a final elongation step (10 min, 72 °C) using a TProfessional thermocycler (Biometra).

2.4.1.2 Agarose gel electrophoresis

Agarose (Biozym Scientific GmbH)

1x TAE buffer: 40 mM Tris-acetate, 1 mM EDTA

Midori Green Advanced (Biozym Scientific GmbH)

100 bp DNA ladder (New England BioLabs)

Amplified DNA fragments were separated at 70 V in a Compact M electrophoresis system (Biometra) using 1.5 % agarose gels containing 0.006 % Midori Green and 1x TAE running buffer. DNA bands were visualized with UV-light (Vilber Lourmat E-Box-VX2-20MX).

2.4.2 qRT-PCR for cytokine measurements

Semi-quantitative real-time PCR was performed to measure cytokine gene expression levels in the brain [207] in collaboration Prof. Dr. Ildiko Dunay and Henning Düsedau.

Briefly, RNA was isolated from the infarct region, the remaining damaged hemisphere, and the intact hemisphere after 1 day of MCAO using the TRIzolTM reagent (Invitrogen) according to the manufacturer's instructions. Following the isolation, RT-PCR was performed using a LightCycler® 480 Instrument II (Roche). Reverse transcription was run for 15 min at 48 °C followed by 10 min at 95 °C. Afterwards, 45 amplification cycles were

performed, including denaturation at 95 °C for 15 s and annealing as well as elongation at 60 °C for 1 min. Relative expression was calculated by normalization to the expression of the housekeeping gene hypoxanthine phosphoribosyltransferase. Obtained results were further normalized to mean values of WT mice and data are shown as mean (± SEM).

2.4.3 Generation of LMP2- and LMP7-fusion protein

E.coli (*Escherichia coli*) BL-21: *E.coli*B F- dcm ompT hsdS(rB-mB-) galλ(DE3) [pLysS Camr]

SOC-media: 5 g/l yeast extract, 20 g/l Bacto-Trypton, 10 mM NaCl, 2.6 mM KCl, 10 mM Mg2So4, 10 mM MgCl2, 20 mM glucose

LB-agar: 15 g agar per 1 l

LB-media: 5 g/l yeast extract, 10 g/l Bacto-Trypton, 5 g/l NaCl

10x PBS: 1.37 M NaCl, 27 mM KCl, 43 mM Na_2HPO_4, 14 mM KH_2PO_4, pH 7.4

50x PI: one tablet complete[TM] protease inhibitor cocktail (Roche) freshly dissolved in 1 ml ddH_2O

Amylose resin (New England BioLabs® Inc.)

2.4.3.1 Transformation of *E. coli* bacteria

The generation of fusion proteins was performed with two constructs, pMal-LMP2 (clone #12) and pMal-LMP7 (clone #24), generated by Dr. Peter Landgraf and Vinita Jagannath. The plasmid-DNA was diluted 1:100 and transformed into chemical competent *E.coli* BL-21 for the expression of the fusion proteins. For this, bacteria and 10 µl of the plasmid solution were incubated for 5 min on ice. After this, the mixture was heated for 45 s at 42 °C and incubated in SOC-media for 1 h at 37 °C with 500 rpm agitation on a thermo cycler (Eppendorf). Bacteria were plated onto LB-agar plates containing 100 µg/ml ampicillin and incubated overnight at 37 °C.

2.4.3.2 Overexpression of the pMal-LMP2 and –LMP7 fusion proteins

Bacterial colonies were picked from the LB agar plates and grown in 100 ml LB-media supplemented with 100 µg/ml ampicillin overnight at 37 °C under permanent agitation (Certomat® IS, Satorius). On the next day, the bacterial cultures were transferred into 1 l LB-media supplemented with 100 µg/ml ampicillin and grown for 1 h at 37 °C under constant agitation. Protein expression was induced by 5 ml 0.1 M IPTG solution and further incubation for 4 h at 37 °C under permanent agitation. Subsequently, bacteria suspensions were centrifuged for 7 min at 4 °C with 5000 x g (Beckman Coulter Avanti® J-E centrifuge, rotor type: J-14). The supernatant was discarded and the remaining pellets resuspended in 25 ml 1x PBS, pH 7.4 and frozen overnight at -80 °C.

2.4.3.3 Extraction and purification of the fusion proteins

For cell lysis and protein extraction, bacteria were slowly thawed at 4 °C under agitation, disrupted with 25 KPSI in a Cell Disrupter System TS 0.75 kW (Constant Systems Ltd.) at

4 °C; respective homogenates were collected on ice and supplemented with 1x PI. Cell debris were sedimented by centrifugation for 20 min at 4 °C with 12.000 x g (Beckman Coulter Optima XPN-80 ultracentrifuge, rotor type: SW 32Ti) and the supernatant containing the protein extract was used for purification of the LMP2- or LMP7-MBP fusion protein. For this, 2 ml of amylose resin were equilibrated twice with 10 ml 1x PBS, pH 7.4 for 5 min at 4 °C under rotation and centrifuged for 5 min at 4 °C with 600 x g. The amylose resin was mixed with the protein extract and incubated for 1 h at 4 °C while spinning in a rotation wheel and subsequently centrifuged as described above. The supernatant was kept at -20 °C, and the amylose resin with bound fusion protein washed three times with 10 ml 1x PBS for 10 min at 4 °C in the spinning wheel. Elution of fusion proteins from the amylose resin was performed with 600 µl 20 mM maltose elution buffer for 10 min at 4 °C under agitation and centrifugation as described above. The supernatant was supplemented with 1x PI and stored at -20 °C until desalting (section 2.4.4). The whole procedure was verified by sample collection of the homogenate, supernatant before and after binding the amylose resin, the resin and the eluate, and following sample solubilization (section 2.4.7), SDS-PAGE (section 2.4.9) and Coomassie staining (section 2.4.10).

2.4.4 Desalting of fusion proteins

Zeba^{TM} spin Desalting Columns 5 ml (Thermo Scientific)

10x PBS: 1.37 M NaCl, 27 mM KCl, 43 mM Na_2HPO_4, 14 mM KH_2PO_4, pH 7.4

50x PI: one complete^{TM} protease inhibitor cocktail tablet (Roche) freshly dissolved in 1 ml ddH_2O

Fusion proteins were desalted using commercially available columns with a high performance size-exclusion resin (Thermo Scientific) for buffer exchange.

First, Zeba^{TM} spin Desalting Columns were equilibrated three times with 2.5 ml 1x PBS and centrifuged for 2 min at 4 °C with 1000 x g. Columns were placed in a new collection tube and fusion proteins were loaded onto columns and centrifuged as described above. MBP-LMP2 and MBP- LMP7 fusion protein solutions were supplemented with 1x and 2x PI, respectively.

Finally, the protein concentration was adjusted to approximately 0.5 µl/µg for both fusion proteins using an Amidoblack assay (section 2.15).

2.4.5 Preparation of subcellular fractions for WB analysis

Hom buffer: 0.32 M sucrose, 5 mM HEPES, 1x PI, pH 7.4

Buffer B: 0.32 M sucrose, 5 mM Tris-HCl, 1x PI, pH 8.1

Buffer C: 0.32 M sucrose, 12 mM Tris-HCl, 1 % Triton X-100, pH 8.1

10x PBS: 1.37 M NaCl, 27 mM KCl, 43 mM Na_2HPO_4, 14 mM KH_2PO_4, pH 7.4

For preparation of synaptic junctions (SJ) [208], 12 to 15-weeks old male WT and LMP7$^{-/-}$ mice were used. For each sample, tissues from two mice of the same age and genotype were combined. All centrifugation steps were performed at 4 °C and samples were kept on ice to avoid degradation processes. Ultracentrifugation (> 12 000 x g) was performed with the Optima XPN-80 Ultracentrifuge from Beckman Coulter (rotor: SW 32 Ti). Mice were anesthetized with isoflurane, decapitated, and brains were rapidly dissected. The cerebellum was removed and the remaining brain tissue was homogenized with 12 strokes at 900 rpm in Hom buffer (10 ml/g brain tissue) using the Potter S from Sartorius. The homogenate (Hom) was centrifuged for 10 min at 4 °C with 100 x g (eppendorf centrifuge 5810R) and the supernatant (S1) was collected. The pellet (P1) containing nuclei and cell debris was discarded. S1 was centrifuged again for 20 min at 4 °C with 12000 x g. The resulting supernatant (S2) was discarded, whereas the pellet (P2) was re-homogenized in 1 mM Tris (1.5 ml/g brain tissue) with 10 strokes at 900 rpm using the Potter S. This fraction was hypo-osmotically shocked by adding 5 volumes of 1 mM Tris-HCl pH 8.1 and stirring for 30 min in an ice bath, followed by centrifugation for 1h at 4 °C with 100 000 x g. The supernatant was discarded and the pellet (P3) was resuspended in buffer B (1.5 ml/g brain tissue) with 6 strokes at 900 rpm using the Potter S. Subsequent, P3 was loaded on a 1.0 and 1.2 M sucrose step gradient and centrifuged for 1.5 h at 4 °C with 90 000 x g. The pre-fraction of synaptic junctions was collected at the 1.0 and 1.2 M sucrose interphase and centrifuged for 1 h at 4 °C with 100 000 x g. The remaining pellet was resuspended in ice-cold PBS (approx. 10 ml/g brain tissue) with 5 strokes at 900 rpm and centrifuged again for 30 min at 4 °C with 100 000 x g. The resulting pellet, defined as the SJ fraction was solved in 300 µl PBS using a glass homogenizer by hand. In addition, samples from the Hom and the S2 fraction were collected, solubilized (section 2.4.7) and stored at -20 °C.

2.4.6 Preparation of S2 fractions for WB analysis

10x PBS: 1.37 M NaCl, 27 mM KCl, 43 mM Na_2HPO_4, 14 mM KH_2PO_4, pH 7.4

50x PI: one complete^{TM} protease inhibitor cocktail tablet (Roche) freshly dissolved in 1 ml ddH_2O

The expression patterns of selected proteins over a period of 4 days post-MCAO were analyzed with homogenate and S2 fractions from WT and LMP7 mice.

Littermates were subjected to MCAO at the same day and sacrificed every 24 h up to 4 days. All following steps were performed on ice to avoid protein degradation. The brains were removed, the cerebella were detached and both hemispheres were separated in damaged and intact hemisphere and collected in 1 ml 1x PBS containing 1x PI each.

Afterwards, the brain tissue was homogenized using a Potter S (Sartorius) with 15 strokes at 1200 rpm. Homogenates were supplemented with 0.1 µl/ml benzonase and 150 µl

samples were collected and solubilized as described in section 2.14. The remaining homogenate was centrifuged for 10 min at 4 °C with 1000 x g. The pellet was discarded and the resulting supernatant S1 was centrifuged for 15 min at 4 °C with 12.000 x g. In this way, the supernatant S2, which contains mainly soluble cytosolic proteins was obtained. After solubilization (see 2.4.7), samples were stored at -20 °C.

2.4.7 Protein solubilization

4x SDS sample buffer: 1 % (v/v) SDS, 40 % (v/v) glycerol, 20 % (v/v) β-Mercaptoethanol, 250 mM Tris pH 6.8, 0.004 % (v/v) Bromophenol blue

1x SDS sample buffer: 0.25 % (v/v) SDS, 10 % (v/v) glycerol, 5 % (v/v) β-Mercaptoethanol, 62.5 mM Tris pH 6.8, 0.001 % (v/v) Bromophenol blue

4x SDS buffer was mixed with sample fractions at a ratio of 1:3. Afterwards, samples were boiled for 5 min at 95 °C and finally centrifuged for 3 min at 21 000 x g. Except for SJ fractions, samples were diluted with 100-200 µl 1x SDS buffer.

2.4.8 Amidoblack assay

U-form 96-well plates (eppendorf)

Amidoblack solution: 1.44 % (w/v) Amidoblack in methanol-acetic acid solution

Methanol/acetic acid solution: 90 % (v/v) methanol, 10 % (v/v) acetic acid

0.1 M NaOH

For measuring total protein concentrations, samples were briefly vortexed and centrifuged for 5 min with 21 000 x g at 4 °C. Standards of the calibration curve were prepared in triplicate from a BSA stock solution (0.5 mg/ml) with BSA concentrations ranging from 0 over 0.02, 0.04, 0.08, 0.12 and 0.16 up to 0.2 µg/µl. Samples were diluted with ddH$_2$O in the ratio 1:20 or 1:50 (triple determination). Standards and samples were incubated for 10 min at RT with 200 µl amidoblack solution per well and afterwards centrifuged for 10 min with 3220 x g (eppendorf centrifuge 5810R). Supernatants were carefully discarded and pellets were washed twice with 300 µl methanol/acetic acid mixture per well by centrifugation for 10 min at 3220 x g. The resulting supernatants were discarded; the pellets were dried for 30 min at RT and dissolved in 300 µl 0.1 M NaOH per well for at least 30 min at RT under constant agitation. The extinction was measured at 620 nm and used for calculation of the total protein concentration according to the Lambert-Beer law.

2.4.9 SDS-PAGE and Western Blot

Separating homogeneous gel buffer: 1.5 M Tris pH 8.8, 0.4 % (v/v) SDS

Separating gradient gel buffer: 1.8 M Tris pH 8.8

Stacking homogeneous gel buffer: 0.5 M Tris pH 6.8, 0.4 % (v/v) SDS

Stacking gradient gel buffer: 0.5 M Tris pH 6.8

PageRuler Prestained Protein Ladder (Thermo Scientific)

Electrophoresis buffer: 25 mM Tris pH 8.3, 192 mM glycine, 0.1 % (v/v) SDS

Western Blot transfer buffer: 25 mM Tris, 192 mM glycine, 0.02 % (v/v) SDS

Odyssey® Nitrocellulose membrane, 0.22 µm, LI-COR Biosciences

Ponceau solution: siehe vorherige Kommentare

TBS: 20 mM Tris, 0.8 % (w/v) NaCl

TBS-T: 20 mM Tris, 0.8 % (w/v) NaCl, 0.1 % (v/v) Tween-20

5 % (w/v) dried milk powder in TBS-T

This method was performed according Towbin et al. [209]. Prior SDS-PAGE, an Amidoblack assay (section 2.4.8) was performed to ensure equal protein concentrations for each sample. For SDS-PAGE homogeneous 9.5 % and 15 % as well as 5-20 % gradient polyacrylamide gels were used. The preparation of 12 SDS-polyacrylamide gels was based on a reagents mixture according to Tab. 3. SDS-PAGE was performed as described by Laemmli [210] with a constant current of 10 mA per gel. Afterwards, gels were blotted onto nitrocellulose membranes (Odyssey® Nitrocellulose membrane, 0.22 µm, LI-COR Biosciences) for 1.5 h at 200 mA. Subsequently, the nitrocellulose membranes were stained for 10 min with Ponceau solution for protein visualization and -fixation and afterwards washed in ddH$_2$O. Blocking of membranes was performed with 5 % milk in TBS for 1 h at RT under gentle agitation to avoid subsequent unspecific AB binding. Primary ABs were incubated overnight at 4 °C under gentle agitation. On the next day, membranes were washed twice for 10 min in TBS and TBS-T and incubated with a species corresponding secondary HRP-conjugated AB (1:7500 in 5 % milk in TBS-T) for 2 h at RT under gentle agitation, followed by the same washing procedure. Immunoblotting was visualized via ECL detection system (Pierce) in an Odyssey Fc (Model: 2800 from LI-COR® Biosciences GmbH). Exposure times were set to 2 or 10 min.

Chemicals	Stacking gel		Separating gel			
	homo-genous	gradient	9.5 %	15 %	5 %	20 %
Separating homogeneous gel buffer (ml)	-	-	15	24	-	-
Separating gradient gel buffer (ml)	-	-	-	-	6.84	6.84
Stacking homogeneous gel buffer (ml)	7	-	-	-	-	-
Stacking gradient gel buffer (ml)	-	9	-	-	-	-
87 % glycerol (ml)	6.4	8.28	4.5	7.2	1.8	7.2
30 % acrylamide (ml)	4.6	5.76	19	48	-	-
40 % acrylamide (ml)	-	-	-	-	4.1	16.2
ddH$_2$O (ml)	9.8	11.88	21	15.84	18.9	1.4
10 % SDS (µl)	-	360	-	-	316.8	316.8
0.2 M EDTA (µl)	-	360	-	-	316.8	316.8
10 % APS (µl)	160	222.3	400	640	115.2	72
TEMED (µl)	40	27.3	40	64	21.6	21.6
0.5 % Bromphenolblau (µl)	-	-	25	40	-	48
Bromphenolred (µl)	25	175	-	-	-	-

Table 3 Composition of SDS-polyacrylamide gels.

2.4.10 Coomassie staining

Coomassie staining solution: 50 % (v/v) methanol, 10 % (v/v) acetic acid, 0.05 % (w/v) Coomassie Brilliant Blue R250

Destaining solution: 5 % (v/v) methanol, 7 % (v/v) acetic acid

Gel drying solution: 50 % (v/v) methanol, 5 % (v/v) glycerol

Gels were placed into Coomassie staining solution and heated for ca. 1 min using a microwave. After cooling, the solution was replaced by destaining solution and gels were heated once again and incubated for several hours at RT under gentle agitation. When bands were clearly visible and background signal was washed out, gels were put into gel drying solution and mounted between two sheets of cellophane (Roth) for long-term preservation.

2.5 Cell biological methods

2.5.1 Cell culture

2.5.1.1 Preparation of primary cortical cell cultures

10x PBS: 1.37 M NaCl, 27 mM KCl, 43 mM Na$_2$HPO$_4$, 14 mM KH$_2$PO$_4$, pH 7.4

Poly-L-Lysin: 50 µg/ml in 1x PBS

10x trypsin: 2.5 % (w/v) trypsin, 7 mM EDTA in Hank´s balanced salt solution (HBSS, Invitrogen), HEPES buffered

trypsin inhibitor: 0.052 % (v/v) trypsin inhibitor, 0.024 % (w/v) DNase I, 0.3 % (w/v) BSA in HBSS, HEPES buffered

DMEM+: DMEM (Gibco), 10 % (v/v) fetal calf serum, 2 mM glutamine (Invitrogen)

NB+: Neurobasal (Gibco), 1x B-27 (life technologies), 0.8 mM glutamine

Preparation of primary cortical neuron-glia co-cultures was performed according to Goslin et al. [211] and recently published in Müller et al., 2015. Briefly, pregnant homozygous WT and LMP7$^{-/-}$ mice were deeply anaesthetized with Isofluran Baxter (Baxter Deutschland GmbH), decapitated, and embryos (E18) were rapidly removed and placed on ice. The brains were dissected, meninges removed, and the cortices underwent enzymatic digestion for 15 min at 37 °C using 1x trypsin. The supernatant was removed and trypsin inhibitor was supplemented for 5 min at RT. Afterwards, cells were washed with HBSS, centrifuged for 3 min at RT with 2000 x g and gently dissociated with cannulas (Sterican® G21 and G25, from B. Braun). Cells were suspended in DMEM+, seeded onto Poly-L-lysine coated coverslips in 24-well plates with a density of 40.000-50.000 cells/well and incubated in a humidified atmosphere at 37°C and 5% CO_2. After 24 h, the medium was replaced with NB+ and subsequently fed once a week with the same medium.

2.5.1.2 Interferon-γ stimulation

PB buffer: 0.1 % (w/v) BSA in 10 mM phosphate buffer, pH 8.0
NB+: Neurobasal (Gibco), 1x B-27 (life technologies), 0.8 mM glutamine
IFN-γ stock: 0.1 mg/ml murine interferon-γ (Peprotech) in PB buffer

After 14 days in vitro (DIV 14) primary cortical cells were stimulated with IFN-γ for 24 h with a final concentration of 10 and 20 ng/ml to mimic an inflammatory milieu. The IFN-γ stock solution was diluted in pre-warmed NB+ medium. For control samples the same volume of PB buffer was diluted in NB+ medium.

2.5.2 Fluorescence *in situ* hybridization in primary cortical cell cultures

PLP-fixative: periodate-lysine-paraformaldehyde fixative after McLean and Nakane (1974) [212]: Freshly prepared: mix 0.084 g sodium metaperiodate resolved in 30 ml Lysine buffer (0.1 M lysine-HCl, 0.05 M dibasic sodium phosphate, pH 7.4) and 0.54 g glucose resolved in 10 ml 16 % PFA

10x PBS (Ambion)

RNAse-free water (Gibco)

ViewRNA™ ISH Cell Assay Kit (Thermo Scientific)

Localization analysis of LMP2 and LMP7 mRNAs was performed under RNAse-free conditions using the commercial QuantiGene ViewRNA™ ISH Cell assay Kit from Affymetrix (Thermo Scientific) with some modifications.
Firstly, cultured cells were rinsed in pre-warmed 1x PBS containing 1 mM $MgCl_2$ and 0.1 mM $CaCl_2$ and fixed with PLP fixative for 30 min at RT. Subsequently, cells were washed three times with 1x PBS for 5 min. Coverslips with fixed cells were transferred into a wet

chamber and rinsed once again with 1x PBS. Next, cells were permeabilized with the detergent solution of the ViewRNA^{TM} ISH cell assay kit for 3 min at RT and three times washed with 1x PBS for 1 min each. The probes were diluted 1:50 in pre-warmed probe set diluent QF of the kit and applied to the cells for 3 h at 40 °C in a hybridization oven (Boekel Scientific, Model 241000) for specific target hybridization. This was followed by three short washing steps with the provided wash buffer, incubation with PreAmp mixture (1:25 diluted in pre-warmed Amplifier Diluent QF) for 1 h at 40 °C, and three washing steps as described above. Next, cells were incubated with Amp mixture (1:25 diluted in pre-warmed Amplifier Diluent QF) and Label Probe mixture (1:25 diluted in pre-warmed Label Probe Diluent QF) in each case for 1 h at 40 °C, followed by three washing steps using the wash buffer. After another three washing steps with 1x PBS, cells were stored overnight at 4 °C. On the next day, an immunocytochemical staining was performed as described from the blocking step onwards in section 2.8. Visualization of probes was achieved with an Axio observer.Z1 microscope with an LSM 710 confocal unit (Carl-Zeiss$^{®}$ Jena) and image acquisition was performed using a 63x oil objective and the ZEN black software (Carl-Zeiss$^{®}$ Jena).

2.5.3 Immunocytochemistry

PLP-fixative: periodate-lysine-paraformaldehyde fixative after McLean and Nakane (1974) [212] (see preparation under section 2.5.2)

10x PBS: 1.37 M NaCl, 27 mM KCl, 43 mM Na_2HPO_4, 14 mM KH_2PO_4, pH 7.4

Blocking buffer (B-Block): 10 % (v/v) horse serum, 5 % (w/v) saccharose, 2 % (w/v) bovine albumin, 0.2 % (v/v) Triton^{TM} X-100 in 1x PBS, pH 7.4

Mowiol: 10 % (w/v) Mowiol, 25 % (v/v) glycerol, 2.5 % (w/v) DABCO in 100 mM Tris-HCl, pH 8.5

Cultured cells were rinsed in 1x PBS supplemented with 1 mM $MgCl_2$ and 0.1 mM $CaCl_2$ and fixed with PLP fixative for 30 min at RT. Afterwards, cells were washed three times with 1x PBS for 10 min and incubated with B-Block for 1 h at RT. Fixed and permeabilised cells were incubated with primary antibodies overnight at 4 °C, washed three times with 0.2 % Triton^{TM} X-100 in 1x PBS for 10 min each, and afterwards incubated with secondary fluorescent antibodies for 1.5 h at RT followed by three washing steps as described above. Nuclear counterstaining was achieved with DAPI incubation (1:5000 in 1x PBS) for 10 min and three additional washing steps with 1x PBS for 5 min. Finally, coverslips were briefly rinsed in ddH$_2$O and mounted in Mowiol.

Immunofluorescent samples were analyzed using an Axio observer.Z1 microscope with an LSM 710 confocal unit and the ZEN black software (all from Carl-Zeiss$^{®}$ Jena).

2.5.4 Immunohistochemistry

For immunohistochemical stainings, mice were sacrificed either 1 or 2 days after MCAO or sham operation.

2.5.4.1 Cresylviolet staining

Cresylviolet solution: 0.5 % (w/v) cresylviolet, 60 mM sodium acetate, 0.34 M acetic acid

Quantification and visualization of the infarct size was realized by Cresylviolet staining of coronal cryosections [213]. In brief, WT and LMP7$^{-/-}$ mice were anesthetized with isoflurane and killed after 1 or 2 d of MCAO or sham surgery. Brains were removed, rapidly frozen in 2-Methylbutan at -35 to -40 °C, and stored at -70 °C. Coronal brain sections of 20 µm thickness were cut on a cryostat (CM3050 from Leica), placed on object slides (HistoBond® from Marienfeld-Superior), dried for 30 min at RT, and stored at -20 °C. Before Cresylviolet staining, sections were dried again for 30 min at RT and slides were sorted into glass cuvettes. Cuvettes were dipped into Cresylviolet solution for 45 min, ddH2O for 1 min, dehydrated in increasing concentrations of isopropanol (70, 80, 90, 100 %) for 1 min each, and twice in Roti®-Histol for 3 min. Afterwards, slides were embedded in DPX Mountant for histology purposes.

The stained slices were scanned with a flat bed scanner (EPSON Perfection V750 Pro) for subsequent image analysis with AdobePhotoshop software. To do so, the infarct volume was measured by selection and calculation of the single infarct area of every brain section via selection tools of AdobePhotoshop software. In addition, the total brain volume was measured. The infarct volumes of LMP7$^{-/-}$ animals were normalized to their WT littermates and expressed as fold increase.

2.5.4.2 Free floating immunofluorescence staining

PLP-fixative: periodate-lysine-paraformaldehyde fixative after McLean and Nakane (1974) [212] (see preparation under section 2.5.2)

TPBS: 0.12 % (w/v) Tris, 0.9 % (w/v) NaCl, 0.025 % (w/v) NaH$_2$PO$_4$*H$_2$O

TPBS-T: 0.12 % (w/v) Tris, 0.9 % (w/v) NaCl, 0.025 % (w/v) NaH$_2$PO$_4$*H$_2$O, 0.3 % (v/v) Triton^{TM} X-100

Avidin-biotin complex (ABC) solution, Vectastain ABC Kit from Vector Laboratories (0.5 % solution A, 0.5 % solution B in TPBS-T)

Biotin-tyramin (BT) solution: 0.15 % (w/v) biotin-tyramin, 0.03 % (v/v) of 30 % H$_2$O$_2$ in TPBS-T

For immunohistochemical stainings, floating coronal cryosections were used from WT as well as LMP7$^{-/-}$ mice 2 d after MCAO.

Mice were anesthetized with 4 % chloral hydrate, fixated on Styrofoam, and the thorax was rapidly opened. Mice were transcardially perfused with 20 ml 0.9 % NaCl and 60 ml PLP fixative. Subsequently, the brain was removed and post-fixed in the same fixative

overnight at RT under gentle shaking. For cryoprotection, brains were incubated in 30 % sucrose for 48 h at 4 °C. Coronal brain sections of 40 µm thickness were prepared on a cryostat (CM3050 from Leica) and stored in TPBS with 0.01 % sodium azide at 4 °C.

On the first day of the immunohistochemical staining procedure, sections were washed three times for 5 min in TPBS. For permeabilization the samples were incubated for 30 min in TPBS/ethanol mixture (1:1) and sections were washed three times for 5 min in TPBS. Afterwards, the samples were blocked in TPBS-T with 3 % horse serum for 1 h and incubated with the first primary antibody (diluted in TPBS-T with 1 % horse serum) overnight at 4 °C in the dark. On the second day, samples were washed four times for 5 min in TPBS-T, incubated for 2 h with a to the host species of the primary AB corresponding, biotin-conjugated IgG (1:500 in TPBS-T with 1 % horse serum) and washed again for three times for 5 min in TPBS-T under gentle shaking.

Subsequently, the samples were incubated for 1 h with ABC solution, freshly prepared 30 min before use, washed three times for 5 min in TPBS-T, and incubated for 20 min with BT solution. After another three washing steps for 5 min in TPBS-T, samples were incubated overnight at 4 °C in the dark with Alexa^{TM} Fluor 488-conjugated streptavidin (1:5000 in TPBS-T containing 1 % horse serum) and with a second primary AB. At the last day of the staining procedure, samples were washed four times for 5 min each in TPBS-T and incubated with the host species corresponding secondary AB (all 1:1000 in TPBS-T with 1 % horse serum) for 4 h at 4 °C in the dark. For counterstaining of nuclei, sections were washed three times for 5 min in TPBS, incubated for 20 min with DAPI (1:5000 in TPBS), and washed again three times for 5 min in TPBS. Sections were mounted on gelatine-coated slides (SuperFrost Weiss, 26 x 76 mm from Roth) and dried for 30 min at 37 °C in the dark. Afterwards, they were rinsed for 2 min in 70, 80, 90, and 100 % isopropanol, consecutively and twice for 5 min in Roti$^®$-Histol. Slides were dried and mounted with Neomount (Millipore) on coverglass (24 x 50 mm from Menzel-Gläser).

Confocal images were acquired with an Axio observer.Z1 microscope with an LSM 710 confocal unit and the ZEN black edition software (all from Carl-Zeiss$^®$ Jena).

2.5.5 Skeleton analysis

The Skeleton analysis was performed as described by Morrison and Filosa [214] with minor modifications. Two days post MCAO striatal (Bregma 1 to 0.8 mm), medial (Bregma -0.2 to -0.4 mm), and hippocampal (Bregma -1.6 to -1.8 mm) coronal brain sections of WT and LMP7$^{-/-}$ littermates were immunohistochemically stained as described above. For quantification of microglia number (defined by Iba1$^+$ cells) and several morphological parameters including the average branch length, branch number, endpoints, and junctions per microglia cell 7.5 µm thick z-stacks at 1.5 µm intervals of 5 different regions were acquired with a 10x objective and an Axio observer.Z1 microscope equipped with an LSM

710 confocal unit (both Carl-Zeiss® Jena). The stacks were merged to maximum intensity projections and the number of microglia cells per frame, defined by a co-localization of DAPI and Iba1 signals, was counted using Adobe Photoshop CS5 software. Then, the Iba1$^+$ channel was separated and images were processed using the *Despeckle* ImageJ plugin as a noise filter for elimination of single-pixel background fluorescence. In the next step, conversion to a binary and subsequent skeletonized image was performed using FIJI software (version 1.49, NIH). The resulting images were analyzed with the ImageJ plugin *AnalyzeSkeleton* to gain the average process length, the sum of branches, endpoints and junctions. Considered were only measurements with at least one junction. Data were normalized to microglia numbers per frame and expressed as mean ± SEM for all analyzed regions.

2.6 Statistics

All statistical analyses were performed with GraphPad Prism 6 software.

Differences between the weight of WT and LMP7$^{-/-}$ mice and in the expression of LMP2 or LMP7 between the damaged versus the intact hemisphere were statistically evaluated using a two-way ANOVA test. This was complemented with a Sidak´s multiple comparison test for the detection of statistical significance in the LMP2 expression pattern of WT and LMP7-/- mice after MCAO. An one-way ANOVA with Sidak´s multiple comparison testing was chosen for the comparison of the protein expression patterns of different subcellular fractions from WT and LMP7$^{-/-}$ mice. For detection of statistical significances in the infarct size after MCAO, a one-way ANOVA with Dunnett´s multiple testing was used. Further, a Students t-test for each region in the Skeleton analysis as well as multiple t-tests in association with the adhesive tape removal test were used for statistical evaluation.

For statistical analysis of the FACS experiments, a two-way ANOVA with a subsequent Fisher´s LSD test was performed. Differences in the levels of cytokine gene expression between groups were analyzed by one-way ANOVA with subsequent post-hoc Tukey's test. Statistical significance was defined as $p < 0.05$.

3 Results

3.1 Validation of applied tools

For these studies, homozygous LMP7-deficient knockout (LMP7$^{-/-}$) mice were used in order to analyze the potential functional role of IPs and the influence of an impaired IP formation in the mouse brain under physiological conditions as well as in the context of cerebral ischemia. As these LMP7$^{-/-}$ mice have not been thoroughly characterized with respect to their behavioral phenotype so far, I conducted a general characterization of these mice before performing actual experiments addressing the functional characterization of the IP with the help of this mouse model.

Furthermore, antibodies raised against the immunoproteasomal subunits LMP2 and LMP7 were generated by the company Pineda Antikörper Service to enable a specific tool for protein detection and characterization. Before the application of the immune sera in experiments aimed at the elucidation of the temporal and cellular expression profiles of both immunoproteasomal subunits, I performed an antibody characterization to test their specificity.

3.1.1 Characterization of LMP7$^{-/-}$ mice

In 1994, Fehling and colleagues generated a mouse strain lacking the entire LMP7 protein in all cells by eliminating exons 1 to 5 of the gene using a deletion-type targeting vector [109]. These mice display a reduced MHCI expression accompanied by a restricted antigen presentation, but are indistinguishable from heterozygous or WT littermates regarding their general viability and fertility. Up until now, there are no published reports concerning the general behavioral phenotype of these mice. As I was planning to perform a small behavioral study in later experiments, a set of experiments was conducted to ensure comparability of the results and to test for effects resulting from phenotypic variations of the different genotypes. At first, this included monitoring of the general state and the weight of the mice. A behavioral characterization using basic standard behavioral tests in WT, LMP7$^{+/-}$ and LMP7$^{-/-}$ littermates were performed in cooperation with the research group of Prof. Dr. M. Fendt.

The overall appearance and activity level of the genotypes appeared very similar including breeding and nest building. By superficial monitoring, there were no obvious differences in sniffing or grooming behavior between WT and LMP7$^{-/-}$ mice observed. The offspring numbers and frequency of litters were comparable with each other. As the body weight can provide some information on the general body condition, I measured the body weights of male and female mice from WT and LMP7$^{-/-}$ colonies over a time frame of 1-12 weeks (Fig. 3). Up to the 3rd week of age, both genotypes exhibit the same body weight gain. But with increasing age, the LMP7$^{-/-}$ mice feature a statistically significant weight reduction

compared to the WT. However, their general health state remains without any noticeable differences.
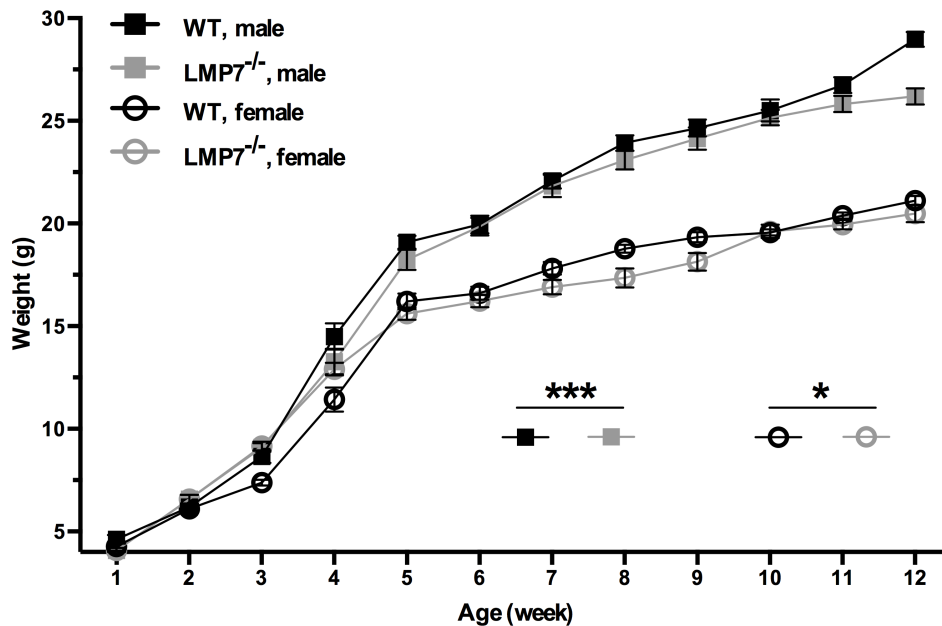
Figure 3: Body weight chart of WT and LMP7$^{-/-}$ mice

The graph illustrates the body weights of WT and LMP7$^{-/-}$ mice of both sexes in a time frame of 1-12 weeks. Both genotypes gain weight in a similar manner, however LMP7$^{-/-}$ mice generally exhibit a reduced weight compared to the WT.
Presented data are mean ± SEM, n=15-20 animals per genotype, sex, and age; statistical analysis was done using two-way ANOVA, ***: p=0.0002, *: p=0.0287.

Further, adult WT, LMP7$^{+/-}$ and LMP7$^{-/-}$ mice, between 10-12 weeks old, performed very similar in the conducted behavioral tests (Fig. 4-6). In the open field test no differences between the genotypes and their performance were obvious as determined by the parameters of total distance the animals travelled (Fig. 4A), the time they remained stationary (Fig. 4B), and the time they spend in the center of the box (Fig. 4C).
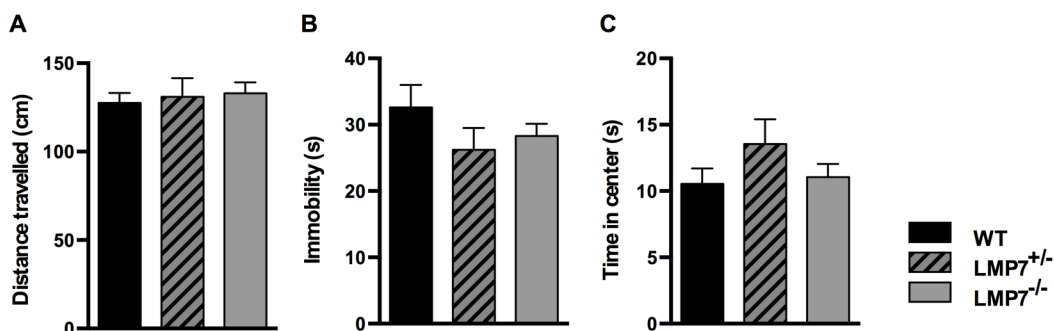
Figure 4: Locomotor activity in the open field test

Displayed are the mean distance travelled (A), the time of immobility (B) and the time spent in the center of the test box (C) of WT, LMP7$^{+/-}$ and LMP7$^{-/-}$ mice littermates. There are no statistically significant differences between the genotypes. The open field test was performed in collaboration with the research group of Prof. Dr. M. Fendt (IPT, OvGU, Magdeburg).
Presented data are mean ± SEM, WT: n=36, LMP7$^{+/-}$: n=22, LMP7$^{-/-}$: n=38 , statistical analysis was done using two-way ANOVA.

A similar result was observed in the light-dark box experiment. Here, means of the percentage distance (Fig. 5A), the time within the bright area (Fig. 5B) as well as the overall distance the animals travelled (Fig. 5C) were similar in all WT, LMP7$^{+/-}$ and LMP7$^{-/-}$ mice tested. All together, the results demonstrate comparable levels of locomotor activity and anxiety in the different genotypes.
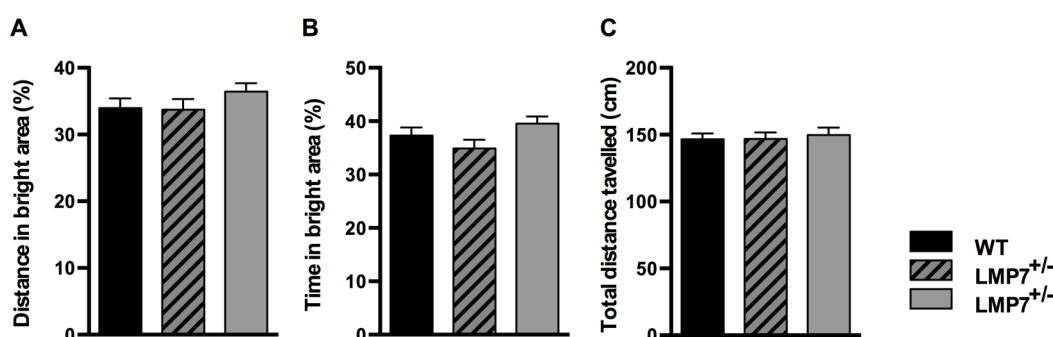
Figure 5: Anxiety assayed in the light-dark box test

Measured was the relative distance (A) and time (B) within the bright area of the light-dark box as well as the total distance travelled (C) of WT, LMP7$^{+/-}$ and LMP7$^{-/-}$ mice littermates. The behavioral assays indicate no difference in unconditioned anxiety between the different genotypes. Experiments were performed in collaboration with the research group of Prof. Dr. M. Fendt (IPT, OvGU, Magdeburg).
Presented data are mean ± SEM, WT: n=29, LMP7$^{+/-}$: n=16, LMP7$^{-/-}$: n=31, statistical analysis was done using two-way ANOVA.

Due to the previous results, were no effects could be observed for heterozygous LMP7$^{+/-}$ littermates and in order to apply good scientific practice following the guidelines of the "Three Rs" [215], [216], innate fear was further tested only for WT and LMP7$^{-/-}$ mice. For this, a carnivore odor-induced fear paradigm was applied [202], in which the mice were exposed to TMT or water as a control condition. Both genotypes exhibit a very similar TMT-avoidance behavior and spent more time outside the odor area when they were exposed to TMT instead of water (Fig. 6A). There seems to be a trend of prolonged phases of immobility in LMP7$^{-/-}$ compared to the WT, irrespective of the odor presence. Therefore, a ratio was calculated to enable a comparison of the TMT effect, but no statistical differences could be observed between the two genotypes (Fig. 6B). According to that, WT and LMP7$^{-/-}$ mice show a similar reduction in overall activity by the distance travelled under TMT exposure and no differences in carnivore-odor induced anxiety.

Further, these data also indicate no differences in the olfactory sense of WT and LMP7$^{-/-}$ mice.
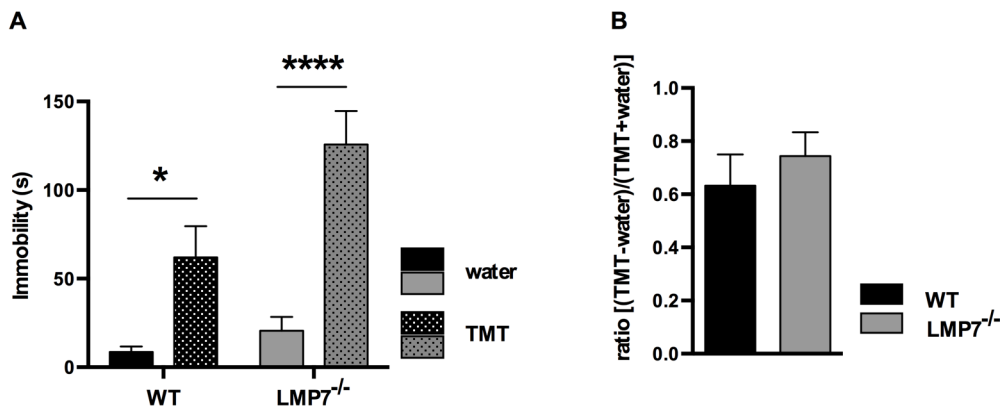
Figure 6: TMT-induced fear behavior

Periods of immobility were significantly increased during exposure to TMT in WT and LMP7$^{-/-}$ mice (A). In contrast, the statistical analysis of the TMT-effect revealed no significant differences between the genotypes but a trend towards reduced locomotor activity in LMP7$^{-/-}$ mice (B). The experiments were conducted in collaboration with the research group of Prof. Dr. M. Fendt (IPT, OvGU, Magdeburg).
Presented data are mean ± SEM, WT: n=9, LMP7$^{-/-}$: n=10, statistical analysis was done using two-way ANOVA with Sidak´s multiple comparisons test, ****: $p<0.0001$, *: $p=0.0285$.

Furthermore, I analyzed the expression level of selected proteins to detect potential disturbances in the cellular protein homeostasis by impaired IP formation under physiological conditions. For this, brains of healthy WT and LMP7$^{-/-}$ mice were collected and different subcellular fractions were prepared according to Smalla et al. [208] with minor modifications in order to enrich specifically the selected proteins for semi-quantitative WB analysis (Fig. 7). Immunodetection of the cellular marker proteins NeuN for neurons, GFAP for astrocytes, and Iba1 for microglia revealed no significant differences in the expression levels for these cell type markers, even though there is a slight tendency towards an increased signal intensity for GFAP and a decreased signal intensity for Iba1 in LMP7$^{-/-}$ mice (Fig. 7A). One major pathway of synaptic plasticity and, thus, brain function is the cAMP/CREB-dependent gene expression [217], [218]. I analyzed the level of CREB and phospho-CREB and calculated the ratio pCREB/CREB in order to pinpoint a possible regulation of this signaling pathway. Notably, there are no alterations in CREB and pCREB expression, but a clear tendency towards an increased CREB phosphorylation in LMP7$^{-/-}$ mice, which could indicate CREB activation in these animals (Fig. 7A). Moreover, I analyzed the expression levels of the constitutive proteasome subunits β1 as well as β5 and the 20S core proteasome subunit α6 in S2 fractions of WT and LMP7$^{-/-}$ mice, which contain mainly cytosolic proteins (Fig. 7B). No differences could be detected between the genotypes except for a minor trend without

statistically significance towards increased expression in α6 in LMP7$^{-/-}$ mice. In addition, I was also interested in the expression of predominant synaptic proteins including subunits of NMDA and AMPA receptors, structural proteins like PSD95 and Shank2, and the presynaptic marker Synaptophysin (Fig. 7C). Overall, LMP7-deficiency caused no changes in expression levels of these proteins under basal conditions and seemed to be similar in both genotypes despite some variations without statistical significance.
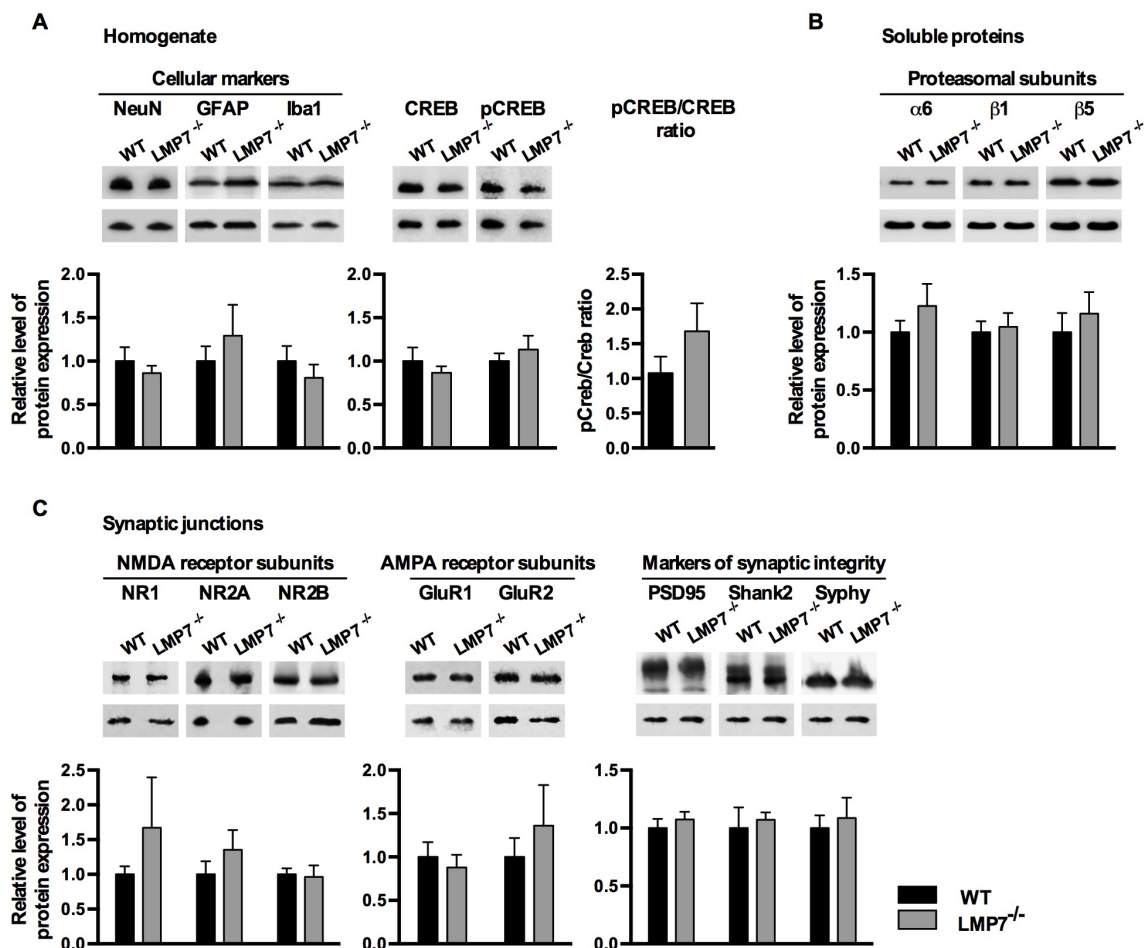
Figure 7: Expression levels of selected proteins in WT and LMP7$^{-/-}$ mice

A subset of subcellular fractions of WT and LMP7$^{-/-}$ mouse brain tissue were prepared using a fractionation protocol [208] and evaluated using semi-quantitative WB analysis. Expression levels of cell type specific marker proteins (A), constitutive proteasome subunits (B), and several synaptic proteins (C) including subunits of the NMDA and AMPA receptor as well as structural synaptic proteins are approximately equally expressed between the genotypes with minor deviations for GFAP, Iba1, alpha6, NR1, and GluR2. However, the differences do not reach statistical significance.
Presented data are mean ± SEM, n=3, statistical analysis was done using one-way ANOVA.

In total, LMP7-deficiency seems to have no obvious pronounced effect on the cellular protein homeostasis,- at least not for cell type markers, components of the proteasomal degradation machinery, and common synaptic proteins, which fits to the observed results from the behavioral phenotyping.

Taken all these results together, I observed no prominent differences between adult WT and LMP7$^{-/-}$ mice in their general health status and behavior, except a minor body weight reduction in the knockout mice, and no changes in the expression level of selected proteins under normal conditions. Due to this, both genotypes appear very similar allowing indeed a comparison of WT and LMP7$^{-/-}$ mice for the intended experiments with robustness and reliability.

3.1.2 IP subunit antibody characterization

An antibody, specifically detecting the protein of interest, is a powerful tool to study whose presence and regulation. At the beginning of this work immune sera raised against LMP2 and LMP7 were generated by the company Pineda Antikörper Service using synthetic peptides for both immunoproteasomal subunits. For each antigen three guinea pigs and three rabbits were immunized either with a peptide of the murine LMP2 sequence (aa 205-219) or of the murine LMP7 sequence (aa 262-276). The resulting anti-sera were obtained after 120 days of immunization.

First, all 12 anti-sera were tested in WB analysis for their sensitivity and specificity in order to establish a protocol with high signal quality, different dilutions of the immune sera, ranging from 1:250, 1:1000, 1:2500 and 1:10.000, were tested. I decided for a dilution of 1:2500 as with this, a notable signal and an economical application was ensured (Fig. S1 and S2). Further, two membrane blocking protocols were tested (data not shown). Membrane blocking with 5 % milk powder in TBS-T resulted in clearer blots with low background signals and, therefore, was used in all subsequent experiments, whereas blocking with 5 % BSA in TBS-T exhibited more unspecific binding and a higher level of background signal.

All generated anti-sera solutions detect an immuno-reactive band at the predicted size of LMP2 or LMP7 (at ca. 22-23 kDa). Interestingly, WBs incubated with anti-LMP7 sera show a double band in the WT samples, probably representing the precursor and the mature protein (Fig S2A, B) of 30 kDa and 23 kDa, respectively. Importantly, immunoreactive signals in spleen samples serving as the positive control can be blocked using either MBP-LMP2 or MBP-LMP7 fusion proteins for pre-adsorption of the respective antibody solutions. These results confirm the necessary specificity of all generated anti-sera for WB analysis. The antibody solutions with the best signal quality were determined (anti-LMP2: guinea pig #3 and rabbit #4; anti-LMP7: guinea pig #2 and rabbit #3) and used for further characterization (Fig. 8 and 9). Spleen homogenates from WT mice served as positive controls whereas spleens derived from LMP2$^{-/-}$ or LMP7$^{-/-}$ mice were used as negative controls: The anti-LMP2 sera from guinea pig #3 and rabbit #4 showed a clear band around 20 kDa, close to the predicted size of the murine LMP2 protein of ca. 23 kDa (Fig. 8). In the brain tissue samples, a very weak immuno-reactive band can be observed in the

homogenates whereas a clear band is visible in the S2 fractions of the WT mice (Fig. 8B). In samples of LMP2$^{-/-}$ mice was no signal at the expected size visible. Interestingly, there are two immuno-reactive bands observed in the LMP7$^{-/-}$ mice spleen samples (Fig. 8A). Since both bands are absent after antibody blocking, it represents most probably the precursor and the mature protein of LMP2. In addition, in all brain samples, several additional binding sites can be detected from 25-130 kDa (Fig. 8B). These bands can be observed in all genotypes and their presence remains unchanged after antibody blocking, which indicates a further affinity of the anti-sera to some unknown proteins.

Figure 8: LMP2 antibody characterization and specificity for WB analysis

The anti-LMP2 antibodies #3 and #4 from guinea pig and rabbit, respectively, were assessed for their specificity of protein recognition in WB. Equal protein amounts of spleen homogenates (A) as well as homogenates and prepared S2 fractions of the mouse brains (B) from WT, LMP2$^{-/-}$ and LMP7$^{-/-}$ mice were loaded. As a control for the necessary specificity blocking of the antibodies was performed with a MBP-LMP2 fusion protein. To exclude interactions of MBP with the antibody, a MBP-LMP7 blocking control was additionally performed. Both antibodies exhibit specific binding in WB analysis. In spleen samples, a clear band can be observed in the WT, no signal is detected in

the LMP2$^{-/-}$ mice and a double band occurred in the LMP7$^{-/-}$ mice. In brain tissue, an obvious immuno-reactive band was detected in S2 fractions and with lower signal intensity in homogenates of WT mice.
Hom: homogenate, S2: supernatant 2 containing mainly cytosolic proteins, MBP: maltose binding protein

However, both LMP2 antibody solutions could be successfully blocked by supplementation and pre-adsorption of the recombinant fusion protein MBP-LMP2 resulting in signal loss compared to unblocked as well as supplemented with a recombinant MBP-LMP7 antibody solution. Only in MBP-LMP2-blocked solutions the detection of the LMP2 immuno-reactive band was missing indicating a specific pre-adsorption of the LMP2 immune sera.
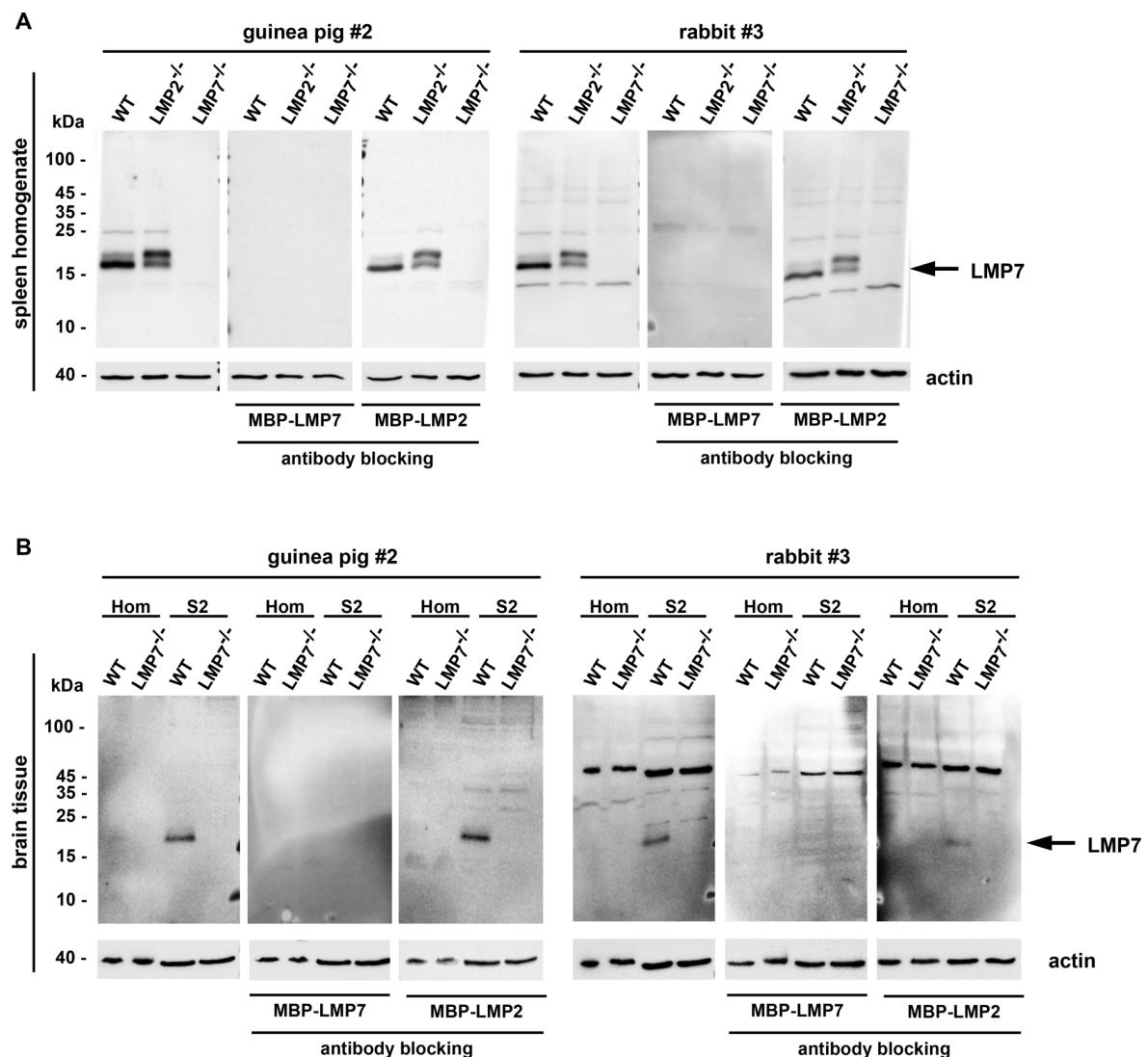
Figure 9: LMP7 antibody characterization for WB analysis

Equal protein amounts of spleen homogenates (A), mouse brain homogenates and S2 fractions (B) of WT, LMP2$^{-/-}$ and LMP7$^{-/-}$ mice were subjected to WB analysis in order to assess the specificity of anti-LMP7 sera #2 and #3 from guinea pig and rabbit, respectively. For blocking assay, antibodies were pre-adsorbed with a MBP-LMP7 fusion protein and additionally with a MBP-LMP2 fusion

protein as positive control. Both LMP7 antibodies exhibit specific binding in WB analysis. In WT and LMP2$^{-/-}$ spleen samples a double band can be observed at the estimated size of LMP7, whereas no signal was detected in samples of LMP7$^{-/-}$ mice. In addition, obtained signals at ca. 20 kDa in the brain tissue of WT mice could be successfully blocked using the fusion protein.
Hom: homogenate, S2: supernatant 2 containing mainly cytosolic proteins, MBP: maltose binding protein

Similar results were obtained with the anti-LMP7 sera of guinea pig #2 and rabbit #3 in WB analysis (Fig. 9). LMP7 has a molecular mass of ca. 30 kDa as a precursor and 23 kDa in its mature form. In WT spleen samples, a clear band at approximately 20 kDa is visible, which is absent on WBs probed with pre-adsorbed immune sera using the fusion protein MBP-LMP7 (Fig. 9A).

A second band of slightly larger molecular mass can be seen in LMP2$^{-/-}$ samples, very similar to the recognition patter of the LMP2 anti-sera in LMP7$^{-/-}$ mice. This immuno-reactive band is also visible in the WT spleen samples, but much less pronounced. The detection of these double bands can be blocked by pre-adsorption of the antibodies with the recombinant MBP-LMP7 fusion protein but not with MBP-LMP2 indicating antibody specificity to the pro- and mature form of the LMP7 peptide. Additionally, application of the rabbit antibody leads to a third immuno-reactive band below 15 kDa in spleen samples (Fig. 9A). Surprisingly, this band is present in the spleen, but absent in the brain tissue samples of LMP7$^{-/-}$ mice (Fig. 9B). Furthermore, this band could be blocked by antibody pre-adsorption. In brain samples, the anti-sera from rabbit #3 recognized additionally some unspecific protein bands between 40-70 kDa.

Next, the generated immune sera against LMP2 and LMP7 were tested for their specific application in immunocytochemical stainings of primary neuronal cell cultures of WT and LMP7$^{-/-}$ mice. To ensure induction of immunoproteasomal subunit expression [56], cells were treated at DIV14 with 20 ng/ml IFN-y for 24 h before immunocytochemistry. Antibody solutions were applied in a 1:2500, 1:5000 and 1:10 000 dilution.
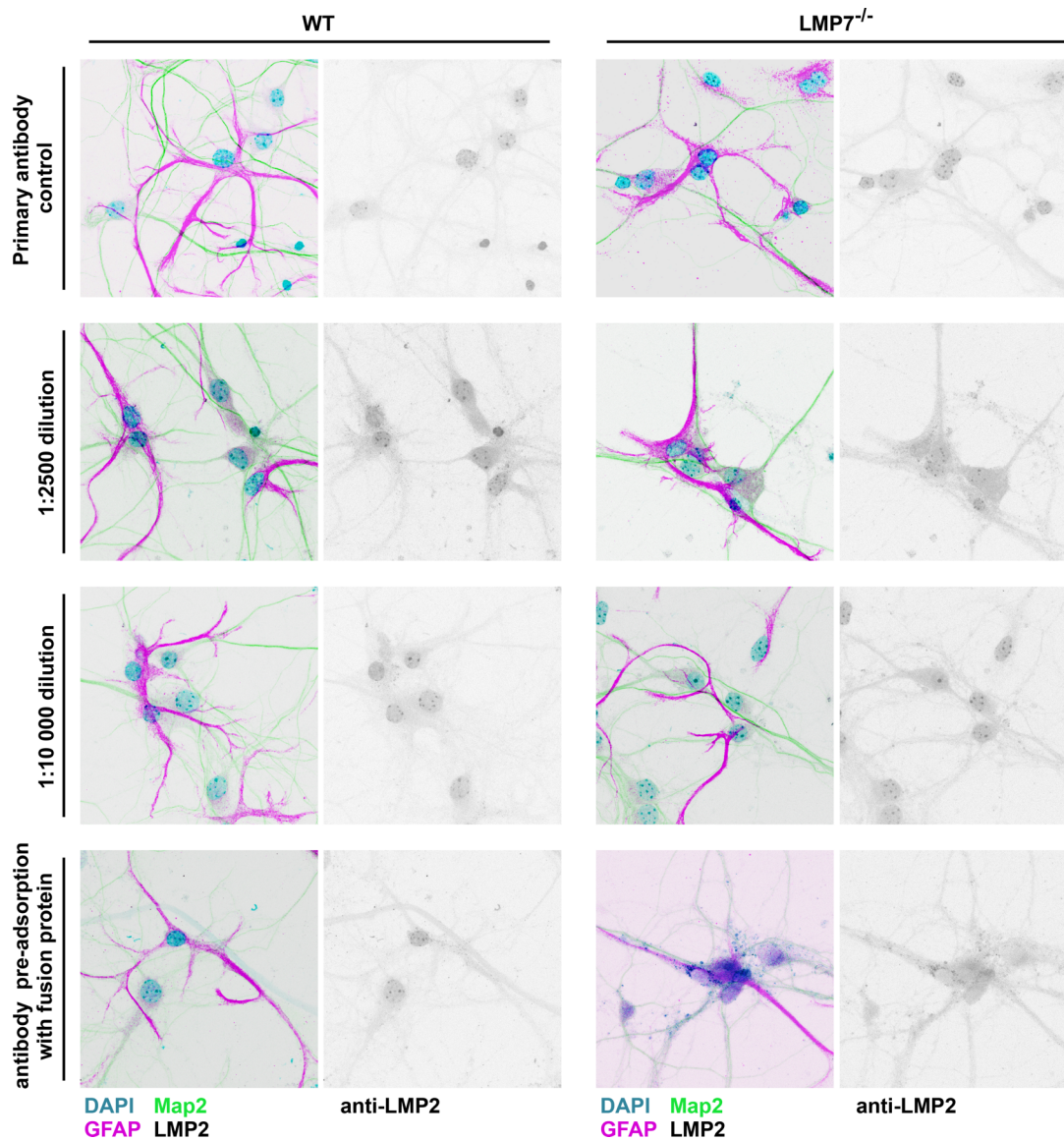
Figure 10: Low signal quality and antibody specificity in immunocytochemistry for LMP2

Representative images of immunocytochemical stainings against LMP2 (exemplarily for anti-LMP2 rabbit #4) and the cell type markers Map2 and GFAP of primary neural cell cultures of WT and in addition of LMP7$^{-/-}$ mice after 24 h IFN-γ stimulation. There were no specific signals well above background detectable.. Instead, the poor immunofluorescence in samples of antibody incubated samples (in both, 1:2500 and 1:10 000 dilution) in relation to the background signals of the primary antibody control and the pre-adsorbed antibody application indicates unspecific binding and a lack of applicability for immunocytochemistry of the LMP2 anti-sera.
Scale bar: 50 μm

Among the different immune sera, no specific signals were observable, neither for LMP2 nor LMP7. Likewise, signal strength was not altered in the different dilutions, beside higher background signals in the highly concentrated antibody solutions (data not shown).
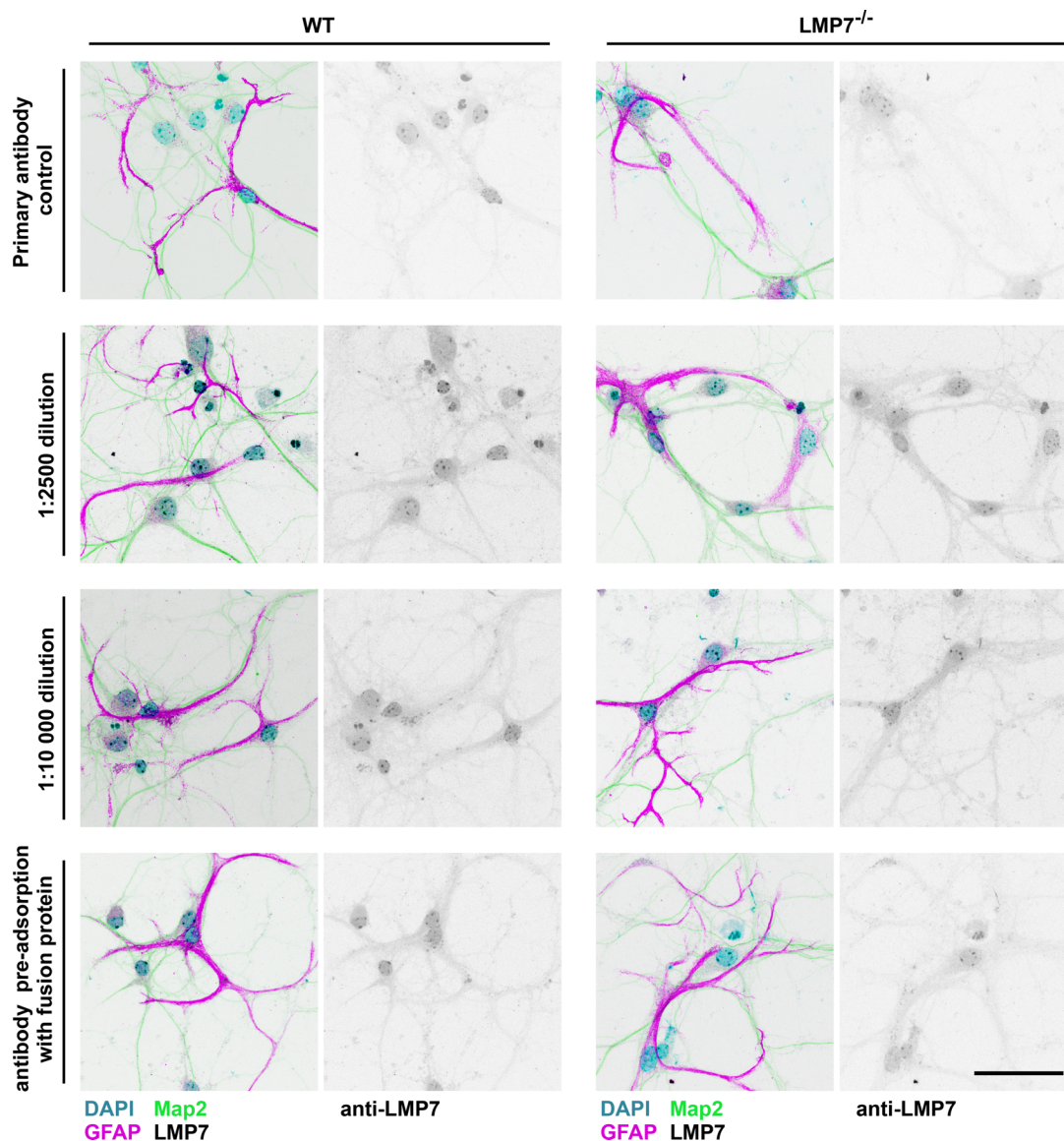
Figure 11: Unspecific antibody binding of anti-LMP7 in immunocytochemistry

Depicted are representatives images (exemplarily for anti-LMP7 rabbit #2) of primary neural cell cultures of WT and LMP7$^{-/-}$ mice after 24 h IFN-γ stimulation, which were immunocytochemically stained for LMP7 and the cell type markers Map2 and GFAP. Comparable low signal strength in WT and LMP7$^{-/-}$ mouse samples as well as after antibody pre-adsorption with a fusion protein (MBP-LMP7) reveals the non-specificity of the applied LMP7 anti-sera.
Scale bar: 50 µm

Representative confocal images of immunocytochemical staining using a 1:2500 and 1:10 000 dilution of sera anti-LMP2 rabbit #4 and anti-LMP7 rabbit #2 are depicted in Fig. 10 and Fig. 11, respectively. The anti-LMP2 sera were additionally tested in LMP7$^{-/-}$ cell cultures in order to capture potential alterations of the antibody specificity in this knockout mouse model. However, confocal images displayed no clear fluorescent signals above the background signal upon comparison to primary antibody controls, which were missing the incubation step with the anti-LMP2 or anti-LMP7. In addition, similar signal intensities for LMP7 in WT and LMP7$^{-/-}$ cell cultures rather indicate the missing specificity of the used

immune sera (Fig. 11). This result implies not only an unsuitability of the anti-LMP7 antibody for specific application in immunocytochemistry, but also for the anti-LMP2 antibody, even though an explicit negative control realized by the use of an LMP2$^{-/-}$ cell culture was not available.

In contrast, immunohistochemically stained brain sections of WT and LMP7$^{-/-}$ mice show precise signals for all LMP2 as well as LMP7 antibodies (selected images in Fig. 12). As described for the WB analysis, immune sera leading to best signal qualities were further characterized.
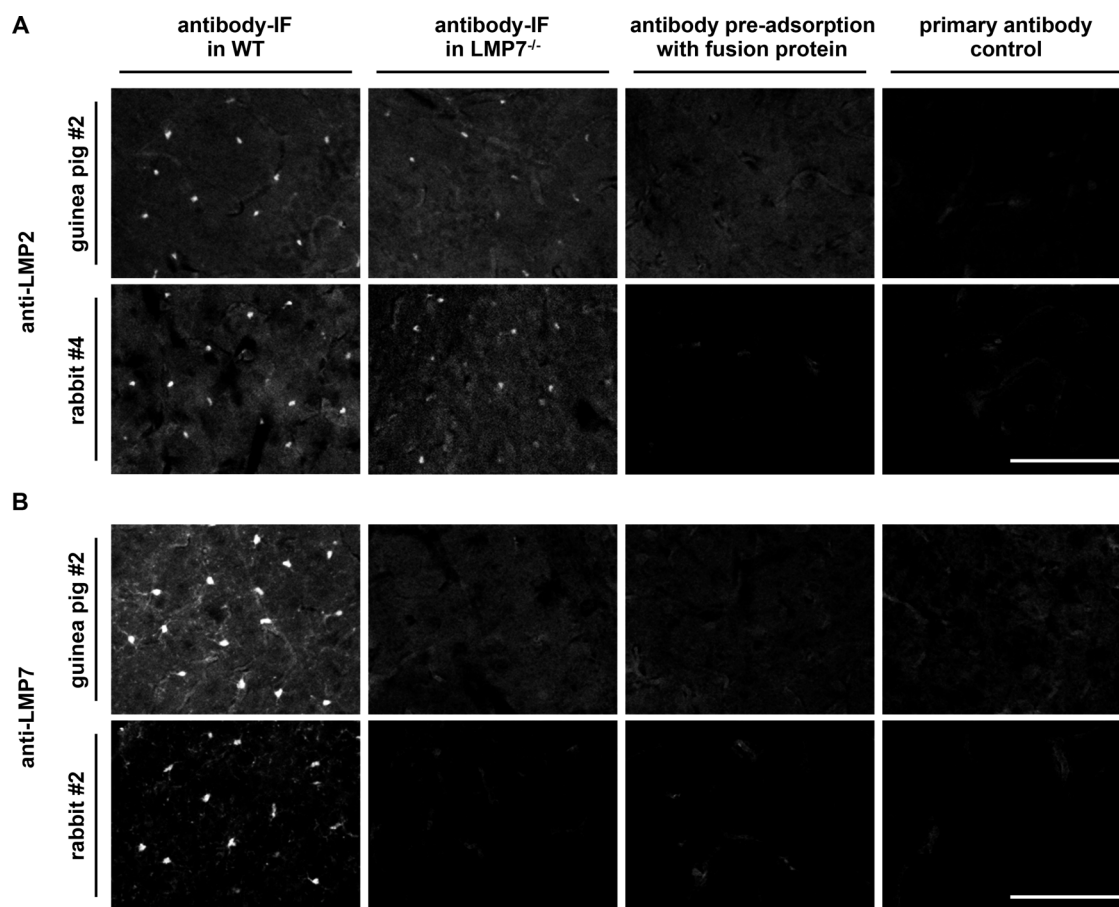
Figure 12: LMP2 and LMP7 antibody specificity in immunohistochemistry

Immune sera against LMP2 and LMP7 from guinea pig and rabbit with the highest signal intensity in preliminary studies were immunohistochemically tested for their specificity and optimized for subsequent applications in free floating coronal brain sections of WT and LMP7$^{-/-}$ mice. Immunofluorescence for LMP2 is detected in sections from both genotypes and vanishes after pre-adsorption of the antibody with the fusion protein MBP-LMP2 (A). In contrast, signals for LMP7 are observed exclusively in WT sections, whereas no fluorescence signal is seen in LMP7$^{-/-}$ samples and after antibody pre-adsorption with a MBP-LMP7 fusion protein (B). The results confirm specific detection of the immunoproteasomal subunits in immunohistochemistry. Potential unspecific binding of the secondary fluorescence dye-coupled antibody could be excluded in the primary antibody control.
IF: immunofluorescence, Scale bar: 100 µm

The anti-LMP2 from guinea pig #2 and rabbit #4 exhibit similar signal intensities in WT brain sections with low background signals and could be successfully block by antibody pre-adsorption using a MBP-LMP2 fusion protein pointing towards the specificity of the used sera. Fluorescent signals in the LMP7$^{-/-}$ mice seem to be slightly lower in signal strength (Fig. 12A). The same results are observed for the anti-LMP7 sera from guinea pig #2 and rabbit #2 apart from fluorescent signals in the LMP7$^{-/-}$ brain slices which should be expected and excludes unspecific binding of the immune sera (Fig. 12B). For both, anti-LMP2 and anti-LMP7 sera, samples of the primary antibody control display no signals excluding unspecific binding of the secondary antibody.

Taken all the results of the antibody characterization together, with the generated immune sera a specific detection of the immunoproteasomal subunits LMP2 and LMP7 can be achieved in WB analysis as well as in immunohistochemistry. However, an application for immunocytochemistry seems to be ineffective due to the low signal intensity and suspected unspecific binding of the available immune sera.

3.2 Cellular and subcellular localization of LMP2 and LMP7

Constitutive, i.e. standard proteasomes are ubiquitously expressed in all eukaryotic cells [13]. The expression of immunoproteasomal subunits was first discovered and investigated in immune relevant tissues, but is induced in various other tissues upon IFN-γ stimulation [21], [219]–[221]. In contrast, the precise cellular expression of IPs in the brain has not yet been completely analyzed. So far, the presence of IPs in brain tissue was mainly associated with neurodegenerative disease or pathological conditions, but somehow contradictory [55]–[60], [144], [187]. To elucidate the functional role of the IPs in the brain, I used a combination of molecular, cell biological and functional tools. I applied a cerebral ischemia mouse model in WT animals before immunohistochemistry in order to ensure a sufficient induction of IP expression due to the high release of inflammatory cytokines [63], [222]. For the same reason, primary neuronal cell cultures were stimulated with IFN-γ prior to immunocytochemistry and the FISH assay. In addition, WB analysis of different biochemical fractions was performed to gain information about the subcellular distribution of immunoproteasomal subunits.

3.2.1 IP subunit expression in microglia

Immunohistochemical co-staining in WT brain sections using antibodies raised against the IP subunits LMP2 or LMP7 and the microglial marker Iba1 display a clear overlap of fluorescent signals for LMP2 as well as LMP7 with Iba1-positive cells (Fig. 13). As LMP7 expression is under basal conditions low, I provoked expression by stroke and afterwards analyzed the cellular localilzation in the mouse brain. Confocal images display close ups of the penumbra after 2 d of MCAO.
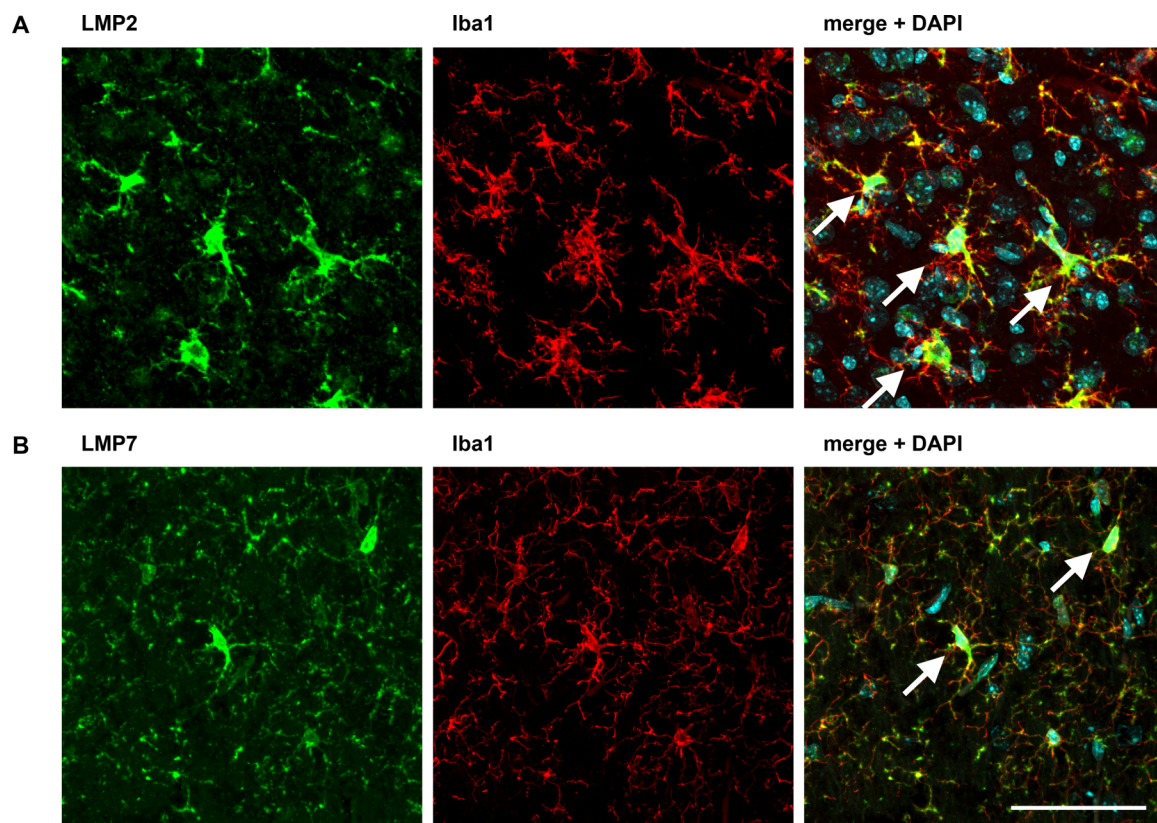
Figure 13: Co-localization of LMP2 and LMP7 in mouse brain sections with the microglial marker Iba1

Immunohistochemical co-stainings using antibodies raised against LMP2 (A) or LMP7 (B) and the microglia marker protein Iba1 in WT mouse brain sections reveal the cellular localization of immunoproteasomal subunits predominantly in microglia cells, indicated by the co-localization of fluorescent signals in merged, representative images for LMP2 and LMP7 with Iba1-positive cells (yellow signals, see arrowheads).
Scale bar: 50 µm

Concerning the inflammatory milieu and the morphology of the Iba1-positive cells, these cells can be assumed as highly activated microglia and/or macrophages. LMP2 and LMP7 appear to be present in all compartments of these cells including thin distal dendrites. This could be confirmed with higher magnifications and the acquisition of confocal stacks, enabling the generation and inspection of cross-sections (Fig. 14). Green fluorescent signals for either LMP2 (Fig. 13A and 14A) or LMP7 (Fig. 13B and 14B) respectively, co-localize with red signals for Iba1 and create yellow signals. Hence, potential superimpositions of the single fluorescent signals, which can be a problem in immunohistochemically stained tissue and often lead to falsified visualizations, can be excluded.
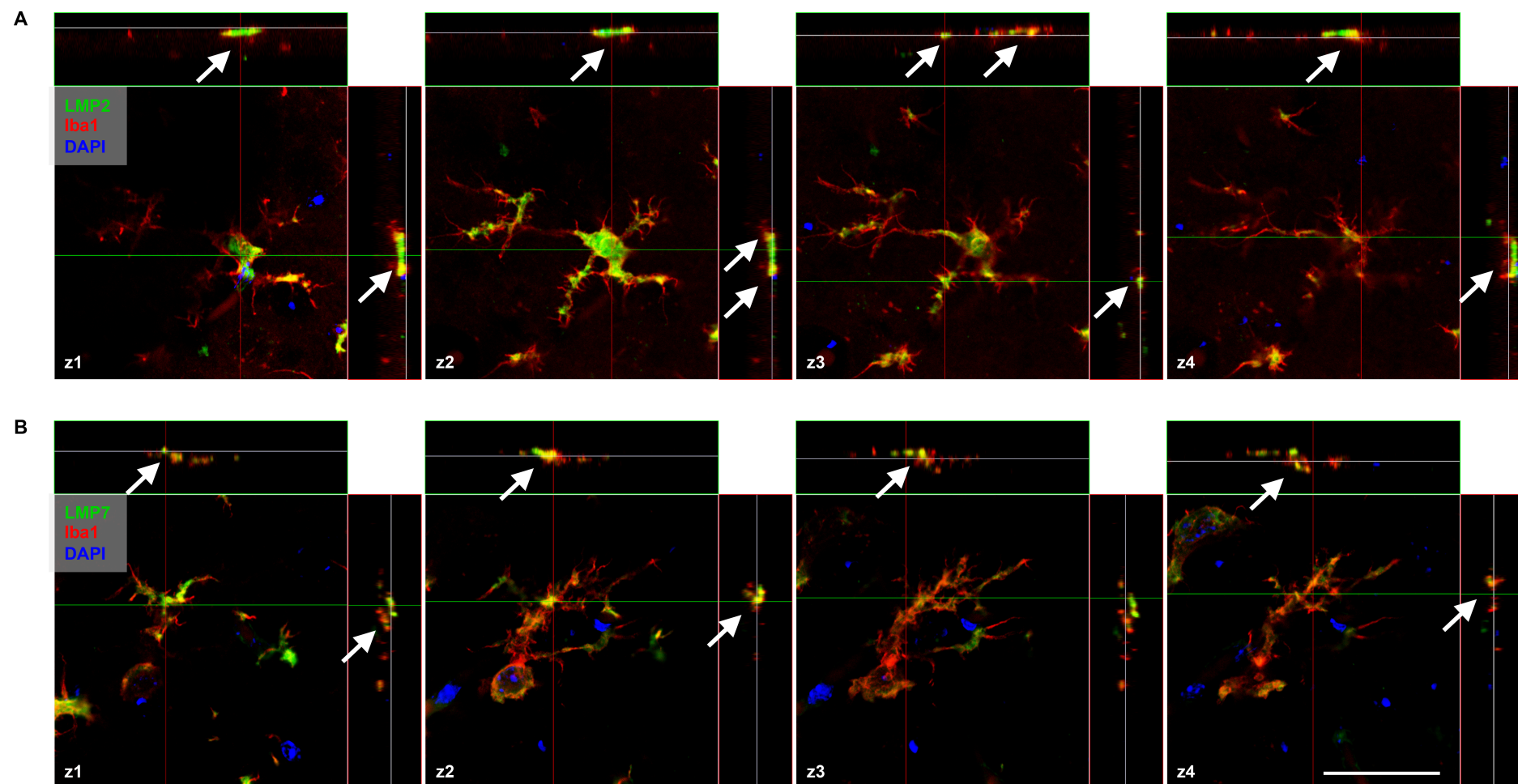
Figure 14: Localization of the immunoproteasomal subunits LMP2 and LMP7 within Iba1-positive cells

Depicted are single z-stacks (z1-z4) and orthogonal cross-sections that were acquired with confocal microscopy of immunohistochemically stained WT mouse brain sections against LMP2 (A) or LMP7 (B) and the microglial marker Iba1. In the cross-sections, yellow signals (see arrowheads) clearly indicate the cellular localization of LMP2 as well as LMP7 (green fluorescent signals) inside of Iba1-positive cells (red fluorescent signals). Scale bar: 2
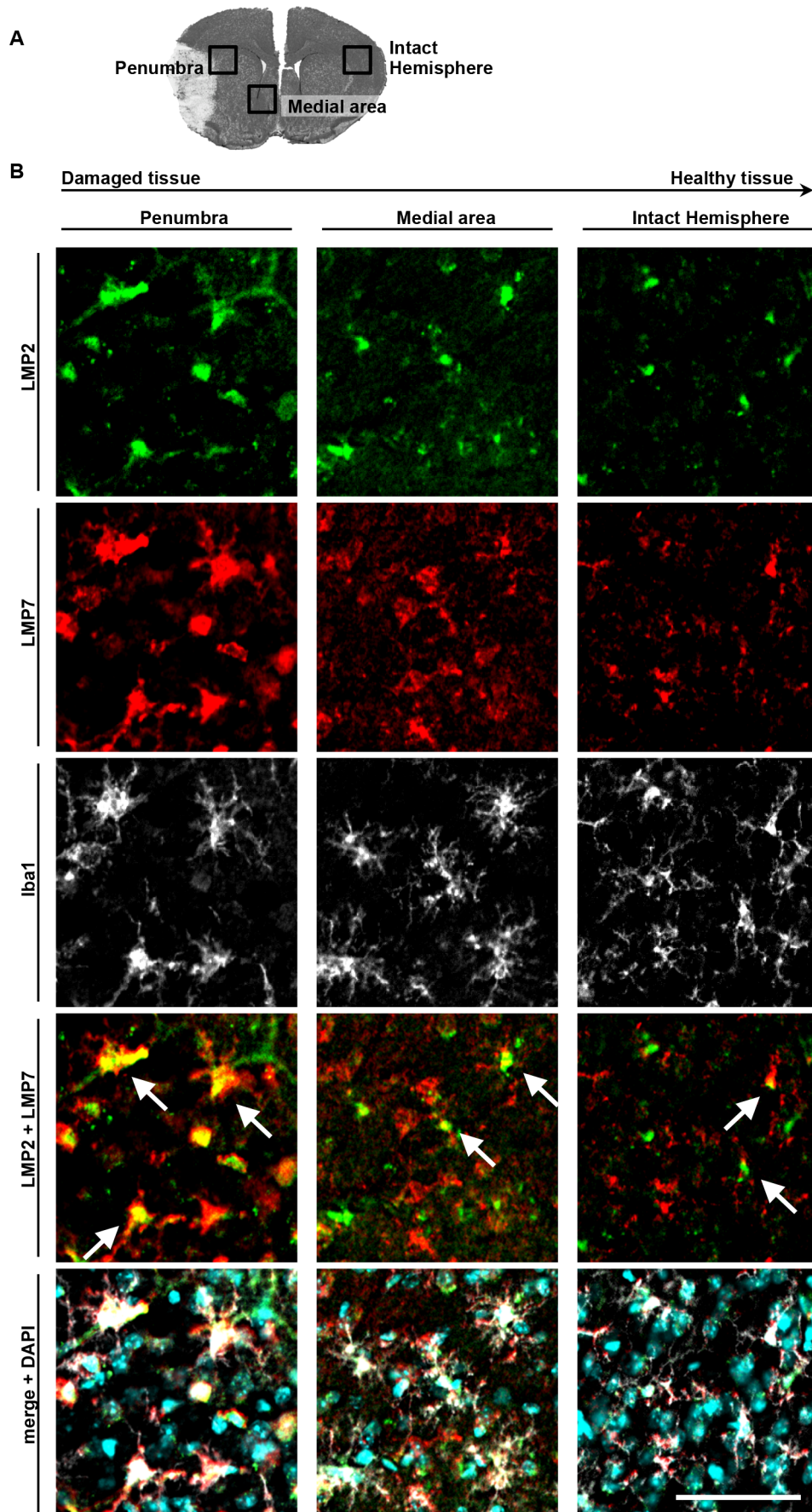
Figure 15: LMP2 and LMP7 co-localize in Iba1-positive cells

Shown are representative confocal images (B) of different regions of WT mouse brains sections after 1 d of MCAO (A) that were immunohistochemically stained for LMP2, LMP7 and Iba1. In the penumbra immediately next to the infarct area, fluorescent signals for LMP2 and LMP7 largely co-localize and seem to be expressed in Iba1-positive cells only. Interestingly, this overlap of LMP2 and LMP7 signals shifts towards more healthy regions. LMP2 signals are located more within the cell soma, close to the nucleus, whereas signals for LMP7 are rather observed in distal parts of Iba1-positive cells. In addition, signals intensities for LMP2 and LMP7 appear decreased in healthy compared to damaged tissue.
Scale bar: 50 µm

In addition, immunohistochemical staining of both IP subunits together and the microglia marker Iba1 were performed (Fig. 15). The co-localization of fluorescent LMP2 and LMP7 signals with Iba1-positive cells could be corroborated, especially in areas of partially damaged tissue such as the penumbra. Moreover, fluorescent signals for LMP2 and LMP7 co-localized with Iba1-positive cells in the intact hemisphere, too (Fig. 15). Expression patterns appear uniform for LMP2 and LMP7 and seem to be present in all compartments of the Iba1-positive cells. Concerning more healthy tissue like medial parts of the sections or the intact hemisphere, LMP2 signals seem to be limited to the cell somata, whereas LMP7 signals were more distally situated. This becomes even more obvious in the images of the merged LMP2 and LMP7 channel, displaying a close proximity of the fluorescent signals but no complete overlap of the fluorescent signals that would result in yellow signals. Moreover, signal intensities for all stained proteins are clearly decreased towards healthy tissue regions.

In conclusion, microglia seem to be the predominant cell type expressing immunoproteasomal subunits in the mouse brain under physiological and ischemic conditions.

3.2.2 IP subunits are not expressed in neurons and astrocytes

Despite the observation that both immunoproteasomal subunits are predominantly detectable only in Iba-1 positive cells, one cannot rule out the possibility that these subunits might be also expressed in other cell types at lower levels. Therefore, the localization of LMP2 and LMP7 was additionally analyzed in relation to the astroglial marker GFAP (Fig. 16) as well as the neuronal marker proteins Map2 and NeuN (Fig. 17). Confocal microscopy revealed no clear overlapping signals for the immunoproteasomal subunits and the cell type markers.
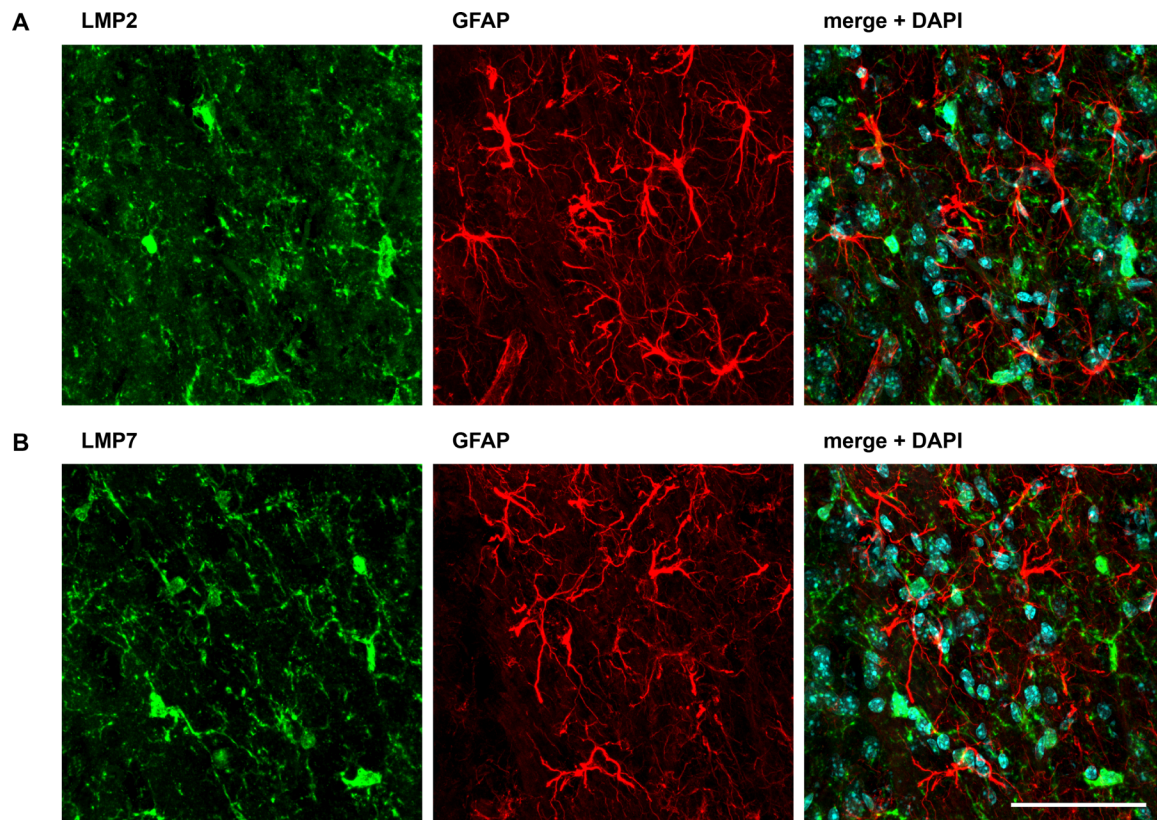
Figure 16: Localization of immunoproteasomal subunits in mouse brain sections in relation to the astroglia marker GFAP

Immunohistochemical co-staining was performed in WT mouse brain sections after 1 d of MCAO using antibodies raised against the IP subunits LMP2 (A) and LMP7 (B) as well as GFAP and analyzed using confocal microscopy. The merged, representative images reveal neither for the LMP2- nor LMP7-immunofluorescent signals a clear co-localization with GFAP signals.
Scale bar: 50 µm
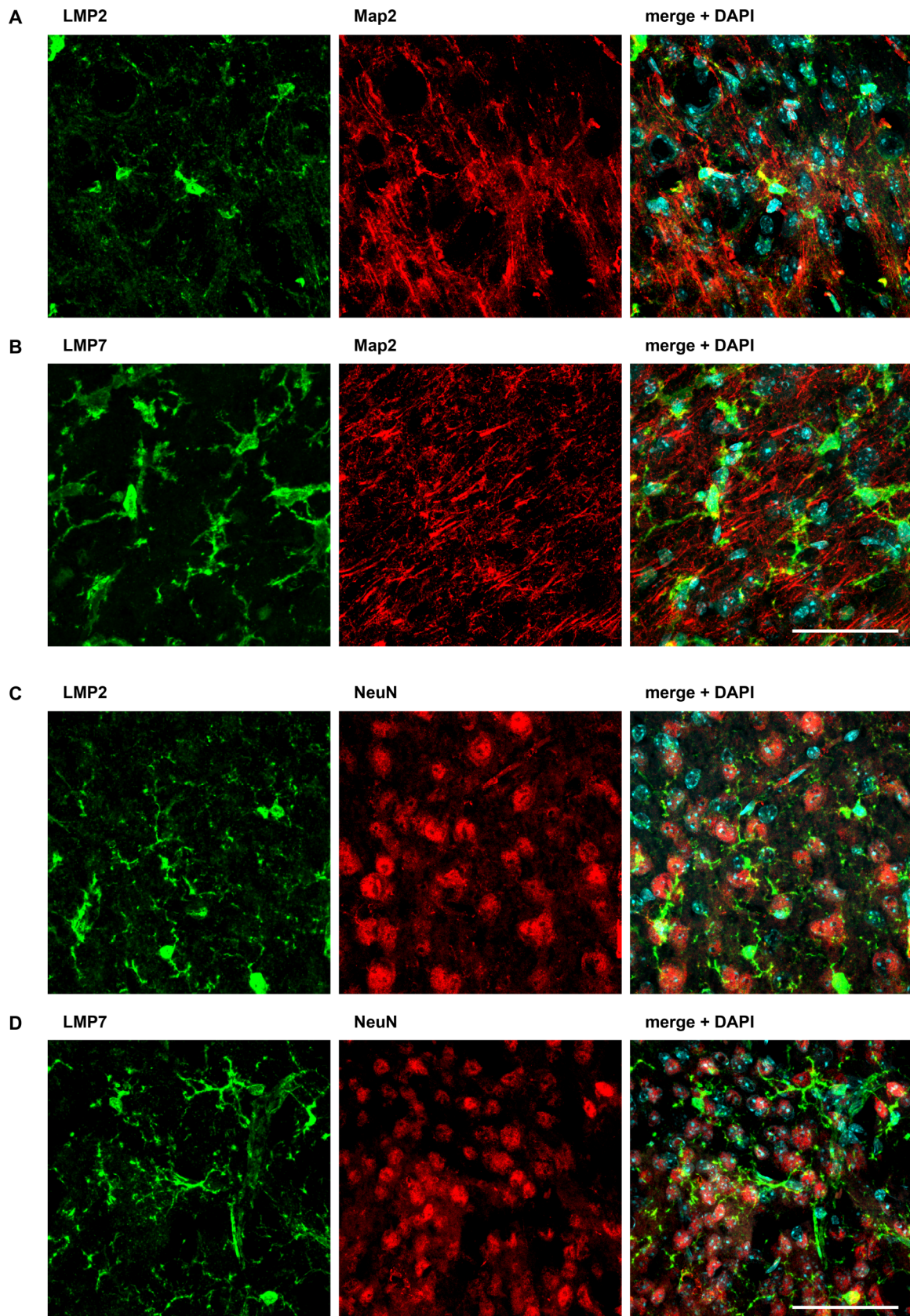
Figure 17: Localization of LMP2 and LMP7 in mouse brain sections with regard to the neuronal markers Map2 and NeuN

After 1 d of MCAO, WT mouse brain section were immunohistochemically co-stained using antibodies raised against the IP subunits LMP2 (A, C) or LMP7 (B, D) and the neuronal marker

proteins Map2 (A, B) and NeuN (C, D). Despite some rare superimpositions, precise co-localizations of LMP2-positive or LMP7-positive cells with fluorescent signals for Map2 and NeuN were not observed. Shown are representative images.
Scale bar: 50 µm

There were no clear co-localizing fluorescent signals for GFAP and the immunoproteasomal subunits observed, neither for LMP2 (Fig. 16A) nor for LMP7 (Fig. 16B). Because of this, an expression of LMP2 and LMP7 seems to be very unlikely in astrocytes under the selected experimental conditions.

Few spots can be observed, where fluorescent signals for LMP2 seem to co-localize with either Map2 (Fig. 17A) or NeuN (Fig. 17C), but are difficult to interpret as these signals do not match the visualized neuronal structures. This impression of superimpositions appears also for co-staining with LMP7 (Fig. 17B,D). Due to this, an additional localization analysis was intended in primary neuronal cell culture. This experimental design would disperse cellular compactness as it occurs in tissue and would enable a higher resolution to avoid misleading superimpositions. However, as the generated immune sera were not suitable for immunocytochemistry (compare to section 3.1.2), I decided to perform a FISH assay using primary neural cells in order to analyze the putative existence of the IP subunits LMP2 and LMP7 at least on transcript level.

3.2.3 LMP2 and LMP7 on transcript level in primary neuronal cell culture

Primary cell cultures were treated with 10 and 20 ng/ml IFN-γ and subjected to a FISH assay with subsequent immunocytochemistry using antibodies raised against the astroglial marker GFAP and the neuron marker Map2. Signals for LMP2 and LMP7 mRNA were detected in WT mouse primary neuronal cell cultures after 24 h IFN-γ stimulation with a concentration of 20 ng/ml IFN-γ, while no signals could be observed for the immunoproteasomal subunits in mock-incubated cell cultures and nearly no signals for 10 ng/ml IFN-γ-treated cell cultures (Fig. 18 and 19, upper row). Thus, an expression of LMP2 and LMP7, at least on transcript level, is predominantly observed in astrocytes, indicated by the overlap of fluorescent signals of the LMP2 and LMP7 probe with GFAP-positive cells (Fig. 18). The amount of LMP2 and LMP7 mRNA levels seem to be similar after 24 h of IFN-γ treatment. The fluorescent signals are found throughout the whole cell body, but seem to be concentrated around the nucleus. In addition, LMP7$^{-/-}$ mouse primary cell cultures were used in order to confirm specificity, at least of the LMP7 probe, in the used FISH assay. As expected, no signals for LMP7 could be detected in the negative controls. As in the WT samples, fluorescent signals for LMP2 mRNA co-localized with GFAP-positive astrocytes in the LMP7$^{-/-}$ cell cultures after IFN-γ treatment. The levels of LMP2 appeared to be indistinguishable between the two genotypes.
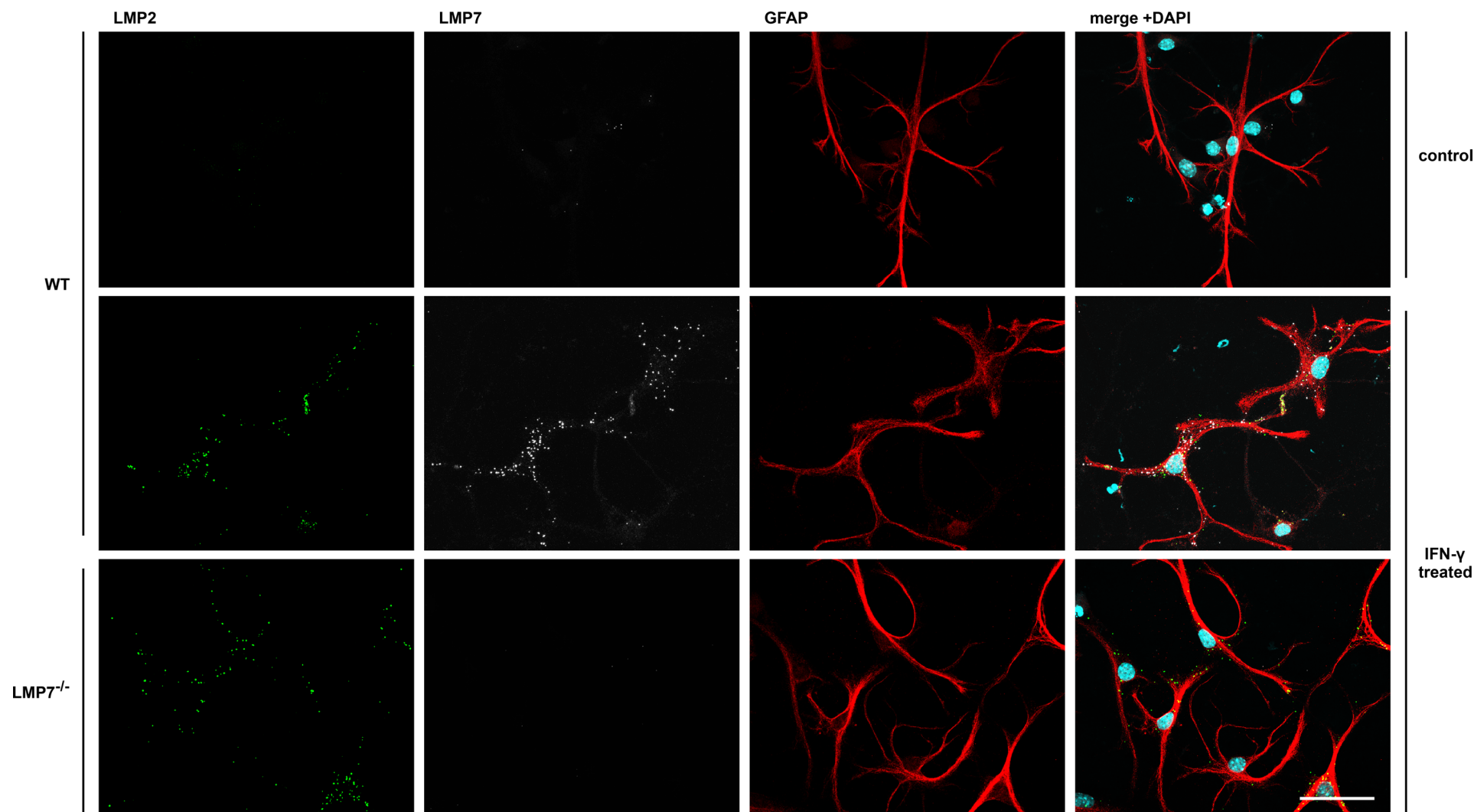
Figure 18: Localization of LMP2 and LMP7 mRNA in primary cell culture in relation to the astroglial marker GFAP

WT and LMP7^{-/-} mouse primary neuron-glia co cultures were incubated with 20 ng/ml IFN-γ for 24 h and subjected to FISH and immunocytochemistry. Fluorescent signals of LMP2 and LMP7 mRNA are mainly observed after IFN-γ stimulation and co-localize with GFAP-positive astrocytes, whereas no signals were observed in mock-incubated cell cultures. No signals for LMP7 in LMP7^{-/-} samples verify the specificity of the used FISH assay. Scale bar of representative images: 50 µm
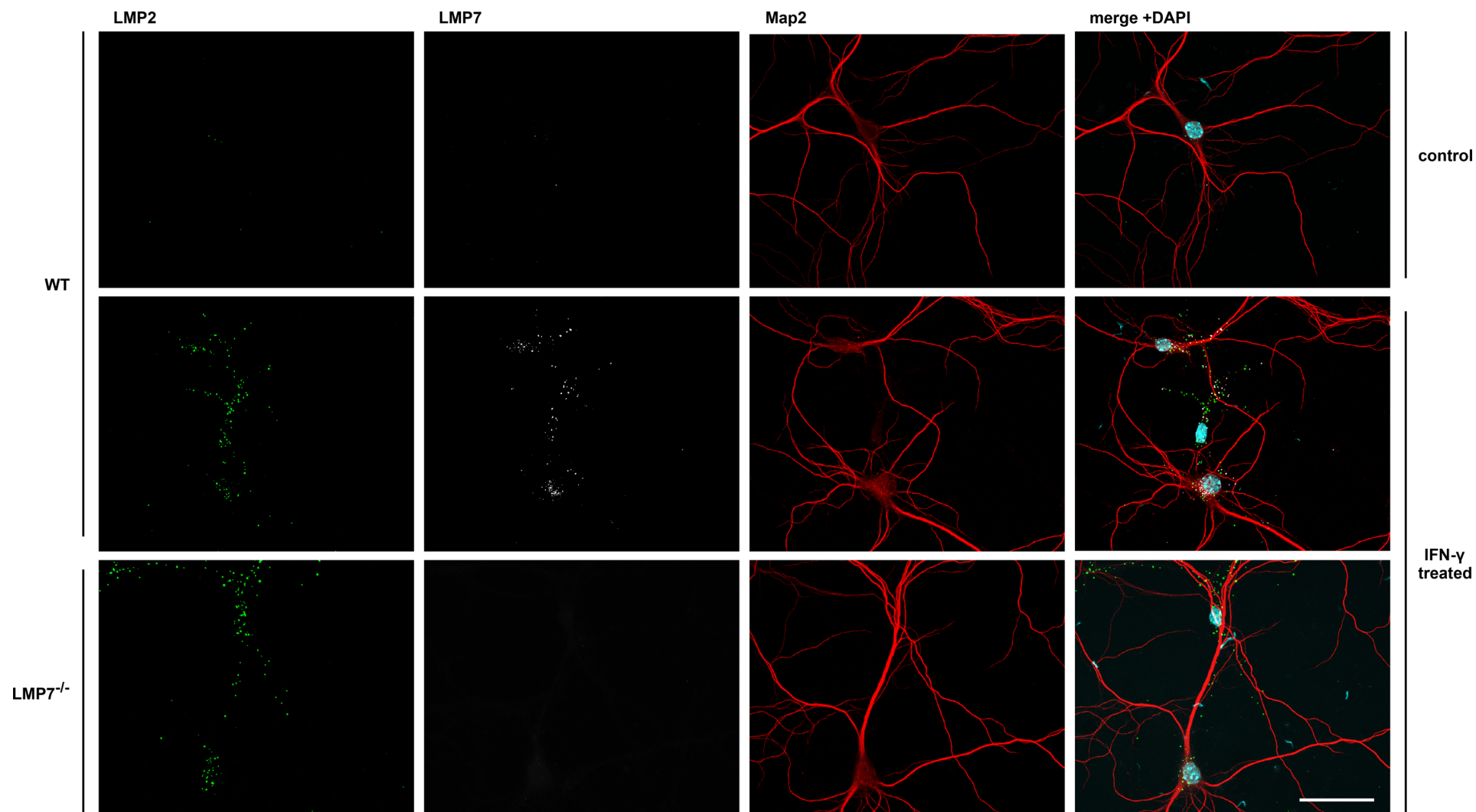
Figure 19: Localization of LMP2 and LMP7 mRNA in primary cell culture in relation to the neuronal marker Map2

Primary neuron-glia co cultures of WT and LMP7^{-/-} mouse were incubated with 20 ng/ml IFN-γ for 24 h and subjected to a FISH assay and immunocytochemistry. After IFN-γ stimulation, fluorescent signals of LMP2 and LMP7 mRNA can be observed in the WT cell cultures. In general, there was no clear overlap of FISH signals and Map2-positive neurons detectable. No signals for LMP7 were noticed in LMP7^{-/-} samples or for both immunoproteasomal subunits in the mock-incubated control samples. Scale bar of representative images: 50 μm

In contrast, fluorescent signals for LMP2 and LMP7 mRNA could be rarely detected in immunocytochemically stained neurons and only after 24 h stimulation with 20 ng/ml IFN-γ (Fig. 19) as already observed in Fig. 18.

However, a few isolated Map2-positive cells could be detected with some overlapping signals for LMP2 and LMP7 mRNA after IFN-γ stimulation (Fig. 20). The quantity of mRNA signals in these neurons is comparable less to the amount of LMP2 and LMP7 mRNA in GFAP-positive astrocytes and their presence seems to be limited to the cell soma around the nucleus. To a lower extent, the described observations were also seen in cell cultures treated for 24 h with 10 ng/ml IFN-γ (data not shown). In mock-incubated control cultures, no fluorescent signals for LMP2 and LMP7 mRNA above the background level were noticed.
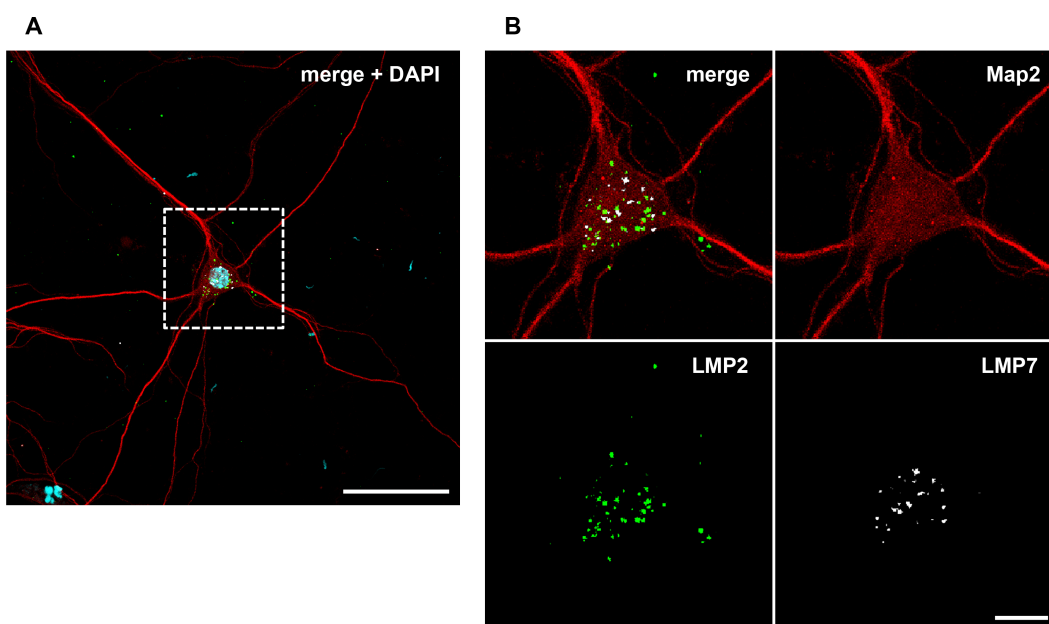
Figure 20: Rare co-localization of LMP2 and LMP7 mRNA with Map2-postive neurons

FISH analysis and immunocytochemistry in WT mouse primary cell cultures after 24 h IFN-γ stimulation (20 ng/ml) revealed occasional overlap of fluorescent signal for LMP2 and LMP7 mRNA with Map2-positive neurons (A), indicating also a induction of immunoproteasomal subunits in neuronal cells under inflammatory conditions. The close up of the confocal image displays the limited presence of LMP2 and LMP7 mRNA to the cell soma (B). Scale bar: 50 µm (A), 10 µm (B)

In additional experiments, I performed immunohistochemical stainings for LMP2 or LMP7 and the previously mentioned cell type markers after 8 d of MCAO in order to discover whether the cellular IP expression might change in the temporal course after an ischemic event. Interestingly, highest signal intensities for LMP2 as well as LMP7 were localized in the former infarct region and the penumbra region. In addition, I could observe numerous

signals for LMP2 and LMP7 in more medial parts of the sections, but however at lower signal intensity.
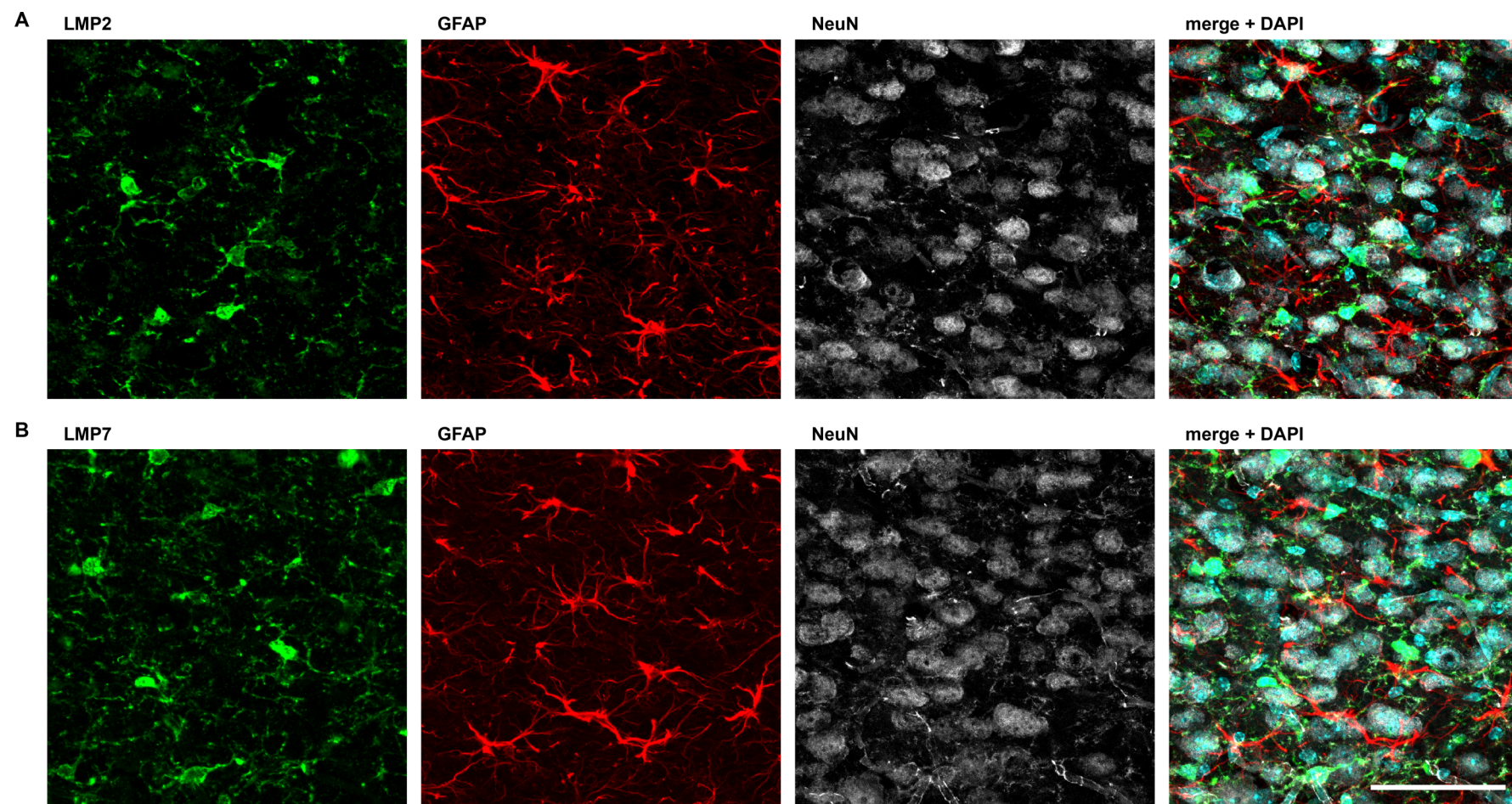
Figure 21: Cellular localization analysis of the immunoproteasomal subunits LMP2 and LMP7 after 8 d of MCAO in mouse brain sections

After 8 d of MCAO, mouse brain section were immunohistochemically stained using antibodies raised against LMP2 (A) or LMP7 (B), the astroglial marker GFAP and the neuronal nucleus marker NeuN. Signals for LMP2 and LMP7 do not co-localize with fluorescent signals for GFAP or NeuN. Scale bar of representative images: 50 µm
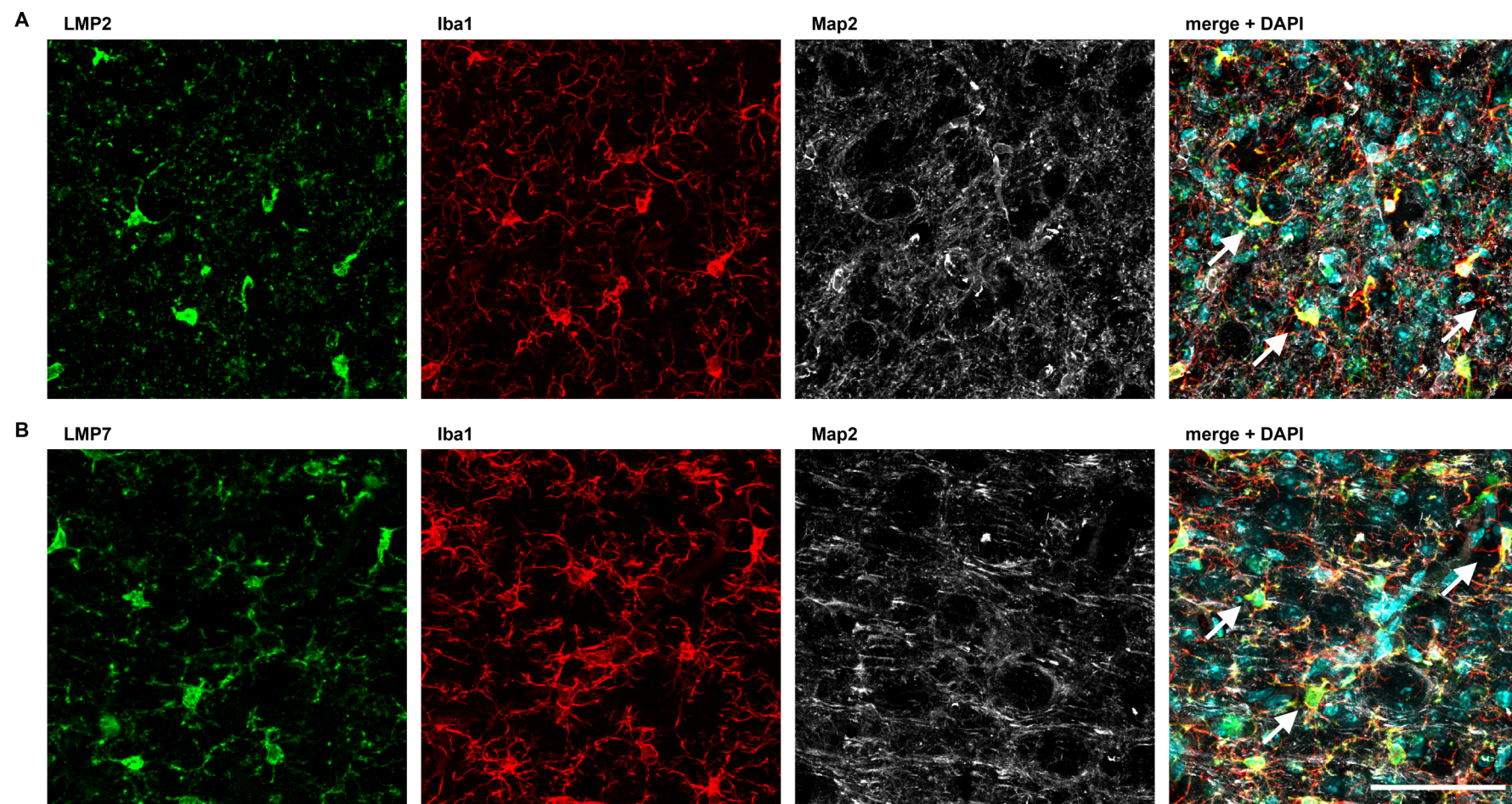
Figure 22: Cellular localization anaylsis of LMP2 and LMP7 in mouse brain sections after 8 d of MCAO

After 8 d of MCAO, mouse brain section were immunohistochemically stained using antibodies raised against the IP subunits LMP2 (A) or LMP7 (B), the microglia marker Iba1, and the neuronal marker protein Map2. Fluorescent signals for LMP2 as well as for LMP7 co-localize with Iba1-positive cells (white arrows), whereas no precise co-localization with the neuronal marker Map2 can be detected. Scale bar of representative images: 50 μm

Fig. 21 and 22 show confocal images of co-stainings for either LMP2 (Fig. 21A and 22A) or LMP7 (Fig. 21B and 22B) together with the astroglial marker GFAP, the neuronal nucleus marker NeuN, the microglial marker Iba1, and the neuronal marker Map2 in the cortical penumbra. Fluorescent signals for the IP subunits and GFAP as well as NeuN do not co-localize suggesting the absent expression of LMP2 and LMP7 in neurons or astrocytes under these conditions. In contrast, as also observed after 1 d of MCAO (compare to Fig. 13), fluorescent signals for LMP2 and LMP7 predominantly co-localize with Iba1-positive cells indicating the potential formation of IPs mainly in microglia and/or macrophages. Rare spots of closely related signals for the immunoproteasomal subunits and Map2 do not appear to be credible co-localizations, but seem to be rather more a results of superimpositions (Fig. 22).

Taken together, microglia and macrophages that feature a high expression of Iba1, especially after activation, seem to express considerable levels of the immunoproteasomal subunits LMP2 and LMP7. These cells are probably the main expressing cell type of IPs *in vivo* under the selected conditions. Moreover, the microglial expression of LMP2 and LMP7 appears to be increased in damaged tissue after an ischemic event and is maintained at least up to 8 d after MCAO. In contrast, no precise co-localization of LMP2 and LMP7 with cell type markers for astrocytes or neurons could be detected in immunohistochemical approaches. Nevertheless, an expression of the two inducible subunits in these other neural cell types is possible as observed by numerous signals for LMP2 and LMP7 on transcript level in astrocytes and, in much lower proportion, in neurons of *in vitro* cell cultures treated with the pro-inflammatory cytokine IFN-γ.

3.2.4 Distribution of LMP2 and LMP7 in subcellular fractions

For a comprehensive localization analysis the subcellular distribution of LMP2 and LMP7 was additionally assessed with biochemical approaches.

WT and LMP7$^{-/-}$ mouse brain tissue could be successfully fractionated as verified by the progressive enrichment of synaptic proteins such as PSD95, Shank2, and Synaptophysin (Fig. 23). Constitutive proteasomes are mainly located in the cytosol as described [13]. Therefore, I expected to find highest levels of LMP2 and LMP7 also in the S2 fraction and diluted these samples to avoid potential non-observance of weak signals adjacent to very strong signal intensities.
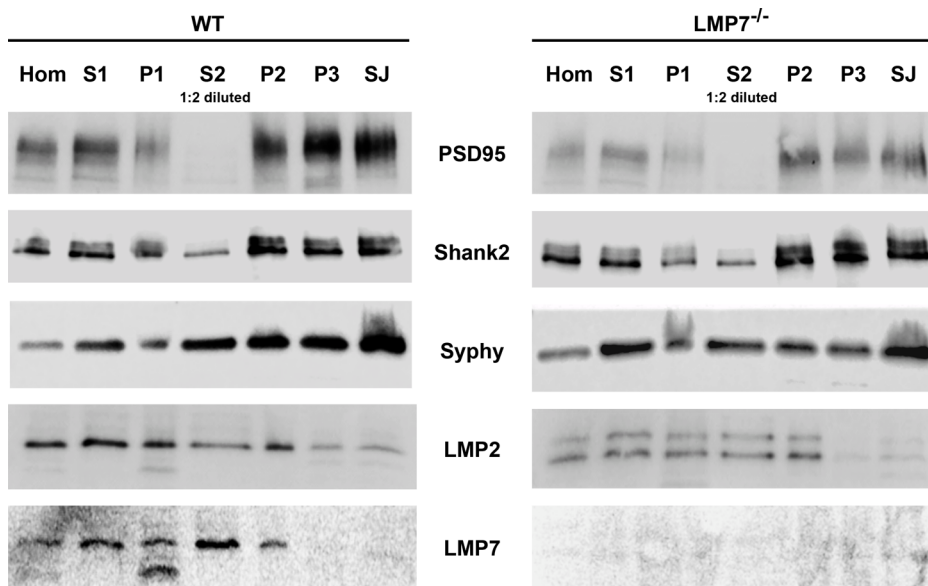
Figure 23: Distribution of immunoproteasomal subunits in subcellular fractions of the mouse brain

Subcellular fractions of WT and LMP7$^{-/-}$ mouse brain tissue were subjected to WB analysis. Increasing concentrations of the synaptic proteins PSD95, Shank2, and Synaptophysin (Syphy) verify the successful enrichment of synaptic material during the fractionation process. Immuno-reactive bands for the immunoproteasomal subunits LMP2 and LMP7 can be detected in all subcellular fractions with higher signal intensities in the first fractions containing cytosolic proteins. Hence, the S2 fraction was diluted 1:2 to avoid signal saturation. In samples of LMP7$^{-/-}$ mice, a double band for LMP2 and no signals for LMP7 were observed indicating the immature form of LMP2 and the absence of LMP7, respectively.

Hom: homogenate, S1: 1st supernatant, P1: nuclei and cell debris, S2: cytosolic-enriched fraction, P2: crude membrane fraction, P3: synaptosome-enriched fraction, SJ: synaptic junctions

Indeed, a very prominent signal for the immunoproteasomal subunit LMP7 can be detected in the WT S2 fraction. Apparent immuno-reactive bands are present in the homogenate (Hom), the 1st supernatant (S1) and the crude membrane fraction (P2), and a double band is visible in the nuclei-enriched pellet (P1). Interestingly, a very faint band for LMP7 is also present in the synaptosome-enriched fraction (P3) and the fraction of synaptic junctions (SJ). Expectedly, WBs of LMP7$^{-/-}$ samples feature no immunoreactivity for the applied LMP7 antibody. In addition, LMP2 seems to be present in all fractions. The signal intensities point towards similar amounts of LMP2 from the homogenate (Hom) up to the crude membrane fraction (P2) in both genotypes, whereby LMP7$^{-/-}$ samples exhibit immuno-reactive double bands. However, very weak signals for LMP2 can be also detected in fractions enriched with synaptic material. The results indicate a putative localization of IPs also in distal parts of dendrites and potentially synapses.

3.3 Functional Relevance of LMP7 in cerebral ischemia

In order to analyze the impact of LMP7 expression and the proper IP formation in the brain under pathophysiological conditions, including neuroinflammation and neuronal

damage, I quantified the infarct volume in WT and LMP7^{-/-} littermates after 1 and 2 d of MCAO. Furthermore, I performed an adhesive tape removal test after Bouet et al. (2009) in WT and LMP7^{-/-} littermates to examine potential long-term sensorimotor deficits after MCAO. Additionally, I monitored the temporal development of the infarction in littermates of both genotypes after MCAO over a period of 2 weeks in collaboration with the research group of Prof. Dr. F. Angenstein (Functional Neuroimaging group, DZNE, Magdeburg). Moreover, immunohistochemical stainings of WT and LMP7^{-/-} brain sections were compared after 8 d of MCAO for their presence of Iba1- and GFAP-positive cells, as the recruitment of peripheral myeloid cells to the brain, beside microglia as well as proliferating glia cells, are supposed to play an important role in the context of putative neural tissue preservation after an ischemic event [223]–[226]. As before, littermates were used to keep the micro- and macromilieu as comparable as possible.

3.3.1 LMP7 expression in microglia restricts the necrotic area after MCAO

The MCAs of adult WT and LMP7^{-/-} mice were occluded as schematically shown in Fig. 24A. After 1 and 2 d of MCAO, mouse brains were collected and infarct volumes were measured using histochemical approaches and subsequent image analysis [213].

The MCAO produced in both genotypes a clear infarct, illustrated by the pale area after Cresylviolet staining (see Fig. 24). The infarct area starts in the cortex and spreads from the striatal to hippocampal parts of the brain, whereas no infarct was seen in sham-operated animals (Fig. 24B). As there was no gender effect observed within the two genotypes, female and male animals were combined. The infarct volume amount on average between 7 - 10 % of the total brain volume. Interestingly, a slightly increased infarct volume can be observed in the LMP7-deficient mice already after 1 d of MCAO. This is massively augmented up to approximately 2.5-fold of the WT infarct volume after 2 d of MCAO with statistical significance (Fig. 24C).

Furthermore, a comparison of the infarct expansion throughout the serial brains sections revealed a trend towards a more widespread infarct in the LMP7^{-/-} mice. These results indicate an increased area of necrosis and, consequently, suggest a larger neural damage in the knockout animals compared to their WT littermates upon an ischemic event.
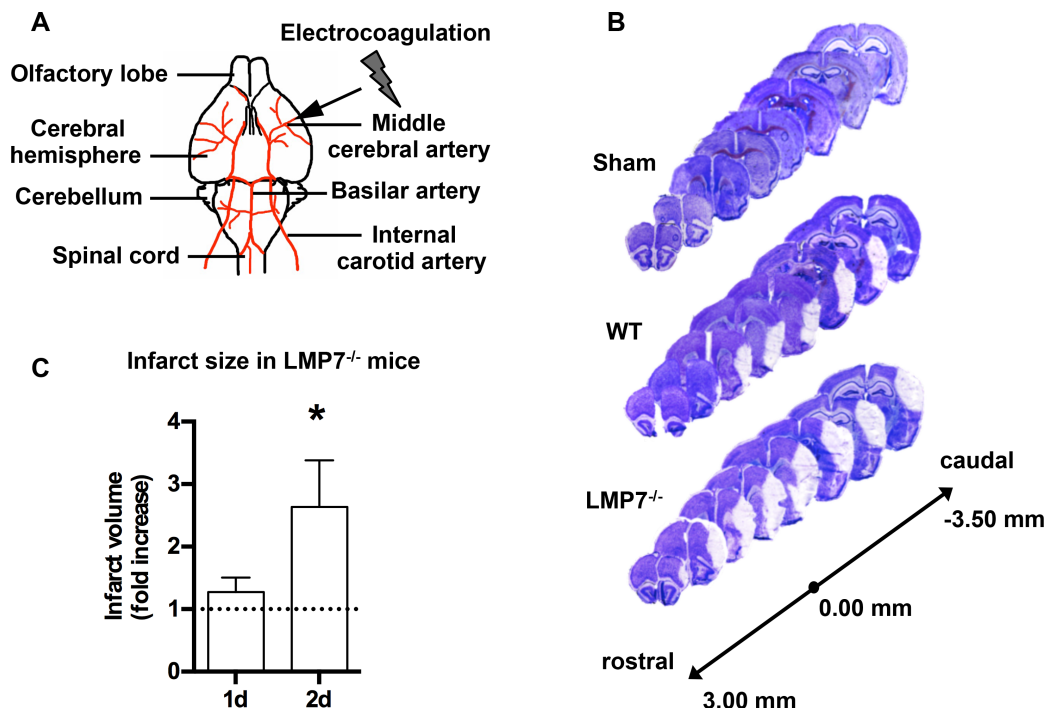
Figure 24: Increased infarct size in LMP7$^{-/-}$ mice after MCAO

MCAs of WT and LMP7$^{-/-}$ littermates were occluded as schematically shown in A on the ventral side of the brain for 1 and 2 d. Living cells of coronal brain sections were immunohistochemically stained with Cresylviolet (B), representative serial sections are shown. Notably, no pale area, usually indicating the infarct region, could be observed in sham-operated animals. In contrast, serial LMP7$^{-/-}$ mouse brain sections exhibit a larger and more expanded infarct compared to the WT. The infarct volume of LMP7$^{-/-}$ mice, normalized to WT littermates, is significantly increased after 2 d up to approximately 2.5-fold (C).

Presented data are mean ± SEM, expressed as fold increase of the infarct volume in LMP7$^{-/-}$ mice normalized to WT littermates, n=17 per time point and group, statistical analysis was done using one-way ANOVA with Dunnett´s multiple comparisons test, *: adjusted p=0.0257.

3.3.2 LMP7 limits sensorimotor deficits after cerebral ischemia

Concerning the increased neural damage in LMP7$^{-/-}$ mice after MCAO, I questioned whether these mice would consequently exhibit increased sensorimotor deficits. The adhesive tape removal test after Bouet et al. (2009) is an established method to evaluate potential long-term sensorimotor deficits after MCAO and, hence, was used in the subsequent evaluation of functional consequences of LMP7-deficiency after MCAO.

For this analysis, exclusively mice showing similar recognition and removal times at both paws in the training were subjected to the test session after 1 d of MCAO. As there were no differences in the performance between male and female mice, animals of both sexes were combined for the statistical analysis. In the training sessions, no statistical significant differences for the time to recognize and remove the tape were detected between WT and LMP7$^{-/-}$ mice. However, there seems to be a slight tendency that LMP7$^{-/-}$ mice require more time to fulfill the task (Fig. 25).
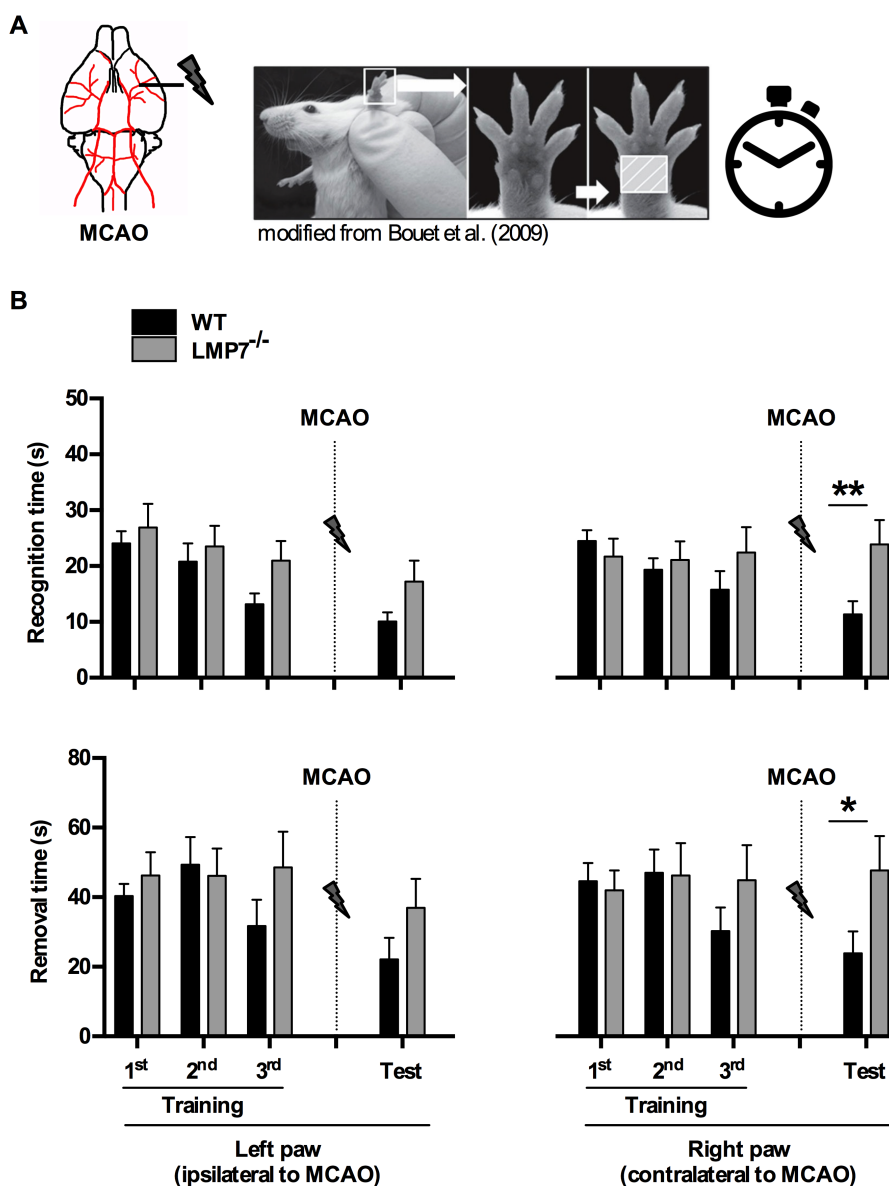
Figure 25: Sensorimotor deficits in LMP7$^{-/-}$ mice after MCAO

An adhesive tape removal test after Bouet et al. (2009) with WT and LMP7$^{-/-}$ littermates was performed after 1 d of MCAO (A). LMP7$^{-/-}$ mice show a slight tendency towards increased recognition and removal times already in the training sessions for both paws (B). After 1 d MCAO, LMP7$^{-/-}$ mice required significantly more time to recognize and remove the tape at their right paw, which is contralateral to the side of MCAO. The worsened performance could indicate stronger sensorimotor impairments in LMP7$^{-/-}$ compared to the WT.
Presented data are mean ± SEM, n=22 for recognition time and n=18 for removal time, statistical analysis was done using multiple t-tests, **: p=0.0076, *: p=0.0449.

After MCAO, LMP7$^{-/-}$ mice display an inferior performance compared to their WT littermates clearly needing more time for recognition and removal of the tape from both fore paws. Thereby, the differences were statistical significant at the right paws, those at

the impaired, contralateral side to MCAO. The prolonged recognition and removal time in LMP7$^{-/-}$ mice could state more severe sensorimotor deficits in these animals compared to the WT littermates, probably due to larger infarct areas measured after MCAO in the LMP7$^{-/-}$ mice (compare to Fig. 24).

3.3.3 LMP7 does not influence temporal development of the infarction

The spatiotemporal development of the infarct region after an ischemic event and the accompanying changes in cell composition of this tissue are still not fully understood [224], [227], [228].

Based on the previous results, the question arises whether both genotypes exhibit the same speed in infarct retrogression after cerebral ischemia. In order to compare the progression of the infarct area in WT and LMP7$^{-/-}$ mice after MCAO, a small study using MRI scans with each two animals per genotype was conducted (in collaboration with the research group of Prof. Dr. F. Angenstein).

The MCA was occluded as described above and MRI measurements were performed after 1, 6 and 14 d of MCAO. A series of anatomical T_2-weighted images was obtained (Fig. 26) and analyzed.
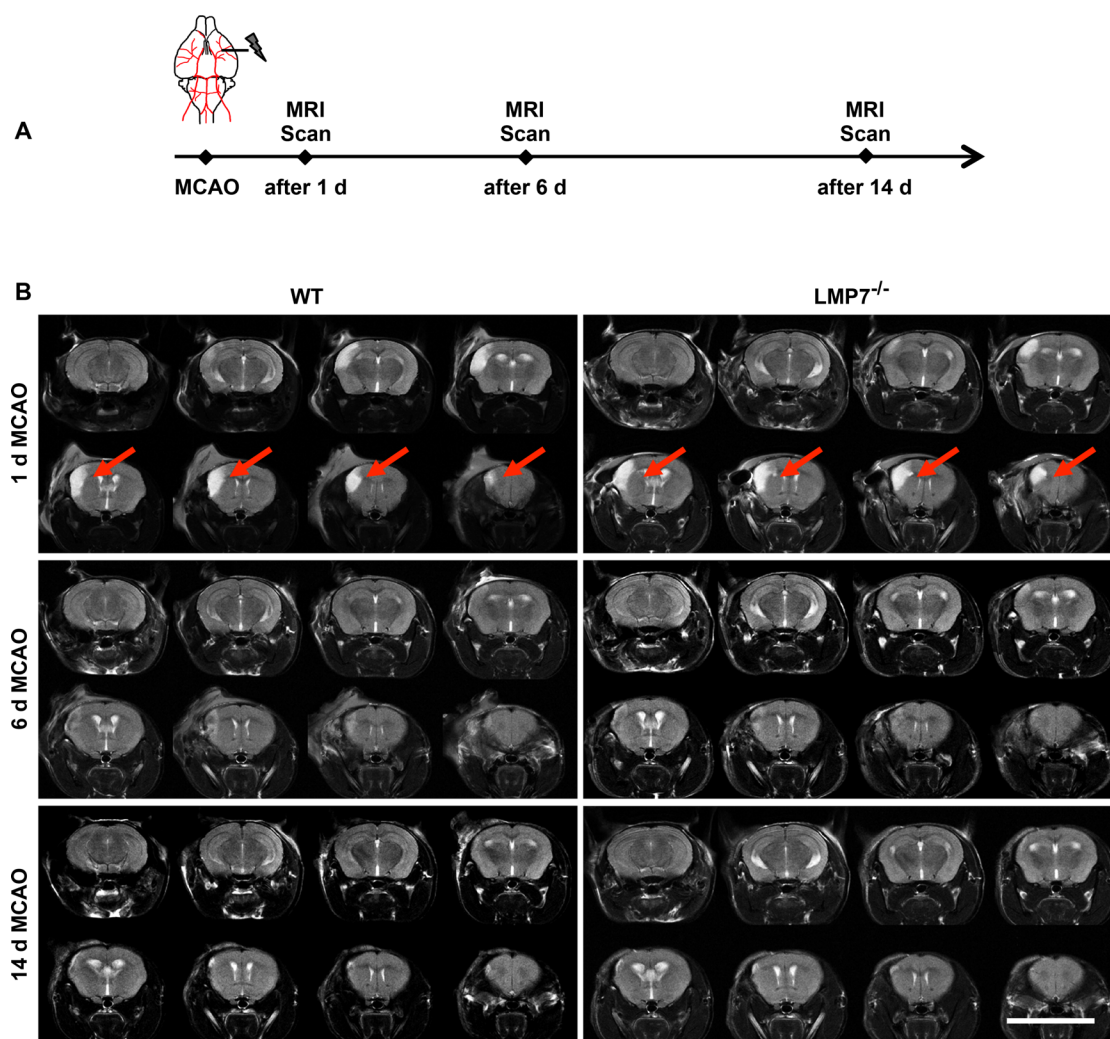
Figure 26: Temporal development of the infarction after MCAO in WT and LMP7$^{-/-}$ mice

The infarct progression in WT and LMP7$^{-/-}$ mice was assessed by MRI scans over 14 days after MCAO (A) (in collaboration with Prof. Dr. F. Angenstein and K. Krautwald, Functional Neuroimaging group, DZNE, Magdeburg).
After 1 d of MCAO, both genotypes exhibit an area of higher signal intensities in coronal T_2-weighted anatomical images in the left cortex, especially in striatal parts of the brain, indicating the infarct area (see arrowheads in B). The infarct regression is similar in WT and LMP7$^{-/-}$ mice, showing a rather fading and small infarct region after 6 d and nearly no differences in signal intensities compared to the surrounding tissue after 14 d of MCAO. Scale bar: 1 cm

In both genotypes an area with bright signal intensity indicating altered tissue properties is observed in the left cortex, which is the ipsilateral side of MCAO. On this basis, one can assume that this region is the infarct area and presumably displays an edema. The size of this area seems to be slightly reduced in the WT animals after 1 d of MCAO, which coincides with the result of the measurement of the infarct volume (compare to 3.3.1), but was not further quantified. The retrogression of this area over the defined time period was similar in both genotypes. After 6 d of MCAO, the originally high signal intensity of the infarct area was drastically diminished and reduced to a minimum in size. This result indicates comprehensive changes in the tissue properties of the infarct and edema region.

A last MRI scan was performed after 14 d of MCAO, at which pronounced signals cannot be observed anymore and the former infarct region is comparable to the adjacent tissue in both genotypes.

However, from the above experiments no information about the cell composition can be obtained. Therefore, I performed immunohistochemical staining using antibodies raised against cell type specific marker proteins in WT and LMP7^{-/-} brain sections after 8 d of MCAO in order to capture the time point at which the immune system changes to an anti-inflammatory phenotype and cellular tissue repair processes are initiated [228], [229]. In both genotypes, Iba1-positive cells with a rather round-shaped morphology were predominantly detected in the former infarct area (Fig. 27 and additional in color in Fig. S3). Apparently, all sections exhibited high Iba1-signal numbers and intensities, whereas these values seem to be increased in the LMP7^{-/-} mice compared to the WT. In addition, Iba1-positive structures within the LMP7^{-/-} animals are located in close proximity and seemed to build a cluster formation. In sections, which were immunohistochemically stained for GFAP, I detected most signals surrounding the initial infarct area after 8 d of MCAO. In both, WT and LMP7^{-/-} mice, there are a high number of GFAP-positive cells that feature strong signal intensity and a ramified morphology indicating the presence of activated astrocytes. According to these observations and their location, the GFAP-positive cells seem to form a border around the previous infarct area also known as "reactive gliosis" [230]. In more medial parts of the sections, further GFAP-positive cells can be detected but in lower numbers and with decreased signal intensities. Taken together, these results suggest a similar participation of astroglia in the process of neuroinflammation for both genotypes. Fluorescent signals for neuronal cell type markers such as NeuN and Map2 were not detected in the former infarct area of WT and LMP7^{-/-} mouse brain sections after 8 d of MCAO (data not shown).

A

Region of image aquisition

8 d MCAO

B

WT   LMP7$^{-/-}$

Iba1 fluorescence

GFAP fluorescence
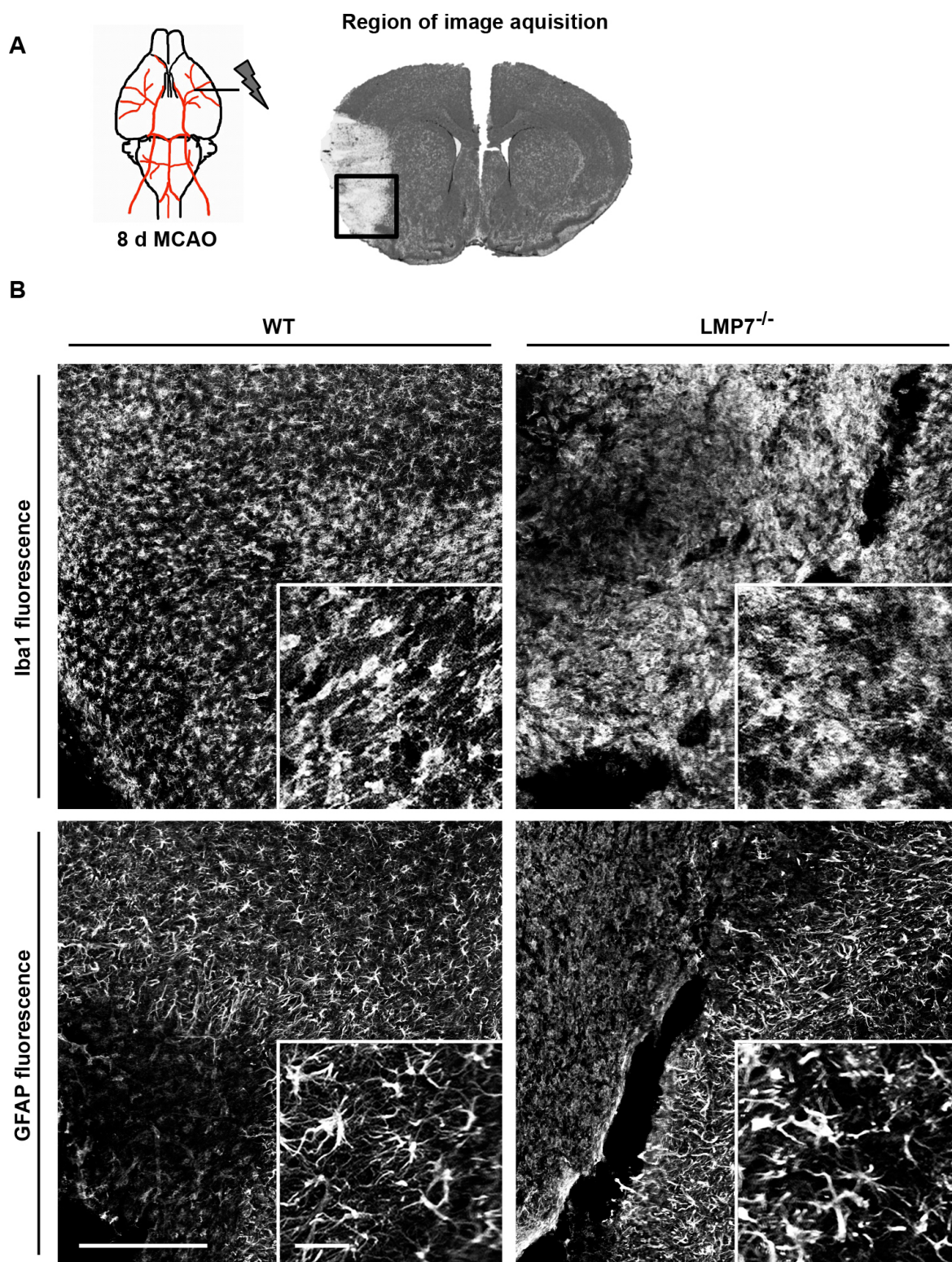
Figure 27: Cell composition in the precedent infarct area after 8 d of MCAO

Immunohistochemical stainings after 8 d of MCAO and subsequent microscopy of the former infarct area (A) reveal the presence of mainly Iba1-positive cells, whereas the number and morphology of these cells seems to differ in WT and LMP7$^{-/-}$ mice. Iba1-positive cells in the LMP7$^{-/-}$ brain sections exhibit more and higher signal intensities and appear more bloated (B). Fluorescence signals for GFAP appear similar in the two genotypes and indicate a high number of reactive astrocytes mainly around the precedent infarct region (B). Scale bar: 250 µm, 100 µm

Taken together, the results indicate the expression of LMP7 seems to have an influence on the outcome of an ischemic event. LMP7 deficiency leads to an increased neural damage and sensorimotor deficits as well as to apparent changes in the number of Iba1-positive cells located at the site of the ischemic injury after 8 d of MCAO. In contrast, the temporal retrogression of the brain tissue seems to be unaffected by LMP7-deficiency, at least at the selected time points.

3.4 Induction of IP subunit expression after cerebral ischemia

The enhanced expression of IPs after the release of inflammatory cytokines such as IFN-y has been well investigated [20], [22], [231], [232]. Here, I asked, how an ischemic stroke that evokes a neuroinflammatory situation alters the expression of standard proteasomal and immunoproteasomal subunits in the mouse brain, which has not been addressed yet. Therefore, the expression levels of LMP2 and LMP7 were examined in immunohistochemically stained mouse brain sections and quantified via semi-quantitative WB analysis of mouse brain tissue samples after MCAO. The LMP2 and LMP7 counterparts of the constitutive standard proteasome subunits β1 and β5 were additionally measured using semi-quantitative WB analysis. In order to analyze a putative regulating effect of the different catalytically active β subunits on each other, I compared samples from WT and LMP7$^{-/-}$ mice with each other.

3.4.1 IP subunits are upregulated after cerebral ischemia

WT and LMP7$^{-/-}$ mice were subjected to MCAO over a period of 2 and 0-4 days as described above and the brains processed for immunohistochemistry and WB analysis. For the detection of protein levels via WB, the brains were separated into damaged and intact hemisphere.

In coronal brain sections, the signal intensities for LMP2 and LMP7 in a selected region of the damaged hemisphere were compared to the corresponding region of the intact hemisphere and to sham-operated animals (Fig. 28). In the penumbra of the damaged hemisphere of WT brain sections, a large number of LMP7 positive cells with high intensity can be observed. In the intact hemisphere of these sections, signals for LMP7 appear in a clearly reduced number of cells and signal intensity.

A very similar observation was made for the distribution of LMP2 signals in WT brain sections, although the signal intensity for LMP2 is slightly reduced compared to the LMP7 signal strength. Due to similar fluorescent signal numbers and intensities for both immunoproteasomal subunits in sham-operated brain sections as well as in intact hemispheres of the brain sections, a clearly increased basal expression of LMP2 and LMP7 in damaged tissue, exposed to an inflammatory challenge, can be assumed.

Due to the impression of overall lower signal intensity for LMP2 in LMP7$^{-/-}$ brain sections, the expression of LMP2 generally seems to be reduced in the penumbra of the damaged hemisphere and to a smaller extent also in the intact hemisphere as well as in sections of sham-operated animals compared to the WT samples. This observation points towards an effect of the LMP7-deficiency on the basal as well as induced expression of LMP2. Nevertheless, an increase in LMP2 signal strength of the damaged hemisphere compared to healthy tissue could be observed within LMP7$^{-/-}$ mice too. For a quantitative assessment of LMP2 and LMP7 expression levels within this context, WB analysis was performed (compare to Fig. 29 and 30.)
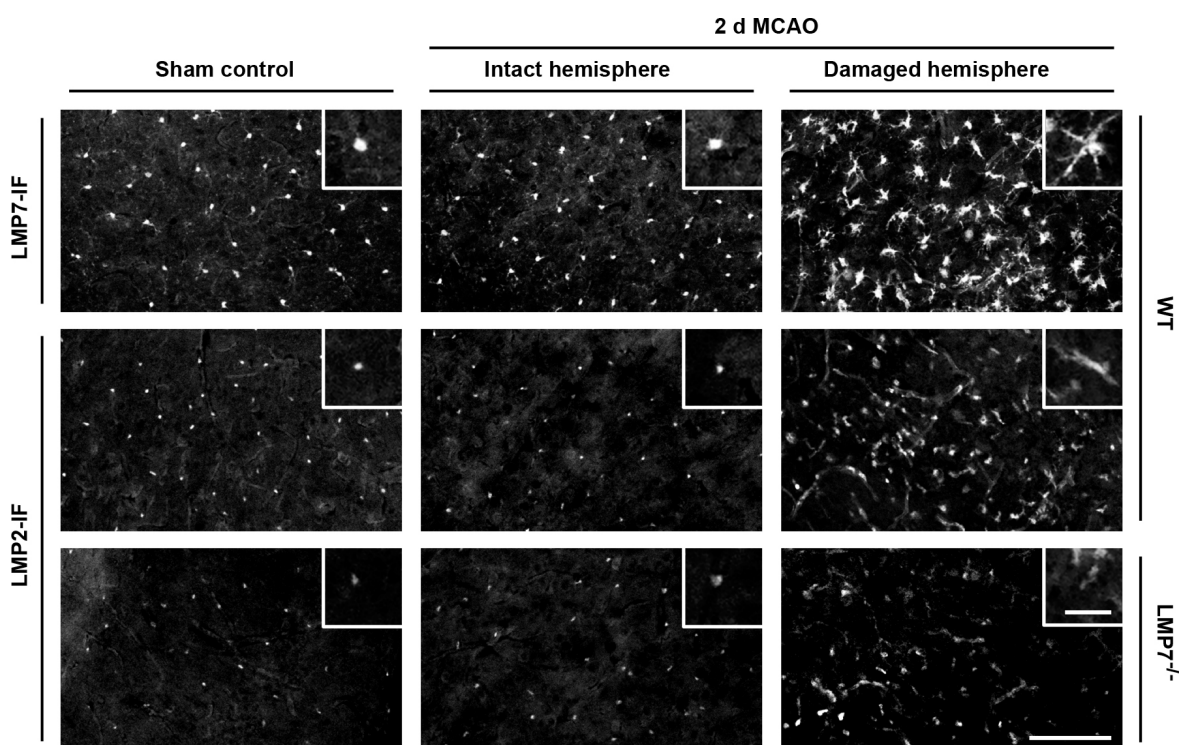
Figure 28: Increased signal intensities for LMP2 and LMP7 in the damaged mouse brain tissue

Depicted are representative immunohistochemical stainings against LMP2 and LMP7 of WT and LMP7$^{-/-}$ brain sections after 2 d of MCAO and sham-operation. Signals intensities for the immunoproteasomal subunits are massively increased in the damaged hemisphere compared to the intact one and the sham control, which apparently exhibit equal expression levels. Compared to the WT, signals for LMP2 appear slightly reduced in the LMP7$^{-/-}$ sections.
Scale bar: 100 µm, 10 µm, IF: immunofluorescence

Furthermore, signals in the damaged hemisphere are suggestive of a LMP2 and LMP7 expression in all compartments of the positively stained cells including distal processes, whereas in the intact hemisphere the expression is limited to the cell somata. The results of the immunohistochemically studied brain sections could be confirmed by semi-quantitative WB analysis.

After MCAO the expression levels of LMP2 and LMP7 are increased in the damaged hemisphere compared to the intact hemisphere up to 4 days after MCAO (Fig. 29).
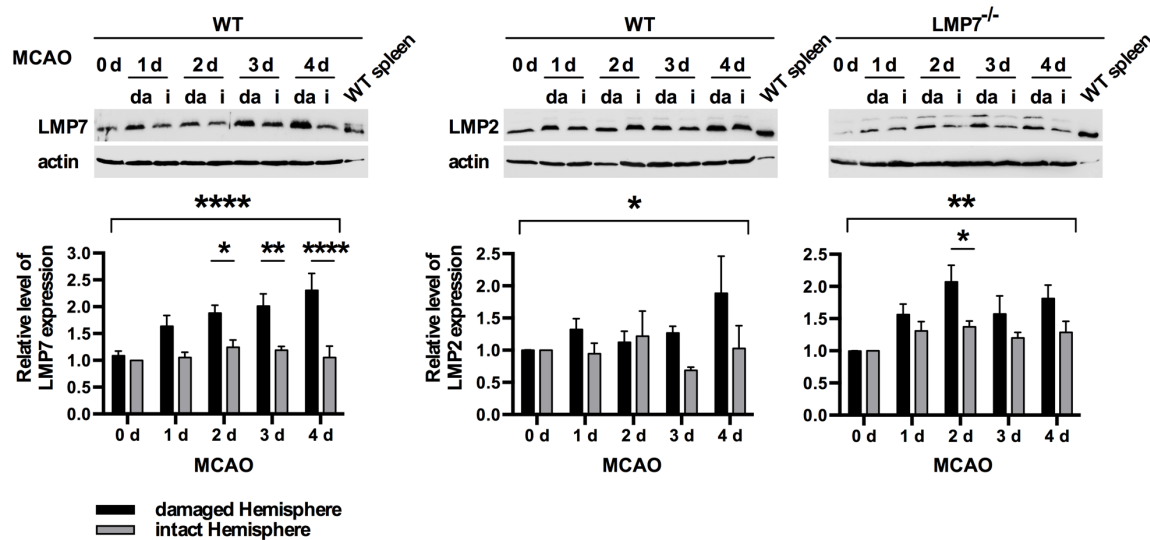
Figure 29: Upregulation of immunoproteasomal subunits after MCAO in the mouse brain

WT and LMP7$^{-/-}$ mice were subjected to MCAO for 1-4 d or 0d, i.e.sham-operation. Subsequently, collected mouse brain samples were biochemically processed and analyzed via semi-quantitative WB analysis. The signal intensities of LMP7- and LMP2-immuno-reactive bands were quantified and analyzed for comparison of protein expression levels in the damaged and intact hemisphere. Overall, the expression levels of LMP7 and LMP2 differ significantly between damaged and intact hemisphere of WT mice whereby both immunoproteasomal subunits are upregulated in the damaged hemisphere. Similarly, LMP2 is increased in the damaged compared to the intact hemisphere of LMP7$^{-/-}$ mice. Notably, the LMP2 signal is showing a double band in WB (pointing towards the detection of the premature and mature form of the protein) and seems to be reduced in LMP7$^{-/-}$ mice in comparison to the WT.
Presented data are mean ± SEM, n=4-5, statistical analysis was done using two-way ANOVA (****: p<0.0001, *: p=0.0298, **: p=0.0015) with Sidak´s multiple comparisons test (*: adjusted p=0.0376 and p=0.0297, **: adjusted p=0.0040, ****: adjusted p<0.0001).

Related to the control samples (0 d sham-operated animals), the expression of LMP7 remains relatively stable in the intact hemisphere of WT samples. In contrast, LMP7 is massively upregulated in a continuous manner over the 4 d of MCAO in the damaged hemisphere. A similar result was observed for the expression of LMP2 in the WT, although this trend was not as clear as for the expression of LMP7. In accordance to this, I also detected an increased expression for LMP2 in the damaged hemisphere of LMP7$^{-/-}$ mice with statistical significance. The results of the immunohistochemistry and the WB analysis clearly reveal an induction of IP subunit expression, which is persistent over the chosen time period of 4 d after MCAO. This observation indicates that the increase in LMP2 and LMP7 is limited to the site of neuroinflammation in the damaged tissue of the hemisphere ipsilateral to MCAO, whereas the intact and healthy hemisphere shows no changes in whose expression levels compared to sham-operated animals.

Remarkably, WBs with the LMP7^{-/-} samples exhibits an immuno-reactive double band for LMP2, which could represent the pro- and mature form of the LMP2 protein. Additionally, LMP2 signal intensities seem to be attenuated in the LMP7^{-/-} samples in relation to the WT samples. According to this and the similar observation of reduced LMP2 signal strength using LMP7^{-/-} samples in immunohistochemistry (compare to Fig. 28), I decided to compare LMP2 expression levels in WT and LMP7^{-/-} mice.

3.4.2 LMP7 deficiency affects LMP2 expression

Biochemical samples of WT and LMP7^{-/-} mice obtained after 0-4 d after MCAO were processed for semi-quantitative WB analysis and loaded next to each other on SDS-gels (Fig. 30).

Figure 30: Decreased LMP2 levels in LMP7^{-/-} mice

Mouse brain samples were subjected to semi-quantitative WB analysis in order to compare the LMP2 expression in WT and LMP7^{-/-} mice (A). Graphs present signal intensities of the lower band predicting the mature form of the protein (B) and total protein amount of the double band (C). Actin

was used as loading control. Levels of LMP2 are clearly reduced in both hemispheres of LMP7$^{-/-}$ mice compared to the WT after 0-4 d of MCAO. Notably, samples of LMP7$^{-/-}$ mice show a pronounced doubl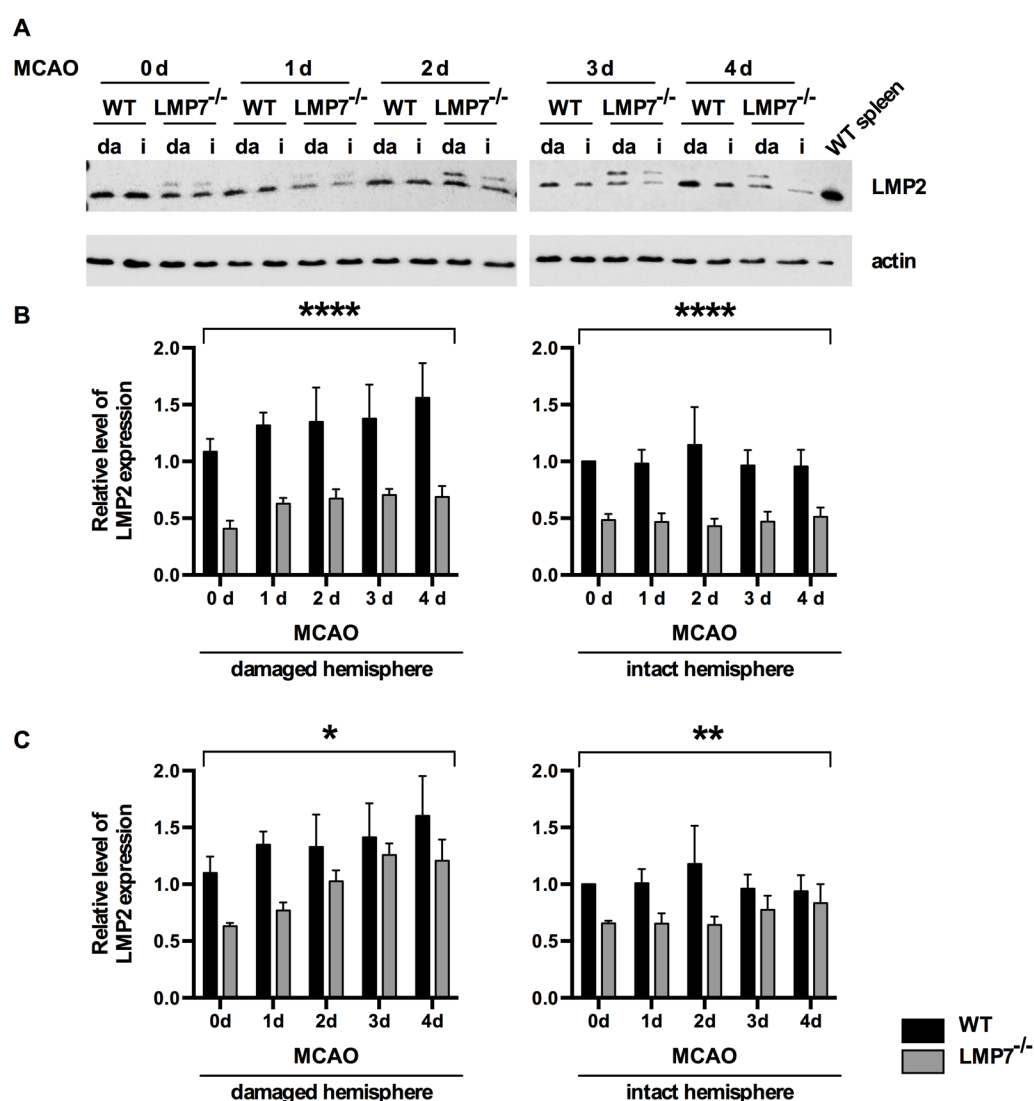e band for LMP2 in WB indicating altered processing of the immature protein. Presented data are mean ± SEM, n=4-5, statistical analysis was done using two-way ANOVA (****: $p<0.0001$, **: $p=0.0028$, *: $p=0.0132$).
da: damaged hemisphere, i: intact hemisphere

As already mentioned, in contrast to the WT, LMP7$^{-/-}$ samples exhibit a double band for LMP2, probably indicating a different ratio of the precursor and mature form of the protein. Signal intensities were measured for the lower immuno-reactive band (Fig. 30B), assuming this as the mature protein and for both immuno-reactive bands to determine the total amount of LMP2 (Fig. 30C). Expression levels of mature LMP2 are reduced in the LMP7$^{-/-}$ mice by approximately 50% compared to WT controls. This can be observed in the control condition as well as in the damaged and the intact hemisphere over the period of 4 d of MCAO. According to this, also the total protein amount of LMP2, including its precursor and mature form, was significantly reduced in both hemispheres of the LMP7$^{-/-}$ mice (Fig. 30C).

This finding suggests a clear effect of the LMP7-deficiency on the protein level and maturation of LMP2 and, hence, presumably also for the general formation of IPs.

3.4.3 LMP7 deficiency does not affect standard proteasome subunit expression

Due to the previous results, I wondered whether an impaired IP formation leads also to putative alterations in the protein levels of standard proteasome subunits, especially in the context of elevated oxidative stress as in ischemia. Semi-quantitative WB analysis of WT and LMP7$^{-/-}$ samples using antibodies raised against the proteasomal subunits β1 and β5 revealed no influence of the LMP7-deficiency on the expression levels (Fig. 31). In contrast to IP subunit expression levels, which increase over 4 d of MCAO, β1 and β5 seems to be mostly increased after 2 d of MCAO. Notably, no clear differences between the genotypes or between the damaged and the intact hemisphere could be observed. Concluding from this, LMP7-deficiency seems to have no influence on the basal expression of β1 and β5 as well as on the amount of standard proteasome in the mouse brain after an ischemic event.
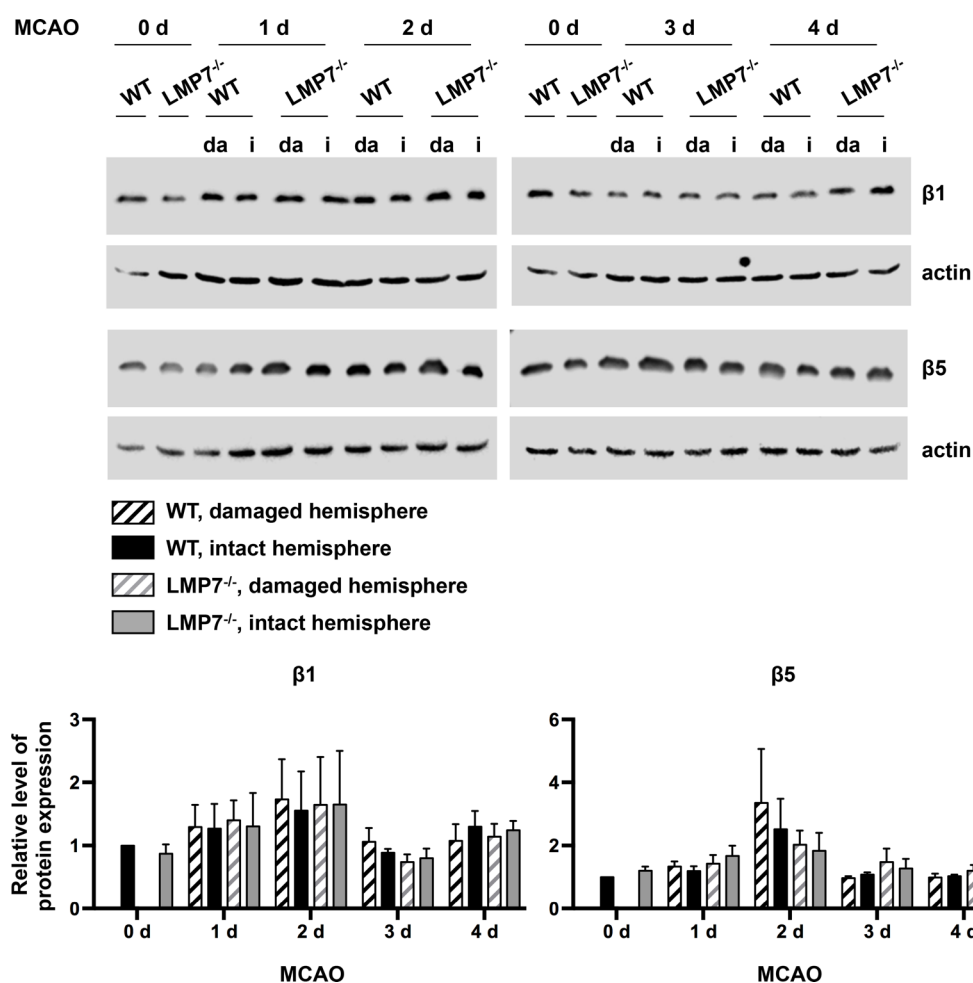
Figure 31: Expression levels of constitutive proteasomal β-subunits after MCAO

Using semi-quantitative WB analysis, expression levels of the constitutive proteasome subunits β1 and β5 were determined over a time period of 4 d after MCAO. Signal quantification displayed a trend towards increased levels of β1 and β5 after 2 d of MCAO without significant differences between the genotypes or the damaged and the intact hemisphere. Actin was used as loading control.

Presented data are mean ± SEM, n=4-5, statistical analysis was done using two-way ANOVA.

da: damaged hemisphere, i: intact hemisphere

3.4.4 LMP7 deficiency does not affect expression levels of ubiquitinated proteins

As a further consequence of the previous findings, levels of ubiquitinated proteins were analyzed in WT and LMP7$^{-/-}$ samples after MCAO using WB analysis with the aim to determine possible disturbances in protein degradation processes caused by an impaired IP formation. Using an antibody (anti-FK2) that detects K^{29}-, K^{48}-, and K^{63}-linked mono- and polyubiquitinated proteins, all samples exhibit similar signal intensities on WB (Fig. 32). Semi-quantification revealed no significant differences between the damaged and the intact hemisphere comparing WT and LMP7$^{-/-}$ mice over the time course of 4 d after MCAO.
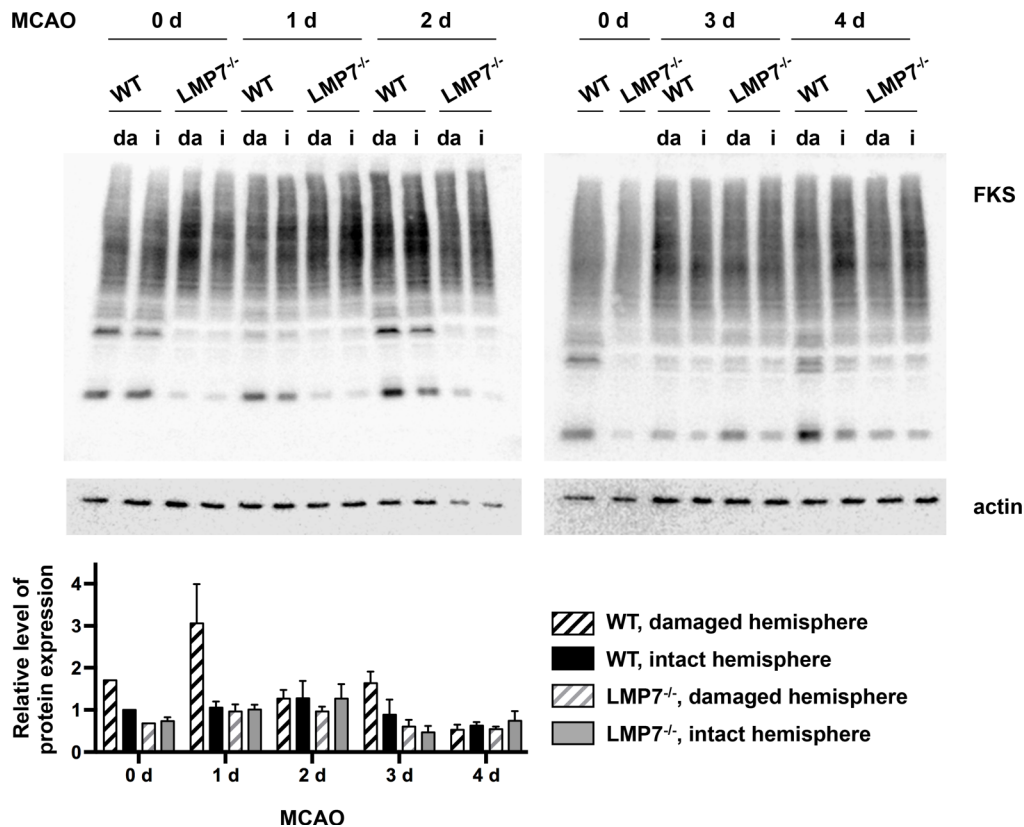
Figure 32: Levels of ubiquitinated proteins after MCAO

After 0-4 d of MCAO, brain samples of the damaged and the intact hemisphere from WT and LMP7$^{-/-}$ littermates were biochemically analyzed using semi-quantitative WB. Detection of ubiquitinated proteins was achieved with an antibody (anti-FK2) raised against K^{29}-, K^{48}-, and K^{63}-linked mono- and polyubiquitinated proteins. Signal quantification showed no obvious changes in the amount of ubiquitinated proteins comparing both genotypes over this time period of MCAO. Presented data are mean ± SEM, n=4-5, statistical analysis was done using two-way ANOVA.
da: damaged hemisphere, i: intact hemisphere

Concluding from that, the pool of ubiquitinated proteins appears to be comparable between WT and LMP7$^{-/-}$ mouse brain tissue during the early phase after an ischemic event.

Taken together, these data display a massive induction of IP subunit expression after cerebral ischemia. Interestingly, LMP7 seems to exert an influence on the expression of LMP2 in the healthy brain as well as after cerebral ischemia. In contrast, a lack of LMP7 has no impact on the expression of constitutive standard proteasome subunits and levels of ubiquitinated proteins in the context of cerebral ischemia.

3.5 Impact of LMP7 on microglia and myeloid cells after cerebral ischemia

Taken into account that on the one hand microglial cells seem to be the main producing cell type of IPs in the brain and on the other hand infiltrating immune cells from the periphery constitutively express immunoproteasomal subunits after an ischemic event, the influence of an impaired IP formation on these cells, including putative consequences on

inflammatory processes, are of great scientific interest. Therefore, the cell recruitment of myeloid subpopulations to the brain after MCAO was examined in collaboration with the research group of Prof. Dr. Ildiko Dunay using FACS analysis. Microglia cells and their expression of activation markers as well as their morphology were analyzed in more detail in both, WT and LMP7$^{-/-}$ mice. Additionally, the expression of selected cytokines was measured on transcript level.

3.5.1 LMP7 affects the cell recruitment to the infarct area after cerebral ischemia

After 1 d of MCAO brains of WT and LMP7$^{-/-}$ littermates were separated into three regions including the infarct area, the remaining damaged hemisphere, and the intact hemisphere (Fig. 33A), and subsequently subjected to FACS analysis(ref.). Alive single cells were determined first by, forward and side scatter and second by singlet gating and subsequent exclusion of dead cells (gating not shown). The numbers of myeloid cells and microglia were gated for CD11b^{high}, CD45^{high} and CD45^{int} expression, respectively. Myeloid-derived leukocytes were further divided into Ly6G^{high} neutrophil granulocytes. The remaining population of mononuclear cells comprises Ly6C^{high} monocytes, Ly6C^{int} dendritic cells and Ly6C^{low} macrophages (Fig. 33B).

In both genotypes, density blots representing the described gating strategy for CD11b-positive cells of the damaged (Fig. S4) and intact (Fig. S5) hemispheres show no differences in the identified subpopulations. In contrast, comparing the intact hemisphere with the infarct region, numbers of myeloid cells are much more reduced indicating the invasion of peripheral immune cells including Ly6G-positive neutrophils as well as monocytes and dendritic cells into the necrotic tissue after the ischemic event. Comparing cell populations in the infarct region of WT and the LMP7$^{-/-}$ mice, numbers differ with statistical significance. Quantification demonstrates an increased number of microglia in the LMP7$^{-/-}$ mice compared to the WT animals. In contrast, myeloid cells including Ly6C^{high} monocytes, Ly6C^{int} dendritic cells, and Ly6C^{low} macrophages are significantly reduced in the knockout animals. The number of Ly6G^{high} neutrophils seems to be very similar in both genotypes (Fig. 33C). As IPs are important in antigen presenting pathways that strongly influences the activation and migration of immune cells, the results leads to the assumption of a potentially impaired recruitment of certain immune cell populations in LMP7$^{-/-}$ mice under neuroinflammatory conditions.
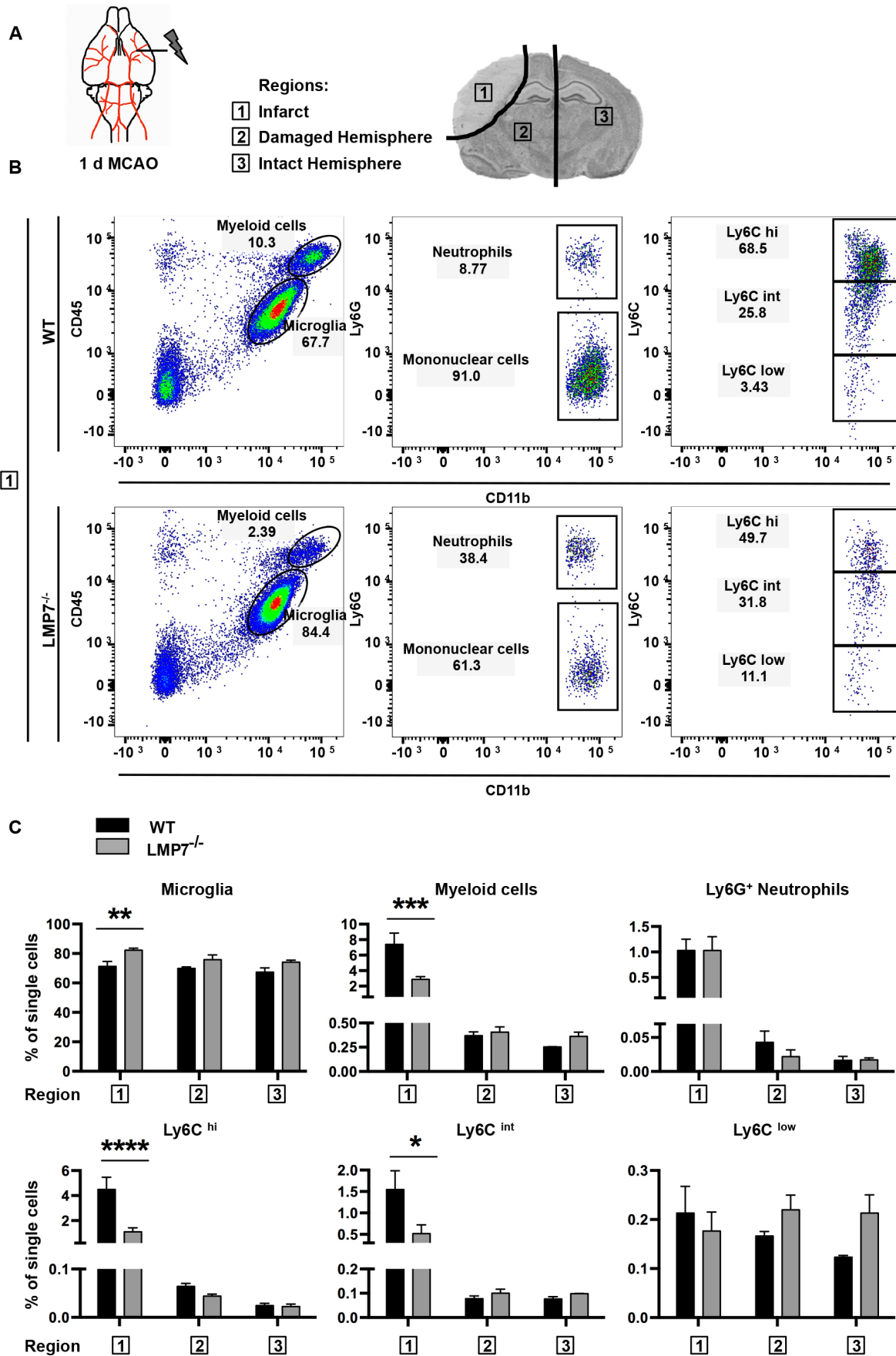
Figure 33: Microglia and myeloid cell populations in WT and LMP7$^{-/-}$ mouse brains after MCAO

After 1 d of MCAO, WT and LMP7$^{-/-}$ mouse brains were dissected into three parts as schematically shown and analyzed via FACS analysis (A). Depicted is the gating strategy for the infarct region of both genotypes (B). Density blots clearly display a reduced number of Ly6C$^{+\ high}$ and Ly6C$^{+\ int}$ cells in LMP7$^{-/-}$ animals. Further, statistical analysis revealed significantly increased numbers of CD45$^{+\ int}$ and CD11b$^{+\ high}$ microglia and decreased numbers of CD45$^{+\ high}$ and CD11b$^{+\ high}$ myeloid cells in LMP7$^{-/-}$ mice compared to the WT littermates (C).

Presented data are mean ± SEM, n=3, statistical analysis was done using two-way ANOVA with Fisher´s LSD test, **: p=0.0066, ***: p=0.0002, ****: p<0.0001, *: p=0.0106.

3.5.2 LMP7 influences microglia activation and morphology after cerebral ischemia

After the observed predominant expression of IP subunits in microglial cells, I wanted to determine the influence of LMP7-deficiency and an impaired IP formation on the phenotype of microglia after an ischemic event. Therefore, after 1 d of MCAO WT and LMP7$^{-/-}$ mouse samples were subjected to FACS analysis and CD11b-positive microglia were further analyzed for their expression of the activation markers CD45, MHCII, F4/80 and CD11c (Fig. 34). Interestingly, only in the damaged hemisphere, microglia of LMP7$^{-/-}$ mice displayed statistically significant increased levels of the surface markers MHCII and F4/80 compared to WT littermates (Fig. 34B,C) but not in any other of the examined brain regions. The expression of the positive regulator of T-cell activation CD45 and the CD11c receptor, involved in inflammatory responses, do not differ between the two genotypes or among the analyzed brain regions after 1 d of MCAO (Fig. 34C). However, in comparison to the WT, this result points towards microglia with a changed phenotype of activation in LMP7$^{-/-}$ animals during the early post-ischemic phase. In addition, the activation state of microglia is tightly connected to their morphology. Based on the either neurotoxic or neuroprotective effect upon microglia activation, two opposite types of microglia polarization can be classified: the M1 and the M2 phenotype, respectively (ref.). While M1 microglia can be found within the first 24 h after an ischemic event, microglia of the M2 phenotype are only observed after the first day of ischemia [228].
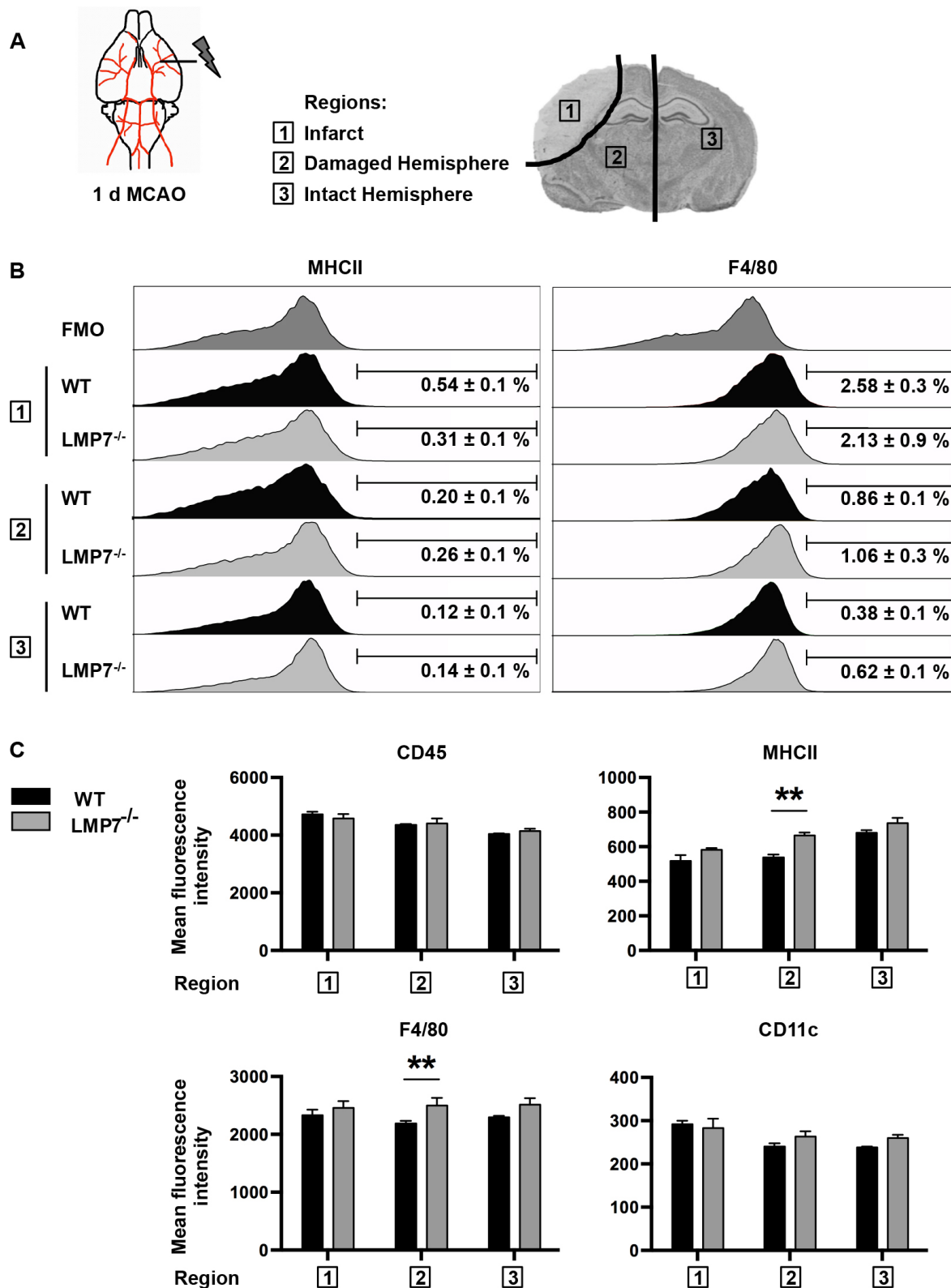
Figure 34: Expression of microglia activation marker following MCAO

WT and LMP7^{-/-} mouse brains were separated into three regions after 1 d of MCAO (A). The expression of the microglial activation markers CD45, MHCII, F4/80 and CD11c were analyzed using flow cytometry. Histograms show the representative expression level of the surface makers MHCII and F4/80 of all three regions of both genotypes in comparison to the corresponding isotype control (FMO), whereby bars represent the percentage of cells positively expressing the indicated surface marker (B). Concerning the damaged hemisphere, a statistically significant increase of the

MHCII and F4/80 expression level was determined for LMP7$^{-/-}$ mice compared to WT littermates (C). Presented data are mean ± SEM, n=3, statistical analysis was done using two-way ANOVA with Fisher´s LSD test, **: p=0.0019, *: p=0.0461.
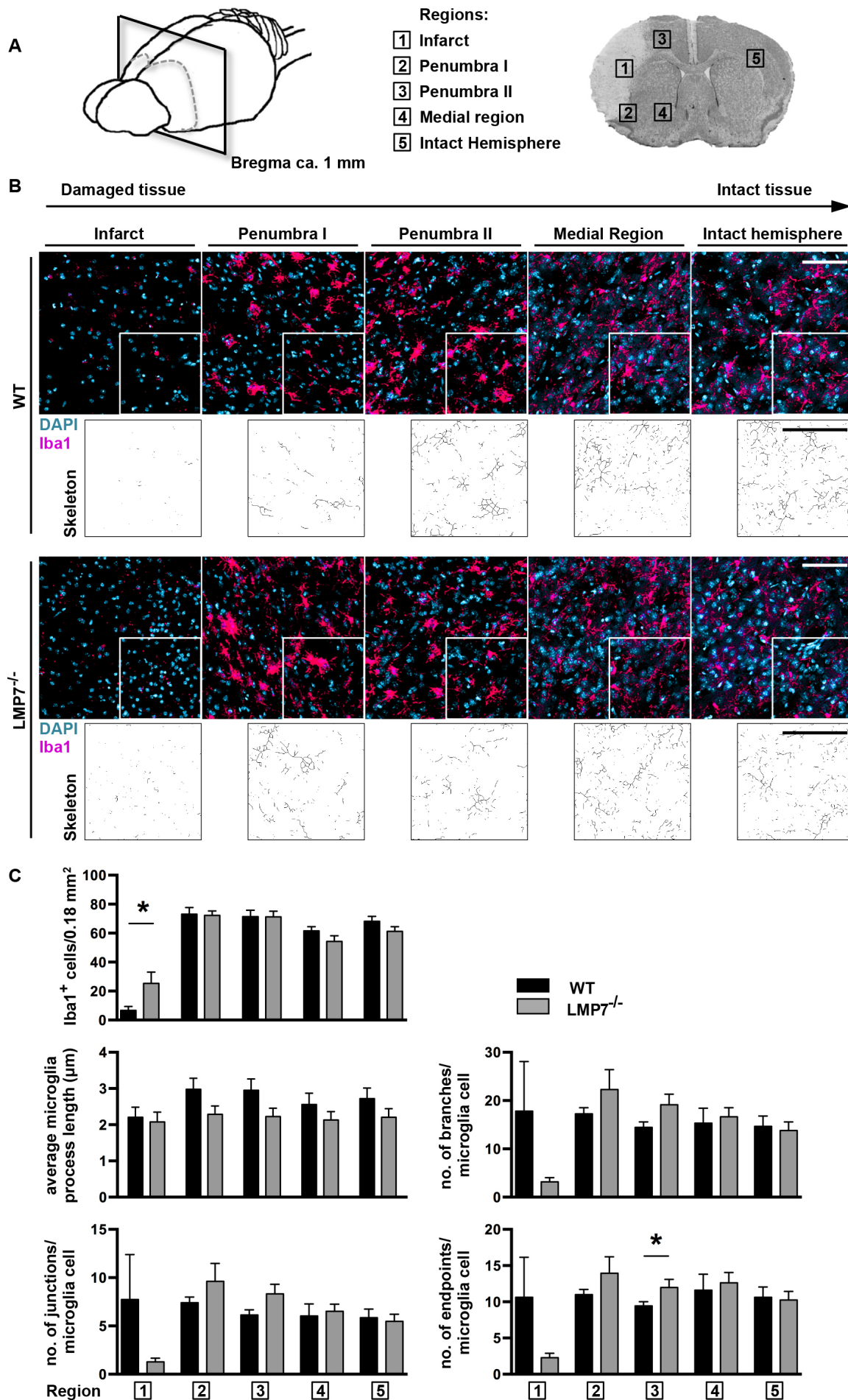
Figure 35: Skeleton analysis of microglia morphology in striatal WT and LMP7$^{-/-}$ brain sections

After 2 d of MCAO, microglia number and morphology was assessed by a Skeleton analysis after Morrison and Filosa (2013). Confocal images were taken from striatal coronal WT and LMP7$^{-/-}$ mouse brain sections (Bregma 1-0.8 mm) and acquired in relation to the infarct region as illustrated (A). Further, maximum intensity projections were generated and skeletonized using ImageJ software (B). Quantification of Iba1-positive cells and their morphological parameters revealed a higher number of Iba1-positive cells in the infarct region of LMP7$^{-/-}$ mice than in WT littermates. The average branch length seems to be reduced whereas the number of branches, junctions and endpoints/cell seems to be increased in LMP7$^{-/-}$ mice.
Presented data are mean ± SEM, n=18 out of 6 independent experiments, statistical analysis was done using Students t-test between the genotypes for each region, *: p=0.0304 and p=0.0495.
Scale bars: 10 µm

In order to obtain a comprehensive overview addressing both potential microglia phenotypes, a Skeleton analysis after Morrison & Filosa (2013) was performed 2 d post MCAO in WT and LMP7$^{-/-}$ mice. Confocal images of Iba1-positive microglia were taken from five regions including damaged as well as healthy tissue in WT and LMP7$^{-/-}$ coronal brain slices, at striatal (Bregma 1 to 0.8 mm), medial (Bregma -0.2 to -0.4 mm) and hippocampal (Bregma -1.6 to -1.8 mm) parts of the brain. As already reported in section 3.3.1, the infarct spreads from striatal to hippocampal regions and is very pronounced in rostral regions. The number of microglia and the morphological parameters including number of junctions, endpoints, and branches per microglia cell as well as the average process length were determined. Consistent with the result of the FACS analysis (compare to Fig. 33) and additionally the previously observed apparent increased number of Iba1-positive cells in immunohistochemical stainings after 8 d of MCAO (compare to Fig. 27, Fig. S3), an increased number of microglia could be observed within the infarct region of LMP7$^{-/-}$ mice compared to the WT (Fig. 35).

Notably, this trend is the opposite in more healthy areas of the tissue (region 4 and 5) from medial and hippocampal sections, where numbers of Iba1-positive cells are reduced in the knockout animals (Fig. 36 and 37). Although the variations in microglia process length between the two genotypes do not reach statistical significance a clear tendency towards shortened processes is obvious in the LMP7$^{-/-}$ animals in all assessed brain regions (Fig. 35-37C). Furthermore, the number of branches per microglia cell appears to be partially increased in LMP7$^{-/-}$ mice as seen in the penumbra (region 2 and 3) and medial parts (region 4) of striatal sections (Fig. 35C). In medial and hippocampal sections, branch numbers are rather similar in WT and LMP7$^{-/-}$ mice. Likewise, the same impression emerged for the number of junctions and endpoints per microglia cell as the mentioned parameter means are higher in the penumbra of LMP7$^{-/-}$ striatal sections compared to the WT, but similar in medial and hippocampal sections of both genotypes (Fig. 36C and 37C).

A

Regions:
1 Infarct
2 Penumbra I
3 Penumbra II
4 Medial region
5 Intact Hemisphere

Bregma ca. -0.4 mm

B

Damaged tissue → Intact tissue
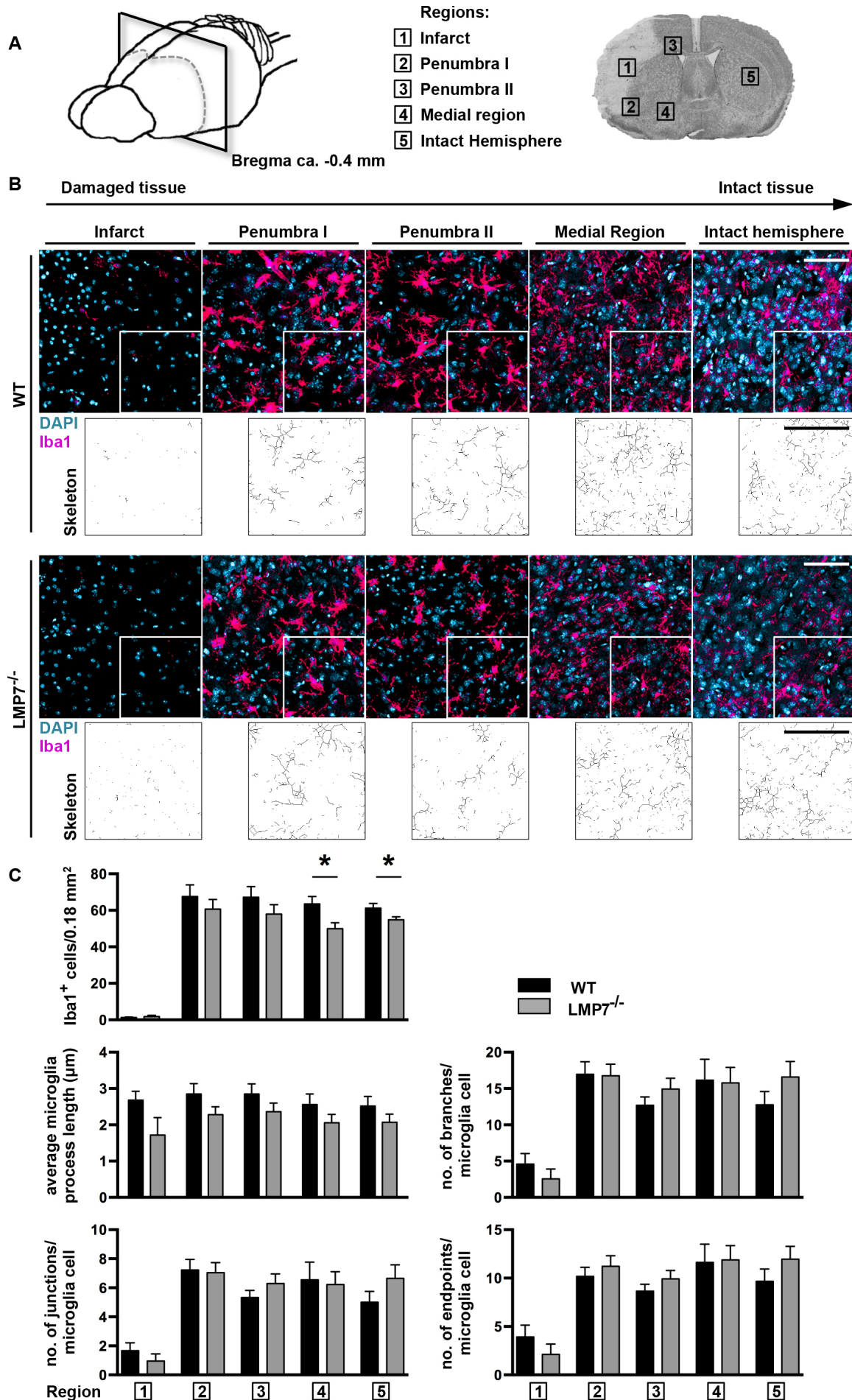
Figure 36: Skeleton analysis of microglia morphology in medial WT and LMP7$^{-/-}$ brain sections

Skeleton analysis in medial WT and LMP7$^{-/-}$ mouse brain sections after 2 d of MCAO was performed using confocal images from different areas as shown in the scheme from medial coronal brain section (Bregma -0.2 to -0.4 mm) (A). Displayed are representative confocal maximum intensity projections from assessed brain regions in WT and LMP7$^{-/-}$ mice and close ups of the skeletonized images (B). The number of microglia, indicated by Iba1-positive cells, is lower in LMP7$^{-/-}$ mice compared to the WT for all analyzed regions. Further, the average process length appears shorter in the LMP7$^{-/-}$ animals. For the number of branches, junctions, and endpoints/cell, no obvious differences between both genotypes could be detected.
Presented data are mean ± SEM, n=18 out of 6 independent experiments, statistical analysis was done using Students t-test between the genotypes for each region, *: p=0.0126, and p=0.05.
Scale bars: 10 µm

Taken together, the LMP7-deficiency and thereby an impaired IP formation seems to alter the phenotype of microglial activation and morphology after an ischemic event as indicated by the enhanced expression of MHCII and F4/80 after 1 d of MCAO as well as altered morphological parameters of microglia and/or macrophages identified via immunohistochemical Iba1-staining in neuroinflammatory regions after 2 d of MCAO in LMP7$^{-/-}$ mice. Moreover, the LMP7-deficient microglia cells appear to be more round-shaped, which would suggest a higher phagocytic state (ref.) compared to microglia from WT littermates.

A

Regions:
1. Infarct
2. Penumbra I
3. Penumbra II
4. Medial region
5. Intact Hemisphere

Bregma ca. -1.7 mm

B

Damaged tissue → Intact tissue

| Infarct | Penumbra I | Penumbra II | Medial Region | Intact hemisphere |

WT — DAPI / Iba1 / Skeleton

LMP7$^{-/-}$ — DAPI / Iba1 / Skeleton

C
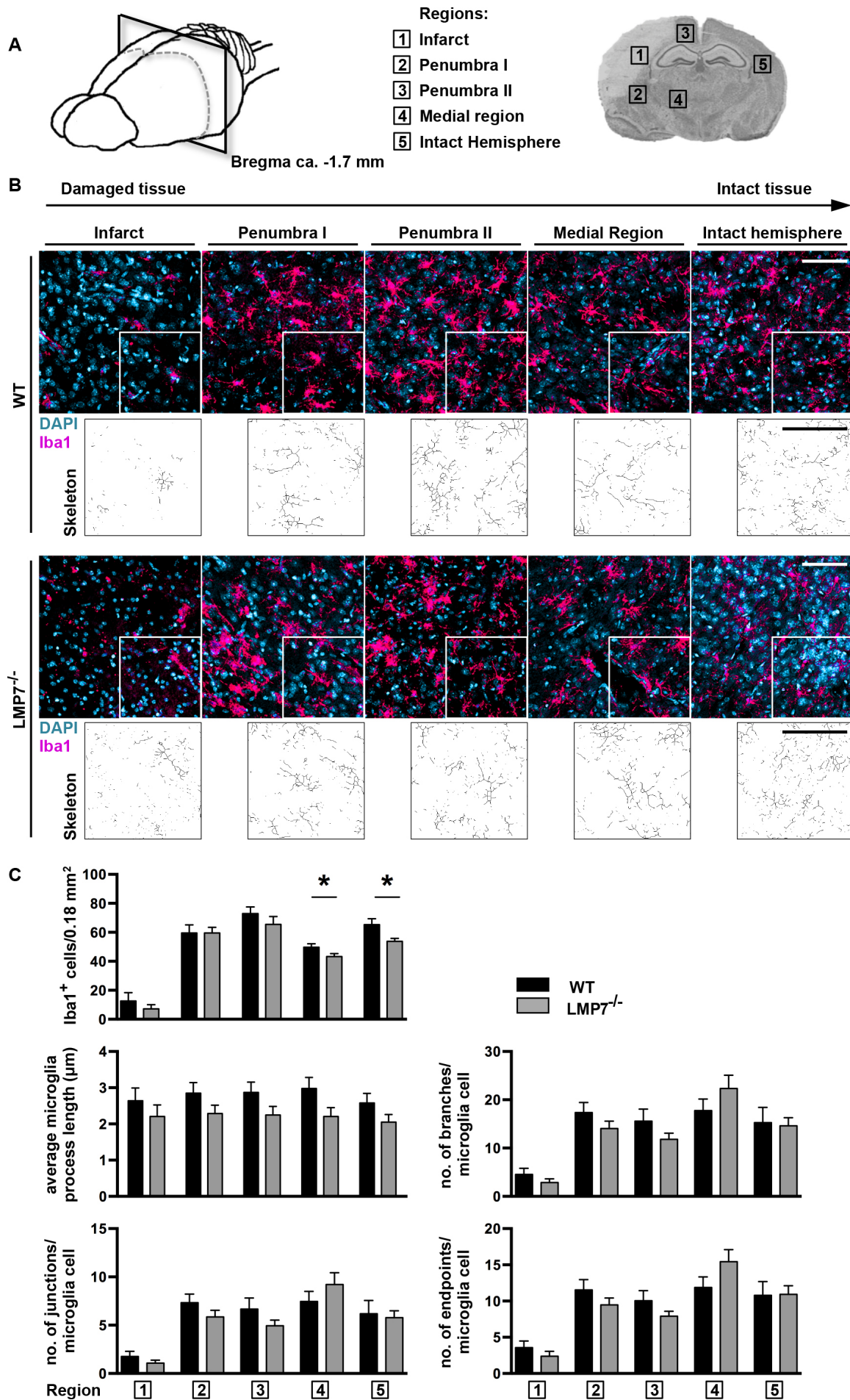
Figure 37: Skeleton analysis of microglia morphology in hippocampal WT and LMP7$^{-/-}$ brain sections

Skeleton analysis in hippocampal WT and LMP7$^{-/-}$ mouse brain sections was carried out 2 d after MCAO. Acquisition of confocal images was performed in the 5 indicated regions from hippocampal coronal brain section (Bregma -1.6 to -1.8 mm) (A). Shown are representative confocal images of WT and LMP7$^{-/-}$ brain slices after immunohistochemistry and close ups of corresponding Skeleton images (B). Decreased numbers of Iba1-positive cells were detected in medial parts of the brain and the intact hemisphere of LMP7$^{-/-}$ mice compared to the WT. In addition, the average process length of assumed microglia is shortened in the knockout animals. For the number of branches, junctions, and endpoints/cell, a trend towards reduced numbers in LMP7$^{-/-}$ mice was detected, except for the medial part of the brain (region 4).
Presented data are mean ± SEM, n=18 out of 6 independent experiments, statistical analysis was done using Students t-test between the genotypes for each region, *: p=0.047 and p=0.0153.
Scale bars: 10 µm

3.5.3 LMP7 seems to influence cytokine induction after cerebral ischemia

Cellular immune responses to pathological conditions such as brain injury commonly involve the production and release of inflammatory modulators such as cytokines. The presence of pro- or anti-inflammatory cytokines, hereby, regulates various cellular processes including cell recruitment, differentiation and induction of gene expression as well as several signaling pathways [233]–[235]. Besides this, also the expression of IPs is upregulated upon IFN-γ or TNF-α stimulation. Based on this and the previous observations that microglia seem to be affected by an impaired IP formation, a comparison of the cytokine levels in WT and LMP7$^{-/-}$ mouse brains after ischemia could reveal further effects and potential functional implications of LMP7 in this context. Thus, expression levels of the pro-inflammatory cytokines TNF- α, IL1b, IL1a and IFN- γ and the anti-inflammatory cytokines TGF-β and IL10 were determined in the infarct area, the remaining damaged hemisphere as well as in the intact hemisphere using RT-PCR (in collaboration with the research group of Prof. Dr. Ildiko Dunay). The statistical analysis revealed no significant differences for all cytokine levels in the assessed brain regions between the two genotypes. Nevertheless, as cytokines are highly potent effector molecules, already small differences could result in biological significance. Therefore, clear tendencies towards increased levels of the classical inflammatory cytokines TNF-α and IL1b as well as the healing process mediating cytokine TGF-β observed within the infarct region of the LMP7$^{-/-}$ samples should be mentioned (Fig. 38). To a smaller extent this trend seems to exist also in the damaged hemisphere. In the intact hemisphere, transcript levels of the cytokines appear to be very similar in WT and LMP7$^{-/-}$ mice, at least after 1 d of MCAO. Notably, this result fits to the previous observations of the putatively stronger activated microglia in LMP7$^{-/-}$ mice in comparison to WT littermates (compare to 3.5.2). Due to the higher release of pro-inflammatory cytokines, a consequently enhanced

activation of microglia would be expected and indeed was confirmed by other approaches (compare to Fig. 27 and sections 3.5.1 and 3.5.2).
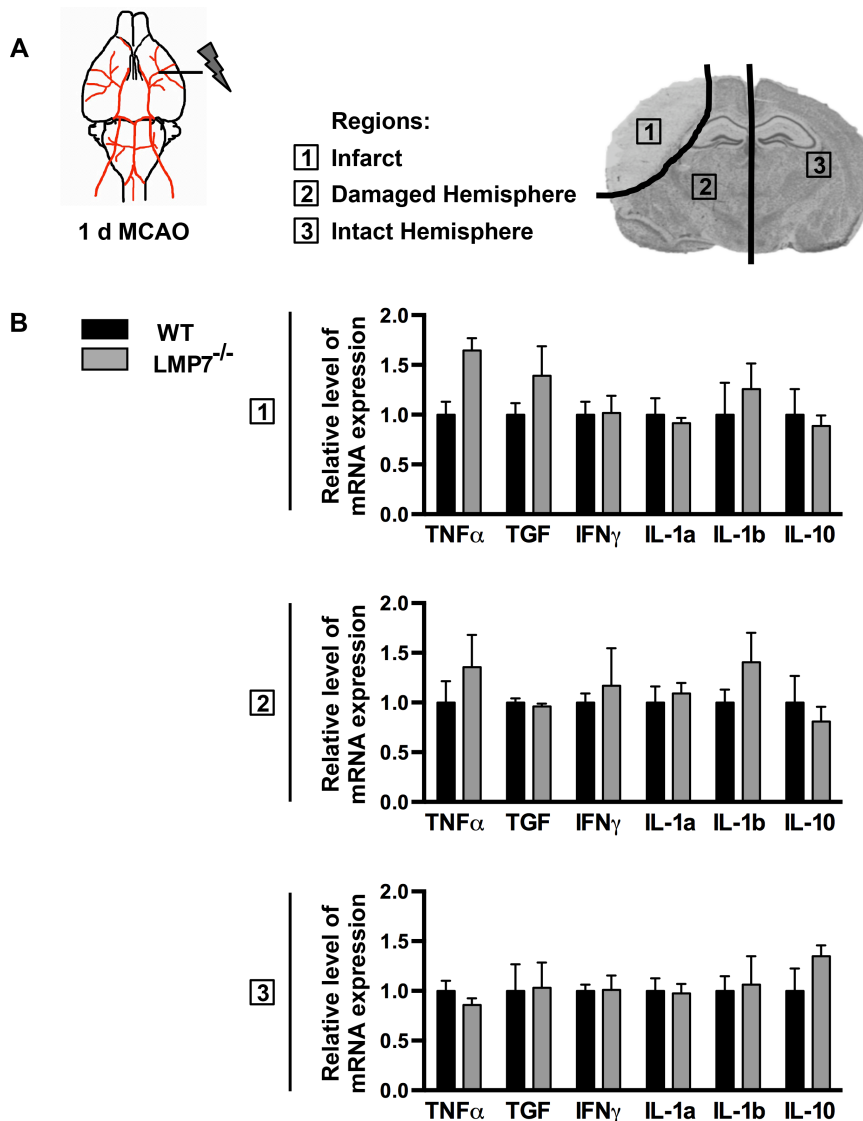
Figure 38: Cytokine production 1 d after MCAO in WT and LMP7$^{-/-}$ mice

After 1 d of MCAO, WT and LMP7$^{-/-}$ mouse brains were dissected into three parts and the relative mRNA expression levels of selected cytokines were determined using qRT-PCR (A). Comparing both genotypes, the statistical analysis revealed no significant differences but a clear trend towards increased pro-inflammatory cytokines like TNFα and IL-1b within the infarct region and to a smaller extend in the damaged hemisphere of LMP7$^{-/-}$ mice. Cytokine production in the intact hemisphere appears very similar in WT and LMP7$^{-/-}$ animals (B).
Presented data are mean ± SEM, n=4, statistical analysis was done using one-way ANOVA.

In summary, the here performed experiments demonstrate a predominant cellular localization of the immunoproteasomal subunits LMP2 and LMP7 *in vivo* in Iba1-positive microglial cells under normal, but especially and to an increased extent under pathological conditions provoked by an ischemic event. A reduced *in vitro* expression of these IP subunits is observed on transcript level additionally in neurons and astrocytes, but could

not be confirmed in tissue samples. Depletion of the LMP7 subunit per se does not produce any obvious phenotype in behavior or selected cellular proteins compared to the WT. Nevertheless, a suppression of LMP7 clearly seems to result in increased neural damage after permanent cerebral ischemia along with increased sensorimotor deficits, but has lesser impact on the temporal retrogression of the infarct area. In addition, the LMP7 affects cellular LMP2 protein levels under normal and ischemic conditions. Further, LMP7 causes an altered activation of microglia indicated by differences in morphology and expression levels of activation markers after ischemia towards a more amoebic cell morphology and increased expression of MHCII and F4/80 in LMP7$^{-/-}$ mice. At the same time, decreased numbers of peripheral myeloid cells in the infarct area were detected in the knockout animals indicating a crucial influence of LMP7 on the recruitment of infiltrating immune cells after an ischemic event.

4. Discussion

The performed experiments were conducted to provide more information about the potential role and function of IPs in the mammalian brain for reasons of both basic understanding and putative therapeutic applications.

The distinct cellular localization of immunoproteasomal subunits in the brain and their presence under physiological but also in neuropathological conditions is still not fully understood. According to this, their functional relevance, especially in the context of putative clinical use is highly warranted.

In this work, I performed a detailed localization analysis on protein level in mouse brain sections and on transcript level in primary neuronal cell cultures revealing microglia most likely as the main producing cells of IPs in the brain (compare to section 3.2.1). Further, the induction and upregulation of LMP2 and LMP7 expression was disclosed using immunohistochemical and protein biochemical approaches in the context of focal cerebral ischemia (compare to section 3.4). Using a LMP7-deficienct mouse model, I could illustrate the impact of impaired IP formation for the outcome of cerebral ischemia including the extent of neural damaged and changes in the microglia cell morphology (compare to section 3.3 and 3.5).

In order to perform these studies, numerous tools including specific antibodies and a basic phenotypic comparison of WT and LMP7$^{-/-}$ mice, had to be established in beforehand (compare to section 3.1).

4.1 Establishment of experimental tools to study IPs in the murine brain

The first parts of this work were designated to establish and verify the selected methods for the project and to ensure applicability of the selected mouse model and the generated antibodies. The LMP7$^{-/-}$ mouse model, initially described by Fehling and colleagues [118] is indeed a suitable tool to analyze the influence of an impaired IP formation in comparison to C57BL/6 WT mice as controls. This was demonstrated by a small behavioral study (Fig. 4-6) and the comparison of the basal expression of selected proteins (Fig. 7). In order to ensure reliability and comparability, littermates were used. Further, the use of littermates was important within the context of the immunosensitive aspect of these studies by the impaired IP formation and presence in the knockout animals.

In general, I observed no peculiarities of LMP7$^{-/-}$ mice compared to their WT littermates in our animal facilities by daily monitoring under physiological conditions. However, a significant weight reduction of adult LMP7$^{-/-}$ mice was observed (Fig. 3). Kimura and colleagues could demonstrate a potential role of LMP7 in the pathology of metabolic disorders such as obesity [236]. They detected no differences in body weight gain

between WT and LMP7$^{-/-}$ mice under normal chow as I did, but their animal numbers were lower and could potentially miss a small difference as I was able to observe. The effect seems to play a more important role under high-fat diet as the body weight and the mass of adipose tissue was significantly reduced in LMP7$^{-/-}$ animals. Nevertheless, a decreased lipid absorption and altered glucose metabolism produced by an impaired IP formation may already have an influence under normal conditions and would explain the observed result in my experiments. Apart from that and also indicated by no other physiologically observed phenotype, the effect could be also a result of slightly different housing conditions of the animal facility. Even though the breeding is standardized, the animal cages are allocated in lower and upper racks, which could lead to slightly different housing conditions concerning light, temperature, and air circulation. These variations were tried to minimize by distribution of both genotypes equally in the racks, but could be also an explanation for the minor weight reduction in LMP7$^{-/-}$ mice.

Overall, there was no phenotype or abnormal behavior of the LMP7$^{-/-}$ mice observed under normal healthy conditions compared to the control WT mice. Both genotypes performed very similar in a small behavioral study that was executed in the lab of Prof. Dr. Markus Fendt. There were no differences in performance observed for an open-field test, the light-dark box and a carnivore-induced fear paradigm (Fig. 4-6). Therefore, I assume no basal effect of the LMP7-deficiency and due to this an impaired IP formation on locomotor activity, basic anxiety as well as unconditioned fear and moreover, on the sense of smell and sensorimotor gating in the examined genotypes. Importantly, based on these findings, the detected differences between WT and LMP7$^{-/-}$ littermates in the performance of the adhesive tape removal test (Fig. 25) can be considered as a genuine effect produced by IP impairment after ischemia and not because of some fundamental locomotor disabilities produced by the lack of the LMP7 subunit.

Furthermore, I detected no obvious differences in the biochemical characterization of subcellular fractions from WT and LMP7$^{-/-}$ mouse brains for well-known protein markers (Fig. 7). According to these results, LMP7 seems to display no strong impact on the basal gene expression of the selected proteins. This observation was important for the later performed biochemical analysis of WT and LMP7$^{-/-}$ samples after ischemia and verifies the effects recognized in these experiments as reliable differences between the genotypes based on the MCAO and not on the knockout *per se*. Moreover, the similar amounts of the β subunits detected in both genotypes allow the assumption that an altered amount of IPs does not globally affect the amount of the constitutive standard proteasome under normal conditions in the mouse brain. In addition, an impaired IP formation seems to have no effect on the expression of important receptor proteins and markers for synaptic integrity and normal brain function, implying no fundamental role of the IP, or more precise the

LMP7 subunit, in synaptic plasticity or for proper proteostasis. Nevertheless, a few tendencies without statistical significance including an increased GFAP, α6, NR1, GluR2 and pCREB ratio as well as a decreased Iba1 level in LMP7$^{-/-}$ should be noted (compare to Fig. 7). As the here used samples originate from individual whole mouse brains, these small differences are probably caused by the biological variations of mouse models. Additionally, two brains were pooled per sample in order to obtain for the synaptic fractions sufficient protein amounts for biochemical analyses, but inevitably increase the biological variability. According to these results, all later observed effects of later experiments between WT and LMP7$^{-/-}$ mice after MCAO contribute to the importance of LMP7 expression in the context of cellular oxidative stress and the inflammatory challenge upon ischemia and not the knockout *per se*. Taken together, these data verify the selected mouse model as a reliable and suitable tool for the later performed experiments.

For the purpose of visualization and characterization of the immunoproteasomal subunits LMP2 and LMP7, 12 antibodies were generated using peptides of the C-terminal region of the proteins in the beginning of this thesis as the availability and specificity of commercial antibodies was limited and (for the brain) mostly lacking, respectively. All antibodies displayed specificity in WB analysis (Fig. S1,S2 and Fig. 8,9) and immunohistochemistry (Fig. 12), thus, the ones with the highest sensitivity were selected for further application.

Notably, in WB analysis a clear double band, which could be blocked, close to the expected size of LMP2 and LMP7 at approximately 20 kDa, was detected in the knockout animals and to a much lesser extent also in the WT samples with all antibodies. Note, that the immunoproteasomal βi subunits are expressed as pro-peptides and further processed after successful maturation of the IPs to their mature form by splicing of the N-terminal end [13], [26]. Due to this, I would assume a specificity of the antibodies for both types of the protein (as the peptide used for immunization lies in the C-terminal region) and the upper immuno-reactive band displaying the premature form of LMP2 and LMP7. Interestingly, the signal ratio of the upper and lower immuno-reactive band seems to differ in WT and LMP2$^{-/-}$ or LMP7$^{-/-}$ samples and is observed and discussed also in later experiments (Fig. 30). Besides, several immuno-reactive bands in the range of 30-130 kDa could be observed in samples of brain tissue and irrespective of whether an antibody for LMP2 or LMP7 was used (Fig. 8,9). These bands were also present after pre-absorption of the antibodies with a fusion protein and indicate some unspecific binding of unknown proteins. The different tissue properties of the samples could be an explanation for the exclusive detection of these bands in the brain tissue samples. However, as for each sample a clearly distinguishable immuno-reactive band at the predicted size of LMP2 and LMP7 was visible that could be blocked by pre-absorption of the anti-sera with

the corresponding fusion protein, a further antibody purification step, and the consequently dilution of the anti-sera, was not necessary.

Besides, the immuno-reactive band below 15 kDa in spleen samples probed with the rabbit antibody raised against LMP7 (compare to Fig. 9A), could be explained by the presence of different posttranslational modification patterns in the different tissues. Another explanation could be also the detection of already degrading protein.

The generated antibodies were also suitable for immunohistochemistry and enabled the visualization of LMP2 and LMP7 in mouse brain slices (compare to section 3.2). As expected and underlining the specificity of the used antibodies, I could observe no signal for LMP7 in the LMP7$^{-/-}$ mice and for both immunoproteasomal subunits after pre-absorption of the respective antibody solution with either a MBP-LMP2 or -LMP7 fusion protein. In addition, no signals could be observed in primary antibody controls, which ensures specific binding of the secondary antibody as well (Fig. 12).

Taken together, these results confirm the applicability of the generated antibodies for the localization analysis in mouse brain slices. However, immunohistochemically stained tissue leads in some cases to difficult results, which are not easily to interpret because of high background and overlapping signals, especially in multiple stainings using various antibodies (Fig. 13,16,17). For this reason, I aimed to additionally apply the localization analysis in a less complex model as primary neuronal cell cultures. Unfortunately, the generated antibodies were not suitable for immunocytochemistry (Fig. 10,11). The observed fluorescent signals, which intrinsically exhibited a low intensity, were also obtained in the LMP7$^{-/-}$ mice for LMP7 and no difference in signal strength could be detected after antibody blocking for both, LMP2 and LMP7. This observation indicates either unspecific binding of the antibodies, which would be in conflict with the specific results of the antibody characterization in WB and immunohistochemistry or demonstrates the limitations of the here generated antibodies as a tool that is not suitable for all methods. In addition and related to the low fluorescent signal intensity compared to the background signal in the primary antibody controls (Fig. 10,11), a further explanation could be the absence of the immunoproteasomal subunits in cultured neural cells. To investigate this issue in more detail, a FISH assay in WT and LMP7$^{-/-}$ neuron-glia co cultures with specific probes for LMP2 and LMP7 mRNA and the use of a commercial kit were performed in order to analyze the expression of the named IP subunits at least on transcript level and will be discussed below.

4.2 Cellular and subcellular localization of IP subunits

The precise cellular localization of the IP subunits within the mammalian CNS has been investigated most probable since 20 years [143], [237], but still remains far to be fully understood.

Within this work, an *in vivo* localization analysis for the immunoproteasomal subunits LMP2 and LMP7 was performed using specific antibodies against the IP subunits and several cell type-specific marker proteins in immunohistochemical double stainings of mouse brain sections. Fluorescent signals for LMP2 and LMP7 were predominantly found in Iba1-positive cells. Iba1 is a cell type marker for microglia and is upregulated after activation of these cells. In the healthy brain, the overlapping fluorescent signals for the immunoproteasomal subunits as well as Iba1 and the observed morphology of the Iba1-positive structures, clearly allow the assumption that both IP subunits are expressed in microglial cells (Fig. 13). Likewise after cerebral ischemia, fluorescent signals for LMP2 and LMP7 mainly co-localized with activated microglia, indicated by the increased Iba1 signal intensity and the altered morphology of these cells [225]. Acquisitions of confocal cross-sections of the immunohistochemically stained samples could verify that the fluorescent signals of LMP2 and LMP7 were in fact localized within Iba1-positive microglia (Fig. 14). These results are in accordance with previous studies of Orre et al., Puttaparthi and Elliott as well as of Chen et al., which all suggest an IP expression, at least of LMP7, in microglia [166], [187], [193]. The assumption that microglia are the predominant cell type of cellular IP expression in the brain is further corroborated by the fact that microglia are the immune cells of the CNS [238] and a constitutive expression of IPs was first discovered in peripheral immune relevant tissue [239], [240]. Especially after an ischemic event such as MCAO, the phagocytic and degrading capabilities of microglia play an important role in the elimination of cell debris produced by apoptotic and necrotic processes [241], [242]. Additionally, IPs were shown to feature a higher proteolytic capacity compared to the standard proteasome [63] and, therefore, enable an accelerated protein degradation, which is necessary within this context of elevated oxidative stress. IP presence in microglia could strongly contribute to the efficient clearance of protein debris produced by the brain injury.

However, after an ischemic event, the blood brain barrier is disrupted and neuroinflammation is induced by the release of cytokines [233]. As a consequence, also peripheral immune cells including monocytes and macrophages are attracted and migrate to the site of injury [224], [241]. Monocytes and macrophages feature likewise microglia high Iba1 expression [243], [244]. Therefore, I cannot exclude the possibility of a considerable proportion of Iba1-positive peripheral monocytes and macrophages besides brain-resident microglia around the infarct site that express LMP2 and LMP7 under the defined experimental circumstances, too.

At the same time, I found neither co-localizing fluorescent signals for LMP2 or LMP7 with fluorescent signals for the neuronal marker proteins NeuN and Map2 nor with the astroglial marker GFAP in the here described immunohistochemical co-stainings (Fig.

16,17). To a small extent, I observed overlapping fluorescent signals for LMP7 and Map2, but these results are difficult to interpret due to the possibility of superimpositions and high background signals in stained tissue samples. Therefore, I aimed to analyze the cellular localization of LMP2 and LMP7 in a more simplified system such as neural primary cell culture. Unfortunately, due to the unspecific binding of the generated antibodies in immunocytochemistry or the possibility of protein expression below detection threshold, I opted to analyze the expression of the IP subunits on transcript level using a FISH assay (Fig. 18-20). Signals for LMP2 and LMP7 mRNA could be observed mainly in GFAP-positive astrocytes and isolated in Map2-positive neurons, too, but only in samples treated with 20 ng/ml IFN-γ for 24 h. With this approach, it remains unclear if the observed mRNA in the here performed *in vitro* cell culture experiments is also translated into proteins. Still, this result indicates that certain levels of inflammatory stimuli, potentially very high and/or chronic inflammatory conditions, might induce the expression and formation of IPs in astrocytes and/or neurons, too. However, these seem to be very low or absent *in vivo* under healthy and ischemic conditions. This results could be an explanation for the observed presence of IP subunits in other studies, which postulate an IP expression also in astrocytes and neurons in the brain [55], [59], [187], [193], [194], [245]. Importantly, those studies observed the cellular localization of the mentioned βi subunits mainly in the context of AD, HD, and ALS models, which all involve a rather moderate but indeed chronic neuroinflammation instead of the acute inflammatory state after an ischemic event as in the study presented here. Based on this, microglia could theoretically express immunoproteasomal subunits on a constitutive level and at first after the onset of brain injury or pathology. Potential modulation of the microglial proteasome content would support their ability to rapidly change their activation status and function in inflammatory cytokine production [246], [247]. However, ongoing activation of microglia and potentially recruited peripheral monocytes could promote then rather neurotoxic conditions that could cause an induction of IPs also in astrocytes and neurons to cope with the inflammatory challenge and the accompanied oxidative stress. Research on neurodegeneration in general emphasizes a time-dependent difference in the metabolic response of the brain cells [248]. Early stages and acute phases of neuropathologies involve the activation of microglia and endothelial cells [88], [238], [246]. Changes in astrocytes and neutrophils occur at later stages of neurodegeneration and can consequently affect neuronal death [249]. Perhaps, these processes are reflected by the diverse expression of IPs in the literature and could explain the in part very different results. Overall, data from the literature as well as from this thesis lead to the assumption that IPs can be expressed most likely in all neural cell types, but the conditions that induce this cell type-specific expression seem to differ in the signal strength of the stimulus.

In order to capture this potential shift in cell type specific IP expression, I conducted the immunohistochemical co-stainings after 8 d of MCAO to investigate the cellular localization at this interface of early and sub-acute phase after ischemia (Fig. 21,22). The expression of LMP2 and LMP7 was once again mainly detected in microglia, indicated by Iba1-positive signals. There were no co-localizing signals for the IP subunits and the neuronal marker proteins NeuN and Map2 or the astroglial marker GFAP. Therefore, I conclude microglia as the IP main producing cell type for IPs under normal as well as acute and sub-acute ischemic conditions. But this conclusion does not exclude the possibility of IP expression in astrocytes or neurons at later stages post-ischemia or under pathological conditions including chronic neuroinflammation.

Another interesting aspect of the localization analysis was the immunohistochemically detected subcellular distribution of the fluorescent signals for LMP2 and LMP7 in the Iba1-positive cells (Fig. 15). In MCAO damaged tissue areas close to the infarct region and in the penumbra, Iba1-positive cells displayed co-localizing signals for LMP2 as well as LMP7 consistently within the entire cell body. Remarkably, in healthy tissue regions of the intact hemisphere, signals for LMP2 seemed to be more concentrated in the cell soma, whereas signals for LMP7 appeared in distal parts of microglial dendrites. This observation would rather indicate the absence of the classical IP composition featuring all three βi subunits under normal conditions in microglia. Different explanations would be, however, also imaginable. On the one hand, the immunoproteasomal subunits could exist as single soluble proteins within the different subcellular compartments. But as the maturation process of the βi subunits involves incorporation into newly generated IPs in order to become spliced at the N-terminal [13], [26], this theory would point to the presence of the premature pro-form of the subunits instead of proteolytically active proteins. Pro-peptides or pro-sequences are part of a wide range of proteins and fulfill several cellular functions, leading partly to very opposite effects compared to the mature protein, as for instance with (pro)neurotrophins [250]–[252]. In case of the immunoproteasomal βi subunits, these pro-pepitides are known to function as inhibitors to keep the protein inactive [32]. Besides this, they could additionally bear a subcellular targeting function as it is known for many proteins featuring an ER signaling peptide. Thereupon, the pro-peptide itself or its molecular interactions with other proteins could promote a sorting or transport of LMP2 and LMP7 into separated different subcellular compartments [253]. A potential explanation for this subcellular localization could be the advantage of a separated intracellular pool of immunoproteasomal βi pro-peptides under physiological conditions in order to prevent a functional IP formation but enables fast IP assembly if required. Especially in the brain, which consists of post-mitotic cells that are very vulnerable to disturbances in the protein homeostasis, a constant accelerated protein

turnover by IP proteolytic activity could rather be more of a disadvantage. The here used antibodies probably have a high potential to detect both the pro- and the mature form of the IP subunits as shown in the performed WB analysis (e.g. Fig. 8,9) as for immunization an peptide of the mature form was used. However, a clear discrimination and investigation of this hypothesis should be performed in the future and was outside the scope of this thesis.

On the other hand and taking various other references into account, the mentioned observation could also indicate the presence of different intermediate or hybrid-proteasomes within microglial cells. Several studies could demonstrate the existence of proteasomes featuring a mixed β subunit composition with specific proteolytic activities and localized in different cellular compartments. For instance, proteasomes bearing either only LMP7 or LMP2 and LMP7 were found in several human tumor cell lines as well as normal human tissue including liver, kidney, small intestine, colon and heart and HeLa Cells [37], [254], [255]. The assumption of intermediate LMP2- or LMP7-proteasomes would be also consistent with the current understanding of proteasome assembly. Generally, the incorporation of βi subunits is preferred compared to the standard β subunits. Thereby, LMP2 is initially incorporated and favors the incorporation of the other two βi subunits MECL-1 and LMP7 [32], [35], [36], [38]. However, LMP7 can be incorporated also independently [34], [37].

As proteasomes in general are known to play a crucial role for the modulation of various cellular signaling pathways and the regulation of gene expression (see section 1.1.3.2), specialized subtypes in different subcellular compartments could target specific substrates such as transcription factors in the cell soma and messenger proteins in the processes.

Next, microglia have to fulfill several, partly very different functions in the brain. The presence of specific intermediate proteasome subtypes in specific compartments could be essential for these diverse functions. For instance, microglia cells are responsible for the homeostatic surveillance of the brain parenchyma. Thereby, microglial processes constantly undergo withdrawal and *de novo* formation [196], [256]. Depending on the perceived environmental stimuli, microglia can rapidly transform to diverse activation phenotypes with diverse functional consequence [246], [247]. Moreover, the surrounding neural structures are vulnerable and command only limited regenerative capacity, which in turn, demands a highly controlled microglia-neuron interaction and subsequent signal processing. Within this context, the presence of certain proteasome subtypes as well as a very specific subcellular activity of the UPS under normal steady state conditions in the brain, could be essential in order to guarantee a precise induction and regulation of these processes and to avoid damage to the surrounding neural tissue.

Another theoretical consequence of subcellular varying proteasome subtypes would/could be the generation of slightly different subcellular sets of oligo-peptides, which could possess so far unknown, but with biological relevance in relation to the heterogeneity of microglia function.

And further, a potential well-balanced mixture of different proteasome subtypes in microglia, especially with regard to the function of IPs in antigen presenting and processing [257], [258], could facilitate a wide-range presentation of antigens and, thus, appropriate immune recognition and/or responses in the CNS. These assumptions could be very interesting scientific questions for future research.

In addition to this, the subcellular distribution of immunoproteasomal subunits was examined under healthy conditions based on the preparation of subcellular fractions and WB analysis (Fig. 23). Strong signal intensities were observed in the fractions containing more soluble proteins and complexes indicating different subcellular localizations of potential IPs in the cytosol as well as in the nucleus of neural cells. Interestingly, weak immuno-reactive bands for LMP2 and LMP7 could be detected in the synaptic material-enriched SJ fraction of healthy adult mouse brains. In the recent concept of the "quad-partite" synapse, astrocytes and microglia processes additionally contribute to the formation, maintenance and removal of synaptic connections beside the pre- and postsynaptic neuron [259]. As a result, the obtained fraction contains mainly components of the pre- and postsynaptic membrane and the synaptic cleft, but includes in addition to neuronal material also components from glial cell origin. Together with the afore mentioned results of the localization analysis, I would assume that the detected signals for LMP2 and LMP7 in Fig. 23 most probably result from material of fine microglial processes. An ensuing question for this hypothesis would be the functional aspect of an IP expression in synaptic structures.

Apart from that, a very low basal *in vivo* expression of IP subunits in astrocytes or even neurons, which declines beneath the detection level of the applied immunohistochemical approach, but could be detected by the comparatively more sensitive WB analysis, cannot be excluded by the here performed experiments. From this point of view, an additional role of IPs for normal brain function and in particular in synaptic plasticity or modulation would be conceivable. Several studies could demonstrate the presence of the standard proteasome in dendritic spines and the involvement of the UPS in synaptic plasticity in answer to synaptic activity [128]. Possibly, a very low basal expression of IPs in addition to the constitutive standard proteasome in neuronal dendrites is needed for rapid protein degradation after strong synaptic activity in order to adapt in an appropriate way. But an importance of the IP in the context of synaptic plasticity, learning as well as memory

formation and the underlying mechanisms and functional purpose cannot be covered with the here performed experiments and should be addressed in future research.

4.3 The impact of IP subunit expression on brain function after cerebral ischemia

In this work, the functional relevance of IPs in the mouse brain was analyzed in the context of focal cerebral ischemia using a LMP7$^{-/-}$ mouse model. The LMP7-deficiency clearly seemed to cause an increase in the area of neural damage (Fig. 24). Furthermore, I observed more severe sensorimotor deficits in LMP7$^{-/-}$ mice compared to WT littermates (Fig. 25), which coincides with the observed increased neural damage in this early phase after MCAO. In the further course of the post-ischemic phase, there was the impression of apparently numerous Iba1-positive cells in the precedent infarct area of LMP7$^{-/-}$ mice, whereas no obvious long-term differences between the two genotypes in the temporal retrogression of the infarction could be observed (Fig. 26,27).

At the same time, a massive increase in gene expression was observed for LMP2 in both WT and LMP7$^{-/-}$ mice as well as LMP7 in the WT mice in the acute and sub-acute phase after ischemia (Fig. 29). However, differences in the amounts of constitutive β-subunits and the pool of ubiquitinated proteins were not observed, neither between the genotypes nor comparing damaged versus intact tissue after MCAO (Fig. 31,32). These results, in relation to the increased area of neural damage in LMP7$^{-/-}$ mice, imply a neuroprotective function of the LMP7 expression, at least in early stages after an ischemic event and, thus, a potentially specific function of the IP within the context of this substantial inflammatory challenge and profound oxidative stress.

LMP7 plays an important role during the maturation process of IPs by cleavage of the pro-peptides of the other two βi-subunits [34], [37]. Due to this an impaired IP formation could be assumed in the chosen knockout mouse model. It is conceivable that intermediate proteasomes, bearing the constitutive β5 subunit, are formed instead of complete IPs in this case. And even though both the LMP7 and β5 subunit possess a chemotrypsin-like activity [61], the resulting proteolytic activity is likely to be altered. Besides, the IP was demonstrated to possess an accelerated turnover of oxidatively modified proteins in comparison to the standard proteasome (compare to section 1.1.3.1). Therefore, an impaired IP formation and altered IP activity could be detrimental within the context of elevated oxidative stress during cerebral ischemia and could cause immense cellular stress. This cellular stress is additionally enforced by the inflammatory circumstances after MCAO and probably leads to an elevated onset of cell death, which is indeed displayed in the results of section 3.3. Another aspect within this context of ischemia is that the IP-producing microglia cells themselves have to manage the high level of oxidative stress in order to maintain not only cellular protein homeostasis and functionality, but more

importantly, to accomplish successful conversion in their reactive states. Regarding this, I would expect consecutive effects of cerebral ischemia primarily on microglia functionality concerning the pattern of cytokines produced, the phagocytic capability as well as cellular degradation rate of these cells in LMP7^{-/-} mice. A few hypothetical implications could include the following aspects:

Regarded as the brain-specific macrophages, microglia are the first to sense the traumatic injury in the course of ischemia by the recognition of certain patterns (DAMPs, damage-associated molecular patterns) via a variety of pattern recognition receptors (PRR) [225], [260]. This leads to the activation of microglia cells within minutes after the ischemic event and the induction of several signaling cascades including the inflammatory NFκB pathway [225], [261], [262]. In the acute phase, microglia activation leads to a rather cytotoxic phenotype in order to defend the afflicted tissue, subsequently promoting the production of pro-inflammatory cytokines as well as the activation of infiltrating peripheral cells. In later stages of the immune response, mechanisms of repair and restoration of the tissue homeostasis become more important, which are also mediated by microglia. Notably, these cells transform to a more phagocytic phenotype, which includes the production of immunosuppressive and neuroprotective factors as well as the uptake of apoptotic cells, clearance of cell debris and damaged extracellular matrix, and finally cell interactions with the immune system via MHC molecules [261], [262]. There is evidence that for all these processes a participation of the UPS in general and possibly for the IP in particular is critical and is disentangled in the following (compare also to section 1.1.3). For instance, LMP7 was demonstrated to exert an influence on cytokine production and to reduce the secretion of pro-inflammatory cytokines [172], [263]. The transcription factor NFκB has a pivotal role for inflammation-associated signaling cascades and is activated only by the proteasomal degradation of its inhibitory IκB molecules [264]. Moreover, the importance of IP expression on antigen processing and presentation has been reliably documented not only for immune cells, but also for non-immune tissue [112], [113], [121], [258], [265]. Beyond that, ubiquitination and proteasomal degradation fulfill a significant function in the down-regulation and conversion of signaling pathways as needed for microglial activation and diversification [247], [266]. Furthermore, the detailed mechanism of phagocytosis still has to be clarified but is supposed to be a very complex process. There is also growing evidence that interactions with proteasomes could play a role, possibly not within the phagosome organelles itself, but might be biologically significant for phagosomal maturation [267]. Concretely, proteasomes could contribute to specific receptor trafficking and phagosomal fission, which involves the presentation of ingested material as antigenic peptides together with MHCII molecules on the cell surface [268], [269]. According to the current state of research and in relation to my work, an impaired IP formation in microglia

would lead therefore e.g. to a potential imbalance in cytokine production. This would have an impact additionally on other neural cells as the secretion of these bioactive factors by microglia after ischemia are known to influence astroglia [270], [271]. Consequently, these astrocytes could be activated in an altered manner. The activation of astrocytes is a process termed as gliosis and known to be important in order to restrict the area of necrosis and inflammation [226], [229], [230]. Although there were no obvious differences of GFAP signals recognized after MCAO in immunohistochemically stained LMP7$^{-/-}$ and WT samples (Fig. 27), a disturbed secretion of the microglial factors could interfere with the astroglial activation and consequently result in increased neural damage.

Next, a delayed clearance of regulatory and immune response-mediating proteins due to an impaired IP formation could impair also the expression of stress response enzymes, apoptosis inhibitors, and consequently disturb the regulation of microglial neurotoxic or -protective effector functions [266], [272]. As there is a need to inactivate the innate microglia-mediated immune response, malfunctioning transformation of the microglia phenotype towards tissue protection and repair due could also explain the increased neural damage upon LMP7-deficiency.

Furthermore, microglia display a broad number of receptors that are important for cell-cell interactions, their ability to communicate with immune cells, and the induction of numerous signaling cascades resulting in the broad range of effector function these cells are capable of [247], [258]. In this context, an elevated IP-mediated proteasomal degradation could be crucial for proper cell functionality. Theoretically imaginable would be a proteolytic activity in combination and/or in addition to the standard proteasome, which is responsible for the mediation of immune responses by presenting antigenic peptides of intracellularly processed proteins to infiltrating cells of the immune system.

All these assumptions would be in conformity with the observed effects in my experiments, but partly contradict other studies demonstrating a rather beneficial effect of impaired IP formation. Notably, inhibition as well as knockout of LMP7 were demonstrated to improve pathological symptoms in mouse models of rheumatoid arthritis and AD [172], [263]. Otherwise, the here observed massive induction the immunoproteasomal subunits LMP2 and LMP7 with an unchanged expression of constitutive proteasome subunits after an ischemic injury is in compliance with other studies [187], [194], [195], [273]. However, depending on the experimental setup this strong induction of IP subunits seems to promote both neuroprotective as well as detrimental consequences.

For instance, Chen and colleagues could demonstrate a beneficial effect of an LMP2 knockdown after MCAO, pointing rather to a pathophysiological role of IP formation in the context of ischemia [187]. By contrast, my results would indicate a neuroprotective function of IP induction in the brain after ischemic injury. Nevertheless, both results do not

necessarily have to be in conflict. The LMP2 knockdown leads to a moderate IP impairment with decreased caspase- and chymotrypsin-like activity of 60-70%. Potentially, this change in proteolytic activity leads to earlier immunosuppressive consequences that result in reduced infarct volumes. Oppositely, a more severe IP impairment produced by a complete gene knockout could be detrimental and possess such a strong effect that the result turns into a reversed outcome after ischemia. Another conceivable explanation for the divergent neural damage in both studies could be the fact that in each case another subunit of the IP was studied. Potentially, the used approaches target two different subtypes as intermediate proteasome bearing only one immunoproteasomal subunit were already suggested. This could include a different functional impact and the outcome of two different effects on neural survival.

Besides that, the different findings could be also related to some significant differences in the used experimental methods that I would like to mention. Chen et al. used an ischemic stroke model involving reperfusion in rats whereas I decided for a permanent stroke model in mice. Transient MCAO and the subsequent reperfusion cause a rapid influx of peripheral cells with a consequent increased leukocyte-derived cytokine production and enhanced inflammation. Following the presumption of section 4.2, a potential attenuation of this stronger inflammatory situations by LMP2 knockdown could promote a rather neuroprotective effect and would also explain the detected induction of IP subunits in astrocytes of WT samples as observed by the authors [187]. This effect is absent in the used permanent MCAO model of my work, but reflects better the majority of human stroke patients. Recanalization therapy with a pharmacologically induced reperfusion is only applied in <10 % of all stroke patients [233], [274]. Further, Chen et al. abolished LMP2 using a lentivirus-mediated LMP2 shRNA, which inhibits the gene expression in a temporally and spatially limited manner and cannot affect already existing products on protein level. In my case, LMP7 was completely and at all times abolished due to the gene knockout. Moreover, Chen et al. examined the infarct volume by TTC staining (Triphenyl tetrazolium chloride) of 2 mm thick brain sections, whereas I performed Cresylviolet staining in 20 µm thick brain sections. These variations might complicate a direct comparison and could be also the reason for the differential findings.

In addition, I observed no evident differences between the used genotypes in the temporal retrogression of the infraction over two weeks post-ischemia, but a tendency towards an increased number and signal strength of Iba1-positive cells in the precedent infarct area of LMP7$^{-/-}$ mice after 8 days of MCAO (Fig. 26,27). An increased numerical density of microglia cells within the infarct area is similarly observed in later experiments of the FACS and Skeleton analysis (compare to Fig. 33 and 35-37).

The expression of Iba1 is upregulated under neuropathological conditions including ischemia and is suggested to play an important role also in the process of phagocytosis by microglia/macrophages [275]–[277]. This could indicate an enhanced recruitment of activated brain-resident microglia and/or Iba1-expressing monocytes as well as macrophages from the periphery to the site of ischemic injury and will be discussed in more detail in the following section 4.4.

Interestingly, the lack of LMP7 exerts an influence on the protein level of the LMP2 subunit (Fig. 30). The in WB observed immuno-reactive double band for LMP2 represents the precursor and mature forms of the peptide. The ratio of signal intensities of the upper and the lower immuno-reactive band clearly differ between the two genotypes (Fig. 8,9,29,30). Apparently, the amount of the pro-peptide is increased and would indicate a disturbed maturation in LMP-deficient mice. In addition, the overall amount of LMP2 is decreased (Fig. 30). On the one hand, this could point towards a shortened lifespan of the LMP2 peptide as the incorporation and maturation into IPs is impaired in the LMP7^{-/-} mice and accumulating pro-peptides undergo enhanced degradation. On the other hand, this could also reflect a difference in the level of protein synthesis. As both the LMP2 as well as the LMP7 gene are located within the MHCII region [35]–[37], [221], potential epigenetic effects due to the DNA damage in LMP7^{-/-} mice could lead to a reduced transcription of the LMP2 gene.

4.4 The role of IP subunit expression on the microglial phenotype after cerebral ischemia

The previous results suggest that microglial expression of LMP7 plays a central role for the course of ischemia including microglia activation. This process involves morphological changes, the secretion of cytokines, and, thus, implications for cells of the adjacent tissue. Therefore, I aimed to investigate the effect of LMP7-deficiency on myeloid cells in more detail by a FACS analysis of the recruited cell populations and the expression of activation markers after MCAO. Further, I performed a Skeleton analysis and a measurement of cytokine production using qRT-PCR in collaboration with the research group of Prof. Dr. Ildiko R. Dunay.

The FACS analysis revealed an increased numerical density of microglia cells but less peripheral myeloid cells within the infarct area of LMP7^{-/-} mice after 24 h of MCAO (Fig. 33C), which could indicate an increased migration of brain-resident microglia towards the site of ischemic injury, potentially due to a reduced recruitment of peripheral myeloid cells. This was supported by the results of the Skeleton analysis (Fig. 35-37). Moreover, the morphological characteristics and the expression of microglial activation markers were altered in LMP7^{-/-} samples suggesting differences in the microglia polarization phenotype caused by the lack of LMP7.

After disruption of the blood brain barrier, highly mobile myeloid cells of the periphery can be recruited to the site of injury and inflamed tissue [224], [227], [228]. Interestingly, clear differences between WT and LMP7$^{-/-}$ mice in the amount of Ly6C^{high} monocytes and Ly6C^{int} dendritic cells indicate an attenuated recruitment of these cells to the infarct area (Fig. 33C). Ly6C^{high} monocytes are also termed as "inflammatory" monocytes and are involved in the regulation of the immune response. Upon tissue infiltration, these cells differentiate into monocyte-derived macrophages with high phagocytic potential and are suggested to assist in the restriction of ischemic damage expansion [224]. In addition, Ly6C^{high} monocytes were demonstrated to foster conversion of adjacent microglia cells and macrophages towards an anti-inflammatory, neuroprotective phenotype [278], [279]. An insufficient influx, as displayed by the reduced numbers of these cells in LMP7$^{-/-}$ mice, could result in an increased neural damage in the sub-acute phase of ischemia as observed in section 3.3 due to a limited phagocytic capacity and suspended assistance in microglial M2 polarization in mechanism of tissue repair and remodeling. Ly6C^{int} myeloid-derived cells represent a subpopulation of brain dendritic cells (DCs) and feature potent antigen presentation capabilities. Their recruitment to ischemic tissue in brain injury was suggested to mediate immunomodulatory properties in the interaction of macrophages and later infiltrating lymphocytes [227], [280], [281]. The significantly reduced numerical density of these Ly6C^{int} DCs in LMP7$^{-/-}$ mice could mirror either improper cell recruitment to the infarction or inappropriate cell loss in the course of inflammation (Fig. 33C). However, both would contribute to an attenuated recruitment and migration of peripheral immune cells to the infarct area. Together, these data suggest a regulatory role for LMP7 within the multifaceted mechanism of ischemia-induced attraction of immune cells after neuroinflammation. Concurrently, the presence of Ly6C^{low} monocytes seems to be unaffected by the LMP7-deficiency. However, there is a trend towards a reduced numerical density of these cells in the infarct and at the same time towards an increased numerical density of these cells in the remaining brain tissue (Fig. 33C). This is an interesting observation with regards to the importance of Ly6C^{low} "patrolling" monocytes/macrophages in vascular integrity and the removal of damaged endothelium [282], but is difficult to interpret because of the small sample size and the missing statistical significance. Likewise, the amount of Ly6G^{high} neutrophils, the most abundant type of phagocytic granulocytes, was in contrast to the other subpopulations apparently not altered. An explanation could be their specialized function in mediating pathogen clearance after infections [283], which perhaps plays a subordinate role in the course of ischemic brain injury as present in my studies and, hence, produces no differences between the genotypes.

The participation of infiltrating peripheral cells after ischemia in concert with brain-resident microglia is known to be important for the regulation and termination of post-ischemic inflammation [224], [284]. An imbalance due to an impaired IP formation or a lack of LMP7 in this complex interplay could explain the observed results.

The quantitative analysis of morphological parameters of Iba1-positive cells after ischemia indicats a more pronounced amoebic microglial morphology including shortened, but more clustered cellular branches in LMP7$^{-/-}$ mice compared to WT littermates (Fig. 35-37 B,C). This could reflect differences in the activation or more specifically polarization phenotype between the present Iba1-positive cells including myeloid-derived macrophages as well as brain-resident microglia. However, the classification into M1 and M2 macrophages describe solely two opposite extremes of a broad range of activation states including diverse effector functions and is supposed to merge during conversion of macrophage polarization as indicated by amplifying diversity of activation characteristics in different pathological models [285]. The dynamics of microglia and myeloid-derived cell activation phenotypes are complex [238], [257], [282], which makes straightforward conclusions difficult. But based on the apparent alterations in morphology, and as mentioned below in the expression of activation markers of LMP7$^{-/-}$ microglia, expression of IP subunits and IP formation could be essential for a fine-tuned balance between both macrophage activation states and associated functional consequences. Potentially, an impaired transformation in LMP7-deficient macrophages into a more M2-related activation phenotype that is characterized by the capability of phagocytosis and is supposed to be rather neuroprotective, mirrors the previously observed increased neural damage in these mice (compare to section 3.3). In accordance, this strengthens the importance of LMP7 and probably of IP formation in controlled microglia conversion, at least during cerebral ischemia.

However, the immunohistochemically observed reduced numerical density of microglial cells in more healthy tissue of LMP7$^{-/-}$ mice could be not confirmed in the FACS analysis (compare Fig. 33C and Fig. 36C, 37C). This discrepancy could be created by the here used methods and the spatially limited investigation of selected brain regions in contrast to complete parts of the brain.

The immunoproteasomal subunits LMP2 and LMP7 are encoded in the genes of the MHCII region and jointly upregulated in antigen-presenting cells during inflammation [20], [35], [112]. In the brain, the expression of MHCII molecules is low and limited to microglia [286]. Due to this, they substantially mediate recruitment and activation of peripheral immune cells. Therefore, the expression of different microglial surface receptors (CD45, MHCII, F4/80, CD11c) in WT and LMP7$^{-/-}$ mice was assessed after 1 d of MCAO using

FACS analysis (Fig. 34). The lack of LMP7 seems to increase the expression of MHCII and F4/80 after cerebral ischemia. The increased levels of MHCII in LMP7$^{-/-}$ microglia would facilitate recognition of extracellular antigens by CD4$^+$ T cells with following potentially enhanced promotion of pro-inflammatory cytokine release and increased cytotoxic effects. The impaired CD4+ T cells that equally lack LMP7 and were suggested to possess altered pro-inflammatory properties would reinforce this effect [287]. Notably, the increased expression of MHCII in LMP7$^{-/-}$ mice is mainly observed in the peri-infarct area that includes the penumbra and remaining parts of the damaged hemisphere. The neuronal cells within this tissue are still capable of survival, but have to cope with the inflammatory environment and are most likely extremely vulnerable to additional disturbances. Similarly, the expression of F4/80 is increased after MCAO in the penumbra and damaged hemisphere of LMP7$^{-/-}$ mice (Fig. 34C) and adds, as a macrophage marker, evidence for a strongly activated state of microglia with potential neurotoxic effects. This could include also enhanced oxidative stress for surrounding neurons due to the massive production of ROS in activated microglia after ischemia [288]. Consequently, the risk of delayed neuronal cell death in the post-ischemic phase is elevated in the peri-infarct region of LMP7$^{-/-}$ animals. At the same time, the LMP7-deficiency seems to have no impact on the expression of the CD45 and CD11c receptors.

Within this context of cerebral ischemia, microglia and macrophages are strongly engaged in the induction, production, and secretion of cytokines. Cytokines are highly potent signaling factors that play a major role in inflammation and transmit various effector functions on cell-cell interactions during an immune response.

Interestingly, the induction of IFN-γ as the major inflammation inducing cytokine seems to be not altered in the two here assessed genotypes. By contrast, mRNA expression levels of TNFα and IL1b, two pro-inflammatory cytokines that are secreted by activated microglia, seem to be increased in the infarct area and the damaged hemisphere after 1d of MCAO (Fig. 38B). In rodent models, a large decrease in infarct volume after ischemia could be demonstrated by pharmacological inhibition of IL1b [233]. This implies a rather promoting effect in infarct expansion of high IL1b levels and possibly reflects the observed brain damage in LMP7$^{-/-}$ mice. The tendency towards increased levels of anti-inflammatory TGF mRNA in those animals would rather refer to enhanced neuroprotective effects, but could also be a consequence of an overall disturbed and altered secretion of inflammatory cytokines in this experimental setup. However, there emerged no effect of LMP7-deficiency on pro-inflammatory IL1a or anti-inflammatory IL10, but in summary a shift within the very complex network of cytokine pathways could be assumed in this case of cerebral ischemia. Moreover, the secretion of pro-inflammatory cytokines like IFN-γ is known to stimulate the expression of IP subunits [246], [247]. Within this context of an

immune response to ischemia, the mentioned characteristics could be part of a negative feedback mechanism in microglia cells that is mediated by the IP. Negative feedback regulation, potentially mediated by the specific presence of LMP7, would allow control over the diverse activation states of microglia. In addition, this mechanism could initiate a conversion towards more anti-inflammatory properties in microglia activation in order to limit neurotoxic processes and promote tissue preservation directly after the acute phase of brain injury. My hypothesis would explain the observed increased neural damage in the LMP7$^{-/-}$ mice caused by an impaired feedback mechanism involving the IP or at least LMP7. In accordance, the observed unaffected protein levels of constitutive standard proteasomes subunits as well as levels of poly-ubiquitinated proteins (Fig. 31,32) would contribute to this hypothesis. The overall proteasomal degradation rate seems to be not impaired by the LMP7 knockout after MCAO and suggests a rather specific function of LMP7, at least within the here investigated context.

4.5 Modulation of IP activity as a putative therapeutic intervention target in cerebral ischemia

My work demonstrates the relevance of increased LMP2 and LMP7 expression in the course of cerebral ischemia caused by permanent MCAO as well as the neuroprotective potential of LMP7 expression itself.

The here-obtained results provide evidence for an important role of LMP7-containing IPs in activated microglia. The derived conclusions about possible functional aspects during cerebral ischemia entail first initiation, preservation, and regulation on microglia activation states including the conversion of M1/M2-associated polarization phenotypes. Secondly, effects on the inflammatory environment and the mediation of cytokine production could be assumed. Thirdly, this includes implications on phagocytic capabilities and the maintenance of general protein homeostasis within this context of oxidative stress. And finally, this comprises an impact on cell-cell interactions and the recruitment as well as activation of adjacent neural cells and infiltrating peripheral immune cells by IP-containing macrophages. In conclusion, an impaired IP formation and changed IP activity within these cells by the lack of LMP7, could produce an imbalance and interruptions in all the processes mentioned and, hence, could promote disease progression in pathologies.

The question remains, how does these results fit, especially in the context of chronic neuroinflammation or auto-immune disease, to numerous studies demonstrating a rather beneficial than detrimental effect of LMP7 inhibition or elimination under pathological conditions?

With regard of the above mentioned regulatory mechanism of IP activity in microglia-mediated neuroinflammation, a spatiotemporal-specific switch of M1/M2-associated phenotypes during the different stages in cerebral ischemia and most probably also in

other neuropathologies, could protect vulnerable tissue and promote repair and rescue mechanism. Besides, another factor that has to be considered is the high number of cellular proteasome subtypes with mixed β and βi subunit compositions and the several possible associations with the regulatory particles that can be formed. The complexity of the UPS and its functional repertoire seems to be further increased by the existence of a varying intracellular proteasome subtype content. This implies on the one hand, various specific cellular functions, but on the other hand it indicates a high compensatory potential to ensure cell vitality. Hence, depending on the time point, localization and extent as well as number of involved subunits, modulations in IP activity could promote advantageous or provoke disadvantageous effects on the progression of disease and pathologies.

In summary, a better understanding of the underlying cellular mechanisms in IP induction, formation and function might unravel the inconsistencies concerning the cytoprotective or -toxic impact of IPs and its single catalytically active subunits, and might help to develop improved therapeutic strategies for a controlled microglia conversion in inflammatory pathologies and providing therapeutic benefit. For instance, a selective inhibition of the IP subunit LMP7 was demonstrated to exhibit low neurotoxicity in comparisan to an overall inhibition of the proteasome in the context of haematopoietic malignancies [186].

5 Outlook

Based on the here presented results, further interesting scientific questions arise for future research.

First of all, future studies could reveal whether there is a similar influence of the other two IP subunits LMP2 and MECL-1 on the outcome of cerebral ischemia using specific knockout mouse models for those subunits. In addition, double and even triple knockout mouse models could be used to obtain a more comprehensive knowledge about the single contributions of the catalytic IP subunits in this context. In comparison with experiments using specific inhibitors of the IP subunits, this could clarify the partially controversial results about the cytoprotective or -toxic role of IPs in cerebral ischemia.

In addition, conditional knockout mice of the single IP subunits would be highly warranted. With such tools, specific functions of the IP in different cell types could be investigated and might help to clarify whether conflicting present facts about the presence, localization and function of IP subunits in the brain and the whole organisms in general.

For a more detailed analysis of inhibition or suppression of IP subunits in neural cells and particular in microglia, organotypical mouse brain slices could be used for diverse pharmacological investigations. This method would allow an elegant simulation of divers pathological conditions such as oxidative stress by H_2O_2 treatment or oxygen deprivation as well as inflammatory stimuli including incubation with pro- and anti-inflammatory cytokines. In addition, the application of specific standard proteasome and IP subunit inhibitors, such as the LMP7 inhibitor ONX-0914, could reveal the functional contribution of single subunits within the complexity of the UPS. At the same time, this more complex model rather mimics the cellular *in vivo* situation as primary neuronal cell cultures. As the ability of specific commercial antibodies raised against the single IP subunits improves, the treated samples could be assessed in immunocytochemical and biochemical terms. This would enable further localization analysis concerning also the subcellular distribution of the IP subunits within neural cells under normal and several other pathological conditions besides ischemia. In addition, supplementation with certain inhibitors of selected signaling cascades could contribute to gain more information about the signaling pathways involved in IP induction and expression.

Furthermore, my studies cover a limited post-ischemic time window of mainly 1 and 2 d after MCAO. A repetition of the FACS, the Skeleton and also biochemical analysis including early as well as later time points would reveal the influence of IP subunits expression in the temporal course of ischemia. This could additionally include a quantification of lymphoid cells and would depict the effects of the IP subunits on the recruitment and activation of other immune cells in cerebral brain ischemia.

As LMP7 seems to exert a significant impact on microglia activity, microglial cultures of WT and knockout animals could be analyzed within a migration assay in order to gain more information for an explanation of the observed altered cell density.

Next, a behavioral characterization of WT and IP-deficient mice after MCAO would reveal the potential of the single IP subunits to affect the loco and sensorimotor abilities of the animals in combination with the observed increased neural damage after cerebral ischemia.

Moreover, and in order to analyze also the opposite situation and the effect of IP subunit overexpression on cell viability under physiological and different neuroinflammatory and/or -pathological conditions, a transfection of primary neuronal cell cultures with the mentioned constructs under normal and pathological stimulations could be performed in future experiments.

And finally, more research on the potential of the IP as a clinical target is highly warranted and could provide better therapeutic options in the treatment of brain injury with neuroinflammation as well as other neurodegenerative disease in the future.

References

[1]   J. Gayon, „Defining Life: Synthesis and Conclusions", *Orig. Life Evol. Biospheres*, Bd. 40, Nr. 2, S. 231–244, Apr. 2010.

[2]   M. Jeuken, „The biological and philosophical definitions of life", *Acta Biotheor.*, Bd. 24, Nr. 1–2, S. 14–21, 1975.

[3]   T. Vellai und G. Vida, „The origin of eukaryotes: the difference between prokaryotic and eukaryotic cells., The origin of eukaryotes: the difference between prokaryotic and eukaryotic cells.", *Proc. R. Soc. B Biol. Sci. Proc. R. Soc. B Biol. Sci.*, Bd. 266, 266, Nr. 1428, 1428, S. 1571, 1571–1577, Aug. 1999.

[4]   E. N. Baker, V. L. Arcus, und J. S. Lott, „Protein structure prediction and analysis as a tool for functional genomics", *Appl. Bioinformatics*, Bd. 2, Nr. 3 Suppl, S. S3-10, 2003.

[5]   J. C. Whisstock und A. M. Lesk, „Prediction of protein function from protein sequence and structure", *Q. Rev. Biophys.*, Bd. 36, Nr. 3, S. 307–340, Aug. 2003.

[6]   B. Alberts, A. Johnson, J. Lewis, M. Raff, K. Roberts, und P. Walter, „Protein Function", 2002.

[7]   O. N. Jensen, „Modification-specific proteomics: characterization of post-translational modifications by mass spectrometry", *Curr. Opin. Chem. Biol.*, Bd. 8, Nr. 1, S. 33–41, Feb. 2004.

[8]   J. Seo und K.-J. Lee, „Post-translational modifications and their biological functions: proteomic analysis and systematic approaches", *J. Biochem. Mol. Biol.*, Bd. 37, Nr. 1, S. 35–44, Jan. 2004.

[9]   E. E. Manasanch und R. Z. Orlowski, „Proteasome inhibitors in cancer therapy", *Nat. Rev. Clin. Oncol.*, Bd. 14, Nr. 7, S. 417–433, Juli 2017.

[10]   L. J. Crawford, B. Walker, und A. E. Irvine, „Proteasome inhibitors in cancer therapy", *J. Cell Commun. Signal.*, Bd. 5, Nr. 2, S. 101–110, Jan. 2011.

[11]   M. Hochstrasser, „Ubiquitin-Dependent Protein Degradation", *Annu. Rev. Genet.*, Bd. 30, Nr. 1, S. 405–439, 1996.

[12]   J. Robert J. Tomko und M. Hochstrasser, „Molecular Architecture and Assembly of the Eukaryotic Proteasome", *Annu. Rev. Biochem.*, Bd. 82, Nr. 1, S. 415–445, 2013.

[13]   T. Jung, B. Catalgol, und T. Grune, „The proteasomal system", *Proteasome*, Bd. 30, Nr. 4, S. 191–296, Aug. 2009.

[14]   R. Raynes, L. C. D. Pomatto, und K. J. A. Davies, „Degradation of oxidized proteins by the proteasome: Distinguishing between the 20S, 26S, and immunoproteasome proteolytic pathways", *Mol. Aspects Med.*, Bd. 50, S. 41, Aug. 2016.

[15]   N. Vigneron und B. Van den Eynde, „Proteasome Subtypes and Regulators in the Processing of Antigenic Peptides Presented by Class I Molecules of the Major Histocompatibility Complex", *Biomolecules*, Bd. 4, Nr. 4, S. 994–1025, Nov. 2014.

[16]   N. Tanahashi, Y. Murakami, Y. Minami, N. Shimbara, K. B. Hendil, und K. Tanaka, „Hybrid Proteasomes INDUCTION BY INTERFERON-γ AND CONTRIBUTION TO ATP-DEPENDENT PROTEOLYSIS", *J. Biol. Chem.*, Bd. 275, Nr. 19, S. 14336–14345, Dez. 2000.

[17]   T. Jung und T. Grune, „Chapter 1 - Structure of the Proteasome", in *Progress in Molecular Biology and Translational Science*, Bd. 109, Supplement C Bde., T. Grune, Hrsg. Academic Press, 2012, S. 1–39.

[18]   M. Unno *u. a.*, „Structure Determination of the Constitutive 20S Proteasome from Bovine Liver at 2.75 Å Resolution", *J. Biochem. (Tokyo)*, Bd. 131, Nr. 2, S. 171–173, Feb. 2002.

[19]   Y. Tomisugi *u. a.*, „New Crystal Forms and Low Resolution Structure Analysis of 20S Proteasomes from Bovine Liver", *J. Biochem. (Tokyo)*, Bd. 127, Nr. 6, S. 941–943, Juni 2000.

[20]   K. Akiyama *u. a.*, „Replacement of proteasome subunits X and Y by LMP7 and LMP2 induced by

interferon-gamma for acquirement of the functional diversity responsible for antigen processing", *FEBS Lett.*, Bd. 343, Nr. 1, S. 85–88, Apr. 1994.

[21]   D. A. Ferrington und D. S. Gregerson, „Immunoproteasomes: Structure, Function, and Antigen Presentation", *Prog. Mol. Biol. Transl. Sci.*, Bd. 109, S. 75–112, 2012.

[22]   J. J. Monaco und H. O. McDevitt, „The LMP antigens: a stable MHC-controlled multisubunit protein complex", *Hum. Immunol.*, Bd. 15, Nr. 4, S. 416–426, Apr. 1986.

[23]   S. Murata *u. a.*, „Regulation of CD8+ T cell development by thymus-specific proteasomes", *Science*, Bd. 316, Nr. 5829, S. 1349–1353, Juni 2007.

[24]   S. Murata, Y. Takahama, und K. Tanaka, „Thymoproteasome: probable role in generating positively selecting peptides", *Curr. Opin. Immunol.*, Bd. 20, Nr. 2, S. 192–196, Apr. 2008.

[25]   K. Takada *u. a.*, „TCR affinity for thymoproteasome-dependent positively selecting peptides conditions antigen responsiveness in CD8+ T cells", *Nat. Immunol.*, Bd. 16, Nr. 10, S. 1069–1076, Aug. 2015.

[26]   K. Tanaka, „The proteasome: Overview of structure and functions", *Proc. Jpn. Acad. Ser. B Phys. Biol. Sci.*, Bd. 85, Nr. 1, S. 12, Jan. 2009.

[27]   L. Budenholzer, C. L. Cheng, Y. Li, und M. Hochstrasser, „Proteasome Structure and Assembly", *Mol. Mech. Regul. Ubiquitin Syst.*, Bd. 429, Nr. 22, S. 3500–3524, Nov. 2017.

[28]   J. M. Belote, M. Miller, und K. A. Smyth, „Evolutionary conservation of a testes-specific proteasome subunit gene in Drosophila", *Gene*, Bd. 215, Nr. 1, S. 93–100, Juli 1998.

[29]   L. Zhong und J. M. Belote, „The testis-specific proteasome subunit Prosα6T of D. melanogaster is required for individualization and nuclear maturation during spermatogenesis", *Development*, Bd. 134, Nr. 19, S. 3517–3525, Okt. 2007.

[30]   M.-X. Qian *u. a.*, „Acetylation-Mediated Proteasomal Degradation of Core Histones during DNA Repair and Spermatogenesis", *Cell*, Bd. 153, Nr. 5, S. 1012–1024, Mai 2013.

[31]   A. R. Kusmierczyk und M. Hochstrasser, „Some Assembly Required: Dedicated Chaperones in Eukaryotic Proteasome Biogenesis", *Biol. Chem.*, Bd. 389, Nr. 9, S. 1143–1151, Sep. 2008.

[32]   S. Murata, H. Yashiroda, und K. Tanaka, „Molecular mechanisms of proteasome assembly", *Nat. Rev. Mol. Cell Biol.*, Bd. 10, Nr. 2, S. 104–115, Feb. 2009.

[33]   P. C. Ramos und R. J. Dohmen, „PACemakers of proteasome core particle assembly", *Struct. Lond. Engl. 1993*, Bd. 16, Nr. 9, S. 1296–1304, Sep. 2008.

[34]   M. De, K. Jayarapu, L. Elenich, J. J. Monaco, R. A. Colbert, und T. A. Griffin, „Beta 2 subunit propeptides influence cooperative proteasome assembly", *J. Biol. Chem.*, Bd. 278, Nr. 8, S. 6153–6159, Feb. 2003.

[35]   T. A. Griffin *u. a.*, „Immunoproteasome assembly: cooperative incorporation of interferon gamma (IFN-gamma)-inducible subunits", *J. Exp. Med.*, Bd. 187, Nr. 1, S. 97–104, Jan. 1998.

[36]   M. Groettrup, S. Standera, R. Stohwasser, und P. M. Kloetzel, „The subunits MECL-1 and LMP2 are mutually required for incorporation into the 20S proteasome", *Proc. Natl. Acad. Sci. U. S. A.*, Bd. 94, Nr. 17, S. 8970–8975, Aug. 1997.

[37]   B. Guillaume *u. a.*, „Two abundant proteasome subtypes that uniquely process some antigens presented by HLA class I molecules", *Proc. Natl. Acad. Sci. U. S. A.*, Bd. 107, Nr. 43, S. 18599–18604, Okt. 2010.

[38]   D. J. Kingsbury, T. A. Griffin, und R. A. Colbert, „Novel propeptide function in 20 S proteasome assembly influences beta subunit composition", *J. Biol. Chem.*, Bd. 275, Nr. 31, S. 24156–24162, Aug. 2000.

[39]   I. Livneh, V. Cohen-Kaplan, C. Cohen-Rosenzweig, N. Avni, und A. Ciechanover, „The life cycle of the 26S proteasome: from birth, through regulation and function, and onto its death", *Cell Res.*, Bd. 26, Nr. 8, S. 869, Aug. 2016.

[40]   T. Jung und T. Grune, „The proteasome and the degradation of oxidized proteins: Part I—structure of

proteasomes", *Redox Biol.*, Bd. 1, Nr. 1, S. 178–182, Jan. 2013.

[41]   M. H. Glickman und A. Ciechanover, „The Ubiquitin-Proteasome Proteolytic Pathway: Destruction for the Sake of Construction", *Physiol. Rev.*, Bd. 82, Nr. 2, S. 373–428, Apr. 2002.

[42]   E. M. Huber und M. Groll, „The Mammalian Proteasome Activator PA28 Forms an Asymmetric α4β3Complex", *Struct. Lond. Engl. 1993*, Bd. 25, Nr. 10, S. 1473-1480.e3, Okt. 2017.

[43]   N. Tanahashi *u. a.*, „Molecular properties of the proteasome activator PA28 family proteins and gamma-interferon regulation", *Genes Cells Devoted Mol. Cell. Mech.*, Bd. 2, Nr. 3, S. 195–211, März 1997.

[44]   P. Cascio, „PA28αβ: The Enigmatic Magic Ring of the Proteasome?", *Biomolecules*, Bd. 4, Nr. 2, S. 566, Juni 2014.

[45]   Z.-X. Wan *u. a.*, „The proteasome activator PA28γ, a negative regulator of p53, is transcriptionally up-regulated by p53", *Int. J. Mol. Sci.*, Bd. 15, Nr. 2, S. 2573–2584, Feb. 2014.

[46]   Z. Zhang und R. Zhang, „Proteasome activator PA28 gamma regulates p53 by enhancing its MDM2-mediated degradation", *EMBO J.*, Bd. 27, Nr. 6, S. 852–864, März 2008.

[47]   X. Li *u. a.*, „The SRC-3/AIB1 coactivator is degraded in a ubiquitin- and ATP-independent manner by the REGgamma proteasome", *Cell*, Bd. 124, Nr. 2, S. 381–392, Jan. 2006.

[48]   X. Li, L. Amazit, W. Long, D. M. Lonard, J. J. Monaco, und B. W. O'Malley, „Ubiquitin- and ATP-independent proteolytic turnover of p21 by the REGgamma-proteasome pathway", *Mol. Cell*, Bd. 26, Nr. 6, S. 831–842, Juni 2007.

[49]   V. Ustrell, L. Hoffman, G. Pratt, und M. Rechsteiner, „PA200, a nuclear proteasome activator involved in DNA repair", *EMBO J.*, Bd. 21, Nr. 13, S. 3516–3525, Juli 2002.

[50]   D. M. W. Zaiss, S. Standera, P.-M. Kloetzel, und A. J. A. M. Sijts, „PI31 is a modulator of proteasome formation and antigen processing", *Proc. Natl. Acad. Sci. U. S. A.*, Bd. 99, Nr. 22, S. 14344–14349, Okt. 2002.

[51]   L. Bedford, S. Paine, P. W. Sheppard, R. J. Mayer, und J. Roelofs, „Assembly, Structure and Function of the 26S proteasome", *Trends Cell Biol.*, Bd. 20, Nr. 7, S. 391–401, Juli 2010.

[52]   M. Funakoshi, R. J. Tomko, H. Kobayashi, und M. Hochstrasser, „Multiple assembly chaperones govern biogenesis of the proteasome regulatory particle base", *Cell*, Bd. 137, Nr. 5, S. 887–899, Mai 2009.

[53]   J. Roelofs *u. a.*, „Chaperone-mediated pathway of proteasome regulatory particle assembly", *Nature*, Bd. 459, Nr. 7248, S. 861–865, Juni 2009.

[54]   E. J. a. M. Sijts und P.-M. Kloetzel, „The role of the proteasome in the generation of MHC class I ligands and immune responses", *Cell. Mol. Life Sci.*, Bd. 68, Nr. 9, S. 1491–1502, Mai 2011.

[55]   M. Díaz-Hernández *u. a.*, „Neuronal induction of the immunoproteasome in Huntington's disease", *J. Neurosci. Off. J. Soc. Neurosci.*, Bd. 23, Nr. 37, S. 11653–11661, Dez. 2003.

[56]   M. Díaz-Hernández, E. Martín-Aparicio, J. Avila, F. Hernández, und J. J. Lucas, „Enhanced induction of the immunoproteasome by interferon gamma in neurons expressing mutant Huntingtin", *Neurotox. Res.*, Bd. 6, Nr. 6, S. 463–468, 2004.

[57]   A. H. P. Jansen, E. A. J. Reits, und E. M. Hol, „The ubiquitin proteasome system in glia and its role in neurodegenerative diseases", *Front. Mol. Neurosci.*, Bd. 7, 2014.

[58]   M. Kremer *u. a.*, „Reduced Immunoproteasome Formation and Accumulation of Immunoproteasomal Precursors in the Brains of Lymphocytic Choriomeningitis Virus-Infected Mice", *J. Immunol.*, Bd. 185, Nr. 9, S. 5549–5560, Nov. 2010.

[59]   M. Mishto *u. a.*, „Immunoproteasome and LMP2 polymorphism in aged and Alzheimer's disease brains", *Neurobiol. Aging*, Bd. 27, Nr. 1, S. 54–66, Jan. 2006.

[60]   D. Vilchez, I. Saez, und A. Dillin, „The role of protein clearance mechanisms in organismal ageing and age-related diseases", *Nat. Commun.*, Bd. 5, S. 5659, Dez. 2014.

[61]   H. K. Johnston-Carey, L. C. D. Pomatto, und K. J. A. Davies, „The Immunoproteasome in Oxidative Stress, Aging, and Disease", *Crit. Rev. Biochem. Mol. Biol.*, Bd. 51, Nr. 4, S. 268, Aug. 2015.

[62]   A. M. Pickering und K. J. A. Davies, „Degradation of Damaged Proteins - The Main Function of the 20S Proteasome", *Prog. Mol. Biol. Transl. Sci.*, Bd. 109, S. 227, 2012.

[63]   U. Seifert *u. a.*, „Immunoproteasomes Preserve Protein Homeostasis upon Interferon-Induced Oxidative Stress", *Cell*, Bd. 142, Nr. 4, S. 613–624, Aug. 2010.

[64]   A. M. Hamilton und K. Zito, „Breaking It Down: The Ubiquitin Proteasome System in Neuronal Morphogenesis", *Neural Plasticity*, 2013. [Online]. Verfügbar unter: https://www.hindawi.com/journals/np/2013/196848/. [Zugegriffen: 18-Okt-2017].

[65]   L. Hicke, „Ubiquitin and proteasomes: Protein regulation by monoubiquitin", *Nat. Rev. Mol. Cell Biol.*, Bd. 2, Nr. 3, S. 195–201, März 2001.

[66]   R. C. Piper, I. Dikic, und G. L. Lukacs, „Ubiquitin-Dependent Sorting in Endocytosis", *Cold Spring Harb. Perspect. Biol.*, Bd. 6, Nr. 1, Jan. 2014.

[67]   A. M. Weissman, „Ubiquitin and proteasomes: Themes and variations on ubiquitylation", *Nat. Rev. Mol. Cell Biol.*, Bd. 2, Nr. 3, S. 169–178, März 2001.

[68]   J. Spence, S. Sadis, A. L. Haas, und D. Finley, „A ubiquitin mutant with specific defects in DNA repair and multiubiquitination.", *Mol. Cell. Biol.*, Bd. 15, Nr. 3, S. 1265–1273, März 1995.

[69]   I. Korovila *u. a.*, „Proteostasis, oxidative stress and aging", *Redox Biol.*, Bd. 13, S. 550–567, Okt. 2017.

[70]   F. Luciani, C. Keşmir, M. Mishto, M. Or-Guil, und R. J. de Boer, „A Mathematical Model of Protein Degradation by the Proteasome", *Biophys. J.*, Bd. 88, Nr. 4, S. 2422–2432, Apr. 2005.

[71]   J. Herrmann, L. O. Lerman, und A. Lerman, „Ubiquitin and ubiquitin-like proteins in protein regulation", *Circ. Res.*, Bd. 100, Nr. 9, S. 1276–1291, Mai 2007.

[72]   C. Cubeñas-Potts und M. J. Matunis, „SUMO: A Multifaceted Modifier of Chromatin Structure and Function", *Dev. Cell*, Bd. 24, Nr. 1, S. 1–12, Jan. 2013.

[73]   R. T. Hay, „SUMO: A History of Modification", *Mol. Cell*, Bd. 18, Nr. 1, S. 1–12, Apr. 2005.

[74]   D. P. Xirodimas, „Novel substrates and functions for the ubiquitin-like molecule NEDD8", *Biochem. Soc. Trans.*, Bd. 36, Nr. 5, S. 802–806, Okt. 2008.

[75]   J. Ying, M. Zhang, X. Qiu, und Y. Lu, „Targeting the neddylation pathway in cells as a potential therapeutic approach for diseases", *Cancer Chemother. Pharmacol.*, S. 1–12, Feb. 2018.

[76]   B. Khoshnood, I. Dacklin, und C. Grabbe, „Urm1: an essential regulator of JNK signaling and oxidative stress in Drosophila melanogaster", *Cell. Mol. Life Sci. CMLS*, Bd. 73, Nr. 9, S. 1939–1954, Mai 2016.

[77]   P. G. A. Pedrioli, S. Leidel, und K. Hofmann, „Urm1 at the crossroad of modifications", *EMBO Rep.*, Bd. 9, Nr. 12, S. 1196–1202, Dez. 2008.

[78]   A. M. Burroughs, S. Balaji, L. M. Iyer, und L. Aravind, „Small but versatile: the extraordinary functional and structural diversity of the beta-grasp fold", *Biol. Direct*, Bd. 2, S. 18, Juli 2007.

[79]   L. Cappadocia und C. D. Lima, „Ubiquitin-like Protein Conjugation: Structures, Chemistry, and Mechanism", 24-Feb-2017. [Online]. Verfügbar unter: http://pubs.acs.org/doi/full/10.1021/acs.chemrev.6b00737. [Zugegriffen: 23-Feb-2018].

[80]   T. Jung, N. Bader, und T. Grune, „Oxidized proteins: Intracellular distribution and recognition by the proteasome", *Arch. Biochem. Biophys.*, Bd. 462, Nr. 2, S. 231–237, Juni 2007.

[81]   U. T. Brunk und A. Terman, „Lipofuscin: mechanisms of age-related accumulation and influence on cell function12 1Guest Editor: Rajindar S. Sohal 2This article is part of a series of reviews on "Oxidative Stress and Aging." The full list of papers may be found on the homepage of the journal.", *Free Radic. Biol. Med.*, Bd. 33, Nr. 5, S. 611–619, Sep. 2002.

[82]   M. Lefaki, N. Papaevgeniou, und N. Chondrogianni, „Redox regulation of proteasome function", *Redox Biol.*, Bd. 13, S. 452–458, Okt. 2017.

[83]   K. J. Davies, „Degradation of oxidized proteins by the 20S proteasome“, *Biochimie*, Bd. 83, Nr. 3–4, S. 301–310, Apr. 2001.

[84]   T. Grune, K. Merker, G. Sandig, und K. J. A. Davies, „Selective degradation of oxidatively modified protein substrates by the proteasome“, *Biochem. Biophys. Res. Commun.*, Bd. 305, Nr. 3, S. 709–718, Juni 2003.

[85]   R. Shringarpure, T. Grune, J. Mehlhase, und K. J. A. Davies, „Ubiquitin conjugation is not required for the degradation of oxidized proteins by proteasome“, *J. Biol. Chem.*, Bd. 278, Nr. 1, S. 311–318, Jan. 2003.

[86]   A. M. Pickering und K. J. A. Davies, „Differential Roles of Proteasome and Immunoproteasome Regulators Pa28αβ, Pa28γ and Pa200 in the Degradation of Oxidized Proteins“, *Arch. Biochem. Biophys.*, Bd. 523, Nr. 2, S. 181–190, Juli 2012.

[87]   A. M. Pickering, A. L. Koop, C. Y. Teoh, G. Ermak, T. Grune, und K. J. A. Davies, „The immunoproteasome, the 20S proteasome and the PA28αβ proteasome regulator are oxidative-stress-adaptive proteolytic complexes“, *Biochem. J.*, Bd. 432, Nr. 3, S. 585–594, Dez. 2010.

[88]   G. H. Danton und W. D. Dietrich, „Inflammatory Mechanisms after Ischemia and Stroke“, *J. Neuropathol. Exp. Neurol.*, Bd. 62, Nr. 2, S. 127–136, Feb. 2003.

[89]   C. H. Y. Wong und P. J. Crack, „Modulation of neuro-inflammation and vascular response by oxidative stress following cerebral ischemia-reperfusion injury“, *Curr. Med. Chem.*, Bd. 15, Nr. 1, S. 1–14, 2008.

[90]   A. J. Williams *u. a.*, „Delayed treatment with MLN519 reduces infarction and associated neurologic deficit caused by focal ischemic brain injury in rats via antiinflammatory mechanisms involving nuclear factor-kappaB activation, gliosis, and leukocyte infiltration“, *J. Cereb. Blood Flow Metab. Off. J. Int. Soc. Cereb. Blood Flow Metab.*, Bd. 23, Nr. 1, S. 75–87, Jan. 2003.

[91]   C. Wojcik und M. Di Napoli, „Ubiquitin-proteasome system and proteasome inhibition: new strategies in stroke therapy“, *Stroke*, Bd. 35, Nr. 6, S. 1506–1518, Juni 2004.

[92]   A. L. Santos und A. B. Lindner, „Protein Posttranslational Modifications: Roles in Aging and Age-Related Disease“, *Oxid. Med. Cell. Longev.*, Bd. 2017, 2017.

[93]   L. Ellgaard und A. Helenius, „Quality control in the endoplasmic reticulum“, *Nat. Rev. Mol. Cell Biol.*, Bd. 4, Nr. 3, S. 181–191, März 2003.

[94]   M. M. Jørgensen, P. Bross, und N. Gregersen, „Protein quality control in the endoplasmic reticulum“, *APMIS. Suppl.*, Nr. 109, S. 86–91, 2003.

[95]   U. Schubert, L. C. Antón, J. Gibbs, C. C. Norbury, J. W. Yewdell, und J. R. Bennink, „Rapid degradation of a large fraction of newly synthesized proteins by proteasomes“, *Nature*, Bd. 404, Nr. 6779, S. 770–774, Apr. 2000.

[96]   F. Wang, L. A. Canadeo, und J. M. Huibregtse, „Ubiquitination of newly synthesized proteins at the ribosome“, *Biochimie*, Bd. 114, S. 127–133, Juli 2015.

[97]   I. Amm, T. Sommer, und D. H. Wolf, „Protein quality control and elimination of protein waste: the role of the ubiquitin-proteasome system“, *Biochim. Biophys. Acta*, Bd. 1843, Nr. 1, S. 182–196, Jan. 2014.

[98]   E. K. Fredrickson und R. G. Gardner, „Selective destruction of abnormal proteins by ubiquitin-mediated protein quality control degradation“, *Semin. Cell Dev. Biol.*, Bd. 23, Nr. 5, S. 530–537, Juli 2012.

[99]   X. L. Fu und D. S. Gao, „Endoplasmic reticulum proteins quality control and the unfolded protein response: the regulative mechanism of organisms against stress injuries“, *BioFactors Oxf. Engl.*, Bd. 40, Nr. 6, S. 569–585, Dez. 2014.

[100]   S.-B. Qian, M. F. Princiotta, J. R. Bennink, und J. W. Yewdell, „Characterization of rapidly degraded polypeptides in mammalian cells reveals a novel layer of nascent protein quality control“, *J. Biol. Chem.*, Bd. 281, Nr. 1, S. 392–400, Jan. 2006.

[101]   I. M. Konstantinova, A. S. Tsimokha, und A. G. Mittenberg, „Role of proteasomes in cellular

regulation“, *Int. Rev. Cell Mol. Biol.*, Bd. 267, S. 59–124, 2008.

[102]   J. R. Skaar und M. Pagano, „Control of cell growth by the SCF and APC/C ubiquitin ligases“, *Curr. Opin. Cell Biol.*, Bd. 21, Nr. 6, S. 816–824, Dez. 2009.

[103]   F. Geng, S. Wenzel, und W. P. Tansey, „Ubiquitin and Proteasomes in Transcription“, *Annu. Rev. Biochem.*, Bd. 81, S. 177–201, 2012.

[104]   T. Yao und A. Ndoja, „Regulation of gene expression by the ubiquitin-proteasome system“, *Semin. Cell Dev. Biol.*, Bd. 23, Nr. 5, S. 523–529, Juli 2012.

[105]   T. Elliott und A. Williams, „The optimization of peptide cargo bound to MHC class I molecules by the peptide-loading complex“, *Immunol. Rev.*, Bd. 207, S. 89–99, Okt. 2005.

[106]   X. C. Li und M. Raghavan, „Structure and function of major histocompatibility complex (MHC) class I antigens“, *Curr. Opin. Organ Transplant.*, Bd. 15, Nr. 4, S. 499–504, Aug. 2010.

[107]   J. S. Blum, P. A. Wearsch, und P. Cresswell, „Pathways of Antigen Processing“, *Annu. Rev. Immunol.*, Bd. 31, Nr. 1, S. 443–473, 2013.

[108]   M. Basler, J. Moebius, L. Elenich, M. Groettrup, und J. J. Monaco, „An Altered T Cell Repertoire in MECL-1-Deficient Mice“, *J. Immunol.*, Bd. 176, Nr. 11, S. 6665–6672, Juni 2006.

[109]   H. J. Fehling *u. a.*, „MHC class I expression in mice lacking the proteasome subunit LMP-7“, *Science*, Bd. 265, Nr. 5176, S. 1234–1237, Aug. 1994.

[110]   E. Z. Kincaid *u. a.*, „Mice completely lacking immunoproteasomes show major changes in antigen presentation“, *Nat. Immunol.*, Bd. 13, Nr. 2, S. 129–135, Feb. 2012.

[111]   L. Van Kaer *u. a.*, „Altered peptidase and viral-specific T cell response in LMP2 mutant mice“, *Immunity*, Bd. 1, Nr. 7, S. 533–541, Okt. 1994.

[112]   M. Basler, C. J. Kirk, und M. Groettrup, „The immunoproteasome in antigen processing and other immunological functions“, *Curr. Opin. Immunol.*, Bd. 25, Nr. 1, S. 74–80, Feb. 2013.

[113]   F. Ebstein, P.-M. Kloetzel, E. Krüger, und U. Seifert, „Emerging roles of immunoproteasomes beyond MHC class I antigen processing“, *Cell. Mol. Life Sci. CMLS*, Bd. 69, Nr. 15, S. 2543–2558, Aug. 2012.

[114]   M. Basler *u. a.*, „Why the structure but not the activity of the immunoproteasome subunit low molecular mass polypeptide 2 rescues antigen presentation“, *J. Immunol. Baltim. Md 1950*, Bd. 189, Nr. 4, S. 1868–1877, Aug. 2012.

[115]   M. Groettrup, C. J. Kirk, und M. Basler, „Proteasomes in immune cells: more than peptide producers?“, *Nat. Rev. Immunol.*, Bd. 10, Nr. 1, S. 73–78, 2010.

[116]   E. S. Schultz *u. a.*, „The Production of a New MAGE-3 Peptide Presented to Cytolytic T Lymphocytes by HLA-B40 Requires the Immunoproteasome“, *J. Exp. Med.*, Bd. 195, Nr. 4, S. 391, Feb. 2002.

[117]   A. J. A. M. Sijts, T. Ruppert, B. Rehermann, M. Schmidt, U. Koszinowski, und P.-M. Kloetzel, „Efficient Generation of a Hepatitis B Virus Cytotoxic T Lymphocyte Epitope Requires the Structural Features of Immunoproteasomes“, *J. Exp. Med.*, Bd. 191, Nr. 3, S. 503–514, Feb. 2000.

[118]   H. Fehling *u. a.*, „MHC class I expression in mice lacking the proteasome subunit LMP-7“, *Science*, Bd. 265, Nr. 5176, S. 1234, Aug. 1994.

[119]   M. Mishto *u. a.*, „Proteasome isoforms exhibit only quantitative differences in cleavage and epitope generation“, *Eur. J. Immunol.*, Bd. 44, Nr. 12, S. 3508–3521, Dez. 2014.

[120]   D. Zanker und W. Chen, „Standard and immunoproteasomes show similar peptide degradation specificities“, *Eur. J. Immunol.*, Bd. 44, Nr. 12, S. 3500–3503, Dez. 2014.

[121]   I. A. York, A. L. Goldberg, X. Y. Mo, und K. L. Rock, „Proteolysis and class I major histocompatibility complex antigen presentation“, *Immunol. Rev.*, Bd. 172, S. 49–66, Dez. 1999.

[122]   A. Dalet, V. Stroobant, N. Vigneron, und B. J. Van den Eynde, „Differences in the production of spliced antigenic peptides by the standard proteasome and the immunoproteasome“, *Eur. J. Immunol.*, Bd. 41, Nr. 1, S. 39–46, Jan. 2011.

[123]   W. Chen, C. C. Norbury, Y. Cho, J. W. Yewdell, und J. R. Bennink, „Immunoproteasomes Shape Immunodominance Hierarchies of Antiviral Cd8+ T Cells at the Levels of T Cell Repertoire and Presentation of Viral Antigens", *J. Exp. Med.*, Bd. 193, Nr. 11, S. 1319–1326, Juni 2001.

[124]   S. Morel *u. a.*, „Processing of some antigens by the standard proteasome but not by the immunoproteasome results in poor presentation by dendritic cells", *Immunity*, Bd. 12, Nr. 1, S. 107–117, Jan. 2000.

[125]   R. Fonseca, R. M. Vabulas, F. U. Hartl, T. Bonhoeffer, und U. V. Nägerl, „A Balance of Protein Synthesis and Proteasome-Dependent Degradation Determines the Maintenance of LTP", *Neuron*, Bd. 52, Nr. 2, S. 239–245, Okt. 2006.

[126]   T. J. Jarome und F. J. Helmstetter, „Protein degradation and protein synthesis in long-term memory formation", *Front. Mol. Neurosci.*, Bd. 7, Juni 2014.

[127]   A. Karpova, M. Mikhaylova, U. Thomas, T. Knöpfel, und T. Behnisch, „Involvement of protein synthesis and degradation in long-term potentiation of Schaffer collateral CA1 synapses", *J. Neurosci. Off. J. Soc. Neurosci.*, Bd. 26, Nr. 18, S. 4949–4955, Mai 2006.

[128]   B. Bingol und E. M. Schuman, „Synaptic protein degradation by the ubiquitin proteasome system", *Curr. Opin. Neurobiol.*, Bd. 15, Nr. 5, S. 536–541, Okt. 2005.

[129]   K. Willeumier, S. M. Pulst, und F. E. Schweizer, „Proteasome inhibition triggers activity-dependent increase in the size of the recycling vesicle pool in cultured hippocampal neurons", *J. Neurosci. Off. J. Soc. Neurosci.*, Bd. 26, Nr. 44, S. 11333–11341, Nov. 2006.

[130]   A. Kato, N. Rouach, R. A. Nicoll, und D. S. Bredt, „Activity-dependent NMDA receptor degradation mediated by retrotranslocation and ubiquitination", *Proc. Natl. Acad. Sci. U. S. A.*, Bd. 102, Nr. 15, S. 5600–5605, Apr. 2005.

[131]   R. S. Saliba, G. Michels, T. C. Jacob, M. N. Pangalos, und S. J. Moss, „Activity-dependent ubiquitination of GABA(A) receptors regulates their accumulation at synaptic sites", *J. Neurosci. Off. J. Soc. Neurosci.*, Bd. 27, Nr. 48, S. 13341–13351, Nov. 2007.

[132]   L. A. Schwarz, B. J. Hall, und G. N. Patrick, „Activity-dependent ubiquitination of GluA1 mediates a distinct AMPA receptor endocytosis and sorting pathway", *J. Neurosci. Off. J. Soc. Neurosci.*, Bd. 30, Nr. 49, S. 16718–16729, Dez. 2010.

[133]   J. Widagdo *u. a.*, „Activity-Dependent Ubiquitination of GluA1 and GluA2 Regulates AMPA Receptor Intracellular Sorting and Degradation", *Cell Rep.*, Feb. 2015.

[134]   J. Widagdo, S. Guntupalli, S. E. Jang, und V. Anggono, „Regulation of AMPA Receptor Trafficking by Protein Ubiquitination", *Front. Mol. Neurosci.*, Bd. 10, S. 347, 2017.

[135]   M. D. Ehlers, „Activity level controls postsynaptic composition and signaling via the ubiquitin-proteasome system", *Nat. Neurosci.*, Bd. 6, Nr. 3, S. 231–242, März 2003.

[136]   A. N. Hegde, „Proteolysis, synaptic plasticity and memory", *Neurobiol. Learn. Mem.*, Bd. 138, Nr. Supplement C, S. 98–110, Feb. 2017.

[137]   C. Dong, S. C. Upadhya, L. Ding, T. K. Smith, und A. N. Hegde, „Proteasome inhibition enhances the induction and impairs the maintenance of late-phase long-term potentiation", *Learn. Mem. Cold Spring Harb. N*, Bd. 15, Nr. 5, S. 335–347, Mai 2008.

[138]   S. C. Upadhya, T. K. Smith, und A. N. Hegde, „Ubiquitin-proteasome-mediated CREB repressor degradation during induction of long-term facilitation", *J. Neurochem.*, Bd. 91, Nr. 1, S. 210–219, Okt. 2004.

[139]   I. B. Zovkic, M. C. Guzman-Karlsson, und J. D. Sweatt, „Epigenetic regulation of memory formation and maintenance", *Learn. Mem. Cold Spring Harb. N*, Bd. 20, Nr. 2, S. 61–74, Jan. 2013.

[140]   J. J. Day und J. D. Sweatt, „Epigenetic mechanisms in cognition", *Neuron*, Bd. 70, Nr. 5, S. 813–829, Juni 2011.

[141]   S. V. Bach, P. R. Tacon, J. W. Morgan, und A. N. Hegde, „Proteasome regulates transcription-

favoring histone methylation, acetylation and ubiquitination in long-term synaptic plasticity", *Neurosci. Lett.*, Bd. 591, S. 59–64, März 2015.

[142]   K. F. Haas und K. Broadie, „Roles of ubiquitination at the synapse", *Biochim. Biophys. Acta*, Bd. 1779, Nr. 8, S. 495, Aug. 2008.

[143]   C. Noda, N. Tanahashi, N. Shimbara, K. B. Hendil, und K. Tanaka, „Tissue distribution of constitutive proteasomes, immunoproteasomes, and PA28 in rats", *Biochem. Biophys. Res. Commun.*, Bd. 277, Nr. 2, S. 348–354, Okt. 2000.

[144]   D. A. Ferrington *u. a.*, „Immunoproteasome responds to injury in the retina and brain", *J. Neurochem.*, Bd. 106, Nr. 1, S. 158, Juli 2008.

[145]   S. Morrison und K. M. Newell, „Aging, Neuromuscular Decline, and the Change in Physiological and Behavioral Complexity of Upper-Limb Movement Dynamics", *Journal of Aging Research*, 2012. [Online]. Verfügbar unter: https://www.hindawi.com/journals/jar/2012/891218/. [Zugegriffen: 20-Mai-2018].

[146]   S. R. Powell *u. a.*, „Aggregates of oxidized proteins (lipofuscin) induce apoptosis through proteasome inhibition and dysregulation of proapoptotic proteins", *Free Radic. Biol. Med.*, Bd. 38, Nr. 8, S. 1093–1101, Apr. 2005.

[147]   R. Shringarpure und K. J. A. Davies, „Protein turnover by the proteasome in aging and disease", *Free Radic. Biol. Med.*, Bd. 32, Nr. 11, S. 1084–1089, Juni 2002.

[148]   A. Terman und S. Sandberg, „Proteasome Inhibition Enhances Lipofuscin Formation", *Ann. N. Y. Acad. Sci.*, Bd. 973, Nr. 1, S. 309–312, Nov. 2002.

[149]   T. C. Squier, „Oxidative stress and protein aggregation during biological aging", *Exp. Gerontol.*, Bd. 36, Nr. 9, S. 1539–1550, Sep. 2001.

[150]   J. M. Ross, L. Olson, und G. Coppotelli, „Mitochondrial and Ubiquitin Proteasome System Dysfunction in Ageing and Disease: Two Sides of the Same Coin?", *Int. J. Mol. Sci.*, Bd. 16, Nr. 8, S. 19458–19476, Aug. 2015.

[151]   E. Kabashi und H. D. Durham, „Failure of protein quality control in amyotrophic lateral sclerosis", *Biochim. Biophys. Acta BBA - Mol. Basis Dis.*, Bd. 1762, Nr. 11, S. 1038–1050, Nov. 2006.

[152]   P. Kumar *u. a.*, „CHIP and HSPs interact with β-APP in a proteasome-dependent manner and influence Aβ metabolism", *Hum. Mol. Genet.*, Bd. 16, Nr. 7, S. 848–864, Apr. 2007.

[153]   M. J. Strong, S. Kesavapany, und H. C. Pant, „The Pathobiology of Amyotrophic Lateral Sclerosis: A Proteinopathy?", *J. Neuropathol. Exp. Neurol.*, Bd. 64, Nr. 8, S. 649–664, Aug. 2005.

[154]   T. J. Jensen, M. A. Loo, S. Pind, D. B. Williams, A. L. Goldberg, und J. R. Riordan, „Multiple proteolytic systems, including the proteasome, contribute to CFTR processing", *Cell*, Bd. 83, Nr. 1, S. 129–135, Okt. 1995.

[155]   G. C. Meacham, C. Patterson, W. Zhang, J. M. Younger, und D. M. Cyr, „The Hsc70 co-chaperone CHIP targets immature CFTR for proteasomal degradation", *Nat. Cell Biol.*, Bd. 3, Nr. 1, S. 100–105, Jan. 2001.

[156]   J. M. Younger *u. a.*, „Sequential Quality-Control Checkpoints Triage Misfolded Cystic Fibrosis Transmembrane Conductance Regulator", *Cell*, Bd. 126, Nr. 3, S. 571–582, Aug. 2006.

[157]   O. Drews und H. Taegtmeyer, „Targeting the ubiquitin-proteasome system in heart disease: the basis for new therapeutic strategies", *Antioxid. Redox Signal.*, Bd. 21, Nr. 17, S. 2322–2343, Dez. 2014.

[158]   J. Herrmann, L. O. Lerman, und A. Lerman, „On to the road to degradation: atherosclerosis and the proteasome", *Cardiovasc. Res.*, Bd. 85, Nr. 2, S. 291–302, Jan. 2010.

[159]   P. J. Elliott, T. M. Zollner, und W.-H. Boehncke, „Proteasome inhibition: a new anti-inflammatory strategy", *J. Mol. Med.*, Bd. 81, Nr. 4, S. 235–245, Apr. 2003.

[160]   S. E. Verbrugge, R. J. Scheper, W. F. Lems, T. D. de Gruijl, und G. Jansen, „Proteasome inhibitors as experimental therapeutics of autoimmune diseases", *Arthritis Res. Ther.*, Bd. 17, S. 17, Jan. 2015.

[161]   A. Calistri, D. Munegato, I. Carli, C. Parolin, und G. Palù, „The Ubiquitin-Conjugating System: Multiple Roles in Viral Replication and Infection", *Cells*, Bd. 3, Nr. 2, S. 386–417, Mai 2014.

[162]   H. Luo, „Interplay between the virus and the ubiquitin-proteasome system: molecular mechanism of viral pathogenesis", *Curr. Opin. Virol.*, Bd. 17, S. 1–10, 2016.

[163]   N. Ahmed, R. Babaei-Jadidi, S. K. Howell, P. J. Beisswenger, und P. J. Thornalley, „Degradation products of proteins damaged by glycation, oxidation and nitration in clinical type 1 diabetes", *Diabetologia*, Bd. 48, Nr. 8, S. 1590–1603, Aug. 2005.

[164]   R. G. Bennett, J. Fawcett, M. C. Kruer, W. C. Duckworth, und F. G. Hamel, „Insulin inhibition of the proteasome is dependent on degradation of insulin by insulin-degrading enzyme", *J. Endocrinol.*, Bd. 177, Nr. 3, S. 399–405, Jan. 2003.

[165]   B. P. Tseng, K. N. Green, J. L. Chan, M. Blurton-Jones, und F. M. LaFerla, „Aβ inhibits the proteasome and enhances amyloid and tau accumulation", *Neurobiol. Aging*, Bd. 29, Nr. 11, S. 1607–1618, Nov. 2008.

[166]   M. Orre *u. a.*, „Reactive glia show increased immunoproteasome activity in Alzheimer's disease", *Brain*, Bd. 136, Nr. 5, S. 1415–1431, Mai 2013.

[167]   Z. Ortega, M. Díaz-Hernández, und J. J. Lucas, „Is the ubiquitin-proteasome system impaired in Huntington's disease?", *Cell. Mol. Life Sci. CMLS*, Bd. 64, Nr. 17, S. 2245–2257, Sep. 2007.

[168]   S. Schipper-Krom *u. a.*, „Dynamic recruitment of active proteasomes into polyglutamine initiated inclusion bodies", *FEBS Lett.*, Bd. 588, Nr. 1, S. 151–159, Jan. 2014.

[169]   T. Yasuda und H. Mochizuki, „The regulatory role of α-synuclein and parkin in neuronal cell apoptosis; possible implications for the pathogenesis of Parkinson's disease", *Apoptosis Int. J. Program. Cell Death*, Bd. 15, Nr. 11, S. 1312–1321, Nov. 2010.

[170]   T. Yasuda, Y. Nakata, und H. Mochizuki, „α-Synuclein and neuronal cell death", *Mol. Neurobiol.*, Bd. 47, Nr. 2, S. 466–483, Apr. 2013.

[171]   C. Zheng, T. Geetha, und J. R. Babu, „Failure of ubiquitin proteasome system: risk for neurodegenerative diseases", *Neurodegener. Dis.*, Bd. 14, Nr. 4, S. 161–175, 2014.

[172]   T. Muchamuel *u. a.*, „A selective inhibitor of the immunoproteasome subunit LMP7 blocks cytokine production and attenuates progression of experimental arthritis", *Nat. Med.*, Bd. 15, Nr. 7, S. 781–787, Juni 2009.

[173]   A. K. Agarwal *u. a.*, „PSMB8 Encoding the β5i Proteasome Subunit Is Mutated in Joint Contractures, Muscle Atrophy, Microcytic Anemia, and Panniculitis-Induced Lipodystrophy Syndrome", *Am. J. Hum. Genet.*, Bd. 87, Nr. 6, S. 866–872, Dez. 2010.

[174]   K. Arima *u. a.*, „Proteasome assembly defect due to a proteasome subunit beta type 8 (PSMB8) mutation causes the autoinflammatory disorder, Nakajo-Nishimura syndrome", *Proc. Natl. Acad. Sci.*, Bd. 108, Nr. 36, S. 14914–14919, Sep. 2011.

[175]   K. Kunimoto *u. a.*, „A New Infant Case of Nakajo-Nishimura Syndrome with a Genetic Mutation in the Immunoproteasome Subunit: An Overlapping Entity with JMP and CANDLE Syndrome Related to PSMB8 Mutations", *Dermatology*, Bd. 227, Nr. 1, S. 26–30, 2013.

[176]   F. Ding, H. Xiao, M. Wang, X. Xie, und F. Hu, „The role of the ubiquitin-proteasome pathway in cancer development and treatment", *Front. Biosci. Landmark Ed.*, Bd. 19, S. 886–895, Juni 2014.

[177]   T. A. Grigoreva, V. G. Tribulovich, A. V. Garabadzhiu, G. Melino, und N. A. Barlev, „The 26S proteasome is a multifaceted target for anti-cancer therapies", *Oncotarget*, Bd. 6, Nr. 28, S. 24733–24749, Sep. 2015.

[178]   T. Jung, B. Catalgol, und T. Grune, „The proteasomal system", *Proteasome*, Bd. 30, Nr. 4, S. 191–296, Aug. 2009.

[179]   L.-P. Li *u. a.*, „Expression of proteasome activator REGγ in human laryngeal carcinoma and

associations with tumor suppressor proteins", *Asian Pac. J. Cancer Prev. APJCP*, Bd. 13, Nr. 6, S. 2699–2703, 2012.

[180]   M. Pagano *u. a.*, „Role of the ubiquitin-proteasome pathway in regulating abundance of the cyclin-dependent kinase inhibitor p27", *Science*, Bd. 269, Nr. 5224, S. 682–685, Aug. 1995.

[181]   M. Shen, S. Schmitt, D. Buac, und Q. P. Dou, „Targeting the ubiquitin-proteasome system for cancer therapy", *Expert Opin. Ther. Targets*, Bd. 17, Nr. 9, S. 1091–1108, Sep. 2013.

[182]   J. B. Almond und G. M. Cohen, „The proteasome: a novel target for cancer chemotherapy", *Leukemia*, Bd. 16, Nr. 4, S. 433–443, Apr. 2002.

[183]   J. Adams, „The proteasome: a suitable antineoplastic target", *Nat. Rev. Cancer*, Bd. 4, Nr. 5, S. 349–360, Mai 2004.

[184]   O. Landgren und K. Iskander, „Modern multiple myeloma therapy: deep, sustained treatment response and good clinical outcomes", *J Intern Med*, Feb. 2017.

[185]   P. G. Richardson, T. Hideshima, C. Mitsiades, und K. Anderson, „Proteasome inhibition in hematologic malignancies", *Ann. Med.*, Bd. 36, Nr. 4, S. 304–314, 2004.

[186]   L. von Brzezinski, P. Säring, P. Landgraf, C. Cammann, U. Seifert, und D. C. Dieterich, „Low Neurotoxicity of ONX-0914 Supports the Idea of Specific Immunoproteasome Inhibition as a Side-Effect-Limiting, Therapeutic Strategy", *Eur. J. Microbiol. Immunol.*, Bd. 7, Nr. 3, S. 234–245, Sep. 2017.

[187]   X. Chen *u. a.*, „Inhibition of immunoproteasome reduces infarction volume and attenuates inflammatory reaction in a rat model of ischemic stroke", *Cell Death Dis.*, Bd. 6, Nr. 1, S. e1626, Jan. 2015.

[188]   D. A. Ferrington *u. a.*, „Immunoproteasome responds to injury in the retina and brain", *J Neurochem*, Bd. 106, Nr. 1, S. 158–69, Juli 2008.

[189]   M. P. Gavilán *u. a.*, „Age‑related increase in the immunoproteasome content in rat hippocampus: molecular and functional aspects", *J. Neurochem.*, Bd. 108, Nr. 1, S. 260–272, Jan. 2009.

[190]   S. Keck, R. Nitsch, T. Grune, und O. Ullrich, „Proteasome inhibition by paired helical filament-tau in brains of patients with Alzheimer's disease", *J. Neurochem.*, Bd. 85, Nr. 1, S. 115–122, Apr. 2003.

[191]   D. Poppek *u. a.*, „Phosphorylation inhibits turnover of the tau protein by the proteasome: influence of RCAN1 and oxidative stress", *Biochem. J.*, Bd. 400, Nr. Pt 3, S. 511–520, Dez. 2006.

[192]   T. Grune *u. a.*, „Tau protein degradation is catalyzed by the ATP/ubiquitin-independent 20S proteasome under normal cell conditions", *Arch. Biochem. Biophys.*, Bd. 500, Nr. 2, S. 181–188, Aug. 2010.

[193]   K. Puttaparthi und J. L. Elliott, „Non-neuronal induction of immunoproteasome subunits in an ALS model: possible mediation by cytokines", *Exp. Neurol.*, Bd. 196, Nr. 2, S. 441–451, Dez. 2005.

[194]   L. Lü und H. Wang, „Transient Focal Cerebral Ischemia Upregulates Immunoproteasomal Subunits", *Cell. Mol. Neurobiol.*, Bd. 32, Nr. 6, S. 965–970, Aug. 2012.

[195]   K. E. Moritz *u. a.*, „The role of the immunoproteasome in interferon-γ-mediated microglial activation", *Sci. Rep.*, Bd. 7, Nr. 1, Dez. 2017.

[196]   U.-K. Hanisch und H. Kettenmann, „Microglia: active sensor and versatile effector cells in the normal and pathologic brain", *Nat. Neurosci.*, Bd. 10, Nr. 11, S. 1387–1394, Nov. 2007.

[197]   S. Cullheim und S. Thams, „Classic major histocompatibility complex class I molecules: new actors at the neuromuscular junction", *Neurosci. Rev. J. Bringing Neurobiol. Neurol. Psychiatry*, Bd. 16, Nr. 6, S. 600–607, Dez. 2010.

[198]   R. K. Stumm *u. a.*, „A Dual Role for the SDF-1/CXCR4 Chemokine Receptor System in Adult Brain: Isoform-Selective Regulation of SDF-1 Expression Modulates CXCR4-Dependent Neuronal Plasticity and Cerebral Leukocyte Recruitment after Focal Ischemia", *J. Neurosci.*, Bd. 22, Nr. 14, S. 5865–5878, Juli 2002.

[199]   F. A. Welsh, T. Sakamoto, A. E. McKee, und R. E. Sims, „Effect of Lactacidosis on Pyridine Nucleotide Stability During Ischemia in Mouse Brain", *J. Neurochem.*, Bd. 49, Nr. 3, S. 846–851, Sep. 1987.

[200]   V. Bouet *u. a.*, „The adhesive removal test: a sensitive method to assess sensorimotor deficits in

mice", *Nat. Protoc.*, Bd. 4, Nr. 10, S. 1560–1564, Okt. 2009.

[201]   R. Khalil und M. Fendt, „Increased anxiety but normal fear and safety learning in orexin-deficient mice", *Behav. Brain Res.*, Bd. 320, S. 210–218, 01 2017.

[202]   M. Fendt, T. Endres, C. A. Lowry, R. Apfelbach, und I. S. McGregor, „TMT-induced autonomic and behavioral changes and the neural basis of its processing", *Neurosci. Biobehav. Rev.*, Bd. 29, Nr. 8, S. 1145–1156, 2005.

[203]   F. Angenstein *u. a.*, „Manganese-Enhanced MRI Reveals Structural and Functional Changes in the Cortex of Bassoon Mutant Mice", *Cereb. Cortex*, Bd. 17, Nr. 1, S. 28–36, Feb. 2006.

[204]   J. Hennig, A. Nauerth, und H. Friedburg, „RARE imaging: A fast imaging method for clinical MR", *Magn. Reson. Med.*, Bd. 3, Nr. 6, S. 823–833, Dez. 1986.

[205]   B. Schumak *u. a.*, „Specific Depletion of Ly6Chi Inflammatory Monocytes Prevents Immunopathology in Experimental Cerebral Malaria", *PLOS ONE*, Bd. 10, Nr. 4, S. e0124080, Apr. 2015.

[206]   L. Möhle *u. a.*, „Ly6Chi Monocytes Provide a Link between Antibiotic-Induced Changes in Gut Microbiota and Adult Hippocampal Neurogenesis", *Cell Rep.*, Bd. 15, Nr. 9, S. 1945–1956, Mai 2016.

[207]   A. Biswas *u. a.*, „Behavior of Neutrophil Granulocytes during Toxoplasma gondii Infection in the Central Nervous System", *Front. Cell. Infect. Microbiol.*, Bd. 7, Juni 2017.

[208]   K.-H. Smalla, P. Klemmer, und U. Wyneken, „Isolation of the Postsynaptic Density: A Specialization of the Subsynaptic Cytoskeleton", *SpringerLink*, S. 265–280, 2013.

[209]   H. Towbin, T. Staehelin, und J. Gordon, „Electrophoretic transfer of proteins from polyacrylamide gels to nitrocellulose sheets: procedure and some applications.", *Proc. Natl. Acad. Sci. U. S. A.*, Bd. 76, Nr. 9, S. 4350, Sep. 1979.

[210]   U. K. Laemmli, „Cleavage of Structural Proteins during the Assembly of the Head of Bacteriophage T4", *Nature*, Bd. 227, Nr. 5259, S. 680–685, Aug. 1970.

[211]   G. Banker und K. Goslin, „Developments in neuronal cell culture", *Nature*, Bd. 336, Nr. 6195, S. 185–186, Nov. 1988.

[212]   I. W. McLean und P. K. Nakane, „Periodate-lysine-paraformaldehyde fixative. A new fixation for immunoelectron microscopy", *J Histochem Cytochem*, Bd. 22, Nr. 12, S. 1077–83, Dez. 1974.

[213]   E. Rousselet, J. Kriz, und N. G. Seidah, „Mouse model of intraluminal MCAO: cerebral infarct evaluation by cresyl violet staining", *J. Vis. Exp. JoVE*, Nr. 69, Nov. 2012.

[214]   H. W. Morrison und J. A. Filosa, „A quantitative spatiotemporal analysis of microglia morphology during ischemic stroke and reperfusion", *J. Neuroinflammation*, Bd. 10, Nr. 1, S. 782, Jan. 2013.

[215]   W. M. S. Russell und R. L. Burch, „The principles of humane experimental technique.", *Princ. Hum. Exp. Tech.*, 1959.

[216]   J. Tannenbaum und B. T. Bennett, „Russell and Burch's 3Rs Then and Now: The Need for Clarity in Definition and Purpose", *J. Am. Assoc. Lab. Anim. Sci. JAALAS*, Bd. 54, Nr. 2, S. 120–132, März 2015.

[217]   E. Benito und A. Barco, „CREB's control of intrinsic and synaptic plasticity: implications for CREB-dependent memory models", *Trends Neurosci.*, Bd. 33, Nr. 5, S. 230–240, Mai 2010.

[218]   C. M. Alberini, „Transcription Factors in Long-Term Memory and Synaptic Plasticity", *Physiol. Rev.*, Bd. 89, Nr. 1, Jan. 2009.

[219]   V. Ortiz-Navarrete, A. Seelig, M. Gernold, S. Frentzel, P. M. Kloetzel, und G. J. Hämmerling, „Subunit of the ‚20S' proteasome (multicatalytic proteinase) encoded by the major histocompatibility complex", *Nature*, Bd. 353, Nr. 6345, S. 662–664, Okt. 1991.

[220]   A. Kelly, S. H. Powis, R. Glynne, E. Radley, S. Beck, und J. Trowsdale, „Second proteasome-related gene in the human MHC class II region", *Nature*, Bd. 353, Nr. 6345, S. 667–668, Okt. 1991.

[221]   R. Glynne, S. H. Powis, S. Beck, A. Kelly, L. A. Kerr, und J. Trowsdale, „A proteasome-related gene between the two ABC transporter loci in the class II region of the human MHC", *Nature*, Bd. 353, Nr. 6342, S.

357–360, Sep. 1991.

[222]   F. Ebstein, P.-M. Kloetzel, E. Krüger, und U. Seifert, „Emerging roles of immunoproteasomes beyond MHC class I antigen processing", *Cell. Mol. Life Sci.*, Bd. 69, Nr. 15, S. 2543–2558, Aug. 2012.

[223]   A. Becerra-Calixto und G. P. Cardona-Gómez, „The Role of Astrocytes in Neuroprotection after Brain Stroke: Potential in Cell Therapy", *Front. Mol. Neurosci.*, Bd. 10, Apr. 2017.

[224]   A. ElAli und N. Jean LeBlanc, „The Role of Monocytes in Ischemic Stroke Pathobiology: New Avenues to Explore", *Front. Aging Neurosci.*, Bd. 8, S. 29, 2016.

[225]   R. Guruswamy und A. ElAli, „Complex Roles of Microglial Cells in Ischemic Stroke Pathobiology: New Insights and Future Directions", *Int. J. Mol. Sci.*, Bd. 18, Nr. 3, Feb. 2017.

[226]   L. B. Haim, M.-A. C. Sauvage, K. Ceyzériat, und C. Escartin, „Elusive roles for reactive astrocytes in neurodegenerative diseases", *Front. Cell. Neurosci.*, Bd. 9, 2015.

[227]   J. C. Felger u. a., „Brain dendritic cells in ischemic stroke: time course, activation state, and origin", *Brain. Behav. Immun.*, Bd. 24, Nr. 5, S. 724–737, Juli 2010.

[228]   S. Vidale, A. Consoli, M. Arnaboldi, und D. Consoli, „Postischemic Inflammation in Acute Stroke", *J. Clin. Neurol. Seoul Korea*, Bd. 13, Nr. 1, S. 1–9, Jan. 2017.

[229]   T. Shichita, R. Sakaguchi, M. Suzuki, und A. Yoshimura, „Post-Ischemic Inflammation in the Brain", *Front. Immunol.*, Bd. 3, Mai 2012.

[230]   Q. Wang, X. N. Tang, und M. A. Yenari, „THE INFLAMMATORY RESPONSE IN STROKE", *J. Neuroimmunol.*, Bd. 184, Nr. 1–2, S. 53–68, März 2007.

[231]   M. Groettrup, S. Khan, K. Schwarz, und G. Schmidtke, „Interferon-γ inducible exchanges of 20S proteasome active site subunits: Why?", *Proteasomes*, Bd. 83, Nr. 3, S. 367–372, März 2001.

[232]   M. Groettrup, R. Kraft, S. Kostka, S. Standera, R. Stohwasser, und P. M. Kloetzel, „A third interferon-gamma-induced subunit exchange in the 20S proteasome", *Eur. J. Immunol.*, Bd. 26, Nr. 4, S. 863–869, Apr. 1996.

[233]   K. L. Lambertsen, K. Biber, und B. Finsen, „Inflammatory cytokines in experimental and human stroke", *J. Cereb. Blood Flow Metab. Off. J. Int. Soc. Cereb. Blood Flow Metab.*, Bd. 32, Nr. 9, S. 1677–1698, Sep. 2012.

[234]   H. Yasukawa, A. Sasaki, und A. Yoshimura, „Negative regulation of cytokine signaling pathways", *Annu. Rev. Immunol.*, Bd. 18, S. 143–164, 2000.

[235]   A. Yoshimura, „The CIS family: negative regulators of JAK-STAT signaling", *Cytokine Growth Factor Rev.*, Bd. 9, Nr. 3–4, S. 197–204, Dez. 1998.

[236]   H. Kimura u. a., „Immunoproteasome subunit LMP7 Deficiency Improves Obesity and Metabolic Disorders", *Sci. Rep.*, Bd. 5, 2015.

[237]   R. Stohwasser u. a., „Biochemical analysis of proteasomes from mouse microglia: induction of immunoproteasomes by interferon-gamma and lipopolysaccharide", *Glia*, Bd. 29, Nr. 4, S. 355–365, Feb. 2000.

[238]   B. Cătălin, A. Cupido, M. Iancău, C. V. Albu, und F. Kirchhoff, „Microglia: first responders in the central nervous system", *Romanian J. Morphol. Embryol. Rev. Roum. Morphol. Embryol.*, Bd. 54, Nr. 3, S. 467–472, 2013.

[239]   T. Frisan, V. Levitsky, A. Polack, und M. G. Masucci, „Phenotype-dependent differences in proteasome subunit composition and cleavage specificity in B cell lines", *J. Immunol. Baltim. Md 1950*, Bd. 160, Nr. 7, S. 3281–3289, Apr. 1998.

[240]   T. Frisan, V. Levitsky, und M. G. Masucci, „Variations in proteasome subunit composition and enzymatic activity in B-lymphoma lines and normal B cells", *Int. J. Cancer*, Bd. 88, Nr. 6, S. 881–888, 2000.

[241]   E. Kim und S. Cho, „Microglia and Monocyte-Derived Macrophages in Stroke", *Neurotherapeutics*, Bd. 13, Nr. 4, S. 702–718, Okt. 2016.

[242]   D. M. Mosser und J. P. Edwards, „Exploring the full spectrum of macrophage activation", *Nat. Rev. Immunol.*, Bd. 8, Nr. 12, S. 958–969, Dez. 2008.

[243]   D. Ito, Y. Imai, K. Ohsawa, K. Nakajima, Y. Fukuuchi, und S. Kohsaka, „Microglia-specific localisation of a novel calcium binding protein, Iba1", *Brain Res. Mol. Brain Res.*, Bd. 57, Nr. 1, S. 1–9, Juni 1998.

[244]   R. Nakamura, T. Nishimura, T. Ochiai, S. Nakada, M. Nagatani, und H. Ogasawara, „Availability of a Microglia and Macrophage Marker, Iba-1, for Differential Diagnosis of Spontaneous Malignant Reticuloses from Astrocytomas in Rats", *J. Toxicol. Pathol.*, Bd. 26, Nr. 1, S. 55–60, März 2013.

[245]   M. Díaz-Hernández, E. Martín-Aparicio, J. Avila, F. Hernández, und J. J. Lucas, „Enhanced induction of the immunoproteasome by interferon gamma in neurons expressing mutant Huntingtin", *Neurotox. Res.*, Bd. 6, Nr. 6, S. 463–468, 2004.

[246]   D. Boche, V. H. Perry, und J. a. R. Nicoll, „Review: activation patterns of microglia and their identification in the human brain", *Neuropathol. Appl. Neurobiol.*, Bd. 39, Nr. 1, S. 3–18, Feb. 2013.

[247]   C. A. Colton, „Heterogeneity of microglial activation in the innate immune response in the brain", *J. Neuroimmune Pharmacol. Off. J. Soc. NeuroImmune Pharmacol.*, Bd. 4, Nr. 4, S. 399–418, Dez. 2009.

[248]   S. Camandola und M. P. Mattson, „Brain metabolism in health, aging, and neurodegeneration", *EMBO J.*, Bd. 36, Nr. 11, S. 1474–1492, 01 2017.

[249]   Z.-J. Ke und G. E. Gibson, „Selective response of various brain cell types during neurodegeneration induced by mild impairment of oxidative metabolism", *Neurochem. Int.*, Bd. 45, Nr. 2–3, S. 361–369, Aug. 2004.

[250]   W. J. Friedman, „Proneurotrophins, seizures, and neuronal apoptosis", *Neurosci. Rev. J. Bringing Neurobiol. Neurol. Psychiatry*, Bd. 16, Nr. 3, S. 244–252, Juni 2010.

[251]   B. L. Hempstead, „Deciphering proneurotrophin actions", *Handb. Exp. Pharmacol.*, Bd. 220, S. 17–32, 2014.

[252]   K. K. Teng, S. Felice, T. Kim, und B. L. Hempstead, „Understanding proneurotrophin actions: Recent advances and challenges", *Dev. Neurobiol.*, Bd. 70, Nr. 5, S. 350–359, Apr. 2010.

[253]   I. V. Demidyuk, A. V. Shubin, E. V. Gasanov, und S. V. Kostrov, „Propeptides as modulators of functional activity of proteases", *Biomol. Concepts*, Bd. 1, Nr. 3–4, S. 305–322, Okt. 2010.

[254]   S. Gohlke u. a., „Adult human liver contains intermediate-type proteasomes with different enzymatic properties", *Ann. Hepatol.*, Bd. 13, Nr. 4, S. 429–438, Aug. 2014.

[255]   N. Klare, M. Seeger, K. Janek, P. R. Jungblut, und B. Dahlmann, „Intermediate-type 20 S Proteasomes in HeLa Cells: "Asymmetric" Subunit Composition, Diversity and Adaptation", *J. Mol. Biol.*, Bd. 373, Nr. 1, S. 1–10, Okt. 2007.

[256]   A. Nimmerjahn, F. Kirchhoff, und F. Helmchen, „Resting microglial cells are highly dynamic surveillants of brain parenchyma in vivo", *Science*, Bd. 308, Nr. 5726, S. 1314–1318, Mai 2005.

[257]   F. Aloisi, „Immune function of microglia", *Glia*, Bd. 36, Nr. 2, S. 165–179, Nov. 2001.

[258]   I. Shaked, Z. Porat, R. Gersner, J. Kipnis, und M. Schwartz, „Early activation of microglia as antigen-presenting cells correlates with T cell-mediated protection and repair of the injured central nervous system", *J. Neuroimmunol.*, Bd. 146, Nr. 1, S. 84–93, Jan. 2004.

[259]   D. P. Schafer, E. K. Lehrman, und B. Stevens, „The "Quad-partite" Synapse: Microglia-Synapse Interactions in the Developing and Mature CNS", *Glia*, Bd. 61, Nr. 1, S. 24–36, Jan. 2013.

[260]   H. Kumar, T. Kawai, und S. Akira, „Pathogen recognition by the innate immune system", *Int. Rev. Immunol.*, Bd. 30, Nr. 1, S. 16–34, Feb. 2011.

[261]   A. Denes u. a., „Proliferating resident microglia after focal cerebral ischaemia in mice", *J. Cereb. Blood Flow Metab. Off. J. Int. Soc. Cereb. Blood Flow Metab.*, Bd. 27, Nr. 12, S. 1941–1953, Dez. 2007.

[262]   R. A. Taylor und L. H. Sansing, „Microglial Responses after Ischemic Stroke and Intracerebral Hemorrhage", *Clin. Dev. Immunol.*, Bd. 2013, 2013.

[263]   L. K. Wagner u. a., „Immunoproteasome deficiency alters microglial cytokine response and improves cognitive deficits in Alzheimer's disease-like APPPS1 mice", *Acta Neuropathol. Commun.*, Bd. 5, 2017.

[264]   B. Hoesel und J. A. Schmid, „The complexity of NF-κB signaling in inflammation and cancer", *Mol. Cancer*, Bd. 12, S. 86, Aug. 2013.

[265]   J. J. Monaco und H. O. McDevitt, „The LMP antigens: A stable MHC-controlled multisubunit protein complex", *Hum. Immunol.*, Bd. 15, Nr. 4, S. 416–426, Apr. 1986.

[266]   G. Zhang und S. Ghosh, „Negative regulation of toll-like receptor-mediated signaling by Tollip", *J. Biol. Chem.*, Bd. 277, Nr. 9, S. 7059–7065, März 2002.

[267]   W. L. Lee, M.-K. Kim, A. D. Schreiber, und S. Grinstein, „Role of Ubiquitin and Proteasomes in Phagosome Maturation", *Mol. Biol. Cell*, Bd. 16, Nr. 4, S. 2077–2090, Apr. 2005.

[268]   G. Griffiths und L. Mayorga, „Phagosome proteomes open the way to a better understanding of phagosome function", *Genome Biol.*, Bd. 8, Nr. 3, S. 207, 2007.

[269]   M. Houde u. a., „Phagosomes are competent organelles for antigen cross-presentation", *Nature*, Bd. 425, Nr. 6956, S. 402–406, Sep. 2003.

[270]   S. A. Liddelow u. a., „Neurotoxic reactive astrocytes are induced by activated microglia", *Nature*, Bd. 541, Nr. 7638, S. 481–487, 26 2017.

[271]   M. V. Sofroniew und H. V. Vinters, „Astrocytes: biology and pathology", *Acta Neuropathol. (Berl.)*, Bd. 119, Nr. 1, S. 7–35, Jan. 2010.

[272]   P. Viatour, M.-P. Merville, V. Bours, und A. Chariot, „Phosphorylation of NF-κB and IκB proteins: implications in cancer and inflammation", *Trends Biochem. Sci.*, Bd. 30, Nr. 1, S. 43–52, Jan. 2005.

[273]   X. Yao, J. Liu, und J. T. McCabe, „Alterations of cerebral cortex and hippocampal proteasome subunit expression and function in a traumatic brain injury rat model", *J. Neurochem.*, Bd. 104, Nr. 2, S. 353–363, Jan. 2008.

[274]   P. Huang, C.-H. Chen, Y.-H. Yang, R.-T. Lin, F.-C. Lin, und C.-K. Liu, „Eligibility for recombinant tissue plasminogen activator in acute ischemic stroke: way to endeavor", *Cerebrovasc. Dis. Basel Switz.*, Bd. 22, Nr. 5–6, S. 423–428, 2006.

[275]   Y. Imai und S. Kohsaka, „Intracellular signaling in M-CSF-induced microglia activation: role of Iba1", *Glia*, Bd. 40, Nr. 2, S. 164–174, Nov. 2002.

[276]   K. Ohsawa, Y. Imai, H. Kanazawa, Y. Sasaki, und S. Kohsaka, „Involvement of Iba1 in membrane ruffling and phagocytosis of macrophages/microglia", *J. Cell Sci.*, Bd. 113 (Pt 17), S. 3073–3084, Sep. 2000.

[277]   K. Ohsawa, Y. Imai, Y. Sasaki, und S. Kohsaka, „Microglia/macrophage-specific protein Iba1 binds to fimbrin and enhances its actin-bundling activity", *J. Neurochem.*, Bd. 88, Nr. 4, S. 844–856, Feb. 2004.

[278]   H. X. Chu, B. R. S. Broughton, H. A. Kim, S. Lee, G. R. Drummond, und C. G. Sobey, „Evidence That Ly6C(hi) Monocytes are Protective in Acute Ischemic Stroke by Promoting M2 Macrophage Polarization", *Stroke*, Bd. 46, Nr. 7, S. 1929–1937, Juli 2015.

[279]   F. Miró-Mur u. a., „Immature monocytes recruited to the ischemic mouse brain differentiate into macrophages with features of alternative activation", *Brain. Behav. Immun.*, Bd. 53, S. 18–33, März 2016.

[280]   P. M. D'Agostino, A. Gottfried-Blackmore, N. Anandasabapathy, und K. Bulloch, „Brain dendritic cells: biology and pathology", *Acta Neuropathol. (Berl.)*, Bd. 124, Nr. 5, S. 599–614, Nov. 2012.

[281]   A. Biswas u. a., „Ly6C(high) monocytes control cerebral toxoplasmosis", *J. Immunol. Baltim. Md 1950*, Bd. 194, Nr. 7, S. 3223–3235, Apr. 2015.

[282]   C. Benakis, L. Garcia-Bonilla, C. Iadecola, und J. Anrather, „The role of microglia and myeloid immune cells in acute cerebral ischemia", *Front. Cell. Neurosci.*, Bd. 8, 2015.

[283]   E. Kolaczkowska und P. Kubes, „Neutrophil recruitment and function in health and inflammation", *Nat. Rev. Immunol.*, Bd. 13, Nr. 3, S. 159–175, März 2013.

[284]   T. Shichita, R. Sakaguchi, M. Suzuki, und A. Yoshimura, „Post-ischemic inflammation in the brain",

*Front. Immunol.*, Bd. 3, S. 132, 2012.

[285]   P. J. Murray *u. a.*, „Macrophage activation and polarization: nomenclature and experimental guidelines", *Immunity*, Bd. 41, Nr. 1, S. 14–20, Juli 2014.

[286]   G. M. Hayes, M. N. Woodroofe, und M. L. Cuzner, „Microglia are the major cell type expressing MHC class II in human white matter", *J. Neurol. Sci.*, Bd. 80, Nr. 1, S. 25–37, Aug. 1987.

[287]   O. Rasid, C. Meulenbroeks, A. Gröne, D. Zaiss, und A. Sijts, „Enhanced Inflammatory Potential of CD4+ T-Cells That Lack Proteasome Immunosubunit Expression, in a T-Cell Transfer-Based Colitis Model", *PLoS ONE*, Bd. 9, Nr. 4, Apr. 2014.

[288]   N. G. Spencer, T. Schilling, F. Miralles, und C. Eder, „Mechanisms Underlying Interferon-γ-Induced Priming of Microglial Reactive Oxygen Species Production", *PloS One*, Bd. 11, Nr. 9, S. e0162497, 2016.

Supplements

A

B
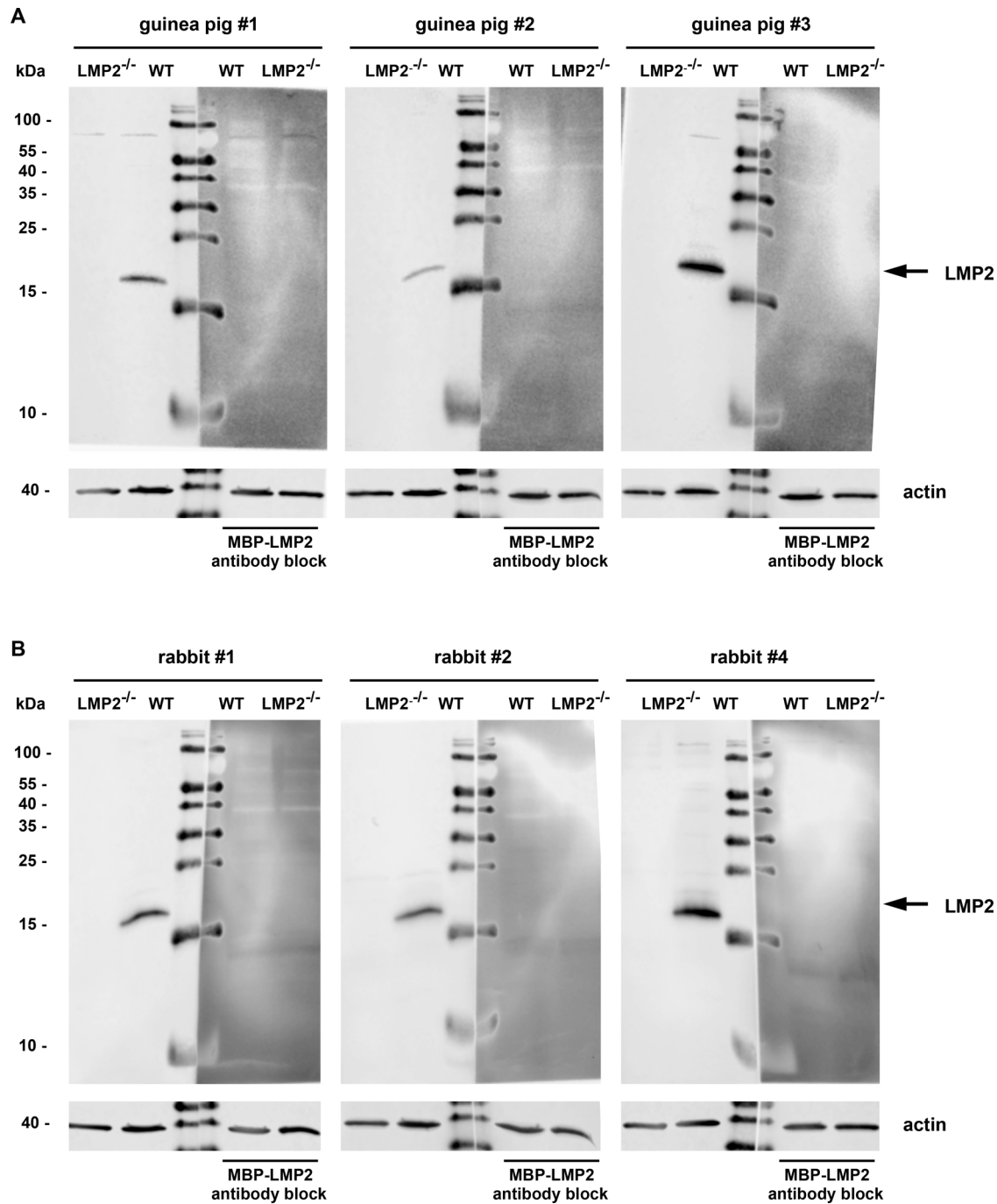
Supplementary Figure S 1: LMP2 anti-sera characterization for WB analysis
All anti-sera against LMP2 from guinea pig #1, #2, #3 (A) and rabbit #1, #2, #4 (B), which were generated by Pineda Antikörper Service, were tested for their applicability in WB analysis using homogenates of WT and LMP2$^{-/-}$ mouse spleens as positive and negative controls, respectively. Both, the guinea pig as well as the rabbit anti-sera detects an immuno-reactive band at the predicted size of LMP2 in the WT samples, whereas no signals could be observed in the knockout samples. Highest signal quality was achieved with the guinea pig #3 (A) and rabbit #4 (B) antibody. Further, specificity of all anti-sera was successfully verified by pre-adsorption of the anti-sera with an MBP-LMP2 fusion protein.
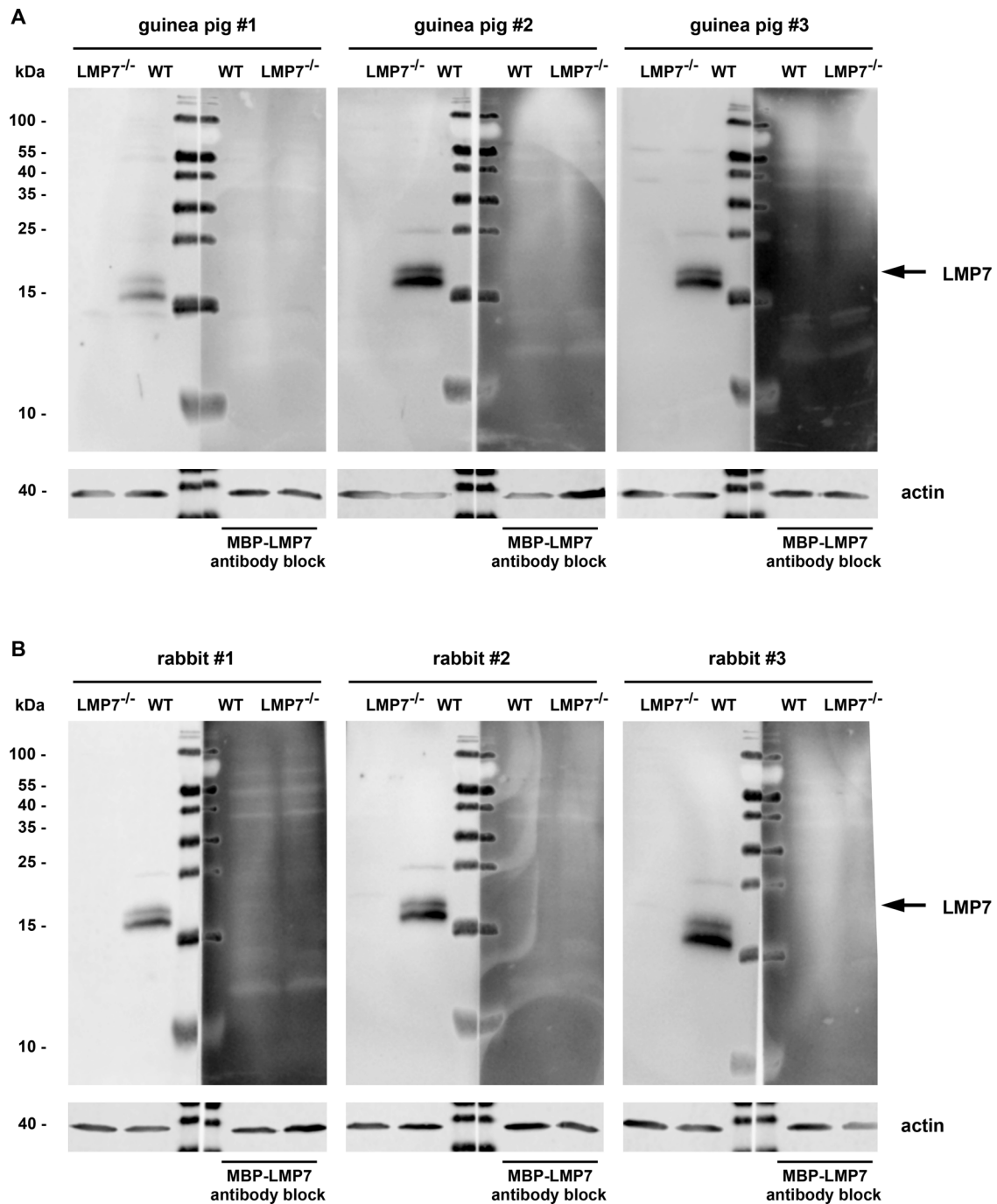
Supplementary Figure S 2: **LMP7 anti-sera characterization for WB analysis**
Anti-sera against LMP7 from guinea pig #1, #2, #3 (A) and rabbit #1, #2, #3 (B), generated by Pineda Antikörper Service, were tested for their applicability in WB analysis using homogenates of WT and LMP7$^{-/-}$ mouse spleens as positive and negative controls, respectively. With both, the guinea pig as well as the rabbit anti-sera immuno-reactive bands were detected at the predicted size of LMP7 in the WT samples, whereas no signals could be observed in the knockout samples. Notably, all anti-sera seem to detect additionally the pro-form of the protein indicated by the double bands. Highest signal quality was achieved with the guinea pig #2 (A) and rabbit #3 (B) antibody. Further, specificity of all anti-sera was successfully verified by pre-adsorption of the anti-sera with a MBP-LMP7 fusion protein, although some blots exhibit high background signals.
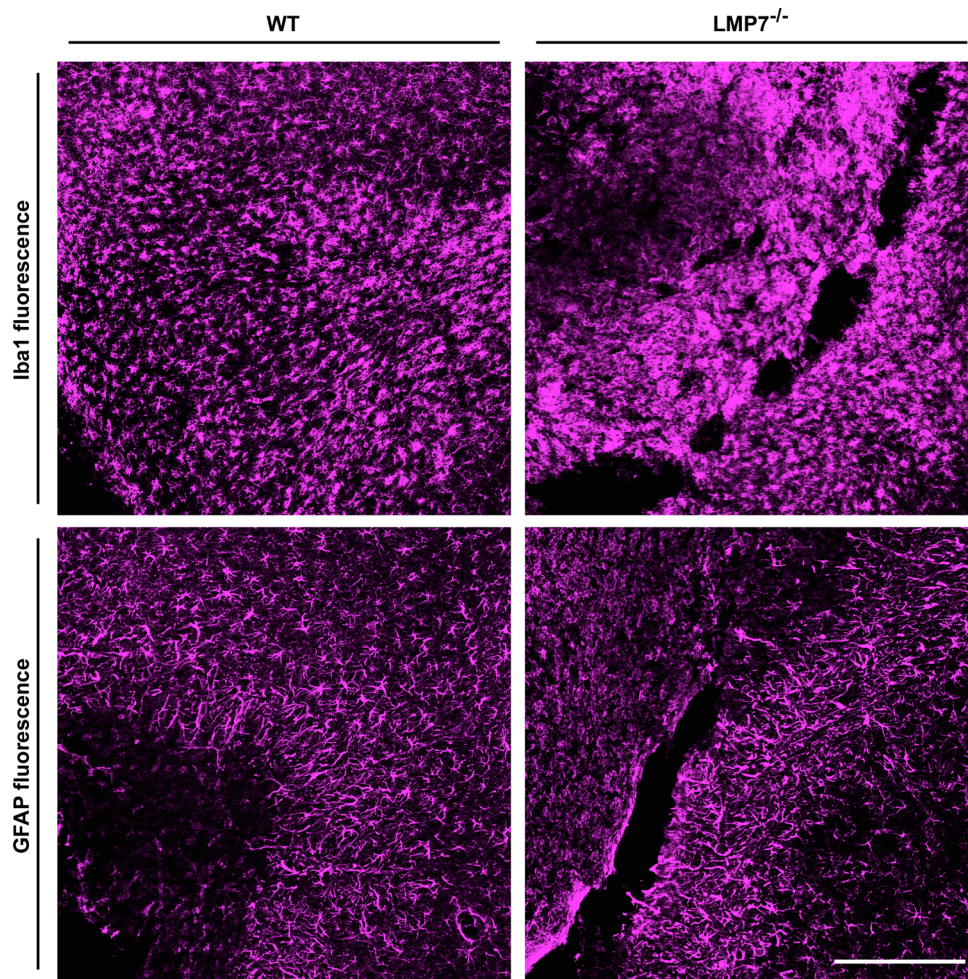
Supplementary Figure S 3: Precedent infarct area after 8 d of MCAO
Signal intensities of Iba1-positive (upper row) and GFAP-positive cells (lower row) in immunohistochemical stainings of WT and LMP7^{-/-} mouse brain sections after 8 d of MCAO.
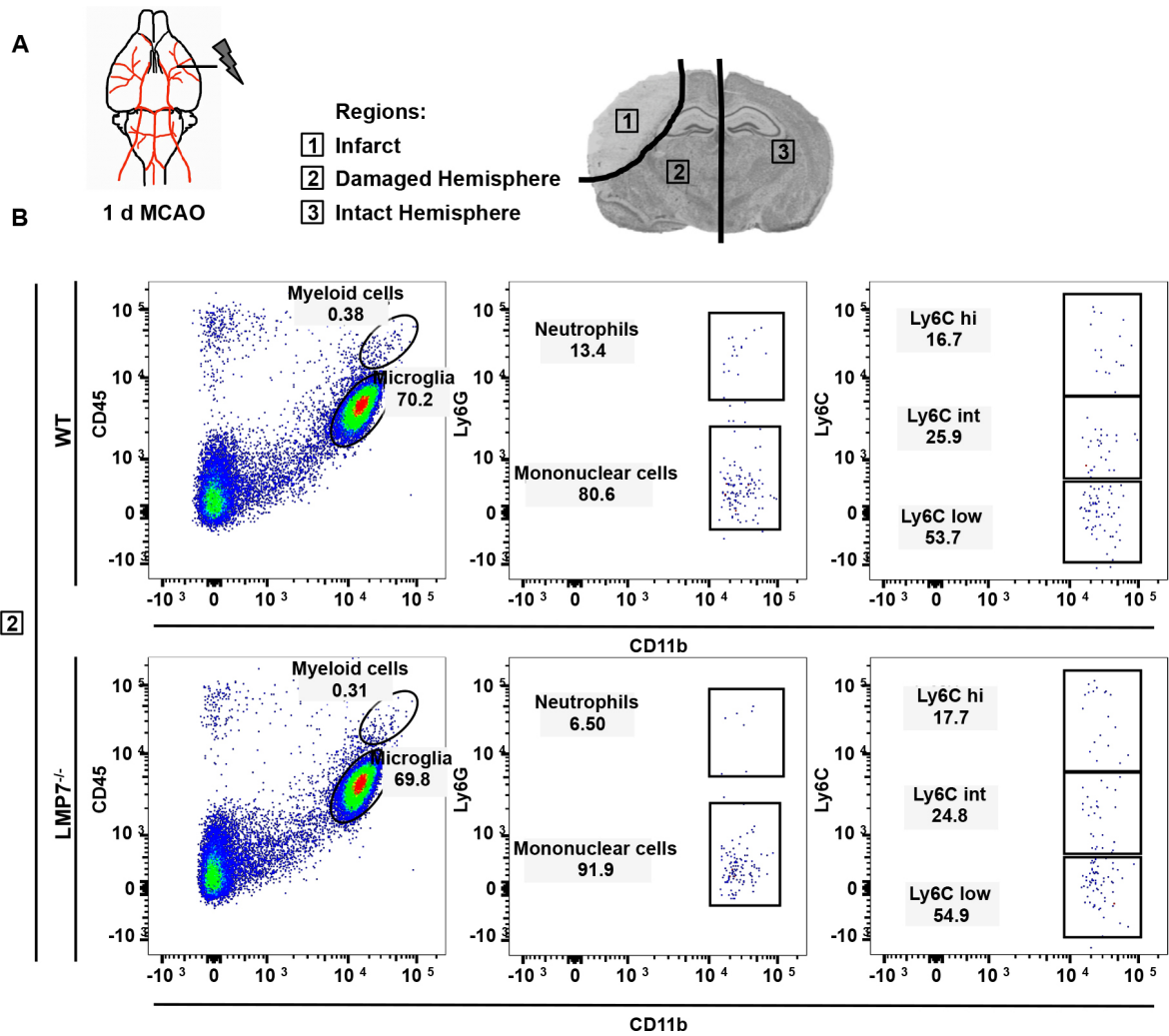
Supplementary Figure S 4: Myeloid cell populations in WT and LMP7$^{-/-}$ mouse brains in the damaged hemisphere after MCAO

After 1 d of MCAO, WT and LMP7$^{-/-}$ mouse brains were dissected into three parts and analysed via FACS analysis (A). Depicted are density blots of the gating strategy for data of the damaged hemisphere of both genotypes (B). There are no obvious differences between WT and LMP7$^{-/-}$ animals.
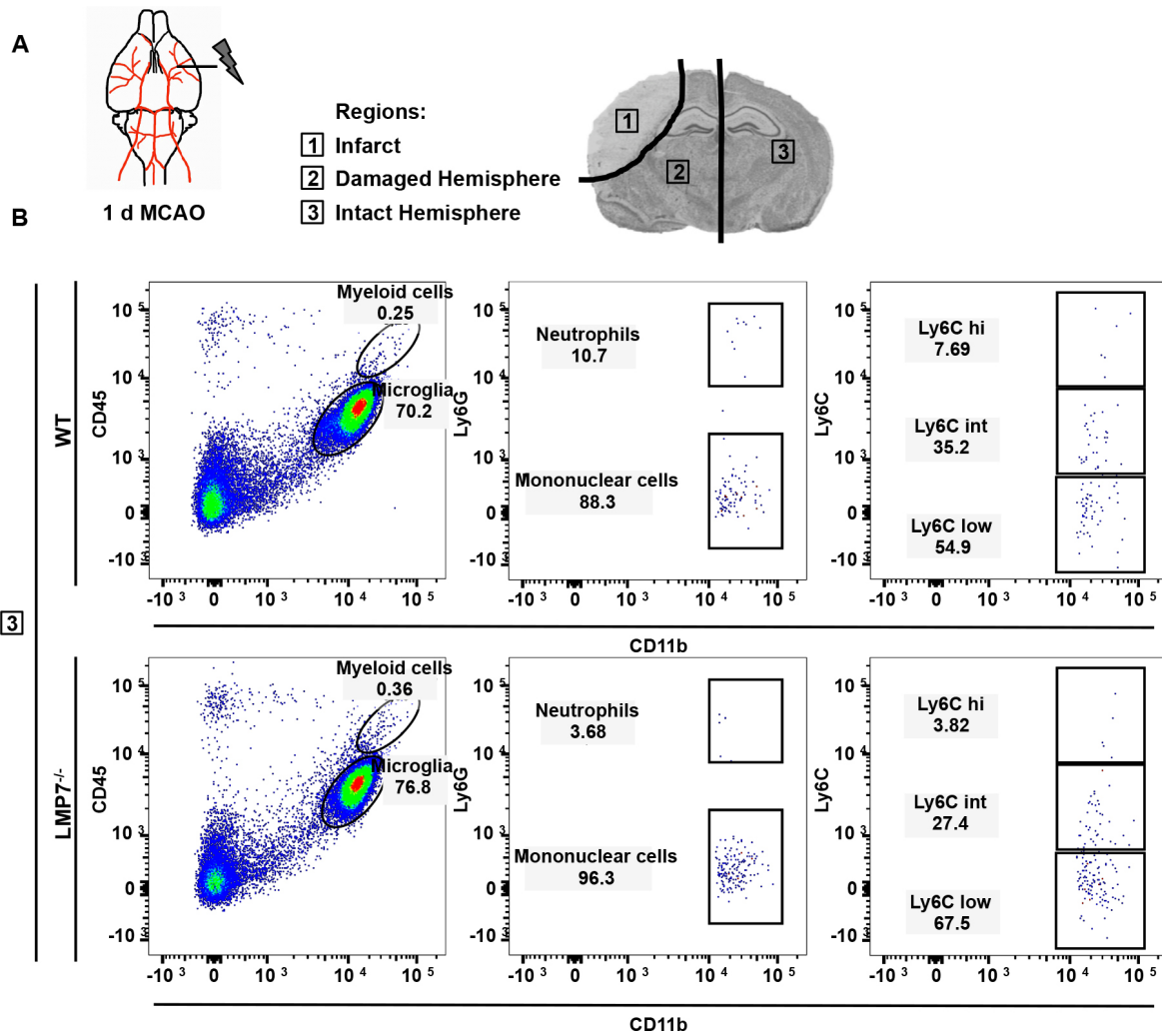
Supplementary Figure S 5: Myeloid cell populations in WT and LMP7^{-/-} mouse brains in the intact hemisphere after MCAO

WT and LMP7^{-/-} mouse brains were dissected into three parts after 1 d of MCAO and analysed via FACS analysis (A). Depicted are density blots of the gating strategy for data of the intact hemisphere of both genotypes (B). There are no obvious differences between WT and LMP7^{-/-} mice.

List of publications

von Brzezinski, L., Säring, P., Landgraf, P., Cammann, C., Seifert, U., and Dieterich, D.C. (2017). Low Neurotoxicity of ONX-0914 Supports the Idea of Specific IP Inhibition as a Side-Effect-Limiting, Therapeutic Strategy. Eur.J.Microbiol.Immunol. 7, 243-245.

Acknowledgement

Statutory declaration

Hiermit erkläre ich, dass ich die von mir eingereichte Dissertation zu dem Thema

Characterization of the Immunoproteasome Subunits LMP2 and LMP7 in the Mouse Brain

selbstständig verfasst, nicht schon als Dissertation verwendet habe und die benutzten Hilfsmittel und Quellen vollständig angegeben wurden.

Weiterhin erkläre ich, dass ich weder diese noch andere Arbeiten zur Erlangung des akademischen Grades doctor rerum naturalium (Dr. rer. nat.) an anderen Einrichtungen eingereicht habe.

Magdeburg, den 22. Mai 2018

Paula Säring